ESTROGEN RECEPTOR ALPHA IN OSTEOBLASTS MEDIATES BONE MASS AND BONE'S RESPONSE TO IN VIVO LOADING

A Dissertation

Presented to the Faculty of the Graduate School

of Cornell University

In Partial Fulfillment of the Requirements for the Degree of

Doctor of Philosophy

by

Katherine Margaret Melville

August 2014

ESTROGEN RECEPTOR ALPHA IN OSTEOBLASTS MEDIATES BONE MASS AND BONE'S RESPONSE TO IN VIVO LOADING

Katherine Margaret Melville, Ph. D.

Cornell University 2014

Decreased bioavailable estrogen levels are a major cause of bone loss in postmenopausal women, but sex hormones are important regulators of bone mass in both sexes. Estrogen signaling in bone occurs mainly through estrogen receptors ERα and ERβ. ERα in particular is important in regulating bone mass and bone's response to mechanical loading, but its particular role in each bone cell type and its cross-talk with BMP signaling are not well studied. `

Osteoblast-specific ERα knockout (pOC-ERαKO) and littermate control (LC) were bred by crossing *Osteocalcin-Cre* and $ER\alpha^{fl/fl}$ mice. The effects of removing ERα in osteoblasts and osteocytes on bone mass, bone strength, and bone's response to mechanical loading were studied in 10-week-old animals. In general, cancellous and cortical bone mass were both reduced in pOC-ERαKO female mice, while bone mass was increased in pOC-ERαKO male mice compared to their sex-matched LC, measured by microCT in the proximal and midshaft tibia, femur, and L5 vertebra. These bone mass changes correlated with decreased vertebral compressive strength in female knockout mice and increased femoral bending strength in male knockout mice. After two weeks of in vivo tibial compression, female pOC-ERαKO mice showed a greater increase in bone mass in the proximal tibia, where baseline bone mass was decreased, and at the tibial midshaft, where baseline bone mass was similar to LC. Male pOC-ERαKO mice exhibited a normal response to mechanical loading.

Next, 10-week-old female pOC-ERαKO and LC mice were administered either

RAP-661, a BMPR1a inhibitor, or placebo, and all mice were subjected to daily in vivo tibial compression for two weeks. RAP-661 markedly increased bone mass in the L5 vertebra and cancellous tibial metaphysis of both genotypes, but not at the femoral midshaft, tibial midshaft, or tibial metaphyseal cortex. In the vertebra, the drug-induced increase in bone mass was less in pOC-ERαKO mice than LC. Animals treated with RAP-661 responded less to mechanical loading in the tibial metaphysis than placebo animals, but similarly at the tibial midshaft. This is the first evidence to indicate that BMPR1a may mediate bone's response to mechanical loading and interact with ERα in osteoblasts in vivo.

BIOGRAPHICAL SKETCH

Katherine Margaret (Povirk) Melville was born in 1987 in Jackson, Michigan, as the second oldest of five children. After graduating as salutatorian from Cumberland Valley High School in 2005, she attended the University of Pittsburgh and earned a Bachelor of Science degree in Bioengineering with summa cum laude in 2009. During her undergraduate career, she was a member of the Zeta Chapter of Phi Sigma Rho, a social sorority for women in engineering, for which she served as Treasurer and President. She also was inducted into Tau Beta Pi. After doing extensive undergraduate research and working for a start-up company in Pittsburgh, she attended Cornell University in the fall of 2009. In 2012, she received her Master of Science degree in Biomedical Engineering. In August 2014, she received her Doctor of Philosophy degree in Biomedical Engineering. While at Cornell, she was funded by a one-year GAANN fellowship, and she also received a prestigious 3-year NSF Graduate Research Fellowship.

I dedicate this work to Evelyn Rose.

ACKNOWLEDGMENTS

I owe gratitude to many people and organizations without whom this work would not have been possible. I acknowledge the U.S. Department of Education for providing me with a one-year Graduate Assistance in Areas of National Need (GAANN) fellowship, and the National Science Foundation for providing me with a three-year Graduate Research Fellowship (GRF). The following grants funded this research: National Institutes of Health R01-AG028664, P30-AR046121, and F32-AR054676.

I want to thank my chair committee member, Dr. Marjolein van der Meulen, for her tremendous support, guidance, and mentorship. My other committee members, Dr. Christopher Hernandez and Dr. John Schimenti, also supported me and this work. Behind the scenes, Judy Thoroughman, Belinda Floyd, and Marcia Sawyer all kept things running smoothly so that I could focus on my research.

This research was completed with the invaluable assistance from many others. I would like to thank many current and past lab members who helped during mouse experiments and data collection: Funmi Adebayo, Daniel Brooks, Daniel Buchalter, Tyler Heck, Derek Holyoak, Stephen Hong, Dr. Frank Ko, Eric Lee, and Gina Surita. I owe a special thanks to Natalie Kelly, who not only assisted in experiments but who traveled to NYC many times in my place to microCT my samples so that I would not have to leave my daughter for several days. When I did travel to NYC, Kirsten Stoner was my gracious host. Drs Maureen Lynch and Russell Main were wonderful mentors who provided guidance throughout my graduate career. I am grateful for the entire Schimenti lab for their support, especially Kerry Schimenti, who helped immensely with mouse genotyping.

I would like to acknowledge many collaborators outside of Cornell for their contributions. At the Hospital for Special Surgery in NYC, Dr. Mathias Bostrom and

his lab group provided valuable feedback on data and conference presentations. Dr. Patrick Ross was instrumental to the design and interpretation of all of this work, and I am very grateful for his expertise. Lyudmila Lukashova helped with microCT scans, even during off hours. Dr. Scott Pearsall at Acceleron collaborated with us for the BMP work. Drs. Thomas Clemens and Sohaib Khan provided mice upon which these experiments were based.

The love of my family and friends was my biggest source of support and encouragement. My parents, Robert and Mary Pat, always encouraged me to use the gifts God gave me to their fullest and helped me to recognize my potential. For six months, my mom and dad traveled to Ithaca every other week for a week at a time to babysit my daughter while my husband and I worked. This tremendous sacrifice of time is just one of the many they have done for me throughout my life. To them, I owe everything. I thank my siblings, Christopher, Stephanie, Sarah, and Jonathan, for late night chats and comic relief, and I am grateful for our closeness. Molly Deuson is my life line, therapist, and best friend, even from 2500 miles away. I cannot imagine my time in Ithaca without the friendships of Dr. Brooke Mason, Dr. Jennifer Puetzer, and Jennifer Richards. I am especially grateful for my friends Shawn and Teresa Carey, who sustained me while I was a single parent for seven months, with weekly meals, ice cream dates, play dates, and unwavering emotional support. You two are incredibly loving and giving. My church, St. Catherine of Siena, and especially the choir members were a wonderful community that I doubt exists in the same capacities elsewhere.

My daughter, Evelyn Rose, is a source of inspiration. Although graduate school in many ways was much more difficult with her in my life, she gave me the perspective I needed to discern what is important, and she helped me to be extremely efficient in my work so that I was able to spend as much time with her as possible.

Last, I cannot even begin to express my love and appreciation for my husband, Alex, who encouraged me to apply to graduate school in the first place. He has supported me in innumerable ways, including forcing me to relax once in a while when it was sorely needed. Every day I feel blessed to be his wife.

TABLE OF CONTENTS

LIST OF FIGURES

LIST OF TABLES

Chapter 1

INTRODUCTION

1.1 Osteoporosis

Osteoporosis, a condition of low bone mass, increases fracture susceptibility. Each year in the United States, 1.5 million Americans suffer from an osteoporotic fracture (1). It is estimated that 1/3 of women and 1/5 of men over the age of 50 will experience an osteoporotic fracture at some point in their lives (2). The healthcare burden of these fractures exceeds $1 billion yearly (3). By the year 2025, over 3 million fractures are expected and healthcare costs are anticipated to rise to $25 billion per year. After a patient experiences one fracture due to osteoporosis, the likelihood of a second fracture is substantially increased, in a pathology known as the "fracture cascade" (4). The need for therapies, treatments, and especially prevention for osteoporosis is clear in our society.

Osteoporosis is characterized by low bone mass and affects 44 million Americans (2). Bone is comprised of two major components: a mineral component, mostly of calcium phosphate, and an organic component, mainly of collagen type 1. Osteoporosis is diagnosed by measuring bone mineral density (BMD) from dual x-ray absorptiometry (DEXA) scans. From DEXA, a T-score or a Z-score is given, which compares the skeleton's BMD to that of the average young adult or the average adult matched for age and sex, respectively. When a patient's T-score is 2.5 standard deviations below that of an average young adult, osteoporosis is the diagnosis. **Figure 1.1** depicts compromised cancellous architecture in human iliac crest bone affected by osteoporosis (5). Bone density and trabecular thickness are both decreased.

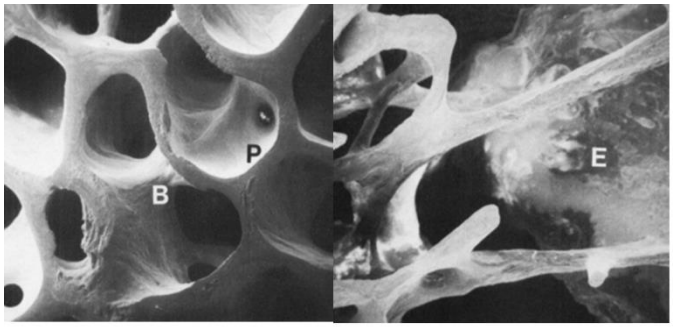

Figure 1.1 Cancellous bone in human iliac crest in normal bone (left) and osteoporotic bone (right). (Used with permission)

Due in part to low estrogen levels, postmenopausal women have the highest susceptibility to develop osteoporosis in their lifetimes, but men are also at risk as well. In **Figure 1.2**, changes in bone mass with age are depicted for both sexes (6). Throughout a person's life, bone is constantly being formed and resorbed in a delicate balance to either gain bone mass in a process called modeling (during growth) or maintain bone mass in a process called remodeling (after peak bone mass is achieved). During growth and maturation, bone is modeled into the respective shapes of each bone in the skeleton, and bone mass steadily increases. Two types of bone are modeled: cortical (compact) bone, found in the shafts of long bones and in flat bones like the skull, and cancellous bone (spongy or trabecular), found in the ends of long bones. Men on average reach a higher peak bone mass, and peak bone mass achieved during growth correlates with bone mass later in life (7). After peak bone mass is achieved around age 30, bone remodeling continues, and the skeleton still is being formed and resorbed. Cortical bone, for example, experiences 2-5% turnover per year in the elderly (8). When this balance is disrupted resulting in the rate of resorption exceeding the rate of formation, bone mass decreases. With age, both females and males show a gradual loss of bone mass, but women show a sharp decrease in bone mass right after menopause. However, men also experience a steeper

decline as they age.

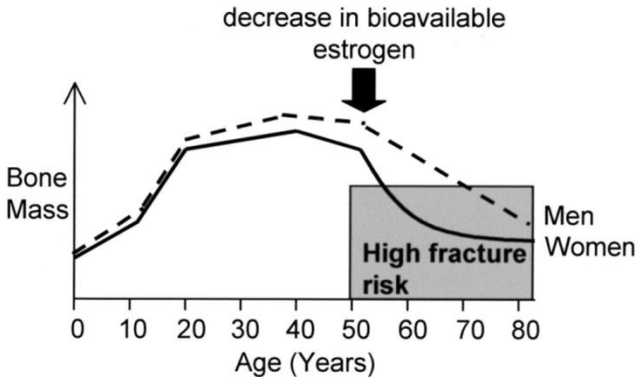

Figure 1.2 Men, on average, reach a higher bone peak bone mass than women. Women begin to rapidly lose bone mass at the onset of menopause. Men also experience a decline in bone mass with age. (Used with permission)

1.2 Estrogen and Bone

Estrogen is a key regulator of bone mass. After menopause, the ovaries stop producing estrogen, drastically decreasing circulating levels of the hormone and contributing to the rapid bone loss often seen in this demographic. However, estrogen is important in bone in both men and women throughout life by regulating both formation and resorption. Estrogen induces osteoblast differentiation and formation and prolongs osteoblast lifespan (9-11). In osteoclasts, estrogen regulates apoptosis (12). In general, men develop higher peak bone mass due to prolonged puberty and increased testosterone levels, which increase periosteal expansion (13, 14). During puberty and beyond, estrogen suppresses periosteal expansion and increases endosteal resorption, and ultimately it is required for growth plate fusion in humans (15).

Estrogen signaling is mediated by two separately coded estrogen receptors (ERs), ERα and ERβ, found in the cytoplasm of cells and members of the nuclear receptor gene superfamily (16). When estrogen binds to either ERα or ERβ, the receptor dimerizes with another ER, and each receptor phosphorylates (**Figure 1.3**). At this point, the ER complex can either directly bind to DNA estrogen response

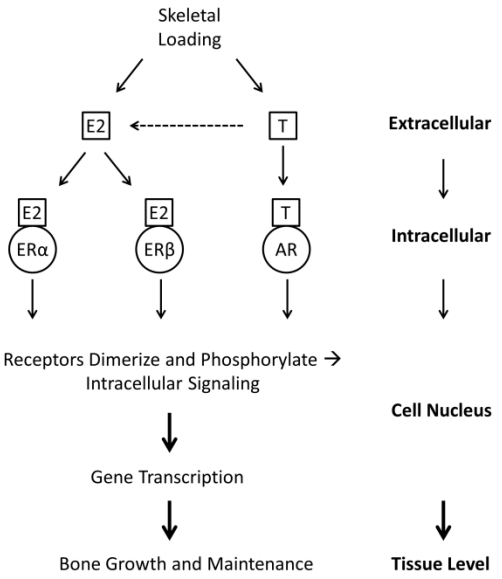

Figure 1.3 Classical sex hormone signaling.
Testosterone can be converted to estrogen by the enzyme aromatase. Estrogen binds to either ERα or ERβ, and the receptor dimerizes and phosphorylates. The complex can be involved in further intracellular signaling or direct gene transcription in the nucleus

elements found in the control regions of target genes, or it can be involved in other intracellular signaling pathways that will ultimately also regulate gene transcription (classical signaling) (7, 17). ERs are present in many cells of the body, including the ovaries, uterus, all bone cells, vasculature, lung, etc (18). In bone cells, ER expression is approximately one-tenth the expression found in reproductive organs (10, 19, 20), and the major signaling path of estrogen in bone is through ERα. ERα expression in bone is regulated by levels of estrogen, even though signaling can occur in estrogen-independent mechanisms (non-classical signaling) (21).

In 1994, clinical data showed unfused growth plates and osteoporosis in a male with an inactivating point mutation in the ERα gene, which has focused research in understanding and elucidating the mechanisms of ERα signaling (22, 23). Further human clinical data have correlated polymorphisms in ESR1, the gene that encodes ERα, with bone mineral density, fracture risk, and bone's response to exercise (24-30).

Because of estrogen's complex signaling environment, via classical and non-classical pathways, ERα is implicated downstream many signaling pathways important to bone, including wnt/β-catenin, insulin-like growth factor 1 (IGF-1), and bone morphogenetic protein (BMP) (31-33).

To model estrogen deficiency that occurs in post-menopausal women, ovariectomy (OVX) in rodents are the gold standard. When the ovaries are removed in rats at 5 months of age, 50% of proximal tibial cancellous bone volume is lost by 14 days post-surgery (34). Skeletally mature rats are preferred to growing rats because the bone loss that occurs more closely resembles the bone loss observed in post-menopausal women (34). Although OVX mice are also used, this model is not as standardized, and bone loss varies among mouse strains (35). OVX has limitations. First, it is major surgery and introduces extra stress on the animals. Second, OVX animals tend to gain a considerable amount of weight compared to their controls (36).

OVX removes the majority of circulating estrogen, which means that any estrogen signaling through ERα, ERβ, or other possible routes are all eliminated. To better focus on one aspect of estrogen signaling, knockout mice (KO) are a valuable tool. Because the mouse genome is fully sequenced and easily manipulated, a technique called cre/lox recombination can generate mice that lack a specific gene or part of a gene, usually corresponding to a protein or a section of a protein rendering it unusable (**Figure 1.4**). In this technique, two types of mice are used: a cre mouse that contains cre recombinase inserted into its genome, and a floxed mouse, that has the gene of interest flanked on either end by loxP sites. When the mice are mated, the cre recognizes the 35 base pair loxP sequences and removes the gene in between those two sites in the pups. The effect of removing genes on mouse development, appearance, behavior, etc., can indicate the role of a specific gene in a particular mechanism. Initially developed ERαKO and ERβKO mice did not completely remove

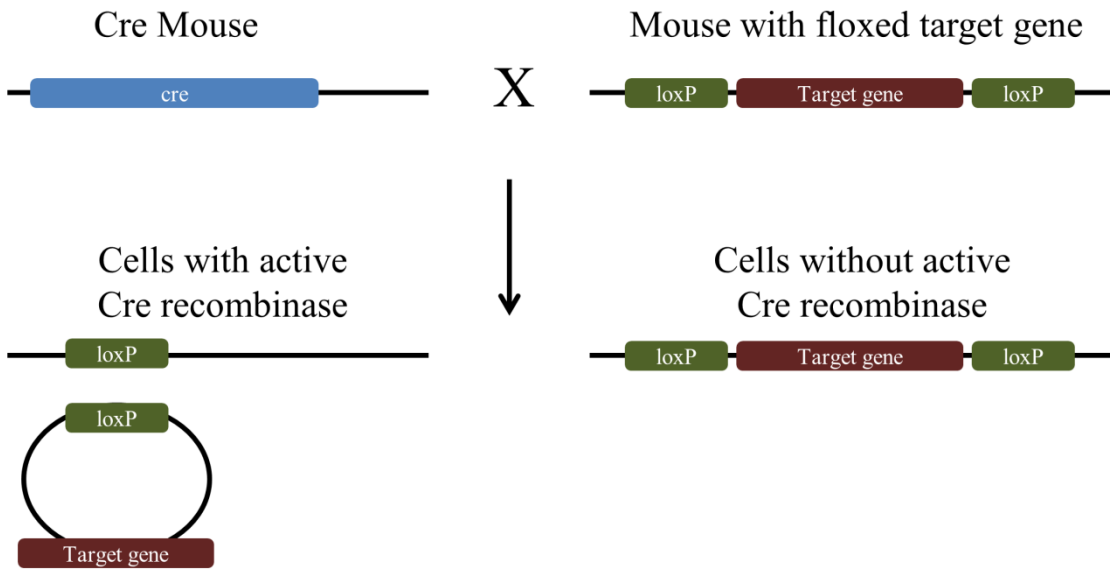

Figure 1.4 Cre-lox technology allows a specific gene, floxed by loxP sites, to be removed from all cells with active cre recombinase when a Cre mouse and a floxed mouse are bred.

all receptor protein production (37-39). In 2000 both complete knockouts were generated by removing sections of exon 3 of each gene, which encodes the first zinc finger of the DNA-binding domain of each receptor (40).

From bone analyses of these knockout animals, ERα was shown to be more important in skeletal development than ERβ. Female ERβKO mice had either increased (41, 42) or no change (43) in long bone lengths. In addition, bone mineral content (BMC) was increased at measurements taken along the whole body, cranium, spine, tibia, and vertebra (44). Cortical thickness at the femoral midshaft (41) and cancellous bone volume fraction in the tibia (43) were both increased, but others have indicated no change in these parameters, depending on the knockout animal source (44). In contrast, male ERβKO mice presented with few skeletal abnormalities. Whole body and site-specific BMC, femoral lengths, and femoral cortical thickness were all similar between knockouts and wildtype animals (43, 44).

Global deletion of ERα had profound effects on bone in both male and female mice. In the incomplete ERαKO female mice, long bone lengths were decreased while BMC and bone mineral density were both increased (41). Cancellous and cortical bone were differentially affected. Tibial cancellous bone volume fraction was increased, but cortical bone thickness at the tibial midshaft was increased. However, in the complete ERαKO, long bone lengths were unaffected. Tibial bone volume fraction was still increased, but bone mineral density in both tibial cortical and cancellous bone were decreased, as was tibial cortical thickness (43). In male mice, the knockout source was of less importance. Femoral lengths were shown to be both decreased (45, 46) and unchanged (43), but cortical and cancellous BMD and cortical thickness in the tibia were decreased (43, 45).

Although ERαKO and ERβKO mice indicate a crucial role of ERs in bone phenotype, confounding characteristics of these global knockout animals make it impossible to determine if bone effects are due solely to a lack of ER, or if caused by a secondary effect of ER's absence in other tissues. For example, IGF-1, an important regulator of bone length, was decreased in female ERαKO and increased in female ERβKO mice (41). Estrogen, a key regulator of bone mass as described earlier, was systemically increased over six-fold in ERαKO female mice (41, 43). Furthermore, ERαKO female mice had increased body weight, increased testosterone levels, and decreased osteocalcin levels (41). Male ERαKO and ERβKO mice also had increased testosterone levels (43). Male and female ERαKO and female ERβKO mice had either reduced or no fertility (40). Furthermore, because ERα is present other tissues, including cardiovascular, brain, adipose, liver, and heart, ERαKO mice become diabetic and develop vascular disease as they age at much greater rates than wildtype mice (46). All of these systemic factors interfere with any skeletal interpretations about ERαKO or ERβKO mice.

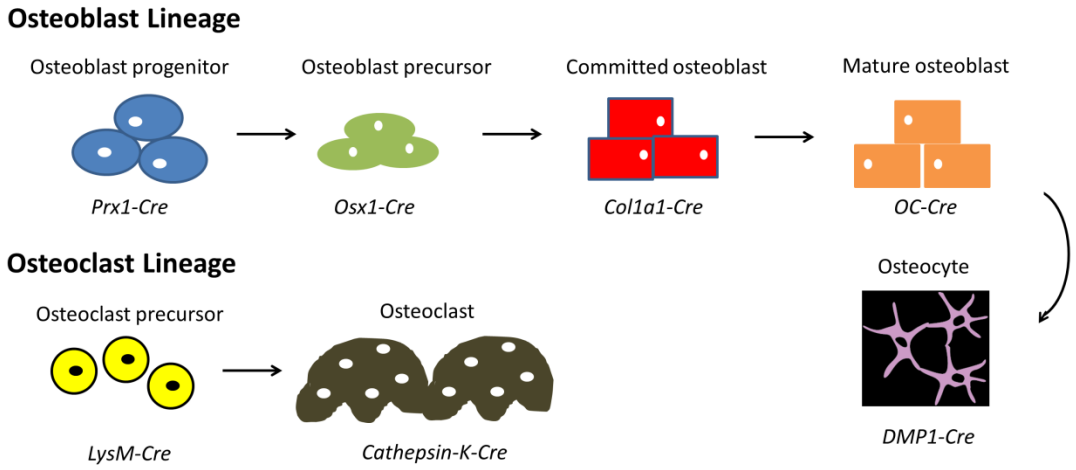

Figure 1.5 Promoter-driven *cre* mice allow a gene to be removed at a specific point in a cell lineage. For example, in the osteoblast lineage, *Prx1-Cre* mice can delete a gene in osteoblast precursor cells and all cells following in the lineage.

To combat the confounding effects in global knockout mice, bone-cell-specific knockouts using promoter-driven cres have provided additional information regarding ERs and bone. When a *cre* is activated by only one promoter, and the promoter is present in only one cell type, a receptor can be removed from a specific cell and all cells following in the lineage. Bone has a variety of promoter-driven cre mice available, which are outlined in **Figure 1.5**. In the past seven years, researchers have selectively removed ERα from osteoclast progenitors, osteoclasts, osteoblast progenitors, osteoblast precursors, committed osteoblasts, mature osteoblasts, and osteocytes (47-52), but the story relating ERα in bone cells to cortical and cancellous bone in males and females is complex and incomplete.

When ERα was conditionally removed from a bone cell type rather than the entire genome, systemic effects seen in the global knockout mice were eliminated. In general, body weight, serum hormone levels, and long bone lengths were similar between tissue-specific ERαKO and littermate controls (47, 50-52). In osteoclasts, ERα protects cancellous bone mass in females but has no effect on male mice (47). In osteoclast-specific ERαKO mice (pCathK-ERαKO), female mice exhibited decreased

BMD and BV/TV of the tibia and femur due to increased osteoclast surface normalized to bone surface (Oc.S/BS) and despite increased bone formation rate and increased MAR. Cortical bone was unaffected. However, when ERα was removed earlier in the osteoclast lineage using the Lysozyme M-cre mouse (LysM-Cre), cortical and cancellous bone mass were overall unaffected, but the number of osteoclasts was increased (48). Bone mass in male pCathK-ERαKO was similar to controls (47).

Table 1.1 Osteoblast-lineage specific *cre* mice have been used to generate cell-specific ERαKO mice. The bone phenotype exhibited by each knockout is displayed below. However, the results are complex regarding bone mass in males and females and in cortical and cancellous bone.

Promoter	Female ERαKO	Male ERαKO
Prx1 (osteoblast progenitors)	No effect on cancellous bone, decreased cortical bone mass	No effect on cancellous bone, decreased cortical bone mass in young mice
Osx1 (osteblast prescursors)	No effect on cancellous bone, decreased cortical bone mass	No effect on cancellous bone, decreased cortical bone mass in young mice
Col1a1 (committed osteoblasts)	No effect on bone mass	No effect on bone mass
OC (mature osteoblasts)	Decreased cortical and cancellous bone	No effect on bone mass but decreased cn BVTV at 6 mo, Increased cn, ct bone mass
DMP-1 (osteocytes)	No effect on bone mass, decreased cancellous bone mass	No effect on cancellous bone, decreased cancellous bone mass

In mice lacking ERα in osteoblast lineage cells, the story is even more complex (**Table 1.1)**. When ERα was removed at the osteoblast progenitor (pPrx1-ERαKO) or osteoblast precursor (pOsx1-ERαKO) stage, cortical bone was decreased in both males and females but cancellous bone was largely unaffected (53). Femoral midshaft cortical thickness, cancellous BV/TV, and periosteal bone formation rate were all decreased in both targeted knockouts, attributed to attenuated osteoblastogenesis detected from cell culture assays. When the same researchers removed ERα from committed osteoblasts (pCol1a1-ERαKO) or osteocytes (pDMP1-ERαKO), cortical and cancellous bone mass were both unchanged between knockouts and controls in both males and females (53). However, others have found conflicting results. In pOC-ERαKO mice, where ERα is removed from mature osteoblasts, female cortical and cancellous bone mass were both reduced in the tibia, due to effects on both osteoblast number and osteoclast number to a greater degree (51). In male pOC-ERαKO mice, bone phenotype was unaffected except at 6 months, where tibial BV/TV was decreased. Furthermore, in opposition to the previous pDMP1-ERαKO mice, others have found that trabecular BV/TV and BFR were decreased while N.Oc/BS remained unchanged (52, 54). Cortical bone in female mice and cortical and cancellous bone in male mice were not affected by ERα absence in osteocytes. Elucidating the role of ERα in osteoblasts, osteocytes, and osteoclasts is incomplete and needs further research to resolve some of these discrepancies.

1.3 Mechanical Loading and Bone

Bone responds to its mechanical environment. In situations of increased loading, bone mass increases. Tennis players show increased cortical thickness in their dominant playing arms compared to the contralateral limb (55). Also, dynamic

jumping exercises have been shown to increase BMC at multiple bone sites in children over a 7-month program (56). At the other end of the spectrum, bone loss can occur in situations of bone disuse, such as with astronauts during space flight or during immobilization (57, 58).

Because of their ability to increase bone mass, controlled loading models in rodent long bones are a promising measure to overcome bone loss and have been widely developed as a means of studying how bone responds to loading. Across many vertebrate animals, bone strains induced by normal physiological activity are similar, despite difference in bone size and loads applied during activity (59). Before beginning any loading experiment, measuring bone stiffness at the cortical midshaft by applying a range of loads is common practice to determine the appropriate peak magnitude of load for a given experimental design.

Two main categories of loading models exist: bending and compression. In four-point bending models of the rat and mouse tibia, up to 100 cycles of loading for 5-12 days were administered to engender 850-3500 microstrain (strain*10^{-6}, με) at the tibial midshaft (60, 61). These models do induce new bone formation, but much of the bone formation is woven bone, which is not as highly organized or as dense as lamellar bone and is more a response to injury than to normal physiologic loading (60, 62).

Because they are more physiologically relevant and produce lamellar bone, axial compression rodent models have replaced the bending controlled loading models (62-66). In rats, loading the ulna at 20N to induce 3500-4500 με at the midshaft produced a clear lamellar cortical bone response after 9 days (62). Frequency variation from 10-20Hz and cycle variation from 1200-12,000 cycles per day had no effect on the amount of bone formation (62). Similar ulnar loading was developed in mice as well, with smaller loads (3-4.3N) 5 days per week for 2 weeks to result in

2000-3000 με at the midshaft (63). In mice, 2000 με corresponded to lamellar formation at the periosteal surface but no formation on the endocortical surface, while 3000 με induced woven bone at the periosteal surface and lamellar bone on the endocortical surface.

Mouse tibial loading models have emerged as valuable tools for studying bone adaption to loading without creating woven bone (64, 65). Its advantages include the possibility of using genetically modified mice (unlike the rat), the ability to study both cortical and cancellous bone (unlike the ulna), and the ability to induce lamellar instead of woven bone formation in a more physiologically relevant axial loading direction. Two main tibial compression protocols, with some variations, are present in the literature. The first model applies strain-, age-, and sex-dependent peak loads that correspond to 1200 με at the midshaft are applied for 1200 cycles each day, at a rate of 4Hz and a dwell of 100ms between each loading cycles (64) (**Figure 1.6**). When applied for 2 weeks, this loading protocol increased bone mass similarly in 10-week-old males and females, with greater increases in the cancellous metaphysis than at the tibial midshaft (67, 68). Older female mice still respond to loading, but a higher load level is required, corresponding to 2100 με. Furthermore, it has been used to rescue bone loss in male mice after orchidectomy (69). The second tibial compression model loads for fewer cycles, fewer days per week, with longer rests between each load cycle (65). Although this loading protocol increased bone mass in 8-week-old animals, trabecular bone mass was lost with loading in 12-week, 20-week, and 26-week-old mice (65, 70). The first loading protocol is more consistently osteogenic than the latter, showing a 65% vs. only 44% increase, respectively, in tibial BV/TV after 6 weeks of loading (71). For a more detailed loading and strain gauging protocol, see **Appendix A.**

In designing and interpreting in vivo loading studies, a variety of factors need

consideration. Ulnar loading measures purely cortical bone response, while tibial loading allows analysis of both cortical and cancellous bone, but a range of loading protocols with varying waveforms, rests between cycles, and number of cycles per day. Growing mice may response differently than those who have reached skeletal maturity, at around 16 weeks of age (72). Strain of mice also plays a role, as some strains are more mechanoresponsive than others (73). In addition, cortical and cancellous bone phenotype varies by mouse strain, which can impact bone response.

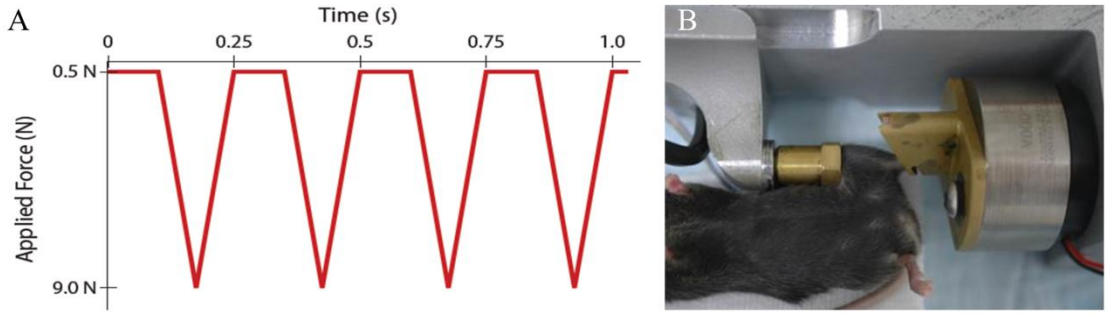

Figure 1.6 A) *In vivo* tibial waveform commonly used to stimulate bone growth in the cancellous metaphysis and the cortical midshaft. B) Mouse situated in custom loading device prepared for *in vivo* tibial loading to begin.

1.4 Mechanotransduction: Estrogen and BMPs

Mechanotransduction is the process by which bone converts mechanical stimuli into chemical, cellular, and tissue-level responses. Controlled mechanical loading initially was used to study the tissue-level responses by looking at changes in bone mass, architecture, and shape with loading. The cellular signaling pathways involved in generating this anabolic response are of particular interest, and cover a wide range of signaling pathways, including wnt/β-catenin, parathyroid hormone (PTH), insulin-like growth factor (IGF-1), hormones including estrogen and testosterone, and bone morphogenetic proteins (BMPs) (31). Many of these pathways are interconnected either directly or indirectly. ERα in particular is proposed to be

involved with many of the above networks. However, much of the signaling research on bone mechanotransduction has been through in vitro studies using cultured osteoblasts stimulated by fluid shear flow over the cells or bending the apparatus on which the cells are seeded. In vivo studies to determine the role of ERα and its interaction with other pathways, such as with BMPs, are needed.

Estrogen and its receptors influence bone mechanoadaptation. In humans, females responded more to exercise pre-puberty than post-puberty after estrogen levels rise (74). Analogously, low dose estrogen administered during rat unlar loading suppressed periosteal bone formation but enhanced endosteal bone growth (75). Furthermore, osteoblast-like cells derived from rats and subjected to four-point bending proliferate in response to strain, estrogen, and even more when the two are combined (76). ERα over ERβ was shown to be highly important in how bone responds to mechanical strain. Expression of ERα is reduced in osteocytes following rat ulnar loading in both sexes, but is increased in osteoblast-like cells after strain in osteoblast-like human cells (77, 78). Osteoblast-like cells from ERαKO mice do not proliferate in response to strain as cells from wildtype mice do (79, 80). Furthermore, in human osteoblast-like cells, proliferative response to strain is abrogated when an ER modulator is administered to block all ERα signaling (81).

To further study ERα's role in bone mechanotransduction, controlled loading models have been applied to both global and cell-specific ERαKO mice. Similar to the in vitro cell cultures from ERαKO mice, female ERαKO mice responded less to in vivo ulnar loading, showing a 70% less increase in Ct.Ar after 2 weeks (6, 80). However, the cancellous bone response to mechanical loading was similar compared to controls (82). In males, global ERα deletion induced a greater response to tibial mechanical loading in both cancellous and cortical bone (82). From sciatic neurectomy, a limb disuse animal model, ERαKO male and female mice lost less

cancellous bone, but similar cortical bone, compared to controls. Importantly, these global ERαKO models exhibit systemic effects, such as increased body weight, as mentioned previously, and so the effects of ERα in each bone cell type cannot be determined. The need for in vivo loading studies in bone cell-specific ERαKO mice is clear, but has not been fully explored, especially in cancellous bone (**Table 1.2**). Female mice deficient in ERα at the osteoblast progenitor or precursor stage showed decreased osteogenic response to loading in cortical bone, but cancellous bone was not studied (83). In mice with ERα removed at the committed osteoblast or osteocyte stage, the cortical response to tibial loading was similar between female knockout and controls, in opposition to the global ERαKO models (54). Again, the response in cancellous bone was not studied. From hindlimb suspension, a limb disuse animal model, female pDmp1-ERαKO mice lost more cancellous bone than controls (52).

Table 1.2 The responses to mechanical loading in cancellous and cortical bone have not been fully explored in mice with ERα removed at particular points along the osteoblast lineage using promoter-drive *cres.*

Promoter	Female ERαKO	Male ERαKO
Prx1 (osteoblast progenitors)	Reduced cortical response	Unknown
Osx1 (osteblast prescursors)	Reduced cortical response	Unknown
Col1a1 (committed osteoblasts)	Normal cortical response	Unknown
OC (mature osteoblasts)	Increased cancellous and cortical response (current work)	Normal response (current work)
DMP-1 (osteocytes)	Normal cortical response	Unknown

BMPs are members of the TGF-β super family of growth factors. Synthesized by skeletal and non-skeletal tissues throughout development, BMPs regulate many cell and tissue processes. BMPs were first identified by their ability to induce ectopic bone formation, but over 20 BMPs are currently identified (84, 85). The BMP cell signaling pathway is complex (**Figure 1.7**). In canonical signaling, BMPs activate type II receptors, which include BMPR1A (Alk-3), AMPR1B (Alk-6), and Act-1a (Alk-2). An activated type II receptor then activates a type I receptor, which phosphorylates and induces phosphorylation of Smad1,5,8. pSmad1,5,8 forms a complex with Smad4, and the entire complex can directly regulate gene transcription in the nucleus (86). Because there are 3 kinds of type I receptors and 3 kind of type II receptors, many signaling combinations are possible and result in varying gene expression or repression. Useful for studying BMP signaling are BMP antagonists, including gremlin, noggin, and follistatin.

In bone, BMPs 2, 4, and 6 are highly expressed (87). BMPs can induce osteoblast differentiation and regulate osteoblastogenesis and osteoclastogeneis (88, 89). BMP2 enhances fracture healing in mice by inducing endochondral ossification and enhance chondrogenesis, BMP2 enhances fracture healing in mice (89-91). Currently, BMPs are FDA-approved for bone regeneration applications such as after fractures and osteotomies.

BMPs have been implicated in bone's response to mechanical loading. In vitro, BMPs were upregulated in osteoblasts to fluid shear (32), and when noggin, an inhibitor, was given, osteoblasts did not proliferate in response to fluid shear. In vivo, BMPs were upregulated in mice after one day of tibial loading (92, 93).

Interactions between estrogen and BMP signaling have been shown in vitro in both competitive and cooperative mechanisms. In fact, BMP Smads and ERα may

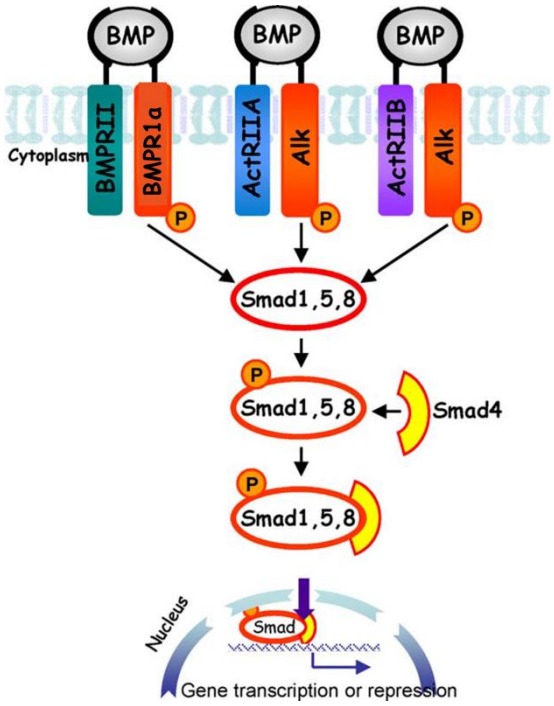

Figure 1.7 Canonical BMP signaling involves type I and type II receptors. When BMP binds to a type II receptor, a type I receptor is activated and phosphorylated. Then, Smad 1,5,8 is phosphorylated and binds to Smad4. This complex can mediate gene transcription in the nucleus. (Used with permission)

directly interact (94). After BMP-2 treatment in myoblasts, ER expression was increased (95). BMP-2 also was shown to induce phosphorylation of Smad 1,5,8, downstream in BMP signaling, and this activity was enhanced with estrogen treatment. In contrast, Smad4 has been shown to inhibit transcription of genes involved in estrogen signaling (96). Antiestrogens suppressed BMP-4 expression in an ERα-dependent manner (97).

Attention has focused on BMPR1a, a type II receptor involved in bone BMP signaling. Although the global BMPR1a KO is embryonically lethal, other animal models have implicated its importance in bone (98). Using the Og2-Cre (osteocalcin 2) mouse, BMPR1a was removed from post-natal osteoblasts (99). Growing mice were smaller than wildtype littermates, but as the mice aged, the knockout mice had

increased bone mass due to decreased bone resorption rates. Similarly, BMPR1a was deleted from osteoblasts through tamoxifen induction, which allows targeted deletion in growing or adult animals for a specified range of time (100). These mice exhibited increased bone mineral density and cancellous bone mass and showed a decrease in both bone formation and, to a greater extend, bone resorption. When BMPR1a was deleted in osteoclasts, bone volume and trabecular thickness were both increased, which correlated with increased bone formation rate (101).

To further study BMPR1a in bone, a soluble BMPR1a was developed that binds to BMP2 and BMP4 with high affinity (102). The drug, RAP-661, prevents canonical BMP signaling through BMPR1a. When administered to wildtype 12-week-old mice, bone mineral density and cancellous bone volume fraction increased in a dose-dependent manner after 2, 4, and 6 weeks. Femoral bending strength was also increased in RAP-661-treated animals, indicating a possible cortical effect as well. Histomorphometry analysis indicated that the drug induces an early increase in osteoblast number followed later by a decrease in osteoclast number. Therefore, soluble BMPR1a may impact both bone formation and bone resorption as a means of increasing bone mass. Possible interactions with ERα and mechanical loading have yet to be determined.

1.5 Aims

Osteoporotic fractures are ultimately the failure of bone to perform its main function, bearing loads. Understanding the cellular and molecular mechanisms that bring about changes in bone in response is critical for prevention and treatment of osteoporosis. Estrogen levels are severely reduced in post-menopausal women, but the hormone is important in both sexes during bone modeling and remodeling. ERα in particular has been implicated in bone's response to mechanical loading. Although

many bone cell-specific ERαKO mice exist, ERα's role in each cell type is incompletely understood. This thesis aims to better understand ERα signaling in osteoblasts by generating pOC-ERαKO mice to examine bone phenotype (Aim 1), studying their response to skeletal mechanical loading (Aim 2), and determining the interactions among ERα, BMP signaling, and mechanical loading (Aim 3).

Aim 1

Because global ERαKO mice have confounding systemic effects, the direct role of ERα in bone is unknown. Because estrogen regulates osteoblasts and osteoclasts, we hypothesized that without ERα in osteoblasts, bone mass would be decreased. We bred female mice with osteoblast-specific ERα deletion (pOC-ERαKO) by crossing *OC-Cre* and $ER\alpha^{fl/fl}$ mice and examined both growing (12 weeks old) and skeletally mature animals (18 weeks old). By measuring body mass, ovary and uterine mass, crown/rump length, and serum levels of estrogen, testosterone, IGF-1, and OC, we ascertained that systemic effects were eliminated in this bone cell-specific ERαKO model. To characterize the effect of genotype on bone mass and architecture in both cortical and cancellous bone, microCT was performed at multiple bone sites: the cortico-cancellous proximal tibia, cortical tibial midshaft, cortico-cancellous L5 vertebra, and the cortico-cancellous distal femur. In addition, both the L5 vertebra and femora were subjected to mechanical testing to failure to determine whole bone stiffness and strength. Changes in osteoblast and osteoclast bone cell activity were measured from immunohistochemistry analysis of the cancellous proximal tibia. Bone formation rate and mineralizing surface were determined from dynamic histomorphometry measurements made at the cancellous proximal tibia.

Aim 2

Both cortical and cancellous bone mass were reduced in female pOC-ERαKO mice (Aim 1), and osteoblast proliferation was reduced in osteoblast-like cells lacking ERα (79). Therefore, we hypothesized that male pOC-ERαKO mice would also show reduced bone mass, and that both sexes of pOC-ERαKO mice would respond less to mechanical loading. To this end, we bred male and female pOC-ERαKO mice backcrossed to a C57Bl/6 background. At ten weeks of age, we measured bone stiffness at the tibial midshaft from in vivo strain gauging to determine parameters for in vivo tibial mechanical loading. Left tibiae from male and female pOC-ERαKO and littermate control (LC) mice were loaded in vivo for two weeks, with the right limb as an internal control. As in Aim 1, we tested for systemic effects in these now backcrossed animals. We measured basal bone phenotype resulting from the osteoblast-specific ERα deletion through microCT of the cortico-cancellous vertebral body and cortical femoral midshaft. Bone strength and stiffness were assessed from femoral and vertebral whole bone mechanical testing. To analyze the response to loading in knockouts vs. LC, microCT was performed at the tibial cortical midshaft and cortico-cancellous tibial metaphysis. Furthermore, osteoblast and osteoclast bone cell activity were measured from immunohistochemistry, and again bone formation rate and mineralizing surface were assessed at both the tibial midshaft and metaphysis.

Aim 3

Elucidating the signaling mechanisms of estrogen and ERα is complex. ERα has been shown to interact with BMP signaling. By inhibiting BMP signaling using RAP-661, a soluble receptor that binds to and prevents signaling through the BMPR1a receptor, bone mass in female mice is increased in a dose- and time-dependent manner. We hypothesized that RAP-661 would rescue bone loss in female pOC-ERαKO mice, and that bone mass could be further increased through mechanical

loading. Also, we hypothesized that in LC animals, both mechanical loading and drug administration would cooperatively increase bone mass. We bred female pOC-ERαKO and LC mice and subjected all animals to 2 weeks of in vivo left tibial mechanical loading. Half of the mice from each genotype were given an IP injection of RAP-661, while the other half were administered a placebo. After euthanasia, basal bone phenotype in drug-treated and placebo-treated mice of both genotypes was assessed from microCT analysis of the L5 vertebra and femoral midshaft. Bone strength and stiffness were determined from whole bone mechanical tests. To determine the combinations of interactions of ERα, RAP-661, and mechanical loading, cancellous and cortical bone mass and architecture were assessed from microCT of the tibial midshaft and metaphysis. Osteoblasts and osteoclast activity were also measured in the cancellous proximal tibia from IHC.

1.6 My contributions

Aim 1 was published in The Journal of Bone and Mineral Research:

> Melville KM, Kelly NH, Khan SA, Schimenti JC, Ross FP, Main RP, van der Meulen MCH. Osteoblast-specific Estrogen Receptor Alpha Knockout Mice Have Compromised Bone Mass and Strength. JBMR 2014. 29(2):370-9.

Previously, I presented part of this Aim at the American Society for Bone and Mineral Research Meeting 2012 as a podium presentation:

> Melville KM, Bruhn TM, Khan SA, Schimenti JC, Ross FP, Main RP, van der Meulen MCH. Osteoblast-specific Estrogen Receptor Alpha Knockout Mice have Compromised Bone Mass and Architecture. American Society for Bone and Mineral Research Annual Meeting 2012. Minneapolis, MN.

The authors' roles for this Aim were: Study design: MCHM, KMM, RPM, FPR, NHK, JSC, SAK. Study conduct: KMM, NHK. Data collection: KMM, NHK. Data analysis: KMM. Data interpretation: KMM, MCHM, FPR. Drafting manuscript: KMM. Revising manuscript content: KMM, MCHM, FPR, NHK, RPM. Approving final version of manuscript: all authors. KMM takes responsibility for the integrity of the data analysis.

Aim 2 is under review for submission to The Journal of Bone and Mineral Research:

> Melville KM, Kelly NH, Surita G, Buchalter DB, Schimenti JC, Main RP, Ross FP, van der Meulen MCH. Estrogen receptor alpha in osteoblast lineage cells regulates bone mass differentially in both sexes and attenuates bone's response to mechanical loading in female mice. JBMR. Under Review.

Previously, I presented part of this Aim at the Proceedings of the 60th Annual Meeting of the Orthopaedic Research Society as a podium presentation:

> Melville, KM, Kelly NH, Surita G, Schimenti JC, Ross FP, Main RP, van der Meulen MCH. ERα in osteoblasts is required for cancellous bone mass but attenuates bone's anabolic response to mechanical loading. Proceedings of the 60th annual meeting of the Orthopaedic Research Society. New Orleans, LA.

The authors' roles for this Aim were: Study design: KMM, FPR, MCHM. Study conduct: KMM, NHK, DBB. Data collection: KMM, NHK, GS, DBB. Data analysis: KMM. Data interpretation: KMM, MCHM, FPR. Drafting manuscript: KMM. Revising manuscript content: KMM, MCHM, FPR, RPM. Approving final version of manuscript: all authors. KMM takes responsibility for the integrity of the data analysis.

Aim 3 is in preparation for submission to The Journal of Bone and Mineral Research:

Melville KM, Kelly NH, Schimenti JC, Ross FP, Pearsall S, van der Meulen MCH. Inhibiting BMP 2/4 signaling increases cancellous bone mass and reduces bone's response to mechanical loading in female mice.

The authors' roles for this Aim were: Study design: KMM, FPR, SP, MCHM. Study conduct: KMM, NHK. Data collection: KMM, NHK. Data anlysis: KMM. Data interpretation: KMM, FPR, MCHM. Drafting manuscript: KMM. Revising manuscript content: KMM, MCHM, FPR. Approving final version of manuscript: all authors. KMM takes responsibility for the integrity of the data analysis.

Appendix A is in press:

Melville KM, Robling AG, van der Meulen MCH (2014) Axial tibial loading of bone. AJ van Wijnen, JJ Westendorf, eds. Osteoporosis and Osteoarthritis, in Methods in Molecular Biology Series, in press.

1.7 References

1. Bone Health and Osteoporosis: A Report of the Surgeon General. Rockville, MD: U.S. Department of Health and Human Services, Office of the Surgeon General; 2004.
2. International Osteoporosis Foundation: Facts and Statistics 2014 [cited 2014]. Available from: http://www.iofbonehealth.org/facts-statistics.
3. Burge R, Dawson-Hughes B, Solomon DH, Wong JB, King A, Tosteson A. Incidence and economic burden of osteoporosis-related fractures in the United States, 2005-2025. J Bone Miner Res. 2007;22(3):465-75.
4. Briggs AM, Greig AM, Wark JD. The vertebral fracture cascade in osteoporosis: a review of aetiopathogenesis. Osteoporos Int. 2007;18(5):575-84.
5. Dempster DW, Shane E, Horbert W, Lindsay R. A simple method for correlative light and scanning electron microscopy of human iliac crest bone biopsies:

qualitative observations in normal and osteoporotic subjects. J Bone Miner Res. 1986;1(1):15-21.
6. Lee KC, Lanyon LE. Mechanical loading influences bone mass through estrogen receptor alpha. Exerc Sport Sci Rev. 2004;32(2):64-8.
7. Khosla S. Pathogenesis of Age-Related Bone Loss in Humans. J Gerontol A Biol Sci Med Sci. 2012.
8. Kaplan FS, Hayes WC, Keaveny TM, Boskey A, Einhorn TA, Iannotti JP. In: Einhorn TA, O'Keefe RJ, Buckwalter JA, editors. Orthopaedic Basic Science. 3rd ed. Rosemont, IL: American Academy of Orthopaedic Surgeons; 2007.
9. Chow J, Tobias JH, Colston KW, Chambers TJ. Estrogen maintains trabecular bone volume in rats not only by suppression of bone resorption but also by stimulation of bone formation. J Clin Invest. 1992;89(1):74-8.
10. Manolagas SC, Kousteni S, Jilka RL. Sex steroids and bone. Recent Prog Horm Res. 2002;57:385-409.
11. Gohel A, McCarthy MB, Gronowicz G. Estrogen prevents glucocorticoid-induced apoptosis in osteoblasts in vivo and in vitro. Endocrinology. 1999;140(11):5339-47.
12. Riggs BL, Khosla S, Melton LJ, 3rd. A unitary model for involutional osteoporosis: estrogen deficiency causes both type I and type II osteoporosis in postmenopausal women and contributes to bone loss in aging men. J Bone Miner Res. 1998;13(5):763-73.
13. Turner RT, Colvard DS, Spelsberg TC. Estrogen inhibition of periosteal bone formation in rat long bones: down-regulation of gene expression for bone matrix proteins. Endocrinology. 1990;127(3):1346-51.
14. Callewaert F, Sinnesael M, Gielen E, Boonen S, Vanderschueren D. Skeletal sexual dimorphism: relative contribution of sex steroids, GH-IGF1, and mechanical loading. J Endocrinol. 2010;207(2):127-34.
15. Riggs BL, Khosla S, Melton LJ, 3rd. Sex steroids and the construction and conservation of the adult skeleton. Endocr Rev. 2002;23(3):279-302.
16. Mangelsdorf DJ, Thummel C, Beato M, Herrlich P, Schutz G, Umesono K, Blumberg B, Kastner P, Mark M, Chambon P, Evans RM. The nuclear receptor superfamily: the second decade. Cell. 1995;83(6):835-9.
17. Shang Y, Brown M. Molecular determinants for the tissue specificity of SERMs. Science. 2002;295(5564):2465-8.
18. Manolagas SC, Bellido T, Jilka RL. Sex steroids, cytokines and the bone marrow: new concepts on the pathogenesis of osteoporosis. Ciba Found Symp. 1995;191:187-96; discussion 97-202.
19. Eriksen EF, Colvard DS, Berg NJ, Graham ML, Mann KG, Spelsberg TC, Riggs BL. Evidence of estrogen receptors in normal human osteoblast-like cells. Science. 1988;241(4861):84-6.
20. Lim SK, Won YJ, Lee HC, Huh KB, Park YS. A PCR analysis of ERalpha and ERbeta mRNA abundance in rats and the effect of ovariectomy. J Bone Miner Res. 1999;14(7):1189-96.
21. Zaman G, Jessop HL, Muzylak M, De Souza RL, Pitsillides AA, Price JS, Lanyon LL. Osteocytes use estrogen receptor alpha to respond to strain but their

ERalpha content is regulated by estrogen. J Bone Miner Res. 2006;21(8):1297-306.
22. Smith EP, Boyd J, Frank GR, Takahashi H, Cohen RM, Specker B, Williams TC, Lubahn DB, Korach KS. Estrogen resistance caused by a mutation in the estrogen-receptor gene in a man. N Engl J Med. 1994;331(16):1056-61.
23. Smith EP, Specker B, Bachrach BE, Kimbro KS, Li XJ, Young MF, Fedarko NS, Abuzzahab MJ, Frank GR, Cohen RM, Lubahn DB, Korach KS. Impact on bone of an estrogen receptor-alpha gene loss of function mutation. J Clin Endocrinol Metab. 2008;93(8):3088-96.
24. Braidman I, Baris C, Wood L, Selby P, Adams J, Freemont A, Hoyland J. Preliminary evidence for impaired estrogen receptor-alpha protein expression in osteoblasts and osteocytes from men with idiopathic osteoporosis. Bone. 2000;26(5):423-7.
25. Braidman IP, Baris C, Selby PL, Adams JE, Freemont AJ, Hoyland JA. Preliminary report of impaired oestrogen receptor-alpha expression in bone, but no involvement of androgen receptor, in male idiopathic osteoporosis. J Pathol. 2000;192(1):90-6.
26. Sonoda T, Takada J, Iba K, Asakura S, Yamashita T, Mori M. Interaction between ESRalpha polymorphisms and environmental factors in osteoporosis. J Orthop Res. 2012;30(10):1529-34.
27. Remes T, Vaisanen SB, Mahonen A, Huuskonen J, Kroger H, Jurvelin JS, Penttila IM, Rauramaa R. Aerobic exercise and bone mineral density in middle-aged finnish men: a controlled randomized trial with reference to androgen receptor, aromatase, and estrogen receptor alpha gene polymorphisms. Bone. 2003;32(4):412-20.
28. Suuriniemi M, Mahonen A, Kovanen V, Alen M, Lyytikainen A, Wang Q, Kroger H, Cheng S. Association between exercise and pubertal BMD is modulated by estrogen receptor alpha genotype. J Bone Miner Res. 2004;19(11):1758-65.
29. Suuriniemi M, Suominen H, Mahonen A, Alen M, Cheng S. Estrogen receptor alpha polymorphism modifies the association between childhood exercise and bone mass: follow-up study. Pediatr Exerc Sci. 2007;19(4):444-58.
30. Gennari L, Merlotti D, De Paola V, Calabro A, Becherini L, Martini G, Nuti R. Estrogen receptor gene polymorphisms and the genetics of osteoporosis: a HuGE review. Am J Epidemiol. 2005;161(4):307-20.
31. Price JS, Sugiyama T, Galea GL, Meakin LB, Sunters A, Lanyon LE. Role of endocrine and paracrine factors in the adaptation of bone to mechanical loading. Curr Osteoporos Rep. 2011;9(2):76-82.
32. Lau KH, Kapur S, Kesavan C, Baylink DJ. Up-regulation of the Wnt, estrogen receptor, insulin-like growth factor-I, and bone morphogenetic protein pathways in C57BL/6J osteoblasts as opposed to C3H/HeJ osteoblasts in part contributes to the differential anabolic response to fluid shear. J Biol Chem. 2006;281(14):9576-88.
33. Sunters A, Armstrong VJ, Zaman G, Kypta RM, Kawano Y, Lanyon LE, Price JS. Mechano-transduction in osteoblastic cells involves strain-regulated estrogen receptor alpha-mediated control of insulin-like growth factor (IGF) I receptor sensitivity to Ambient IGF, leading to phosphatidylinositol 3-kinase/AKT-dependent Wnt/LRP5 receptor-independent activation of beta-catenin signaling. J Biol Chem.

2010;285(12):8743-58.
34. Thompson DD, Simmons HA, Pirie CM, Ke HZ. FDA Guidelines and animal models for osteoporosis. Bone. 1995;17(4 Suppl):125S-33S.
35. Bouxsein ML, Myers KS, Shultz KL, Donahue LR, Rosen CJ, Beamer WG. Ovariectomy-induced bone loss varies among inbred strains of mice. J Bone Miner Res. 2005;20(7):1085-92.
36. Jee WS, Yao W. Overview: animal models of osteopenia and osteoporosis. J Musculoskelet Neuronal Interact. 2001;1(3):193-207.
37. Lubahn DB, Moyer JS, Golding TS, Couse JF, Korach KS, Smithies O. Alteration of reproductive function but not prenatal sexual development after insertional disruption of the mouse estrogen receptor gene. Proc Natl Acad Sci U S A. 1993;90(23):11162-6.
38. Krege JH, Hodgin JB, Couse JF, Enmark E, Warner M, Mahler JF, Sar M, Korach KS, Gustafsson JA, Smithies O. Generation and reproductive phenotypes of mice lacking estrogen receptor beta. Proc Natl Acad Sci U S A. 1998;95(26):15677-82.
39. Couse JF, Curtis SW, Washburn TF, Lindzey J, Golding TS, Lubahn DB, Smithies O, Korach KS. Analysis of transcription and estrogen insensitivity in the female mouse after targeted disruption of the estrogen receptor gene. Mol Endocrinol. 1995;9(11):1441-54.
40. Dupont S, Krust A, Gansmuller A, Dierich A, Chambon P, Mark M. Effect of single and compound knockouts of estrogen receptors alpha (ERalpha) and beta (ERbeta) on mouse reproductive phenotypes. Development. 2000;127(19):4277-91.
41. Lindberg MK, Alatalo SL, Halleen JM, Mohan S, Gustafsson JA, Ohlsson C. Estrogen receptor specificity in the regulation of the skeleton in female mice. J Endocrinol. 2001;171(2):229-36.
42. Windahl SH, Hollberg K, Vidal O, Gustafsson JA, Ohlsson C, Andersson G. Female estrogen receptor beta-/- mice are partially protected against age-related trabecular bone loss. J Bone Miner Res. 2001;16(8):1388-98.
43. Sims NA, Dupont S, Krust A, Clement-Lacroix P, Minet D, Resche-Rigon M, Gaillard-Kelly M, Baron R. Deletion of estrogen receptors reveals a regulatory role for estrogen receptors-beta in bone remodeling in females but not in males. Bone. 2002;30(1):18-25.
44. Windahl SH, Vidal O, Andersson G, Gustafsson JA, Ohlsson C. Increased cortical bone mineral content but unchanged trabecular bone mineral density in female ERbeta(-/-) mice. J Clin Invest. 1999;104(7):895-901.
45. Vidal O, Lindberg MK, Hollberg K, Baylink DJ, Andersson G, Lubahn DB, Mohan S, Gustafsson JA, Ohlsson C. Estrogen receptor specificity in the regulation of skeletal growth and maturation in male mice. Proc Natl Acad Sci U S A. 2000;97(10):5474-9.
46. Lee HR, Kim TH, Choi KC. Functions and physiological roles of two types of estrogen receptors, ERalpha and ERbeta, identified by estrogen receptor knockout mouse. Lab Anim Res. 2012;28(2):71-6.
47. Nakamura T, Imai Y, Matsumoto T, Sato S, Takeuchi K, Igarashi K, Harada Y, Azuma Y, Krust A, Yamamoto Y, Nishina H, Takeda S, Takayanagi H, Metzger D,

Kanno J, Takaoka K, Martin TJ, Chambon P, Kato S. Estrogen prevents bone loss via estrogen receptor alpha and induction of Fas ligand in osteoclasts. Cell. 2007;130(5):811-23.
48. Martin-Millan M, Almeida M, Ambrogini E, Han L, Zhao H, Weinstein RS, Jilka RL, O'Brien CA, Manolagas SC. The estrogen receptor-alpha in osteoclasts mediates the protective effects of estrogens on cancellous but not cortical bone. Mol Endocrinol. 2010;24(2):323-34.
49. Almeida M, Han L, O'Brien C A, Kousteni S, Manolagas SC. Classical genotropic versus kinase-initiated regulation of gene transcription by the estrogen receptor alpha. Endocrinology. 2006;147(4):1986-96.
50. Melville KM, Kelly NH, Khan SA, Schimenti JC, Ross FP, Main RP, van der Meulen MC. Female mice lacking estrogen receptor-alpha in osteoblasts have compromised bone mass and strength. J Bone Miner Res. 2014;29(2):370-9.
51. Maatta JA, Buki KG, Gu G, Alanne MH, Vaaraniemi J, Liljenback H, Poutanen M, Harkonen P, Vaananen K. Inactivation of estrogen receptor alpha in bone-forming cells induces bone loss in female mice. FASEB J. 2012.
52. Kondoh S, Inoue K, Igarashi K, Sugizaki H, Shirode-Fukuda Y, Inoue E, Yu T, Takeuchi JK, Kanno J, Bonewald LF, Imai Y. Estrogen receptor alpha in osteocytes regulates trabecular bone formation in female mice. Bone. 2014;60:68-77.
53. Almeida M, Iyer S, Martin-Millan M, Bartell SM, Han L, Ambrogini E, Onal M, Xiong J, Weinstein RS, Jilka RL, O'Brien CA, Manolagas SC. Estrogen receptor-alpha signaling in osteoblast progenitors stimulates cortical bone accrual. J Clin Invest. 2013;123(1):394-404.
54. Windahl SH, Borjesson AE, Farman HH, Engdahl C, Moverare-Skrtic S, Sjogren K, Lagerquist MK, Kindblom JM, Koskela A, Tuukkanen J, Divieti Pajevic P, Feng JQ, Dahlman-Wright K, Antonson P, Gustafsson JA, Ohlsson C. Estrogen receptor-alpha in osteocytes is important for trabecular bone formation in male mice. Proc Natl Acad Sci U S A. 2013;110(6):2294-9.
55. Jones HH, Priest JD, Hayes WC, Tichenor CC, Nagel DA. Humeral hypertrophy in response to exercise. J Bone Joint Surg Am. 1977;59(2):204-8.
56. Fuchs RK, Bauer JJ, Snow CM. Jumping improves hip and lumbar spine bone mass in prepubescent children: a randomized controlled trial. J Bone Miner Res. 2001;16(1):148-56.
57. Jaworski ZF, Liskova-Kiar M, Uhthoff HK. Effect of long-term immobilisation on the pattern of bone loss in older dogs. J Bone Joint Surg Br. 1980;62-B(1):104-10.
58. Schneider V, Oganov V, LeBlanc A, Rakmonov A, Taggart L, Bakulin A, Huntoon C, Grigoriev A, Varonin L. Bone and body mass changes during space flight. Acta Astronaut. 1995;36(8-12):463-6.
59. Rubin CT, Lanyon LE. Dynamic strain similarity in vertebrates; an alternative to allometric limb bone scaling. J Theor Biol. 1984;107(2):321-7.
60. Turner CH, Akhter MP, Raab DM, Kimmel DB, Recker RR. A noninvasive, in vivo model for studying strain adaptive bone modeling. Bone. 1991;12(2):73-9.
61. Gross TS, Srinivasan S, Liu CC, Clemens TL, Bain SD. Noninvasive loading of the murine tibia: an in vivo model for the study of mechanotransduction. J Bone

Miner Res. 2002;17(3):493-501.
62. Torrance AG, Mosley JR, Suswillo RF, Lanyon LE. Noninvasive loading of the rat ulna in vivo induces a strain-related modeling response uncomplicated by trauma or periostal pressure. Calcif Tissue Int. 1994;54(3):241-7.
63. Lee KC, Maxwell A, Lanyon LE. Validation of a technique for studying functional adaptation of the mouse ulna in response to mechanical loading. Bone. 2002;31(3):407-12.
64. Fritton JC, Myers ER, Wright TM, van der Meulen MC. Loading induces site-specific increases in mineral content assessed by microcomputed tomography of the mouse tibia. Bone. 2005;36(6):1030-8.
65. De Souza RL, Matsuura M, Eckstein F, Rawlinson SC, Lanyon LE, Pitsillides AA. Non-invasive axial loading of mouse tibiae increases cortical bone formation and modifies trabecular organization: a new model to study cortical and cancellous compartments in a single loaded element. Bone. 2005;37(6):810-8.
66. Moustafa A, Sugiyama T, Saxon LK, Zaman G, Sunters A, Armstrong VJ, Javaheri B, Lanyon LE, Price JS. The mouse fibula as a suitable bone for the study of functional adaptation to mechanical loading. Bone. 2009;44(5):930-5.
67. Lynch ME, Main RP, Xu Q, Walsh DJ, Schaffler MB, Wright TM, van der Meulen MC. Cancellous bone adaptation to tibial compression is not sex dependent in growing mice. J Appl Physiol (1985). 2010;109(3):685-91.
68. Main RP, Lynch ME, van der Meulen MC. Load-induced changes in bone stiffness and cancellous and cortical bone mass following tibial compression diminish with age in female mice. J Exp Biol. 2014;217(Pt 10):1775-83.
69. Fritton JC, Myers ER, Wright TM, van der Meulen MC. Bone mass is preserved and cancellous architecture altered due to cyclic loading of the mouse tibia after orchidectomy. J Bone Miner Res. 2008;23(5):663-71.
70. Brodt MD, Silva MJ. Aged mice have enhanced endocortical response and normal periosteal response compared with young-adult mice following 1 week of axial tibial compression. J Bone Miner Res. 2010;25(9):2006-15.
71. Holguin N, Brodt MD, Sanchez ME, Kotiya AA, Silva MJ. Adaptation of tibial structure and strength to axial compression depends on loading history in both C57BL/6 and BALB/c mice. Calcif Tissue Int. 2013;93(3):211-21.
72. Beamer WG, Donahue LR, Rosen CJ, Baylink DJ. Genetic variability in adult bone density among inbred strains of mice. Bone. 1996;18(5):397-403.
73. Robling AG, Turner CH. Mechanotransduction in bone: genetic effects on mechanosensitivity in mice. Bone. 2002;31(5):562-9.
74. Bass SL, Saxon L, Daly RM, Turner CH, Robling AG, Seeman E, Stuckey S. The effect of mechanical loading on the size and shape of bone in pre-, peri-, and postpubertal girls: a study in tennis players. J Bone Miner Res. 2002;17(12):2274-80.
75. Saxon LK, Turner CH. Low-dose estrogen treatment suppresses periosteal bone formation in response to mechanical loading. Bone. 2006;39(6):1261-7.
76. Damien E, Price JS, Lanyon LE. Mechanical strain stimulates osteoblast proliferation through the estrogen receptor in males as well as females. J Bone Miner Res. 2000;15(11):2169-77.
77. Ehrlich PJ, Noble BS, Jessop HL, Stevens HY, Mosley JR, Lanyon LE. The

effect of in vivo mechanical loading on estrogen receptor alpha expression in rat ulnar osteocytes. J Bone Miner Res. 2002;17(9):1646-55.
78. Jessop HL, Sjoberg M, Cheng MZ, Zaman G, Wheeler-Jones CP, Lanyon LE. Mechanical strain and estrogen activate estrogen receptor alpha in bone cells. J Bone Miner Res. 2001;16(6):1045-55.
79. Jessop HL, Suswillo RF, Rawlinson SC, Zaman G, Lee K, Das-Gupta V, Pitsillides AA, Lanyon LE. Osteoblast-like cells from estrogen receptor alpha knockout mice have deficient responses to mechanical strain. J Bone Miner Res. 2004;19(6):938-46.
80. Lee K, Jessop H, Suswillo R, Zaman G, Lanyon L. Endocrinology: bone adaptation requires oestrogen receptor-alpha. Nature. 2003;424(6947):389.
81. Cheng MZ, Rawlinson SC, Pitsillides AA, Zaman G, Mohan S, Baylink DJ, Lanyon LE. Human osteoblasts' proliferative responses to strain and 17beta-estradiol are mediated by the estrogen receptor and the receptor for insulin-like growth factor I. J Bone Miner Res. 2002;17(4):593-602.
82. Saxon LK, Galea G, Meakin L, Price J, Lanyon LE. Estrogen receptors alpha and beta have different gender-dependent effects on the adaptive responses to load bearing in cancellous and cortical bone. Endocrinology. 2012;153(5):2254-66.
83. Iyer S, Kim H, Ucer SS, Bartell S, Warren A, Crawford J, Skinner R, Dallas M, Johnson M, Weinstein RS, Jilka RL, O'Brien C A, Almeida M, Manolagas SC. ERα Signaling in Osterix1 and Prx1 Expressing Cells, Respectively, Mediates the Anabolic Effect of Mechanical Loading in the Murine Periosteum and the Protective Effects of Estrogens on Endocortical Resorption. J Bone Miner Res. 2013;28(S1).
84. Urist MR. Bone: formation by autoinduction. Science. 1965;150(3698):893-9.
85. Wozney JM, Rosen V, Celeste AJ, Mitsock LM, Whitters MJ, Kriz RW, Hewick RM, Wang EA. Novel regulators of bone formation: molecular clones and activities. Science. 1988;242(4885):1528-34.
86. Rosen V. BMP2 signaling in bone development and repair. Cytokine Growth Factor Rev. 2009;20(5-6):475-80.
87. Canalis E. Growth factor control of bone mass. J Cell Biochem. 2009;108(4):769-77.
88. Fukuda T, Kokabu S, Ohte S, Sasanuma H, Kanomata K, Yoneyama K, Kato H, Akita M, Oda H, Katagiri T. Canonical Wnts and BMPs cooperatively induce osteoblastic differentiation through a GSK3beta-dependent and beta-catenin-independent mechanism. Differentiation. 2010;80(1):46-52.
89. Canalis E, Economides AN, Gazzerro E. Bone morphogenetic proteins, their antagonists, and the skeleton. Endocr Rev. 2003;24(2):218-35.
90. Tsuji K, Bandyopadhyay A, Harfe BD, Cox K, Kakar S, Gerstenfeld L, Einhorn T, Tabin CJ, Rosen V. BMP2 activity, although dispensable for bone formation, is required for the initiation of fracture healing. Nat Genet. 2006;38(12):1424-9.
91. Yu YY, Lieu S, Lu C, Colnot C. Bone morphogenetic protein 2 stimulates endochondral ossification by regulating periosteal cell fate during bone repair. Bone. 2010;47(1):65-73.
92. Zaman G, Saxon LK, Sunters A, Hilton H, Underhill P, Williams D, Price JS,

Lanyon LE. Loading-related regulation of gene expression in bone in the contexts of estrogen deficiency, lack of estrogen receptor alpha and disuse. Bone. 2010;46(3):628-42.
93. McKenzie JA, Bixby EC, Silva MJ. Differential gene expression from microarray analysis distinguishes woven and lamellar bone formation in the rat ulna following mechanical loading. PLoS One. 2011;6(12):e29328.
94. Yamamoto T, Saatcioglu F, Matsuda T. Cross-talk between bone morphogenic proteins and estrogen receptor signaling. Endocrinology. 2002;143(7):2635-42.
95. Matsumoto Y, Otsuka F, Takano M, Mukai T, Yamanaka R, Takeda M, Miyoshi T, Inagaki K, Sada KE, Makino H. Estrogen and glucocorticoid regulate osteoblast differentiation through the interaction of bone morphogenetic protein-2 and tumor necrosis factor-alpha in C2C12 cells. Mol Cell Endocrinol. 2010;325(1-2):118-27.
96. Wu L, Wu Y, Gathings B, Wan M, Li X, Grizzle W, Liu Z, Lu C, Mao Z, Cao X. Smad4 as a transcription corepressor for estrogen receptor alpha. J Biol Chem. 2003;278(17):15192-200.
97. van den Wijngaard A, Mulder WR, Dijkema R, Boersma CJ, Mosselman S, van Zoelen EJ, Olijve W. Antiestrogens specifically up-regulate bone morphogenetic protein-4 promoter activity in human osteoblastic cells. Mol Endocrinol. 2000;14(5):623-33.
98. Mishina Y, Suzuki A, Ueno N, Behringer RR. Bmpr encodes a type I bone morphogenetic protein receptor that is essential for gastrulation during mouse embryogenesis. Genes Dev. 1995;9(24):3027-37.
99. Mishina Y, Starbuck MW, Gentile MA, Fukuda T, Kasparcova V, Seedor JG, Hanks MC, Amling M, Pinero GJ, Harada S, Behringer RR. Bone morphogenetic protein type IA receptor signaling regulates postnatal osteoblast function and bone remodeling. J Biol Chem. 2004;279(26):27560-6.
100. Kamiya N, Ye L, Kobayashi T, Lucas DJ, Mochida Y, Yamauchi M, Kronenberg HM, Feng JQ, Mishina Y. Disruption of BMP signaling in osteoblasts through type IA receptor (BMPRIA) increases bone mass. J Bone Miner Res. 2008;23(12):2007-17.
101. Okamoto M, Murai J, Imai Y, Ikegami D, Kamiya N, Kato S, Mishina Y, Yoshikawa H, Tsumaki N. Conditional deletion of Bmpr1a in differentiated osteoclasts increases osteoblastic bone formation, increasing volume of remodeling bone in mice. J Bone Miner Res. 2011;26(10):2511-22.
102. Baud'huin M, Solban N, Cornwall-Brady M, Sako D, Kawamoto Y, Liharska K, Lath D, Bouxsein ML, Underwood KW, Ucran J, Kumar R, Pobre E, Grinberg A, Seehra J, Canalis E, Pearsall RS, Croucher PI. A soluble bone morphogenetic protein type IA receptor increases bone mass and bone strength. Proc Natl Acad Sci U S A. 2012;109(30):12207-12.

Chapter 2

FEMALE MICE LACKING ESTROGEN RECEPTOR-ALPHA IN OSTEOBLASTS HAVE COMPROMISED BONE MASS AND STRENGTH[1]

2.1 Introduction

Osteoporosis, characterized by low bone mass, greatly increases skeletal fracture risk. Each year in the United States, osteoporotic fractures affect 1.5 million individuals and cost $17 billion in treatment (1). Due to the increasingly aged population, by 2025 treatment costs are predicted to rise to $25 billion (2). To reduce this economic burden and the cost of patient suffering, clinical strategies to maintain and even increase bone mass are essential and require understanding the complexity of cell signaling in bone.

Bone mass is regulated by a number of factors, including the sex hormones estrogen and testosterone, circulating parathyroid hormone (PTH) and insulin-like growth factor (IGF-1), and biophysical stimuli including the mechanical environment. By suppressing bone resorption and remodeling, estrogen regulates bone mass in both men and women during pubertal growth and throughout adulthood (3-5). At the onset of menopause, women experience a sharp decline in circulating estrogen that is accompanied by decreased bone mineral density, which can lead to osteoporosis and increased fracture risk (6, 7). Primarily due to this rapid hormonal decline, the majority of osteoporosis-related fractures occur in women (8). However, reduced bone mass and unfused growth plates were found in a male with an inactivating point mutation in the estrogen receptor alpha (ERα) gene, indicating that estrogen plays a role in bone mass in both sexes (9). Other research has also highlighted the

[1] Reprinted with permission: Melville KM, Kelly NH, Khan SA, Schimenti JC, Ross FP, Main RP, van der Meulen MCH. Osteoblast-specific Estrogen Receptor Alpha Knockout Mice Have Compromised Bone Mass and Strength. JBMR 2014. 29(2):370-9.

importance of estrogen in the male skeleton and the pathogenesis of osteoporosis (10).

While estrogen acts through two estrogen receptors (ER), ERα and ERβ, coded by separate genes, the steroid impacts bone mainly via ERα, which is present in chondrocytes, osteoblasts, osteocytes, and osteoclasts (3). Studies of global ERα knockout (ERαKO) mice show that ERα has a profound effect on bone tissue in growing and adult animals (11-13). Focusing on females, ERαKO mice had shorter bones compared to littermate controls during growth and maturation, in addition to increased cancellous and cortical bone mineral density in the tibia (14-17). Importantly, estrogen acts through ERα and/or ERβ in many organ systems, not limited to bone, resulting in confounding systemic effects in female global ERαKO mice, including increased body and uterine masses (15, 17). Also, serum levels of estrogen and testosterone were both increased (12, 17, 18), while that of serum IGF-1 was decreased (17). Because estrogen and IGF-1 are major independent regulators of bone mass, the role of ERα in bone is difficult to isolate and interpret in mice lacking the gene globally. Given these facts, a logical approach is to delete the gene in individual bone cell types with the goal of gaining a better understanding of the cell-specific effects of estrogen signaling, knowledge that will contribute to prevention of fractures and new treatments for osteoporosis.

Recent generation of bone-specific ERαKO mice revealed that expression of the receptor in chondrocytes, osteoblast progenitors, osteoblasts, osteocytes, or osteoclasts is important for maintaining bone mass during both growth and aging. However, the relationships between ERα and cancellous and cortical bone in females and males are complex and conflicting (19-23). Osteoclast-specific female ERαKO mice exhibited osteoporosis with cancellous architecture similar to that seen in post-menopausal women, due to reduced apoptosis of osteoclasts and subsequent high bone turnover rates, but cortical bone was unaffected (22, 23). When ERα was deleted from

osteoblast progenitors, cortical but not cancellous bone mass was reduced in males and females (19). In osteocyte-specific ERαKO mice, cortical bone was unaffected in both sexes, while cancellous bone was reduced in males but not females (21). Use of *OC-Cre* mice to delete ERα in osteoblasts reduced cancellous and cortical bone mass in females only, but no changes in bone mass in either sex were found when the gene was deleted in osteoblasts using *col1a1-Cre* mice (19, 20). To study the skeletal structural compromise that occurs with osteoporosis, bone strength, which is dependent upon bone mass, bone architecture, and material properties, must be considered (24). Importantly, the effect of ERα deletion in osteoblasts on whole bone strength at cortical and cancellous sites has not been studied in these models.

Therefore, the aim of this work was to determine the role of ERα in osteoblasts and osteocytes on cortical and cancellous bone mass and strength. To this end, we bred female osteoblast-specific ERαKO mice using the *osteocalcin-Cre* mouse. Having eliminated the possible role of systemic effects, we focused on relating bone mechanics to skeletal phenotype using micro-computed tomography, histology, dynamic histomorphometry, and whole bone mechanical testing in growing and skeletally mature mice.

2.2 Methods

2.2.1 Generation of osteoblast-specific ERαKO mice (pOC-ERαKO)

pOC-ERαKO mice were generated by breeding mice with exon 3 of the DNA-binding domain of the ERα gene (*Esr1*) flanked by loxP sequences, $ERα^{fl/fl}$ (13), to mice containing a transgene encoding *Cre* recombinase driven by the human osteocalcin promoter, *OC-Cre*, provided by Dr. Thomas Clemens (The Johns Hopkins University, Baltimore, MD) (25, 26). The resulting compound heterozygous mice, *OC-Cre*;$ERα^{fl/+}$, were bred back to $ERα^{fl/fl}$ mice to produce female osteoblast-specific

ERα knockout mice, *OC-Cre;ERα*$^{fl/fl}$ (pOC-ERαKO), and littermate controls, *ERα*$^{fl/+}$ (LC). The *OC-Cre* mice were inbred to the C57BL/6 strain, while *ERα*$^{fl/fl}$ mice were on a mixed C57Bl/6 and 129Sv background. Mice were housed 3-5 per cage with 12:12 light:dark hour cycles with ad libitum access to food and water. All animal procedures were approved by Cornell University's Institutional Animal Care and Use Committee.

Mouse genotyping was conducted by lysed tail PCR using the primers: 5'-CAAATAGCCCTGGCAGAT-3' (forward) and 5'-TGATACAAGGGACATCTTCC-3' (reverse) to detect the *Cre* transgene, while the floxed ERα gene was detected using the primers: 5'-TGGGTTGCCCGATAACAATAAC-3' (forward) and 5'-AAGAGATGTAGGGCGGGAAAAG-3' (reverse).

Femoral shaft DNA was purified for PCR to detect the floxed ERα gene using the primers above. Briefly, femurs were dissected, the bone marrow was flushed, and bone ends were cut off to isolate the diaphysis. DNA purification was performed following the manufacturer's instructions (QIAamp DNA mini kit, Qiagen).

2.2.2 Mass and Serum Hormone Measurements

Female LC and pOC-ERαKO mice were aged to 12 (LC n=16, pOC-ERαKO n=17) and 18 weeks of age (LC n=10, pOC-ERαKO n=10). Body mass was recorded at 4, 8, 12, and 18 weeks of age. Ovarian and uterine mass were measured at 12 and 18 weeks of age. Blood was collected through cardiac puncture at euthanasia, kept on ice for 4 hours, and then stored at 4°C overnight. Blood was centrifuged at 2,000g for 20 min to obtain serum, which was stored at -20°C. Serum was assayed using kits for estrogen (E2, CalBiotech EW180S-100, Spring Valley, CA), testosterone (T, CalBiotech TE187S-100, Spring Valley, CA, 12wk mice only), osteocalcin (OC, ALPCO 31-50-1300, Salem, NH), IGF-1 (ALPCO 22-IGF-R21, Salem, NH), and

TRACP5b (IDS SB-TR103, Scottsdale, AZ). T, OC, and IGF-1 assays were performed by the MECORE Laboratory (St. Joseph Hospital, Bangor, ME).

2.2.3 Microcomputed Tomography

Right tibiae were harvested and fixed in 4% paraformaldehyde for 24hr at 4°C and then transferred to 70% ethanol. Right femora and L5 vertebrae were harvested, wrapped in PBS-soaked gauze, and stored at -20°C. Bones were scanned using microcomputed tomography (microCT) at room temperature with an isotropic voxel resolution of 15μm (μCT35, Scanco Medical AG, Switzerland; 55kVp, 145μA, 600ms integration time). In each tibia, two volumes of interest (VOIs) were analyzed: a cancellous region manually contoured in the proximal tibia excluding the cortical shell beginning ~0.5mm distal to the growth plate and extending 10% of total bone length, and a cortical region centered at the midshaft and extending 2.5% of total bone length. In the distal femur, cortical bone was manually separated from cancellous bone beginning ~0.5mm proximal to the distal growth plate and extending 2mm proximally. In each vertebra, cortical bone was manually separated from cancellous bone extending the entire height of the vertebra. Measurable outcomes for cancellous regions included bone volume fraction (BV/TV), trabecular thickness (Tb.Th), trabecular separation (Tb.Sp), and cancellous tissue mineral density (cn.TMD). Measurable outcomes for the cortical regions included cortical area (Ct.Ar), marrow area (Ma.Ar, tibia only), total area (T.Ar, tibia only), maximum and minimum moments of inertia (I_{MAX}, I_{MIN}), cortical thickness (Ct.Th), and cortical tissue mineral density (ct.TMD). Mineralized tissue was separated from non-mineralized tissue using age- and bone-specific thresholds.

2.2.4 Dynamic Histomorphometry

Ten and 3 days before euthanasia, mice were administered calcein through

intraperitoneal injection (30mg/kg). Left tibiae were dissected at euthanasia and fixed in 70% ethanol. Bones were embedded in acrylosin and sectioned with a D profile tungsten-carbide blade to 5μm thickness using a rotary microtome (Leica RM2265, Germany) by the Bone Histology/Histomorphometry Laboratory (Yale University Department of Orthopaedics and Rehabilitation, New Haven, CT). Two slides per mouse and 4-5 mice per genotype were analyzed to measure single and double fluorescent labels on cancellous bone in longitudinal sections of the proximal tibia and on cortical bone in transverse sections of the tibial midshaft (OsteomeasureXP v3.2.1.7, Osteometrics, Decatur, GA). Outcome measures were mineralizing surface (MS), mineral apposition rate (MAR), and bone formation rate (BFR).

2.2.5 Histology

After microCT scanning, right tibiae from both 12- and 18-week-old animals were decalcified for 2 weeks in 10% EDTA, embedded in paraffin, and sectioned longitudinally in the sagittal plane at 6μm thickness using a rotary microtome (Leica RM2255, Germany).

To measure growth plate thickness, five evenly spaced lines were averaged for 2 slides per mouse, 6 mice per genotype on sections stained with Safranin O/Fast Green/Alcian Blue (OsteomeasureXP v3.2.1.7, Osteometrics, Decatur, GA).

To quantify osteoclast number, sections of the proximal tibiae were stained for tartrate-resistant acid phosphatase (TRAP). Sections were deparaffinized and rehydrated, and then placed in TRAP buffer for 10 min (3.28g Na-acetate, 46.01g Na-tartrate in 1L distilled water; Sigma-Aldrich). Sections were then incubated at 37°C in TRAP staining solution for 100min (40mg Napthol AS-MIX, 4mL N-N-dimethylformamide, 240mg Fast Red Violett LB Salt, 2mL Triton X-100; Sigma-Aldrich, in 200mL TRAP buffer). After counterstaining with hematoxylin, sections

were dehydrated and cover slipped. Beginning distal to the primary spongiosa, the number of positively-stained osteoclasts in the cancellous tissue normalized to bone surface was counted for 2 slides per mouse, 6 mice per genotype.

For pro-collagen I and ERα immunostaining, longitudinal sections of the proximal tibiae were deparaffinized and rehydrated. Antigen retrieval was achieved using 0.1M hot citrate buffer (20min pro-collagen I, 10min ERα). Endogenous peroxidase blocking was performed with 2% hydrogen peroxide (5 min), 2.5% periodic acid (5 min) and 0.02% sodium borohydride (5 min). Protein blocking was done using serum-free protein block for 20min for pro-collagen I (Dako) and using goat normal serum for 4hr for ERα (Vectastain ABC kit). Sections were incubated in either anti-pro-collagen I primary antibody (undiluted, SP1.D8, Developmental Studies Hybridoma Bank, Iowa City, IOWA) or anti-ERα primary antibody (1:100, abcam 75635, Cambridge, MA) overnight. Secondary antibody was delivered for 1hr (anti-mouse IgG for pro-collagen I and anti-rabbit IgG for ERα, Vectastain ABC kits), and staining was visualized using diaminobenzidine. Sections were dehydrated and cover slipped. For osteoblast activity, the number of positively-stained osteoblasts for pro-collagen I was counted and normalized to bone surface for 2 slides per mouse, 6 mice per genotype in the cancellous tissue beginning distal to the primary spongiosa.

2.2.6 Mechanical Testing

Prior to testing all bones were thawed to room temperature and kept moist in PBS. Femur length, and vertebral height, length, and width were measured using calipers. Right femora were loaded to failure in three-point bending in the anterior-posterior direction with a span length of 6 mm at a rate of 0.1 mm/s (858 Mini Bionix, MTS, Eden Prairie, MN). L5 vertebrae were loaded in compression at a rate of 0.05 mm/s to failure. For femora, bending strength and stiffness were calculated from load

and displacement data. For vertebrae, compressive strength and stiffness were calculated (27).

2.2.7 Statistics

Differences between pOC-ERαKO and LC mice for mass, serum (except for TRAP5b), and histomorphometry were determined using Student's t-tests in each age group. For microCT, mechanical testing, TRAP5b serum levels, and histology (pro-collagen I, TRAP, growth plate thickness), a 2-factor ANOVA (age, genotype) with interaction was used with Tukey's HSD post-hoc (JMP Pro 10). Significance was set at $p<0.05$.

2.3 Results

2.3.1 Generation and characterization of pOC-ERαKO mice

To study the effects of ERα absence in osteoblasts on bone strength, we crossed mice expressing the floxed ERα gene with animals transgenic for *Cre* driven by the human osteocalcin promoter. Mice were viable and born at the expected Mendelian ratio. The absence of ERα in osteoblasts in pOC-ERαKO mice was confirmed by PCR of genomic DNA of femoral shafts and ERα IHC in the proximal tibia (**Figure B.1**).

As others have reported, we found *Cre* expression in hypertrophic chondroctyes in addition to osteoblasts and osteocytes when *OC-Cre* mice were crossed with *ROSA26-Cre* reporter mice and longitudinal tibial sections were stained with X-Gal to detect β-galactosidase activity (data not shown) (28). However, we found no subsequent growth plate effects in the pOC-ERαKO mice. Specifically, the growth plates in the pOC-ERαKO mice had normal cell alignment and organization, and did not differ in thickness compared to LC mice at 12 or 18 weeks of age (**Figure 2.1, Table 2.1**). In addition, femoral and tibial lengths were not different between

pOC-ERαKO and LC mice in either age group, indicating normal endochondral ossification and longitudinal bone growth (**Figure B.2**).

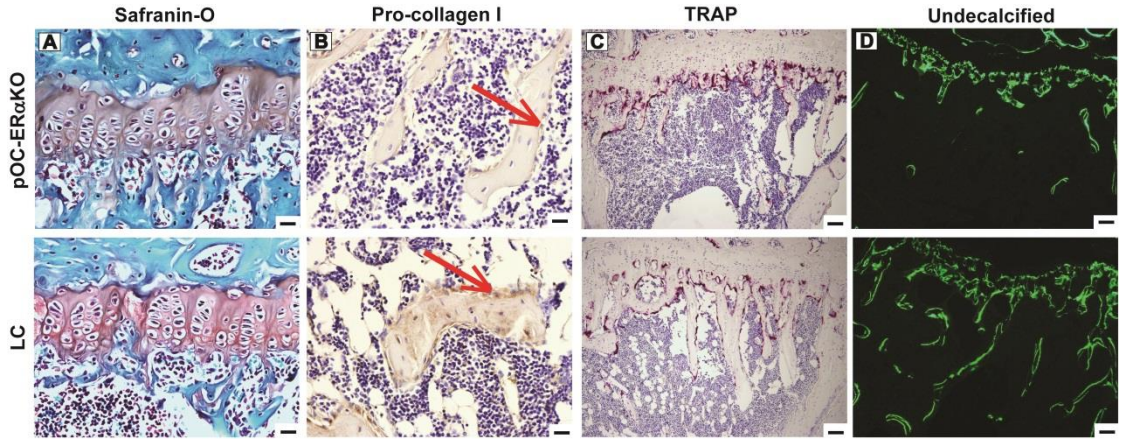

Figure 2.1 Representative IHC, histology, and dynamic histomorphometry images for sagittal sections of the proximal tibiae of pOC-ERαKO and LC female mice. (A) Tibial growth plate thickness did not differ between pOC-ERαKO and LC based upon measures from growth plates stained with Safranin-O. (B) In the cancellous bone of the proximal tibia, fewer osteoblasts per bone surface were positive for pro-collagen I activity (red arrow) in pOC-ERαKO compared to LC. (C) Osteoclast number normalized to bone surface was similar between pOC-ERαKO and LC mice at both age groups as indicated by TRAP staining in cancellous bone in the proximal tibia. (D) Reduced cancellous bone volume fraction is apparent in undecalcified sections of the proximal tibiae in pOC-ERαKO mice compared to LC. Dynamic histomorphometry measurements from double calcein labeling were not significantly different between genotypes. Scale bar = 20μm for A, B; 80μm for C, D. A, B, C, are at 12wk and D is at 18wk.

Table 2.1 IHC and histology quantification for the proximal tibia of pOC-ERαKO and LC mice

	12wk		18wk	
	LC	**pOC-ERαKO**	**LC**	**pOC-ERαKO**
GP.Th (mm)	0.117 ± 0.0051	0.114 ± 0.0038	0.106 ± 0.014	0.109 ± 0.024
N.Ob/BS (mm^{-1})	3.44 ± 1.8	2.00 ± 0.88[a]	2.07 ± 0.98	1.36 ± 1.1[a]
N.Ocl/BS (mm^{-1})	3.44 ± 0.21	3.47 ± 0.60	2.06 ± 0.65[b]	1.43 ± 0.46[b]

Data are represented as mean ± SD. GP.Th, growth plate thickness; N.Ob, number of positively stained osteoblasts for pro-collagen I; BS, bone surface; N.Ocl, number of positively stained osteoclasts for TRAP.

[a]pOC-ERαKO different from LC, [b]18wk different from 12wk, $p < 0.05$ by 2-factor ANOVA with interaction.

In contrast to the global ERαKO mice, systemic effects were not present in our osteoblast-specific ERαKO mice. No differences in body, ovarian, or uterine mass were measured between female pOC-ERαKO and LC mice (**Table B.1**). Altered serum levels of E2, T, IGF-1, and OC found in the global ERαKO mouse that may have produced secondary skeletal effects were eliminated in this tissue-specific knockout model; these parameters were all similar between pOC-ERαKO female mice and LC (**Figure 2.2**).

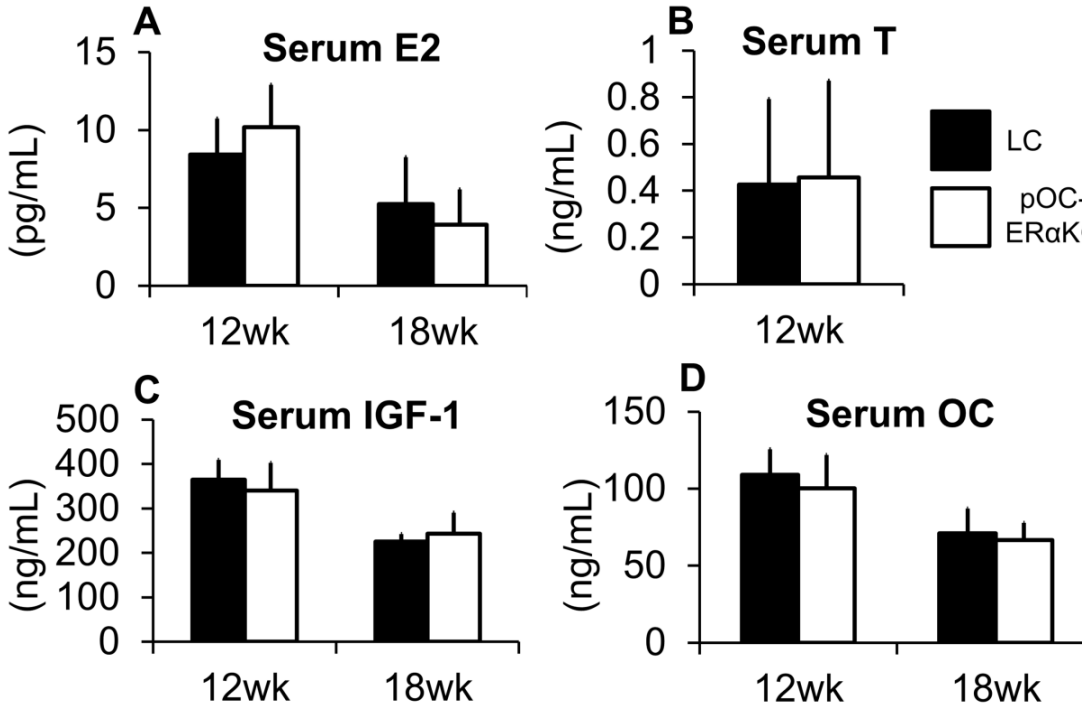

Figure 2.2 Unlike global ERαKO mice, serum levels of estrogen (A), testosterone (B), IGF-1 (C), and osteocalcin (D) were unaltered in female pOC-ERαKO mice compared to controls at both 12 and 18 weeks of age (n=6-10 per genotype per age). Data are represented as mean ± SD.

2.3.2 Bone mass and architecture

Previously, bone mass was altered in both global and bone-specific ERαKO mice. In our osteoblast-specific ERαKO mouse, cancellous bone mass was severely reduced at the three sites examined compared to LC mice at 12 weeks of age (**Figure 2.3, Table 2.2**). Bone volume fraction (BV/TV) was significantly reduced in the proximal tibia (-35%), L5 vertebral body (-35%), and distal femur (-30%). The same decrease in all measured parameters continued in 18-week-old animals. Mean BV/TV

remained significantly less in the proximal tibia (-7%), vertebra (-44%), and distal femur (-33%) of pOC-ERαKO mice at 18 weeks of age as well.

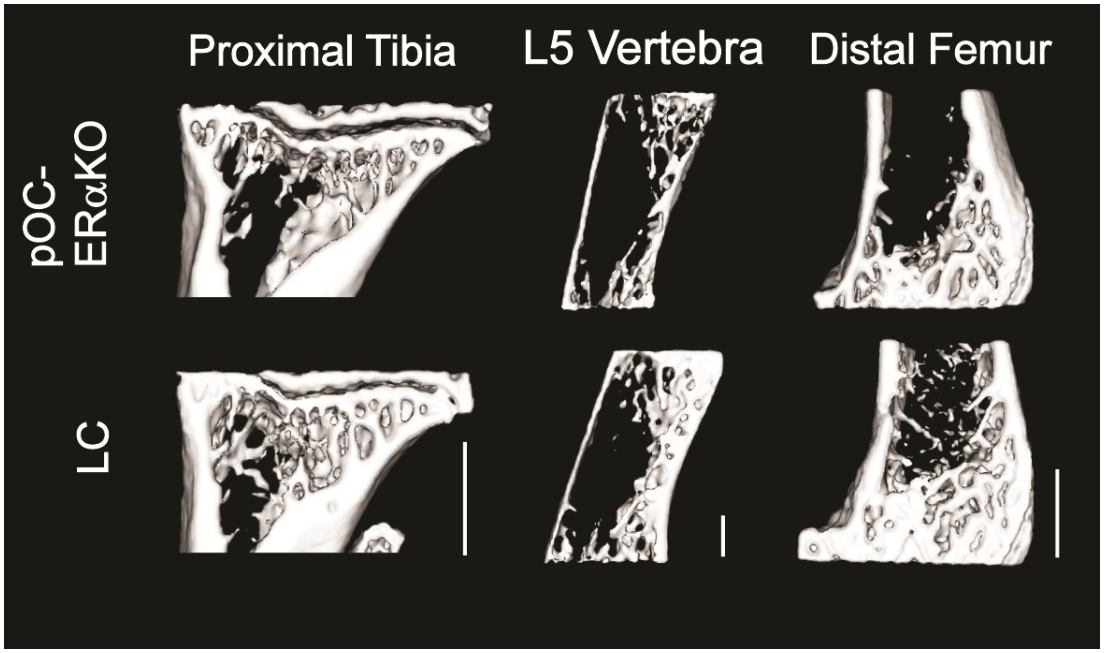

Figure 2.3 Lack of ERα in osteoblasts significantly reduced cancellous and cortical bone mass in pOC-ERαKO female mice. Sagittal sections through the proximal tibiae, L5 vertebrae, and distal femora are shown from representative microCT scans of 12-week-old female pOC-ERαKO and LC mice. Bone volume fraction was reduced 35% in the proximal tibia, 35% in the L5 vertebra, and 30% in the distal femur. Cortical area was reduced 4% in the L5 vertebra and 13% in the distal femur. Scale bar = 0.5mm for tibia and vertebra and 1.0mm for femur.

Table 2.2 Cancellous parameters measured by microCT for the proximal tibia, L5 vetebral body, and distal femur of 12- and 18-week-old female pOC-ERαKO and LC mice

		Proximal Tibia		L5 Vertebra		Distal Femur	
		LC	**pOC-ERαKO**	**LC**	**pOC-ERαKO**	**LC**	**pOC-ERαKO**
12wk	BV/TV	0.0964 ± 0.023	0.0630 ± 0.016[a]	0.246 ± 0.054	0.160 ± 0.041[a]	0.118 ± 0.028	0.0819 ± 0.019[a]
	Tb.Th (μm)	51.4 ± 4.2	50.0 ± 3.2	55.4 ± 5.7	47.6 ± 4.4[a]	55.9 ± 3.3	52.6 ± 3.2
	Tb.Sp (μm)	333 ± 44	484 ± 47[a]	236 ± 33	269 ± 31[a]	264 ± 31	368 ± 79[a]
	cn.TMD (mg HA/cc)	771 ± 16	775 ± 18	657 ± 43	667 ± 41	706 ± 21	709 ± 20
18wk	BV/TV	0.134 ± 0.020[b]	0.125 ± 0.035[a,b]	0.272 ± 0.047	0.154 ± 0.025[a]	0.0968 ± 0.031[b]	0.0648 ± 0.022[a,b]
	Tb.Th (μm)	64.2 ± 6.3[b]	68.5 ± 5.3[b]	63.9 ± 13[b]	50.6 ± 2.7[a,b]	53.7 ± 7.3	53.2 ± 5.3
	Tb.Sp (μm)	352 ± 55[b]	563 ± 122[a,b]	249 ± 28[b]	311 ± 37[a,b]	308 ± 32[b]	542 ± 122[a,b]
	cn.TMD (mg HA/cc)	750 ± 16[b]	737 ± 14[b]	674 ± 27	660 ± 13	732 ± 14[b]	772 ± 18[b]

Data are represented as mean ± SD. BV/TV, bone volume fraction; Tb.Th, trabecular thickness; Tb.Sp, trabecular separation; cn.TMD, cancellous tissue mineral density.

[a]pOC-ERαKO different from LC, [b]18wk different from 12wk, $p<0.05$ by 2-factor ANOVA with interaction.

Changes in cancellous trabecular architecture correlated with decreased bone mass (**Table 2.2**). Reduced BV/TV in pOC-ERαKO mice was due primarily to increased trabecular separation (Tb.Sp), which was markedly increased in all three cancellous sites at both ages. The proximal tibia had the greatest increase in Tb.Sp, which was increased 45% at 12wk and 60% at 18wk in pOC-ERαKO mice. In the distal femur, Tb.Sp was increased in pOC-ERαKO mice compared to LC in both 12- and 18-week-old animals (+40% and +76%, respectively), and in the vertebra (+14% and +25% for 12wk and 18wk, respectively). Regardless of bone site or genotype, Tb.Sp increased with age in all animals. Trabecular thickness (Tb.Th) was decreased in pOC-ERαKO mice compared to LC in both age groups only in the vertebra (-14% and -21% at 12 and 18wk, respectively), contributing to the overall reduced vertebral BV/TV. Tb.Th, like Tb.Sp, increased significantly with age in the tibiae and vertebra, but not in the femur.

Cancellous tissue mineral density (cn.TMD) was not affected by osteoblast-specific deletion of ERα (**Table 2.2**). However, cn.TMD decreased significantly with age at the proximal tibia (-3% LC, -5% pOC-ERαKO) but increased with age in the distal femur (+4% LC, +2% pOC-ERαKO).

The cancellous changes in the corticocancellous distal femur and vertebra of pOC-ERα mice were accompanied by analogous but smaller cortical changes (**Table 2.3**). Cortical area (Ct.Ar) was reduced in the distal femur and L5 vertebra cortexes in pOC-ERαKO mice compared to LC at 12wk (-13% and -4%, respectively) and 18wk (-14% and -11%, respectively). This decrease in bone mass corresponded with lower overall cortical thickness (Ct.Th) at both sites at 12wk (-8% for femur, -10% for vertebra) and 18wk (-14% for both bones). In the distal femur only, maximum and minimum moments of inertia ($I_{MAX,}$ I_{MIN}) were reduced at 12wk in pOC-ERαKO mice (-16% and -17%, respectively) and at 18wk (-11% and -12%, respectively). In both

genotypes, femoral Ct.Ar was greater in 18wk than 12wk mice (+11% for LC, +10% for pOC-ERαKO) as were I_{MAX} and I_{MIN} (+16% for both in LC, +23% for both in pOC-ERαKO). Tissue mineral density in the cortical shell (ct.TMD) was reduced in pOC-ERαKO mice compared to LC at both ages in the distal femur (-2% at 12wk, -3% at 18wk), but not in the L5 vertebra. However, ct.TMD increased with age in the L5 vertebra, by 2% in LC and 3% in pOC-ERαKO mice. In the corticocancellous regions of the distal femur and L5 vertebra, decreased bone mass in pOC-ERαKO mice was present in both the cortical shell and the cancellous region.

Cortical bone mass was also reduced compared to LC in the tibial diaphysis, but less so than in the cancellous envelope of the metaphysis (**Figure 2.4**). At the tibial midshaft, Ct.Ar was decreased in both 12- and 18-week-old female pOC-ERαKO mice compared to LC (-8% and -7%, respectively) (**Table 2.3**). At both ages, this decrease in bone mass was due to decreased Ct.Th (-7% at both ages) and lower ct.TMD (-2% at 12wk, -1% at 18wk). In older animas, Ct.Th and ct.TMD were significantly greater than younger animals for both genotypes. I_{MAX} at the tibial

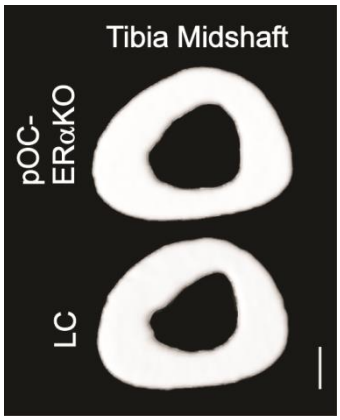

Figure 2.4 Deletion of ERα from osteoblasts reduced cortical bone mass. Transverse sections at the tibial midshaft from microCT scans of 12-week-old female pOC-ERαKO (top) and LC mice (bottom) are shown. Cortical area was 8% less in 12-week-old pOC-ERαKO mice compared to LC. Scale bar = 0.25mm.

Table 2.3 Cortical parameters measured by microCT for the tibial midshaft, L5 vertebra, and distal femur of 12- and 18-week-old female pOC-ERαKO and LC mice

		Tibial Midhaft		L5 Vertebra		Distal Femur	
		LC	**pOC-ERαKO**	**LC**	**pOC-ERαKO**	**LC**	**pOC-ERαKO**
12wk	Ct.Ar (mm^2)	0.654 ± 0.057	0.601 ± 0.071[a]	0.477 ± 0.065	0.460 ± 0.058[a]	1.09 ± 0.12	0.948 ± 0.10[a]
	T.Ar (mm^2)	0.928 ± 0.083	0.871 ± 0.10	--	--	--	--
	Ma.Ar (mm^2)	0.275 ± 0.041	0.270 ± 0.054	--	--	--	--
	Ct.Th (mm)	0.240 ± 0.014	0.223 ± 0.0097[a]	0.0909 ± 0.010	0.0817 ± 0.0056[a]	0.168 ± 0.014	0.154 ± 0.023[a]
	I_{MAX} (mm^4)	0.0791 ± 0.015	0.0747 ± 0.018	0.198 ± 0.037	0.213 ± 0.047	0.554 ± 0.10	0.465 ± 0.099[a]
	I_{MIN} (mm^4)	0.0514 ± 0.0094	0.0415 ± 0.010[a]	0.0614 ± 0.018	0.0575 ± 0.014	0.277 ± 0.069	0.231 ± 0.049[a]
	ct.TMD (mg HA/cc)	1020 ± 17	1000 ± 15[a]	713 ± 27	707 ± 18	882 ± 29	868 ± 37[a]
18wk	Ct.Ar (mm^2)	0.677 ± 0.059	0.628 ± 0.063[a]	0.501 ± 0.052	0.445 ± 0.039[a]	1.21± 0.083[b]	1.04 ± 0.10[a,b]
	T.Ar (mm^2)	0.923 ± 0.098	0.887 ± 0.10	--	--	--	--
	Ma.Ar (mm^2)	0.246 ± 0.055	0.259 ± 0.061	--	--	--	--
	Ct.Th (mm)	0.256 ± 0.016[b]	0.237 ± 0.017[a,b]	0.0948 ± 0.0051	0.0816 ± 0.0048[a]	0.175 ± 0.013	0.150 ± 0.0094[a]
	I_{MAX} (mm^4)	0.0796 ± 0.020	0.0764 ± 0.016	0.219 ± 0.052	0.209 ± 0.033	0.643 ± 0.076[b]	0.573 ± 0.097[a,b]
	I_{MIN} (mm^4)	0.0511 ± 0.0092	0.0439 ± 0.011[a]	0.0621 ± 0.010	0.0628 ± 0.011	0.322 ± 0.049[b]	0.285 ± 0.045[a,b]
	ct.TMD (mg HA/cc)	1040 ± 12[b]	1020 ± 14[a,b]	724 ± 32[b]	725 ± 21[b]	899 ± 18	875 ± 14[a]

Data are represented as mean ± SD. Ct.Ar, cortical area; T.Ar, total area; Ma.Ar, marrow area; Ct.Th, cortical thickness; I_{MAX} and I_{MIN}, maximum/minimum moment of inertia; ct.TMD, cortical tissue mineral density

[a]pOC-ERαKO different from LC, [b]18wk different from 12wk, $p<0.05$ by 2-factor ANOVA with interaction.

midshaft was not affected by osteoblast-specific ERα deletion, but the minimum moment of inertia I_{MIN} was significantly reduced in pOC-ERαKO mice at both ages (-19% at 12wk and -14% at 18wk). Marrow area in the tibial midshaft was also unchanged by ERα deletion in osteoblasts; thus, the smaller cortex reflected a lack of periosteal expansion along the minimum axis.

2.3.3 Bone cell activity

Decreased BV/TV in the cancellous tissue of the proximal tibiae of pOC-ERαKO mice reflected changes in osteoblast activity (**Figure 2.1**). When normalized to bone surface, the number of pro-collagen I-positive osteoblasts was decreased in pOC-ERαKO females compared to LC at 12wk (-42%) and 18wk (-34%) (**Table 2.1**). Systemically, serum TRACP5b levels were reduced in pOC-ERαKO mice at both 12wk (-29%) and 18wk (-37%), reflecting the decreased cancellous bone mass (**Figure 2.5**). However, local osteoclast number indicated by TRAP staining was not different between genotypes at either age when normalized to bone surface in the proximal tibia (**Figure 2.1, Table 2.1**).

Decreased bone mass was evident in undecalcified longitudinal sections of the proximal tibia of pOC-ERαKO animals **(Figure 2.1)**, but dynamic histomorphometric measurements were not statistically different between genotypes for either cancellous bone in the proximal tibia or at endosteal or periosteal surfaces at the tibial midshaft.

2.3.4 Whole bone strength

The decreases in cortical and cancellous bone mass and compromised architecture resulting from deletion of ERα in osteoblasts corresponded to compromised whole bone strength. In both age groups, vertebral and femoral strength were reduced in pOC-ERαKO mice compared to LC, as determined through

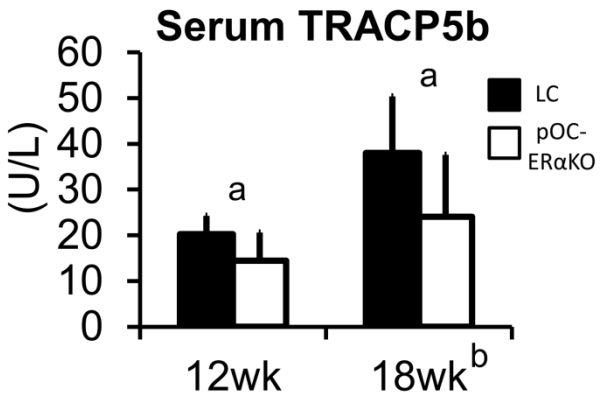

Figure 2.5 pOC-ERαKO mice had significantly lower TRACP5b levels at both 12 and 18 weeks of age, indicating reduced osteoclast number resulting from lower bone mass. Data are represented as mean ± SD. [a]pOC-ERαKO different from LC, [b]18wk different from 12wk, $p<0.05$ by 2-factor ANOVA with interaction.

mechanical testing to failure (**Figure 2.6**). Femoral bending strength was reduced 11% at 12wk and 10% at 18wks, while vertebral strength was reduced 25% at both ages in pOC-ERαKO mice. Bone strength increased significantly with age (+27% femur, +17% vertebra for pOC-ERαKO; +26% femur, +18% vertebra for LC). Interestingly, vertebral compressive strength correlated linearly with BV/TV for LC but not pOC-ERαKO mice through regression analysis (**Figure B.3**). BV/TV accounted for 43% of the variation in vertebral compressive strength for LC mice ($p=0.0006$) but BV/TV had no predictive value for vertebral strength in pOC-ERαKO mice. Although femoral bending stiffness was decreased in pOC-ERαKO mice compared to LC at both 12wk (-13%) and 18wk (-15%), vertebral compressive stiffness was not significantly different between genotypes. Femoral and vertebral stiffness also increased significantly with age (+40% femur, +43% vertebra for pOC-ERαKO; +42% femur, +34% vertebra for LC).

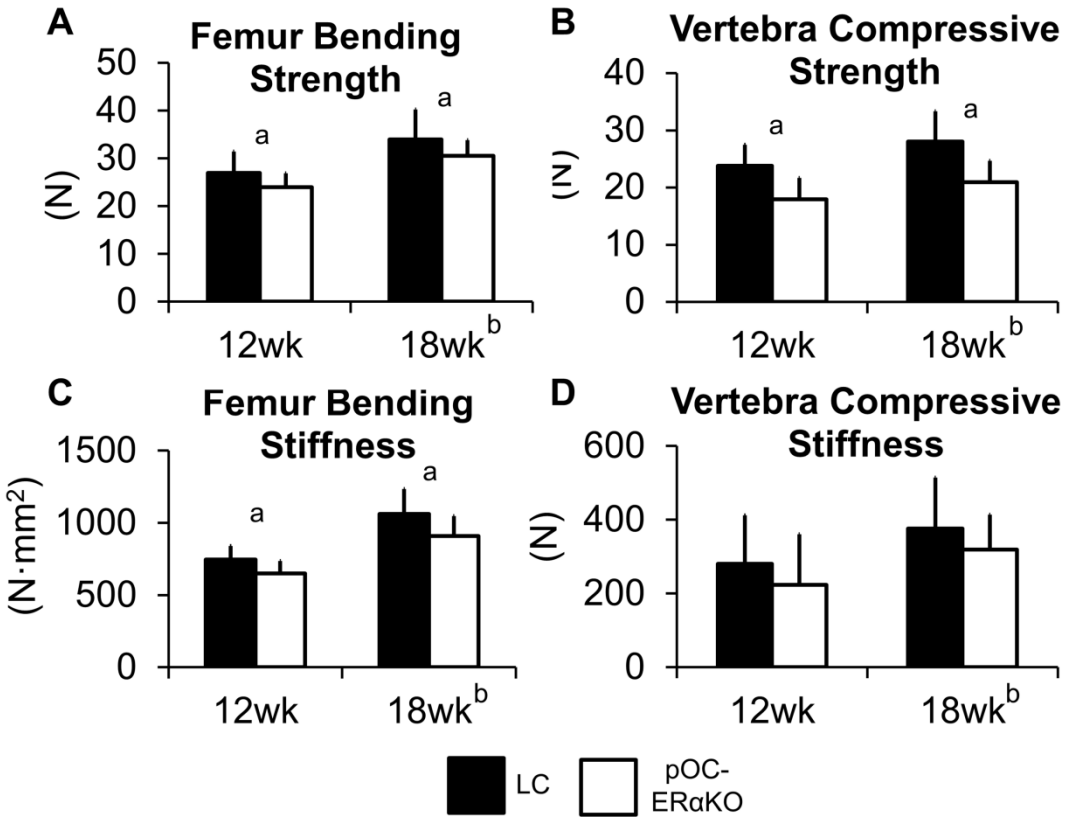

Figure 2.6 Whole bone strength and stiffness were compromised in pOC-ERαKO female mice. (A) In three-point bending to failure, pOC-ERαKO female mice had decreased femoral bending strength at both 12 weeks (-11%) and 18 weeks (-10%) of age. (B) L5 vertebrae of pOC-ERαKO female mice were 25% weaker at both 12 and 18 weeks of age in compression testing to failure. (C) Femur bending stiffness was reduced 13% and 15% in 12- and 18-week-old pOC-ERαKO mice, respectively, compared to LC. (D) Vertebral compressive stiffness was not different between genotypes. n=10-17 per genotype and age. Data are represented as mean ± SD. [a]pOC-ERαKO different from LC, [b]18wk different from 12wk, $p<0.05$ by 2-factor ANOVA with interaction.

2.4 Discussion

We successfully deleted ERα from osteoblasts and osteocytes in female mice by mating *ERα*$^{fl/fl}$ and *OC-Cre* mice without producing systemic hormone effects. Serum E2, T, IGF-1, and OC were unchanged in pOC-ERαKO mice, as were ovarian and uterine masses, confirming the lack of systemic effects that may independently alter bone phenotype. During growth, the pOC-ERαKO and LC mice did not differ in

body mass, and long bone lengths were similar between genotypes at both 12 and 18 weeks of age. In contrast, the pOC-ERαKO mice had decreased cancellous and cortical bone mass compared to littermate controls, which negatively impacted whole bone strength and stiffness, indicating that ERα in osteoblasts is a critical component of successful accrual of bone mass and strength in female mice.

The role of ERα in bone was studied initially using global ERαKO mice, which have a drastically different skeletal phenotype opposite that seen in our pOC-ERαKO and other osteoblast-specific ERαKO mouse models (11-13). While our pOC-ERαKO female mice had decreased cancellous and cortical bone mass, the global ERαKO female mice had increased bone mass and bone mineral density (16, 17). However, systemic effects indicate that other tissues were affected by global ERα deletion. Female mice had increased serum estrogen levels leading to increased uterine mass and decreased serum IGF-1 levels resulting in shorter bones (12, 15, 17, 18). Because estrogen and IGF-1 have major indirect actions on bone (29, 30), the skeletal phenotype seen in the global ERαKO mice is influenced by these secondary effects and those arising from the direct role of ERα in bone. These conflicting results led researchers to create conditional knockouts, such as our pOC-ERαKO mouse.

Estrogen acts in bone-residing cells primarily through ERα to alter gene transcription, but also exhibits non-genomic effects (31, 32) and so is likely to have distinct effects on different lineages as they mature and differentiate, as has been shown though osteoblast lineage deletions of RANKL (28). Recently, two other conditional ERαKO mouse models focusing on osteoblasts were generated, with results that are similar to ours or in significant conflict with ours. Määttä *et al.* also used the *OC-Cre* promoter transgenic mouse to create animals with an osteoblast-specific deletion of ERα ($ER\alpha^{\Delta OB/\Delta OB}$) (20). Bone phenotype was analyzed in both males and females at 3.5, 6, and 12 months of age. As in our 12- and 18-week-old

pOC-ERαKO mice, BV/TV in the proximal tibia and cortical bone volume at the tibial diaphysis were reduced in female $ER\alpha^{\Delta OB/\Delta OB}$ mice at 3.5 months. However, this phenotype disappeared with age. At 6 months, bone mass was still decreased in the proximal tibia, but Tb.Sp was no longer different between genotypes, while by 12 months of age, no tibial cancellous phenotype difference was seen by microCT analysis in the tibiae. We cannot confirm their results for older mice, as our study only included growing (12 wk) and skeletally mature (18 wk) animals.

In contrast to the work of Määttä *et al.* and our study, Almeida *et al.* found no cortical or cancellous bone phenotype in a female osteoblast-specific ERαKO mouse ($ER\alpha^{f/f}$*;Col1a1-Cre*), using the *Col1a1-Cre* promoter, which is expressed in mature osteoblasts and osteocytes (19). Femoral cancellous bone mass and cortical thickness were unaltered in 12- and 26-week-old female mice, and spine and femoral BMD were unchanged in female mice from 4 to 12 weeks of age. However, when the same authors deleted ERα in osteoblast progenitor cells using either *Osx-Cre* or *Prx-Cre* mice, BMD of the femur and cortical thickness in the femur mid-diaphysis were decreased in female mice, but cancellous bone mass remained unchanged at the proximal femur. These findings indicate that ERα is not required in either osteoblasts or their progenitors for cancellous bone mass accrual in females; in contrast, cortical bone was affected by absence of ERα in osteoblast progenitors but not mature osteoblasts. Much of the discrepancy in the results found in $ER\alpha^{f/f}$*;Col1a1-Cre* model vs. the $ER\alpha^{\Delta OB/\Delta OB}$ models and our pOC-ERαKO models can be attributed to the use of different *Cre* models and timing of their cellular effects. The *OC-Cre* targets osteoblasts during the mineralization phase, while the *Col1a1-Cre* targets osteoblasts earlier, during the matrix maturation phase (33). Interestingly, when ERα was ablated only in mature osteocytes using the 10kb *DMP1-Cre* mouse, cancellous and cortical bone were both unaffected in female mice, suggesting that ERα may play a stronger

role in osteoblasts than in osteocytes when combined with our study's results (21).

The *OC-Cre* mouse is an established model used to ablate genes in mature osteoblasts and osteocytes (26). Crossing these mice with *ROSA26-Cre* reporter mice has shown that *Cre* expression is limited to osteoblasts and osteocytes, but expression in hypertrophic chondrocytes has been reported (28, 34). Because hypertrophic chondroctyes differentiate into osteoblasts during endochondral ossification, the possible effects of ERα in growth plate cartilage cannot be ignored in examining the bone phenotypes of pOC-ERαKO mice. In a cartilage-specific ERαKO female mouse, the skeleton developed normally during growth, but continued to grow beyond 4 months of age, resulting in increased femur length compared to controls (35). Femoral growth plate height, however, was not different between cartilage-specific ERαKO mice and controls, which is consistent with our results, in which tibial growth plate height and long bone lengths were similar between pOC-ERαKO and LC. In contrast, female $ERα^{\Delta OB/\Delta OB}$ at 3.5 months of age had increased tibial growth plate height compared to controls but no difference in bone length (20). While we cannot explain the growth plate discrepancy between similarly generated mice, we can infer that the skeletal phenotype seen in pOC-ERαKO is indeed bone-mediated as opposed to an effect on cartilage because bone lengths and growth plate structure were unaffected.

Although mouse models cannot directly translate to human clinical data, ERα clearly plays an important role in both the mouse and human skeletons. In human clinical data, a mutation in the ERα gene increased bone mineral density and resulted in osteopenic bone (9). Polymorphisms in ERα are correlated with bone mass in humans (36). Our data show that when ERα is deleted from osteoblasts, bone mass and strength are compromised at cortical and corticocancellous sites in female mice, pointing to a crucial role of ERα in these cells. The receptor has been proposed to be involved in a number of bone signaling networks, including those activated estrogen,

IGF-1, wnt/β-catenin, and BMP-2 (37-39). The majority of these studies examined the interaction between estrogen signaling and other signaling pathways using osteoblast cultures *in vitro*. Availability of osteoblast-specific ERαKO mice will facilitate future studies on osteoblastic ERα signaling *in vivo*. As we increase our understanding of estrogen signaling in bone, we may have the opportunity to develop new drugs for preventing and treating osteoporosis, especially in post-menopausal women, in whom estrogen signaling is most relevant.

2.5 References

1. Bone Health and Osteoporosis: A Report of the Surgeon General. Rockville, MD: U.S. Department of Health and Human Services, Office of the Surgeon General; 2004.
2. Burge R, Dawson-Hughes B, Solomon DH, Wong JB, King A, Tosteson A. Incidence and economic burden of osteoporosis-related fractures in the United States, 2005-2025. J Bone Miner Res. 2007;22(3):465-75.
3. Manolagas SC, Bellido T, Jilka RL. Sex steroids, cytokines and the bone marrow: new concepts on the pathogenesis of osteoporosis. Ciba Found Symp. 1995;191:187-96; discussion 97-202.
4. Eastell R. Role of oestrogen in the regulation of bone turnover at the menarche. J Endocrinol. 2005;185(2):223-34.
5. Riggs BL. The mechanisms of estrogen regulation of bone resorption. J Clin Invest. 2000;106(10):1203-4.
6. Richelson LS, Wahner HW, Melton LJ, 3rd, Riggs BL. Relative contributions of aging and estrogen deficiency to postmenopausal bone loss. N Engl J Med. 1984;311(20):1273-5.
7. Riggs BL. Endocrine causes of age-related bone loss and osteoporosis. Novartis Found Symp. 2002;242:247-59; discussion 60-4.
8. Johnell O, Kanis JA. An estimate of the worldwide prevalence and disability associated with osteoporotic fractures. Osteoporos Int. 2006;17(12):1726-33.
9. Smith EP, Boyd J, Frank GR, Takahashi H, Cohen RM, Specker B, Williams TC, Lubahn DB, Korach KS. Estrogen resistance caused by a mutation in the estrogen-receptor gene in a man. N Engl J Med. 1994;331(16):1056-61.
10. Khosla S, Amin S, Orwoll E. Osteoporosis in men. Endocr Rev. 2008;29(4):441-64.
11. Lubahn DB, Moyer JS, Golding TS, Couse JF, Korach KS, Smithies O. Alteration of reproductive function but not prenatal sexual development after insertional disruption of the mouse estrogen receptor gene. Proc Natl Acad Sci U S A. 1993;90(23):11162-6.

12. Couse JF, Curtis SW, Washburn TF, Lindzey J, Golding TS, Lubahn DB, Smithies O, Korach KS. Analysis of transcription and estrogen insensitivity in the female mouse after targeted disruption of the estrogen receptor gene. Mol Endocrinol. 1995;9(11):1441-54.
13. Dupont S, Krust A, Gansmuller A, Dierich A, Chambon P, Mark M. Effect of single and compound knockouts of estrogen receptors alpha (ERalpha) and beta (ERbeta) on mouse reproductive phenotypes. Development. 2000;127(19):4277-91.
14. Lee KC, Jessop H, Suswillo R, Zaman G, Lanyon LE. The adaptive response of bone to mechanical loading in female transgenic mice is deficient in the absence of oestrogen receptor-alpha and -beta. J Endocrinol. 2004;182(2):193-201.
15. Vidal O, Lindberg M, Savendahl L, Lubahn DB, Ritzen EM, Gustafsson JA, Ohlsson C. Disproportional body growth in female estrogen receptor-alpha-inactivated mice. Biochem Biophys Res Commun. 1999;265(2):569-71.
16. Sims NA, Dupont S, Krust A, Clement-Lacroix P, Minet D, Resche-Rigon M, Gaillard-Kelly M, Baron R. Deletion of estrogen receptors reveals a regulatory role for estrogen receptors-beta in bone remodeling in females but not in males. Bone. 2002;30(1):18-25.
17. Lindberg MK, Alatalo SL, Halleen JM, Mohan S, Gustafsson JA, Ohlsson C. Estrogen receptor specificity in the regulation of the skeleton in female mice. J Endocrinol. 2001;171(2):229-36.
18. Parikka V, Peng Z, Hentunen T, Risteli J, Elo T, Vaananen HK, Harkonen P. Estrogen responsiveness of bone formation in vitro and altered bone phenotype in aged estrogen receptor-alpha-deficient male and female mice. Eur J Endocrinol. 2005;152(2):301-14.
19. Almeida M, Iyer S, Martin-Millan M, Bartell SM, Han L, Ambrogini E, Onal M, Xiong J, Weinstein RS, Jilka RL, O'Brien CA, Manolagas SC. Estrogen receptor-alpha signaling in osteoblast progenitors stimulates cortical bone accrual. J Clin Invest. 2013;123(1):394-404.
20. Maatta JA, Buki KG, Gu G, Alanne MH, Vaaraniemi J, Liljenback H, Poutanen M, Harkonen P, Vaananen K. Inactivation of estrogen receptor alpha in bone-forming cells induces bone loss in female mice. FASEB J. 2012.
21. Windahl SH, Borjesson AE, Farman HH, Engdahl C, Moverare-Skrtic S, Sjogren K, Lagerquist MK, Kindblom JM, Koskela A, Tuukkanen J, Divieti Pajevic P, Feng JQ, Dahlman-Wright K, Antonson P, Gustafsson JA, Ohlsson C. Estrogen receptor-alpha in osteocytes is important for trabecular bone formation in male mice. Proc Natl Acad Sci U S A. 2013;110(6):2294-9.
22. Nakamura T, Imai Y, Matsumoto T, Sato S, Takeuchi K, Igarashi K, Harada Y, Azuma Y, Krust A, Yamamoto Y, Nishina H, Takeda S, Takayanagi H, Metzger D, Kanno J, Takaoka K, Martin TJ, Chambon P, Kato S. Estrogen prevents bone loss via estrogen receptor alpha and induction of Fas ligand in osteoclasts. Cell. 2007;130(5):811-23.
23. Martin-Millan M, Almeida M, Ambrogini E, Han L, Zhao H, Weinstein RS, Jilka RL, O'Brien CA, Manolagas SC. The estrogen receptor-alpha in osteoclasts mediates the protective effects of estrogens on cancellous but not cortical bone. Mol Endocrinol. 2010;24(2):323-34.

24. van der Meulen MC, Jepsen KJ, Mikic B. Understanding bone strength: size isn't everything. Bone. 2001;29(2):101-4.
25. Clemens TL, Tang H, Maeda S, Kesterson RA, Demayo F, Pike JW, Gundberg CM. Analysis of osteocalcin expression in transgenic mice reveals a species difference in vitamin D regulation of mouse and human osteocalcin genes. J Bone Miner Res. 1997;12(10):1570-6.
26. Zhang M, Xuan S, Bouxsein ML, von Stechow D, Akeno N, Faugere MC, Malluche H, Zhao G, Rosen CJ, Efstratiadis A, Clemens TL. Osteoblast-specific knockout of the insulin-like growth factor (IGF) receptor gene reveals an essential role of IGF signaling in bone matrix mineralization. J Biol Chem. 2002;277(46):44005-12.
27. Turner CH, Burr DB. Basic biomechanical measurements of bone: a tutorial. Bone. 1993;14(4):595-608.
28. Xiong J, Onal M, Jilka RL, Weinstein RS, Manolagas SC, O'Brien CA. Matrix-embedded cells control osteoclast formation. Nat Med. 2011;17(10):1235-41.
29. Khosla S, Oursler MJ, Monroe DG. Estrogen and the skeleton. Trends Endocrinol Metab. 2012;23(11):576-81.
30. Canalis E. Growth factor control of bone mass. J Cell Biochem. 2009;108(4):769-77.
31. Almeida M, Han L, O'Brien C A, Kousteni S, Manolagas SC. Classical genotropic versus kinase-initiated regulation of gene transcription by the estrogen receptor alpha. Endocrinology. 2006;147(4):1986-96.
32. Kousteni S, Bellido T, Plotkin LI, O'Brien CA, Bodenner DL, Han L, Han K, DiGregorio GB, Katzenellenbogen JA, Katzenellenbogen BS, Roberson PK, Weinstein RS, Jilka RL, Manolagas SC. Nongenotropic, sex-nonspecific signaling through the estrogen or androgen receptors: dissociation from transcriptional activity. Cell. 2001;104(5):719-30.
33. Lian JB, Stein JL, Stein GS, Montecino M, van Wijnen AJ, Javed A, Gutierrez S. Contributions of nuclear architecture and chromatin to vitamin D-dependent transcriptional control of the rat osteocalcin gene. Steroids. 2001;66(3-5):159-70.
34. Zhong Z, Zylstra-Diegel CR, Schumacher CA, Baker JJ, Carpenter AC, Rao S, Yao W, Guan M, Helms JA, Lane NE, Lang RA, Williams BO. Wntless functions in mature osteoblasts to regulate bone mass. Proc Natl Acad Sci U S A. 2012;109(33):E2197-204.
35. Borjesson AE, Lagerquist MK, Liu C, Shao R, Windahl SH, Karlsson C, Sjogren K, Moverare-Skrtic S, Antal MC, Krust A, Mohan S, Chambon P, Savendahl L, Ohlsson C. The role of estrogen receptor alpha in growth plate cartilage for longitudinal bone growth. J Bone Miner Res. 2010;25(12):2690-700.
36. Wang KJ, Shi DQ, Sun LS, Jiang X, Lu YY, Dai J, Chen DY, Xu ZH, Jiang Q. Association of estrogen receptor alpha gene polymorphisms with bone mineral density: a meta-analysis. Chin Med J (Engl). 2012;125(14):2589-97.
37. Lau KH, Kapur S, Kesavan C, Baylink DJ. Up-regulation of the Wnt, estrogen receptor, insulin-like growth factor-I, and bone morphogenetic protein pathways in C57BL/6J osteoblasts as opposed to C3H/HeJ osteoblasts in part contributes to the differential anabolic response to fluid shear. J Biol Chem. 2006;281(14):9576-88.
38. Price JS, Sugiyama T, Galea GL, Meakin LB, Sunters A, Lanyon LE. Role of

endocrine and paracrine factors in the adaptation of bone to mechanical loading. Curr Osteoporos Rep. 2011;9(2):76-82.
39. Sunters A, Armstrong VJ, Zaman G, Kypta RM, Kawano Y, Lanyon LE, Price JS. Mechano-transduction in osteoblastic cells involves strain-regulated estrogen receptor alpha-mediated control of insulin-like growth factor (IGF) I receptor sensitivity to Ambient IGF, leading to phosphatidylinositol 3-kinase/AKT-dependent Wnt/LRP5 receptor-independent activation of beta-catenin signaling. J Biol Chem. 2010;285(12):8743-58.

Chapter 3

ESTROGEN RECEPTOR ALPHA IN OSTEOBLAST LINEAGE CELLS REGULATES BONE MASS DIFFERENTIALLY IN BOTH SEXES AND ATTENUATES BONE'S RESPONSE TO MECHANICAL LOADING IN FEMALE MICE

3.1 Introduction

Sex hormones are important regulators of bone mass in males and females. During puberty, estrogens inhibit, while androgens stimulate, periosteal bone formation in humans, contributing to generally higher bone mass in males (1). The decline in estrogen associated with menopause is a primary contributor to post-menopausal osteoporosis in females (2-4). In men sex hormone levels also decline with age and correlate with gradual bone loss (5-7). Point mutation in estrogen receptor alpha (ERα), the primary receptor effector of estrogen in bone, caused unfused growth plates and osteoporosis in a single reported human case (8). Since then, the role of ERα in skeletal health in both males and females has been a focus (9-11).

To better understand the role of estrogen in bone cells, global ERα knockout (ERαKO) and cell-specific ERαKO mice that remove ERα at specific points in the osteoblast-osteocyte lineage were developed. However, outcomes are conflicting concerning the cortical and cancellous bone status in males and females. Global deletion of ERα increased cancellous and cortical tibial bone mineral density in females, but decreased cortical and cancellous bone mass in males (12-16). However, systemic effects that include altered hormone levels and body weight differences confound bone results in global knockouts (14, 16). When ERα was removed from osteoblast progenitors or precursors, using *Prx1*- or *Osx-Cre* mice, respectively, cortical bone mass decreased in females and young males, while cancellous bone was

unaffected (17). ERα deletion in mature osteoblasts (*OC-Cre*) decreased cortical and cancellous bone mass (18, 19), but bone mass was unchanged with deletion in committed osteoblasts in females (*Col1a1-Cre)* (17). Bone mass in young and growing male mice was unaffected by ERα deficiency in osteoblasts in both targeted knockouts. Finally, when ERα was removed from osteocytes (*Dmp-1-Cre*), female and male mice exhibited no change in or decreased bone mass, respectively (20, 21).

Bone is mechanosensitive. Bone mass can increase in response to dynamic loading, but decreases with disuse in adult animals (22, 23). In vivo rodent loading models are established methods for studying the response of cancellous and cortical bone to controlled, dynamic bone loading (24-26). Although ERα has been implicated in bone mechanotransduction (27, 28), the response to mechanical loading has not been well-studied in bone cell-specific ERαKO mice. ERα in females has no effect on bone's anabolic response to mechanical loading when removed at the osteocyte stage of the lineage (20). In male mice, the response to mechanical loading has not been reported in any bone cell-specific ERαKO mouse.

No study to date has investigated cancellous and cortical bone adaptation to mechanical loading in male and female mice generated using the *OC-Cre* to remove ERα at the stage of mature osteoblasts (pOC- ERαKO). To generate these animals and littermate controls we crossbred *OC-Cre* and ERα floxed mice. At 10 weeks of age, we subjected the left tibiae to two weeks of in vivo mechanical loading, with the right limb as an internal control, and analyzed bone mass and architecture through microCT, dynamic histomorphometry, and immuno-histochemistry (IHC). In addition, we examined bone mass, morphology, and strength of L5 vertebrae and femoral midshafts in LC and targeted animals. We hypothesized that ERα deficiency in mature osteoblasts and osteocytes would decrease bone mass in both female and male mice, and that the response to mechanical loading would be attenuated in pOC-

ERαKO mice.

3.2 Methods

3.2.1 Generation of osteoblast-specific ERαKO mice

pOC-ERαKO and littermate control (LC) mice were generated by breeding mice containing a transgene encoding *Cre* recombinase driven by the human osteocalcin promoter (*OC-Cre*, provided by Dr. Thomas Clemens, The Johns Hopkins University, Baltimore, MD) (29, 30) with mice in which exon 3 of the DNA-binding domain of the ERα gene (*Esr1*) was flanked by loxP sequences ($ER\alpha^{fl/fl}$, provided by Dr. Kahn, University of Cincinnati, Cincinnati, OH) (31). Mice were inbred to be >99% pure C57Bl/6 by speed congenics (DartMouse Speed Congenic Core Facility, Geisel School of Medicine at Dartmouth, Hanover, NH) and genotyped as described (19). Mice were housed 3-5 per cage with ad libitum access to food and water. All animal procedures were approved by Cornell University's IACUC.

3.2.2 In vivo tibial mechanical loading

At ten weeks of age, single element strain gauges (EA-06-015LA-120, Micromeasurements) were surgically attached to the tibial midshafts of female and male LC and pOC-ERαKO mice (n=5-6 per genotype). A series of cyclic compressive loads (-2 to -12N) were applied to the left and right tibiae in our custom tibial loading device, and bone stiffness was calculated from the load and strain data as previously described (32). Bone stiffness was used to calculate the peak load required to induce 1200 microstrain (με) at the tibial midshaft during compressive tibial loading. Bone stiffness was similar among pOC-ERαKO and LC male and female mice (0.00671 ± 0.0010 N/με LC female, 0.00763 ± 0.00068 N/με pOC-ERαKO female, 0.00760 ± 0.00029 N/με LC male, 0.00767 ± 0.00016 N/με pOC-ERαKO male). A peak load of -

9.0N was applied to all animals in the subsequent loading experiment.

The left tibiae of male and female LC and pOC-ERαKO mice (n=12-14 per group) were loaded in compression in vivo for 2 weeks (32). In brief, a cyclic compressive load was applied at a rate of 4Hz for 1200 cycles per day, 5 days per week, in a triangular waveform with a peak load of -9.0N, dwell of 100ms between successive load cycles, and dwell load of -0.5N.

3.2.3 Mass and serum marker measurements

Three days after the last day of mechanical loading, mice were euthanized via isoflurane overdose and cardiac puncture. Blood was stored overnight at 4°C and centrifuged at 2,000rpm for 20min to separate serum. Serum was assayed (n=8-10 per group) for estrogen (E2, females only, CalBiotech EW180S-100, Spring Valley, CA), insulin-like growth factor 1 (IGF-1, ALPCO 22-IGF-R21, Salem, NH), osteocalcin (OC, ALPCO 31-50-1300), tartrate-resistant acid phosphatase 5b (TRAP5b, IDS SB-TR103, Scottsdale, AZ), and pro-collagen I N-terminal peptide (PINP, MyBioSource 703389). Body mass and female uterine and ovarian masses were recorded at euthanasia.

3.2.4 Microcomputed tomography

At euthanasia, left and right tibiae were stored overnight in 4% paraformaldehyde or 70% ethanol and then scanned in 70% ethanol at 15μm voxel resolution (μCT35, Scanco Medical AG, Switzerland; 55kVp, 145μA, 600ms integration time). Mineralized tissue was separated from non-mineralized tissue using gender- and bone-specific thresholds. For each tibia, the metaphyseal cancellous core and cortex were analyzed separately, and the cortical midshaft analyzed as previously described (19).

Right femora and L5 vertebrae were wrapped in PBS-soaked gauze and stored at -20°C prior to microCT scanning at 15um resolution. The cancellous core and cortical shell of the vertebrae were analyzed as previously described (19). For the femur, a cortical volume of interest extending 0.5 mm, centered at the midshaft, was analyzed.

Cancellous bone outcome measures were bone volume fraction (BV/TV), trabecular thickness (Tb.Th), trabecular separation (Tb.Sp), and cancellous tissue mineral density (cn.TMD). Cortical bone outcome measures were cortical area (Ct.Ar), marrow area (Ma.Ar, tibial and femoral midshaft only), maximum and minimum moments of inertia (I_{MAX}, I_{MIN}), cortical thickness (Ct.Th), and cortical tissue mineral density (ct.TMD).

3.2.5 Dynamic histomorphometry

Ten and three days before euthanasia, mice (n=6-7 per group) received injections of calcein (30mg/kg IP). After microCT scanning, tibiae were embedded in acrylosin and sectioned by the Bone Histology/Histomorphometry Laboratory (Yale University Department of Orthopaedics and Rehabilitation, New Haven, CT). Both transverse sections of the tibial midshaft and longitudinal sections of the tibial metaphysis were analyzed to measure single and double fluorescent labels on bone surfaces (2 slides per animal, OsteomeasureXP v3.2.1.7, Osteometrics, Decatur, GA). Measurable outcomes were mineralizing surface (MS), mineral apposition rate (MAR), bone formation rate (BFR), and woven bone area (Wo.Ar).

3.2.6 Histology

Left and right tibiae not used for dynamic histomorphometry were decalcified in 10% EDTA for two weeks, processed, and embedded in paraffin (n=6-7 per group).

Tibiae were sectioned longitudinally at 6μm using a rotary microtome (Leica RM2255, Germany). Sections were stained for TRAP and pro-collagen I as previously described (19). The number of positively-stained osteoclasts (TRAP) or osteoblasts (pro-collagen I) in the cancellous metaphysis was quantified and normalized to bone surface (2 slides/animal, OsteomeasureXP v3.2.1.7). Growth plate thickness was quantified from sections stained with Safranin O/Fast Green/Alcian Blue by averaging five evenly spaced lines (2 slides per mouse, n=6 mice/group, OsteomeasureXP v3.2.1.7).

3.2.7 Mechanical testing

Prior to mechanical testing, femora and L5 vertebrae were thawed to room temperature and kept moist with PBS. Femora were testing in three-point bending to failure, and vertebrae were tested in compression to failure in the cranial-caudal direction as previously described (858 Mini Bionix, MTS, Eden Prairie, MN) (19). Whole bone strength and stiffness were determined from the load-displacement data for bending and compression.

3.2.8 Statistics

For serum, bone lengths, in vivo bone stiffness, vertebral and femoral microCT, and mechanical testing data, a one-way ANOVA was used for each sex. In comparing the loaded and control tibiae for tibial microCT, dynamic histomorphometry, histology, and IHC data, a repeated measures ANOVA with interaction was used for each sex with a Tukey HSD post-hoc test. The between-subject factor was genotype, and the within-subject factor was loaded (left) vs. control (right). Significance was set at $p<0.05$.

3.3 Results

3.3.1 Generation and characterization of pOC-ERαKO mice

To determine the role of ERα in osteoblasts in bone growth and in their response to mechanical loading, we generated male and female pOC-ERαKO and LC by mating *OC-Cre* and *ERα*$^{fl/fl}$ mice. Because the global ERαKO mouse possessed systemic effects that confound the role of ERα in bone alone (13, 14, 16, 33), we measured body weight, crown/rump length, ovarian and uterine weight (females only), tibia and femur length, and serum levels of E2 and IGF-1 (**Figure C.1, Table C.1**). All outcome measures were similar between pOC-ERαKO and LC within each sex, except for femoral length, which was greater in pOC-ERαKO males vs. LC.

3.3.2 Female pOC-ERαKO mice exhibit decreased bone mass

To assess changes in bone structure and geometry, microCT analysis was performed on the L5 vertebrae, femoral midshafts, and proximal and mid-diaphyseal control tibiae (**Table 3.1, Table 3.2**). Cancellous BV/TV was lower in pOC-ERαKO female mice by 16% in the vertebral body and by 25% in the tibial metaphysis, due to lower Tb.Th in the vertebra (-6.2%), and due to increased Tb.Sp in the tibia (+28%) (**Figure 3.1, Table 3.2**). Analogously, cortical bone at these two cortico-cancellous sites was also affected, but to a lesser extent than the cancellous tissues. In the vertebral shell, both Ct.Ar (-11%) and Ct.Th (-11%) were lower in the knockouts compared to LC. From compression testing, the lower bone mass found in both cortical and cancellous regions of the pOC-ERαKO vertebra correlated with lower compressive strength (-18%), but compressive stiffness was unchanged. The tibial metaphyseal cortical shell was 9.3% thinner in female pOC-ERαKO mice.

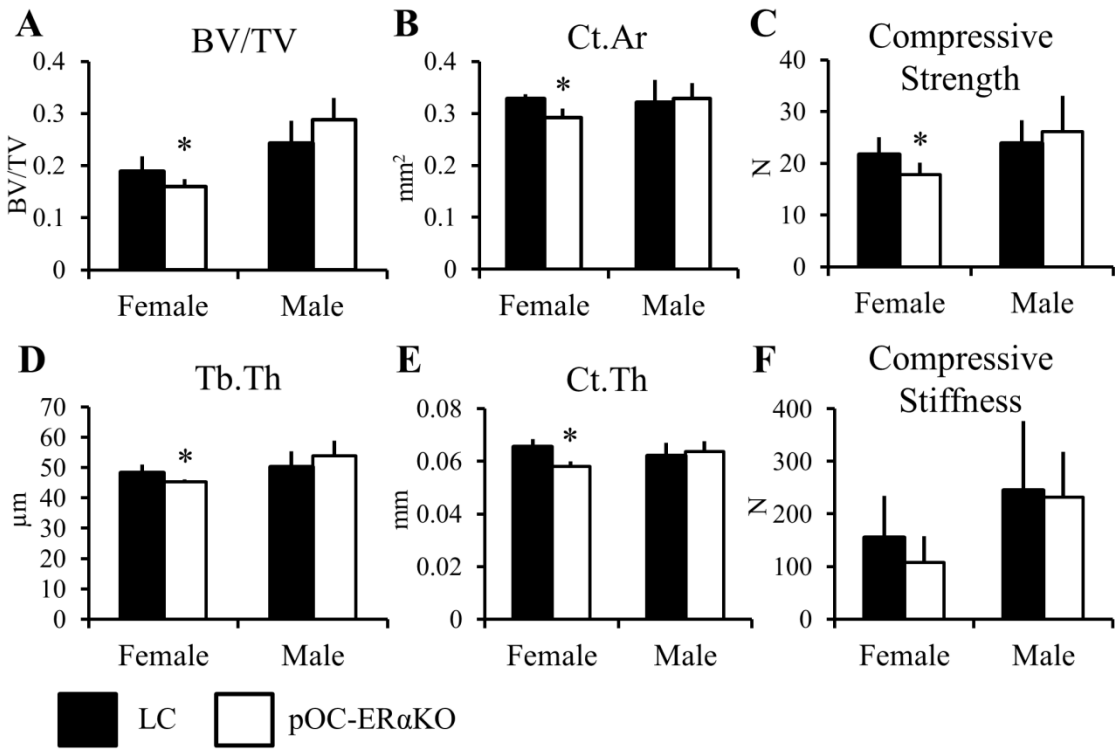

Figure 3.1 Vertebral cancellous and cortical bone morphology and strength were differentially affected by ERα deletion in osteoblasts in 12-week-old pOC-ERαKO females and males compared to LC. (A) Vertebral body BV/TV was decreased due to (D) decreased Tb.Th in female knockouts compared to LC. (A) In male pOC-ERαKO mice, BV/TV in the vertebral shell was similar between genotypes. (E) The vertebral shell had thinner cortices in female pOC-ERaKO mice compared to LC, resulting in (B) decreased Ct.Ar. Vertebral shell Ct.Ar and Ct.Th in pOC-ERaKO male mice were not different from LC. The cortical and cancellous morphology changes seen in female and male pOC-ERαKO mice contributed to (C) a decrease in compressive strength in vertebral compression tests in females, but no change in compressive strength in male knockouts or (F) in compressive stiffness in either sex.

Table 3.1 Cancellous and cortical bone in general were differentially affected by ERα deletion in 10-week-old pOC-ERαKO females and males measured by microCT in the vertebral body, vertebral shell, and femoral midshaft.

	Female		**Male**	
	LC	**pOC-ERαKO**	**LC**	**pOC-ERαKO**
BV/TV	0.189 ± 0.029	0.160 ± 0.015*	0.243 ± 0.042	0.288 ± 0.042
Tb.Th (μm)	48.3 ± 2.7	45.3 ± 0.85*	50.2 ± 5.1	53.9 ± 5.0
Tb.Sp (μm)	225 ± 21	277 ± 16	175 ± 13	158 ± 10*
cn.TMD (mg HA/cc)	632 ± 10	639 ± 7.6	646 ± 22	653 ± 17
Ct.Ar (mm^2)	0.329 ± 0.0084	0.292 ± 0.017*	0.321 ± 0.043	0.329 ± 0.029
Ct.Th (μm)	65.5 ± 3.0	58.0 ± 2.0*	62.1 ± 4.9	63.6 ± 4.0
I_{MAX} (mm^4)	0.142 ± 0.0088	0.139 ± 0.014	0.136 ± 0.019	0.141 ± 0.020
I_{MIN} (mm^4)	0.0297 ± 0.0026	0.0284 ± 0.0025	0.0333 ± 0.0073	0.0338 ± 0.0044
ct.TMD (mg HA/cc)	791 ± 7.5	787 ± 8.1	795 ± 6.3	798 ± 9.0
Ct.Ar (mm^2)	0.726 ± 0.027	0.675 ± 0.021*	0.934 ± 0.088	1.06 ± 0.097*
Ma.Ar (mm^2)	0.890 ± 0.046	0.908 ± 0.053	1.17 ± 0.096	1.24 ± 0.13
Ct.Th (mm)	0.180 ± 0.0040	0.167 ± 0.0095*	0.193 ± 0.0077	0.202 ± 0.011
I_{MAX} (mm^4)	0.195 ± 0.020	0.175 ± 0.015*	0.351 ± 0.063	0.430 ± 0.072*
I_{MIN} (mm^4)	0.107 ± 0.0077	0.103 ± 0.0072	0.167 ± 0.029	0.206 ± 0.039*
ct.TMD (mg HA/cc)	945 ± 8.9	933 ± 9.1*	925 ± 8.2	930 ± 6.8

Data are mean ± SD. BV/TV, bone volume fraction; Tb.Th, trabecular thickness; Tb.Sp, trabecular separation; cn.TMD, cancellous tissue mineral density; Ct.Ar, cortical area; Ma.Ar, marrow area; Ct.Th, cortical thickness; I_{MAX} and I_{MIN}, maximum and minimum moments of inertia; ct.TMD, cortical tissue mineral density*pOC-ERαKO different from LC, $p<0.05$ by one-factor ANOVA for each sex.

Table 3.2 Female10-week-old pOC-ERαKO mice responded more to 2 weeks of tibial compression than LC while male pOC-ERαKO mice responded similarly to LC, measured by microCT in the proximal tibia and tibial midshaft.

			Female		Male	
			LC	**pOC-ERαKO**	**LC**	**pOC-ERαKO**
Cancellous Metaphysis	BV/TV	Control	0.0779 ± 0.019	0.0584 ± 0.0095*	0.121 ± 0.041	0.162 ± 0.037*
		Loaded	0.111 ± 0.014†	0.115 ± 0.015†	0.143 ± 0.030	0.156 ± 0.016
	Tb.Th (μm)	Control	48.4 ± 2.4	46.4 ± 2.2	46.0 ± 5.2	52.4 ± 5.6*
		Loaded	67.3 ± 4.4†	74.2 ± 4.2*†	58.7 ± 3.0†	61.0 ± 5.7*†
	Tb.Sp (μm)	Control	323 ± 35	413 ± 41*	227 ± 28	225 ± 36
		Loaded	327 ± 32	436 ± 52*	225 ± 31	230 ± 36
	cn.TMD (mg HA/cc)	Control	767 ± 13	757 ± 14	765 ± 9.1	774 ± 15
		Loaded	798 ± 12†	791 ± 15†	796 ± 11†	794 ± 13†
Cortical Shell Metaphysis	Ct.Ar (mm^2)	Control	0.964 ± 0.092	0.866 ± 0.050	1.11 ± 0.12	1.18 ± 0.14
		Loaded	1.28 ± 0.097†	1.27 ± 0.049†	1.31 ± 0.084†	1.39 ± 0.11†
	Ct.Th (mm)	Control	0.141 ± 0.010	0.128 ± 0.0049*	0.134 ± 0.013	0.141 ± 0.015
		Loaded	0.179 ± 0.011†	0.174 ± 0.0090†	0.156 ± 0.0076†	0.158 ± 0.0082†
	I_{MAX} (mm^4)	Control	0.373 ± 0.055	0.339 ± 0.032	0.553 ± 0.086	0.613 ± 0.11*
		Loaded	0.534 ± 0.070†	0.540 ± 0.047†	0.670 ± 0.063†	0.771 ± 0.12*†
	I_{MIN} (mm^4)	Control	0.301 ± 0.040	0.268 ± 0.035*	0.421 ± 0.061	0.440 ± 0.061
		Loaded	0.433 ± 0.061†	0.429 ± 0.037†	0.530 ± 0.064†	0.598 ± 0.085†
	ct.TMD (mg HA/cc)	Control	833 ± 23	816 ± 19	817 ± 11	815 ± 14
		Loaded	843 ± 20†	883 ± 12†	827 ± 17	815 ± 7.8
Cortical Midshaft	Ct.Ar (mm^2)	Control	0.560 ± 0.029	0.534 ± 0.026	0.769 ± 0.080	0.823 ± 0.053*
		Loaded	0.717 ± 0.034†	0.755 ± 0.042*†	0.791 ± 0.049†	0.834 ± 0.052*†
	Ma.Ar (mm^2)	Control	0.333 ± 0.017	0.348 ± 0.021	0.432 ± 0.029	0.450 ± 0.024*
		Loaded	0.317 ± 0.028†	0.325 ± 0.027†	0.420 ± 0.030	0.465 ± 0.031*
	Ct.Th (mm)	Control	0.205 ± 0.0095	0.194 ± 0.0062	0.241 ± 0.018	0.249 ± 0.012
		Loaded	0.253 ± 0.011†	0.258 ± 0.013†	0.246 ± 0.008	0.248 ± 0.0072
	I_{MAX} (mm^4)	Control	0.0603 ± 0.0054	0.0598 ± 0.0065	0.121 ± 0.022	0.141 ± 0.017*
		Loaded	0.0926 ± 0.0098†	0.105 ± 0.0089*†	0.127 ± 0.017†	0.1474 ± 0.020*†
	I_{MIN} (mm^4)	Control	0.0505 ± 0.0034	0.0470 ± 0.0046	0.0849 ± 0.014	0.0936 ± 0.010*
		Loaded	0.0646 ± 0.0064†	0.0687 ± 0.0057†	0.0883 ± 0.010†	0.0985 ± 0.012*†
	ct.TMD (mg HA/cc)	Control	1020 ± 16	1020 ± 8.4	1040 ± 12	1050 ± 17
		Loaded	1010 ± 18†	1010 ± 12†	1040 ± 11	1050 ± 10

Data are mean ± SD. BV/TV, bone volume fraction; Tb.Th, trabecular thickness; Tb.Sp, trabecular separation; cn.TMD, cancellous tissue mineral density; Ct.Ar, cortical area; Ma.Ar, marrow area; Ct.Th, cortical thickness; I_{MAX} and I_{MIN}, maximum and minimum moments of inertia; ct.TMD, cortical tissue mineral density

*pOC-ERαKO different from LC, †Loaded tibia different from Control, $p<0.05$ by repeated measures ANOVA with interaction for each sex.

At the tibial midshaft, the non-loaded right limbs in pOC-ERαKO female mice showed no difference from LC mice in Ct.Ar, Ct.Th, I_{MAX}, I_{MIN}, or other parameters (**Table 3.2**). At the femoral midshaft, however, Ct.Ar (-7.0%) and Ct.Th (-7.3%) were lower, as were I_{MAX} and ct.TMD (-10% and –1.3%, respectively) (**Figure 3.2, Table 3.1**). These changes in bone geometry and architecture at the femoral midshaft did not correspond with changes in either maximum moment or bending stiffness in 3-point bending tests in targeted mice compared to LC.

Female pOC-ERαKO mice had similar PINP and OC but decreased TRAP5b serum levels compared to LC, probably reflecting the overall lower bone mass and therefore overall lower bone turnover in the knockouts.

3.3.3 Male pOC-ERαKO mice exhibit increased bone mass

The bone phenotype seen in male pOC-ERαKO mice compared to their littermate controls was opposite that seen in females (**Table 3.1, Table 3.2**). In the vertebral body, Tb.Sp was lower in knockouts (-9.9%) while Tb.Th remained unchanged, but these changes did not result in an overall alteration in BV/TV (**Figure 3.1**). In the right tibial metaphysis, cancellous BV/TV was greater by 34%, due largely to increased Tb.Th (+14%) (**Table 3.2**). In the cortical shell of the tibial metaphysis, pOC-ERαKO mice had larger I_{MAX} (+15%) compared to LC, but unchanged Ct.Ar, I_{MIN}, Ct.Th, and ct.TMD. The cortical shell of the vertebrae was unaffected by ERα deletion in osteoblasts and osteocytes. Compressive strength and stiffness were not different in pOC-ERαKO males compared to LC, reflecting the cortical bone mass and geometry at that site.

At two purely cortical regions, the right femoral and tibial midshafts, cortical bone mass was significantly greater in male pOC-ERαKO mice. In the femur, Ct.Ar (+14%), I_{MAX} (+23%), and I_{MIN} (+23%) were larger, which were reflected in greater

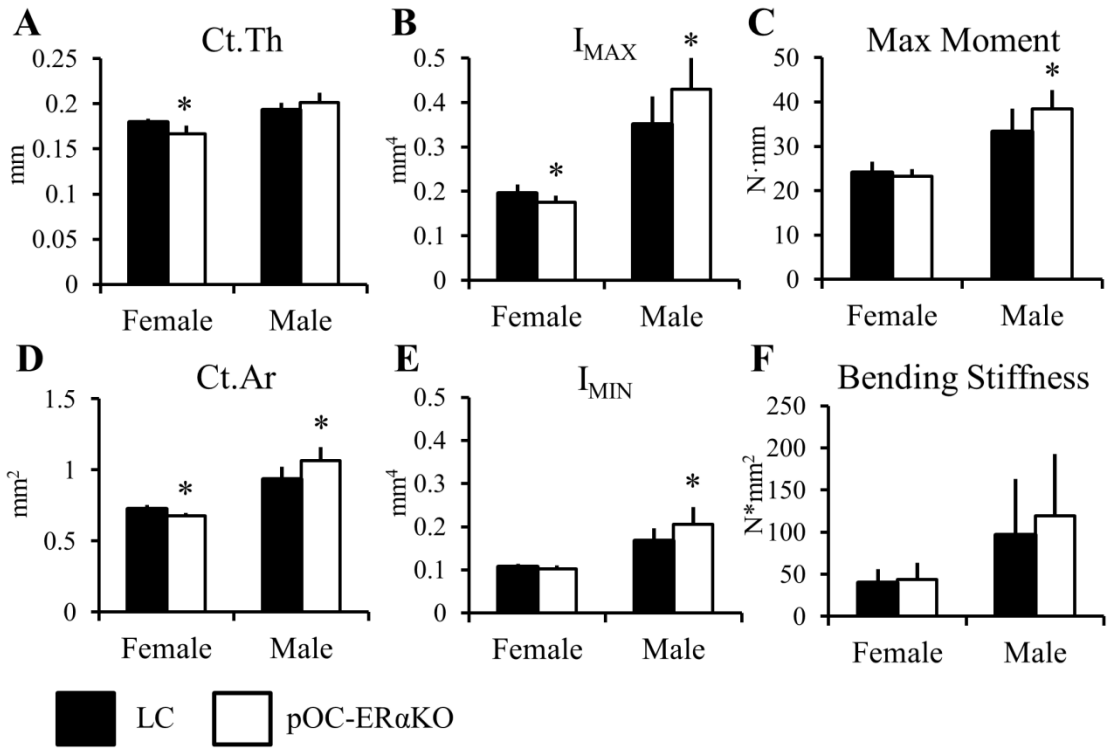

Figure 3.2 Femoral midshaft bone morphology and strength were differentially affected in 12-week-old pOC-ERαKO females and males compared to LC. Female pOC-ERαKO mice had (A) decreased Ct. Th, (D) decreased Ct.Ar , and (B) decreased I_{MAX} compared to LC. (C,F) Maximum moment and bending stiffness were not different between genotypes in females from 3-point bending mechanical tests. Male pOC-ERαKO mice exhibited an opposite bone phenotype compared to LC than that found in females. (D) Ct.Ar , (B) I_{MAX}, and (E) I_{MIN} were all increased in male pOC-ERαKO mice, which resulted in (C) increased maximum moment in 3-point bending tests. Ct.Ar, cortical area; Ct.Th, cortical thickness; I_{MAX} and I_{MIN}, maximum and minimum moments of inertia. Data are mean ± SD, n=8-12 per group. *pOC-ERαKO different from LC, $p<0.05$ by one-way ANOVA for each sex.

maximum bending moment (+15%) but no change in whole bone stiffness from bending tests (**Figure 3.2**). Similarly, at the right tibial midshaft, male pOC-ERαKO mice had larger Ct.Ar (+6.9%), I_{MAX} (+16%), and I_{MIN} (+10%).

Serum levels of PINP and TRAP5b in males were similar between genotypes. Serum osteocalcin levels were decreased in knockouts, despite the higher bone mass found in male pOC-ERαKO mice.

3.3.4 ERα in osteoblasts suppresses the anabolic response to mechanical loading in female mice

At the tibial metaphysis, cancellous bone responded robustly to mechanical loading in both LC and gene-deleted females (**Figure 3.3**). BV/TV, Tb.Th, and cn.TMD were increased after two weeks of loading (**Table 3.2**). Likewise, cancellous MS, MAR, and BFR were increased in loaded vs control limbs (**Table 3.3**). Osteoblast activity from pro-collagen I IHC normalized to bone surface was increased in loaded vs. control tibiae (**Figure 3.5**), as expected with increased bone mass (**Table 3.3**). Both BV/TV and Tb.Th increased significantly more in response to mechanical loading in mice lacking ERα in mature osteoblasts than in LC. BV/TV increased 97% in pOC-ERαKO and 43% in LC, due to increased Tb.Th (+60%, +39%, respectively). Although BV/TV was lower in knockout mice in the control limbs compared to LC, Tb.Th was not different between control right tibiae. Osteoclast number measured by TRAP histology normalized to bone surface was not affected by loading or by genotype; however systemic levels of TRAP5b were lower in female pOC-ERαKO mice compared to LC (**Figure 3.5**), most likely due to overall lower bone mass found in these animals. Serum levels of PINP were similar between genotypes (**Figure C.1**). Tibial growth plate thickness increased with loading, and was increased in control limbs of knockouts (**Table 3.3**).

Similar to the cancellous region of the tibial metaphysis, Ct.Ar, Ct.Th, I_{MAX}, I_{MIN}, and ct.TMD in the cortical shell of the tibial metaphysis increased in response to mechanical loading. Both I_{MIN} and Ct.Th were decreased in the control tibiae of pOC-ERαKO female mice compared to LC, yet these two parameters responded more to mechanical loading in pOC-ERαKO mice. I_{MIN} increased 64% in pOC-ERαKO but only 44% in LC. Ct.Th increased 37% in knockouts but 27% in LC. Ct.Ar responded similarly to mechanical loading as LC and was not different in right control limbs.

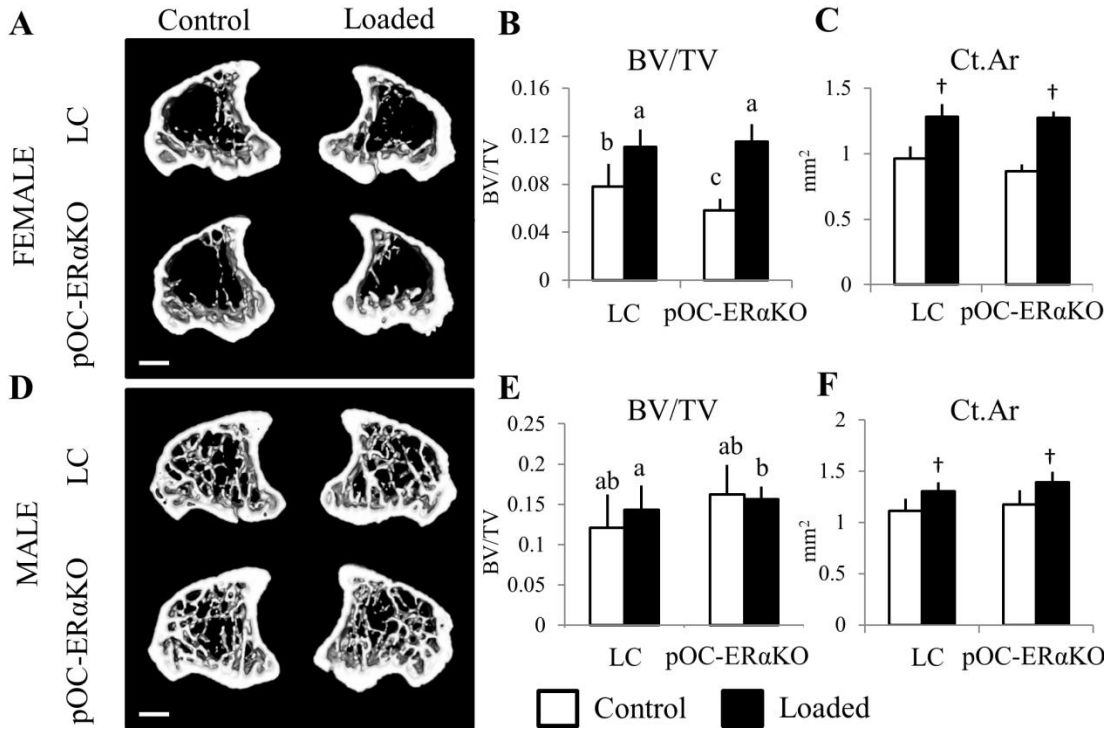

Figure 3.3 Tibial metaphyseal bone mass was in general reduced in pOC-ERαKO female mice but increased in pOC-ERαKO male mice, and pOC-ERαKO female mice responded more to 2 weeks of tibial compression. Representative transverse 3D microCT reconstructions (0.51mm thick) of the tibial metaphysis in (A) female and (D) male 12-week-old LC (top) and pOC-ERaKO mice (bottom) after 2 weeks of left tibial loading. (B) Cancellous bone in female pOC-ERaKO mice had 25% lower BV/TV in the unloaded right tibia compared to LC. After two weeks of tibial loading, BV/TV increased more (+97%) in pOC-ERaKO mice than in LC mice (+43%). (E) Male pOC-ERaKO had increased BV/TV in the tibial metaphysis compared to LC, but 2 weeks of loading did not alter BV/TV in left vs. right limbs for either genotype. (C,F) Cortical shell bone area increased similarly between genotypes within each sex after loading, and Ct.Ar was unaffected by ERα deletion in both sexes.

BV/TV, bone volume fraction; Ct.Ar, cortical area. Data are mean ± SD, n=12-14 per group. †Loaded tibia different from Control, $p<0.05$ by repeated measures ANOVA with interaction for each sex. Bars not sharing same letter are significantly different from one another from Tukey HSD post-hoc only when interaction term (load*genotype) was significant. Scale bar = 1.0mm.

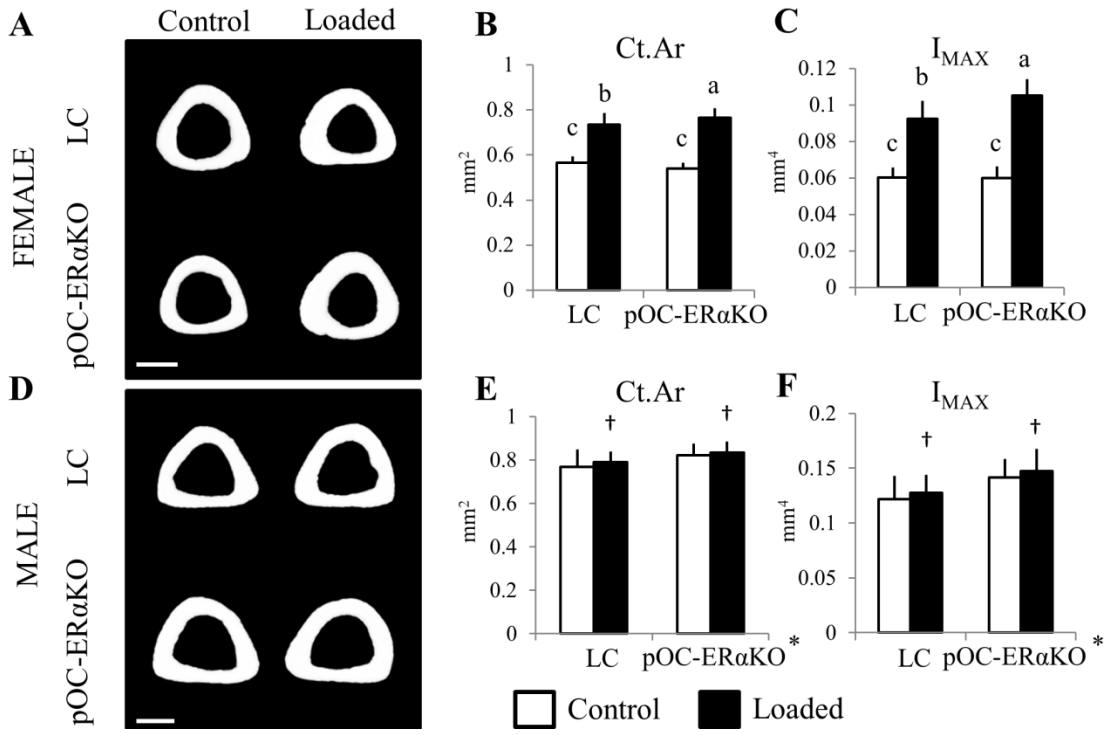

Figure 3.4 Tibial midshaft cortical bone mass was similar between pOC-ERαKO and LC mice, but knockouts responded more to 2 weeks of tibial compression; male pOC-ERαKO had increased cortical bone mass but responded similarly to loading as LC mice. Representative transverse 3D microCT reconstructions (45um thick) of the tibial midshaft in (A) female and (D) male 12-week-old LC (top) and pOC-ERaKO mice (bottom) after 2 weeks of left tibial loading. (B,C) Although Ct.Ar was not different between LC and pOC-ERaKO female mice in the right, control limb, after 2 weeks of tibial loading, Ct.Ar increased more in pOC-ERaKO mice (+41%) vs. LC (+28%), as did I_{MAX}. (E,F) Male pOC-ERaKO mice had increased Ct.Ar and I_{MAX} at the tibial midshaft in the right unloaded limbs, and both genotypes showed a similar increase in Ct.Ar and I_{MAX} after 2 weeks of mechanical loading.
Ct.Ar, cortical area; I_{MAX}, maximum moment of inertia. Data are mean ± SD, n=12-14 per group. *pOC-ERαKO different from LC, †Loaded tibia different from Control, $p<0.05$ by repeated measures ANOVA with interaction for each sex. Bars not sharing same letter are significantly different from one another from Tukey HSD post-hoc only when interaction term (load*genotype) was significant. Scale bar = 0.5mm.

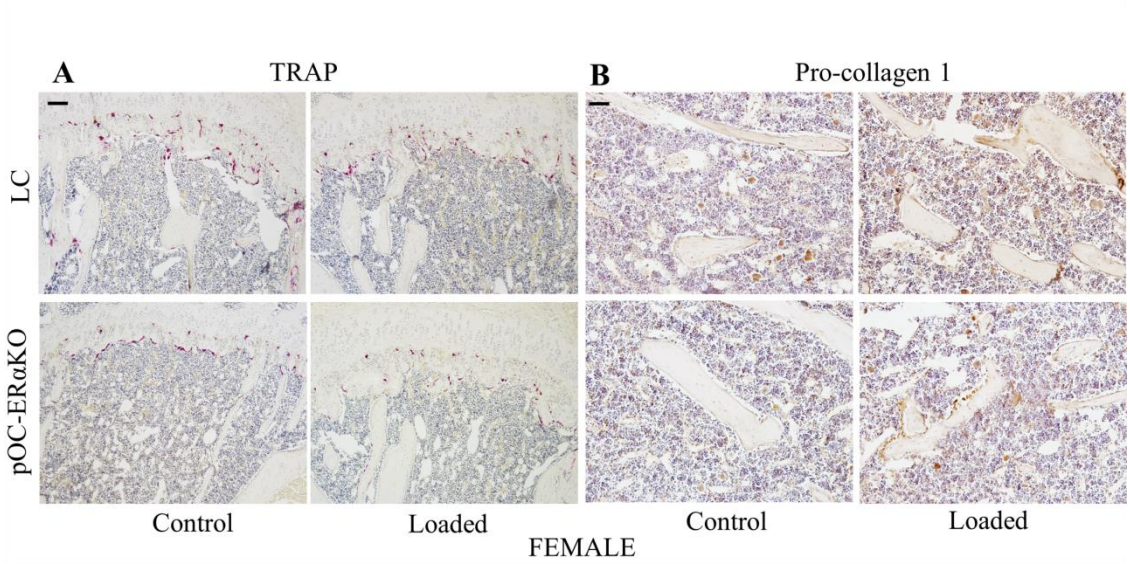

Figure 3.5 Representative IHC and histology images for sagittal sections of the proximal tibiae of LC (top) and pOC-ERαKO (bottom) female mice in loaded and control limbs. (A) N.Oc/BS was unchaged between genotypes and was not altered with 2 weeks of tibial mechanical loading in either pOC-ERαKO or LC mice. (B) N.Ob/BS increased with 2 weeks of in vivo tibial loading similarly in both genotypes. N.Ob/BS, number of osteoblasts staining positively for pro-collagen I normalized to bone surface; N.Oc/BS, number of osteoclasts staining positively for TRAP normalized to bone surface. Scale bar = 80μm for A, 20μm for B

At the tibial midshaft, female pOC-ERαKO mice responded more to mechanical loading than LC despite having similar bone architecture in contralateral limbs (**Figure 3.4**). Ct.Ar increased more in pOC-ERαKO mice (+41%) than in LC (+28%), as did I_{MAX} (+76% in pOC-ERαKO and +53% in LC) (**Table 3.2**). Ct.Th, I_{MIN}, and ct.TMD increased similarly between genotypes with two weeks of tibial loading. New bone formed on both the periosteal and endosteal surfaces of the tibial midshaft, as indicated by increased MS, MAR, and BFR at the periosteum and increased MAR and BFR at the endosteum (**Table 3.3**). As such, Ma.Ar decreased with loading (-4.9% pOC-ERαKO, -6.5% LC). Of note, woven bone formation was present at the tibial midshaft of both genotypes of female mice in response to loading, but not in the metaphysis.

3.3.5 The response to mechanical loading is unchanged in male pOC-ERαKO mice

After 2 weeks of tibial loading in male mice, cancellous trabeculae thickened (+16% pOC-ERαKO, +28% LC) and cn.TMD increasd (+2.6% pOC-ERαKO, +4.0% LC) in the loaded limb compared to the contralateral limb in both genotypes in the tibial metaphysis (**Table 3.2**). Overall BV/TV did not change with loading as in previous similar experiments with male C57Bl/6 mice (26, 34) (**Figure 3.3**). Although overall bone mass was unchanged with loading, osteoblast activity and osteoclast number normalized to bone surface were both increased in loaded vs. contralateral tibial metaphyses, as was tibial growth plate thickness (**Table 3.3, Figure 3.6**). Cancellous MS increased 12% in pOC-ERαKO and 16% in LC with loading, but MAR and BFR were unchanged (**Table 3.3**).

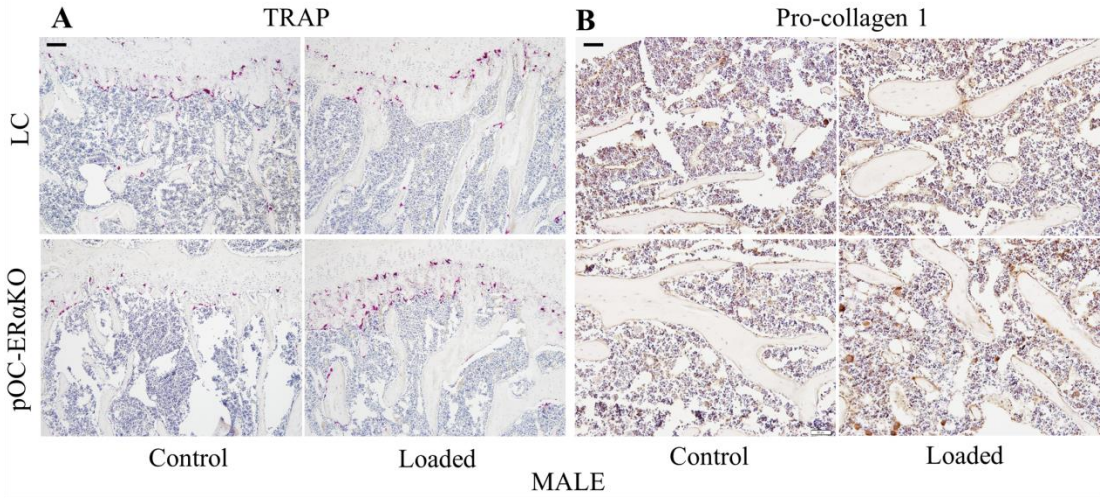

Figure 3.6 Representative IHC and histology images for sagittal sections of the proximal tibiae of LC (top) and pOC-ERαKO (bottom) male mice in loaded and control limbs. (A,B) Osteoclast number and osteoblast activity normalized to bone surface both increased after 2 weeks of in vivo tibial mechanical loading in male pOC-ERαKO and LC mice. N.Ob/BS, number of osteoblasts positively stained for pro-collagen I normalized to bone surface; N.Oc/BS, number of osteoclasts positively stained for TRAP normalized to bone surface. Scale bar = 80μm for A, 20μm for B.

In the cortical shell of the metaphysis, Ct.Ar, I_{MAX}, and I_{MIN} increased in response to 2 weeks of mechanical loading. Despite pOC-ERαKO mice having higher bone mass in the cancellous metaphysis and increased I_{MAX} in the cortical shell metaphysis, LC and pOC-ERαKO showed similar responses to in vivo tibial loading.

At the cortical tibial midshaft, Ct.Ar increased 1.4% in pOC-ERαKO with loading and 2.8% in LC (**Figure 3.4**). Most new bone formation reflected periosteal expansion, as shown through increased Per.MS and Per.MAR, but no change in Ma.Ar. However, endosteal MS increased with loading in both genotypes, while I_{MAX} and I_{MIN} also were higher. Cortical geometry in pOC-ERαKO male mice responded similarly to mechanical loading as LC mice.

3.4 Discussion

We generated 10-week-old female and male mice lacking ERα in mature osteoblasts and osteocytes by breeding $ER\alpha^{fl/fl}$ and *OC-Cre* mice. Serum measurements, bone length, and growth plate analyses revealed that systemic effects were not present in females and limited in males, who showed decreased serum osteocalcin levels and increased femur length. When ERα was removed in mature osteoblasts, cancellous and cortical bone mass were lower at most sites in females; in contrast, pOC-ERαKO male mice in general showed increased cancellous and cortical bone mass. When mice were subjected to two weeks of in vivo mechanical tibial loading, female pOC-ERαKO mice formed more bone in response to loading than LC. In contrast, genotype did not affect the skeletal response to mechanical loading in males.

ERα in osteoblasts clearly has a role in bone mass accrual and its response to mechanical loading, depending upon the stage of deletion. Our previous work and that

of Määttä *et al.*, found similar reduced bone mass in female mice when ERα was deleted in mature osteoblasts using the OC-Cre-driven promoter (18, 19). Määttä *et al.* did not find genotype differences in males, except at 6 months of age, at which time tibial BV/TV and Tb.N were lower in knockouts. Of note, our current study examined 10-week-old mice, whereas the Määttä study analyzed older mice at 3.5, 6, and 12 months of age. In addition, genetic background can profoundly affect bone structure and mass (35, 36). Our mice were backcrossed fully to a C57Bl/6 background, whereas the background of Määttä, *et al.* was not reported.

ERα mediates mechanosensitivity in bone. In osteoblast cultures, cells lacking ERα responded less to mechanical strain (37). Similarly, the response to mechanical loading was decreased in global ERαKO female mice compared to controls, but has not been widely studied yet in bone cell-specific ERαKO mice of either sex (12). In the present study, when ERα is deleted in mature osteoblasts and osteocytes using the *OC-Cre* promoter, female pOC-ERαKO mice showed an increased anabolic response to tibial loading compared to controls, whereas male knockouts responded similarly to LC. In contrast, lack of ERα osteoctyes did not alter cortical bone's anabolic response to mechanical loading in female mice, pointing to a critical role of ERα in osteoblasts in the female skeletal response to increased mechanical loading (20). However, Kondoh *et al.* performed hindlimb unloading in Dmp1-ERαKO female mice and showed an accelerated loss of bone mass compared to littermate controls (21). Coupled with our data, ERα in osteoblasts but not osteocytes regulates the magnitude of bone's response to loading, but ERα in osteocytes regulates bone mass during disuse. Whether mechanical stimuli are increased or decreased, the absence of ERα in mature osteoblasts or osteoctyes enhances sensitivity to the loading environment in ER-deficient bone (38).

During puberty, sex steroids promote bone growth and are major contributors

to sexual skeletal dimorphism in humans (1). Later in puberty, estrogen suppresses periosteal apposition and leads to growth plate fusion in both sexes (38, 39). Adult males have greater bone mass due to a prolonged puberty and high testosterone levels that increase periosteal apposition (40). In pOC-ERαKO male mice, because the growth-suppressive effects of estrogen do not act on mature osteoblasts or osteocytes via ERα, the stimulating effects of testosterone on bone growth may be enhanced and might help to explain the higher bone mass phenotype found in these animals. Females lacking an estrogenic response via ERα in mature osteoblasts may accrue bone mass during growth more slowly resulting in the decreased bone mass found in female pOC-ERαKO mice.

The formation of woven bone in response to mechanical loading at both the periosteal and endosteal surfaces of the tibial midshaft in female pOC-ERαKO and LC mice is a limitation of this study, as we aimed to analyze lamellar bone formation from skeletal loading. A peak load of -9.0N was required to produce 1200με at the midshaft cortex, and similar load levels have been used previously for mouse tibial loading (32, 41). Following mechanical loading, the amount and variety of differentially expressed genes depends on whether lamellar or woven bone is being generated (42). The possible effects of woven vs. lamellar bone on data interpretation from the current study cannot be discounted. However, female pOC-ERαKO also responded more to mechanical loading in the proximal tibiae, where woven bone was not present, indicating that ERα does regulate the skeletal response to mechanical loading during accrual of lamellar bone. Bone mass in the proximal tibiae of pOC-ERαKO female mice was lower than that of LC mice. Because load levels were normalized for a target strain level at the cortical midshaft, a site at which bone mass and stiffness were similar between genotypes, we cannot distinguish whether the increased response to mechanical load in the cancellous tissues of the female pOC-

ERαKO was caused purely by genotypic effects or a combination of genotype and different strains in the cancellous tissues of the knockouts relative to the LC.

Use of a cre-recombinase driven by the OC promoter (pOC) has been widely used in the literature (30). Although the *OC-Cre* mouse has been a tool to knockout specific receptors and proteins in mature osteoblasts and subsequent osteocytes, *cre* expression has been detected in the growth plate (43). Previously in our mixed background strain of female pOC-ERαKO mice, we found no differences in growth plate thickness or in tibial or femoral lengths compared to LC (19). However, in the current animals, on a pure C57Bl/6 background, female pOC-ERαKO mice had thicker tibial growth plates but no differences in tibial or femoral bone length. In contrast, growth plate thickness was not different in pOC-ERαKO males, yet femoral length was increased and tibial length was unaffected. Määttä *et al.* found increased tibial lengths in male pOC-ERαKO mice at 3 months of age (18). These results are difficult to interpret, as mouse growth plates never fuse and cannot be directly correlated to the actions of human growth plates. OC-Cre expression in the growth plate may affect growth plate thickness and bone length. However, overall body mass and crown/rump length were not altered in pOC-ERαKO mice of either sex.

Because declining sex hormones contribute greatly to osteoporosis in the elderly, especially post-menopausal women who have severely decreased estrogen levels, recent research has focused on understanding the role of estrogen signaling via its receptors in bone (9, 44). Here ERα in mature osteoblasts and osteocytes differentially regulated bone mass in males and females. Removing ERα increased the skeletal response to mechanical loading at cortical and cancellous sites in females, but did not affect skeletal adaption to physical stimuli in male mice. Further research should emphasize elucidating the cellular mechanisms and signaling pathways involved in estrogen signaling in bone, which may provide valuable insight into the

pathogenesis of osteoporosis.

3.5 References

1. Callewaert F, Sinnesael M, Gielen E, Boonen S, Vanderschueren D. Skeletal sexual dimorphism: relative contribution of sex steroids, GH-IGF1, and mechanical loading. J Endocrinol. 2010;207(2):127-34.
2. Richelson LS, Wahner HW, Melton LJ, 3rd, Riggs BL. Relative contributions of aging and estrogen deficiency to postmenopausal bone loss. N Engl J Med. 1984;311(20):1273-5.
3. Riggs BL. Endocrine causes of age-related bone loss and osteoporosis. Novartis Found Symp. 2002;242:247-59; discussion 60-4.
4. Eastell R. Role of oestrogen in the regulation of bone turnover at the menarche. J Endocrinol. 2005;185(2):223-34.
5. Khosla S, Amin S, Orwoll E. Osteoporosis in men. Endocr Rev. 2008;29(4):441-64.
6. Callewaert F, Boonen S, Vanderschueren D. Sex steroids and the male skeleton: a tale of two hormones. Trends Endocrinol Metab. 2010;21(2):89-95.
7. Falahati-Nini A, Riggs BL, Atkinson EJ, O'Fallon WM, Eastell R, Khosla S. Relative contributions of testosterone and estrogen in regulating bone resorption and formation in normal elderly men. J Clin Invest. 2000;106(12):1553-60.
8. Smith EP, Boyd J, Frank GR, Takahashi H, Cohen RM, Specker B, Williams TC, Lubahn DB, Korach KS. Estrogen resistance caused by a mutation in the estrogen-receptor gene in a man. N Engl J Med. 1994;331(16):1056-61.
9. Price JS, Sugiyama T, Galea GL, Meakin LB, Sunters A, Lanyon LE. Role of endocrine and paracrine factors in the adaptation of bone to mechanical loading. Curr Osteoporos Rep. 2011;9(2):76-82.
10. Vico L, Vanacker JM. Sex hormones and their receptors in bone homeostasis: insights from genetically modified mouse models. Osteoporos Int. 2010;21(3):365-72.
11. Khosla S. Pathogenesis of age-related bone loss in humans. J Gerontol A Biol Sci Med Sci. 2013;68(10):1226-35.
12. Lee KC, Jessop H, Suswillo R, Zaman G, Lanyon LE. The adaptive response of bone to mechanical loading in female transgenic mice is deficient in the absence of oestrogen receptor-alpha and -beta. J Endocrinol. 2004;182(2):193-201.
13. Vidal O, Lindberg M, Savendahl L, Lubahn DB, Ritzen EM, Gustafsson JA, Ohlsson C. Disproportional body growth in female estrogen receptor-alpha-inactivated mice. Biochem Biophys Res Commun. 1999;265(2):569-71.
14. Lindberg MK, Alatalo SL, Halleen JM, Mohan S, Gustafsson JA, Ohlsson C. Estrogen receptor specificity in the regulation of the skeleton in female mice. J Endocrinol. 2001;171(2):229-36.
15. Vidal O, Lindberg MK, Hollberg K, Baylink DJ, Andersson G, Lubahn DB, Mohan S, Gustafsson JA, Ohlsson C. Estrogen receptor specificity in the regulation of

skeletal growth and maturation in male mice. Proc Natl Acad Sci U S A. 2000;97(10):5474-9.
16. Parikka V, Peng Z, Hentunen T, Risteli J, Elo T, Vaananen HK, Harkonen P. Estrogen responsiveness of bone formation in vitro and altered bone phenotype in aged estrogen receptor-alpha-deficient male and female mice. Eur J Endocrinol. 2005;152(2):301-14.
17. Almeida M, Iyer S, Martin-Millan M, Bartell SM, Han L, Ambrogini E, Onal M, Xiong J, Weinstein RS, Jilka RL, O'Brien CA, Manolagas SC. Estrogen receptor-alpha signaling in osteoblast progenitors stimulates cortical bone accrual. J Clin Invest. 2013;123(1):394-404.
18. Maatta JA, Buki KG, Gu G, Alanne MH, Vaaraniemi J, Liljenback H, Poutanen M, Harkonen P, Vaananen K. Inactivation of estrogen receptor alpha in bone-forming cells induces bone loss in female mice. FASEB J. 2012.
19. Melville KM, Kelly NH, Khan SA, Schimenti JC, Ross FP, Main RP, van der Meulen MC. Female mice lacking estrogen receptor-alpha in osteoblasts have compromised bone mass and strength. J Bone Miner Res. 2014;29(2):370-9.
20. Windahl SH, Borjesson AE, Farman HH, Engdahl C, Moverare-Skrtic S, Sjogren K, Lagerquist MK, Kindblom JM, Koskela A, Tuukkanen J, Divieti Pajevic P, Feng JQ, Dahlman-Wright K, Antonson P, Gustafsson JA, Ohlsson C. Estrogen receptor-alpha in osteocytes is important for trabecular bone formation in male mice. Proc Natl Acad Sci U S A. 2013;110(6):2294-9.
21. Kondoh S, Inoue K, Igarashi K, Sugizaki H, Shirode-Fukuda Y, Inoue E, Yu T, Takeuchi JK, Kanno J, Bonewald LF, Imai Y. Estrogen receptor alpha in osteocytes regulates trabecular bone formation in female mice. Bone. 2014;60:68-77.
22. Cavolina JM, Evans GL, Harris SA, Zhang M, Westerlind KC, Turner RT. The effects of orbital spaceflight on bone histomorphometry and messenger ribonucleic acid levels for bone matrix proteins and skeletal signaling peptides in ovariectomized growing rats. Endocrinology. 1997;138(4):1567-76.
23. Jones HH, Priest JD, Hayes WC, Tichenor CC, Nagel DA. Humeral hypertrophy in response to exercise. J Bone Joint Surg Am. 1977;59(2):204-8.
24. Turner CH, Akhter MP, Raab DM, Kimmel DB, Recker RR. A noninvasive, in vivo model for studying strain adaptive bone modeling. Bone. 1991;12(2):73-9.
25. De Souza RL, Matsuura M, Eckstein F, Rawlinson SC, Lanyon LE, Pitsillides AA. Non-invasive axial loading of mouse tibiae increases cortical bone formation and modifies trabecular organization: a new model to study cortical and cancellous compartments in a single loaded element. Bone. 2005;37(6):810-8.
26. Fritton JC, Myers ER, Wright TM, van der Meulen MC. Loading induces site-specific increases in mineral content assessed by microcomputed tomography of the mouse tibia. Bone. 2005;36(6):1030-8.
27. Lee KC, Lanyon LE. Mechanical loading influences bone mass through estrogen receptor alpha. Exerc Sport Sci Rev. 2004;32(2):64-8.
28. Ehrlich PJ, Noble BS, Jessop HL, Stevens HY, Mosley JR, Lanyon LE. The effect of in vivo mechanical loading on estrogen receptor alpha expression in rat ulnar osteocytes. J Bone Miner Res. 2002;17(9):1646-55.
29. Clemens TL, Tang H, Maeda S, Kesterson RA, Demayo F, Pike JW, Gundberg

CM. Analysis of osteocalcin expression in transgenic mice reveals a species difference in vitamin D regulation of mouse and human osteocalcin genes. J Bone Miner Res. 1997;12(10):1570-6.
30. Zhang M, Xuan S, Bouxsein ML, von Stechow D, Akeno N, Faugere MC, Malluche H, Zhao G, Rosen CJ, Efstratiadis A, Clemens TL. Osteoblast-specific knockout of the insulin-like growth factor (IGF) receptor gene reveals an essential role of IGF signaling in bone matrix mineralization. J Biol Chem. 2002;277(46):44005-12.
31. Dupont S, Krust A, Gansmuller A, Dierich A, Chambon P, Mark M. Effect of single and compound knockouts of estrogen receptors alpha (ERalpha) and beta (ERbeta) on mouse reproductive phenotypes. Development. 2000;127(19):4277-91.
32. Lynch ME, Main RP, Xu Q, Walsh DJ, Schaffler MB, Wright TM, van der Meulen MC. Cancellous bone adaptation to tibial compression is not sex dependent in growing mice. J Appl Physiol (1985). 2010;109(3):685-91.
33. Couse JF, Curtis SW, Washburn TF, Lindzey J, Golding TS, Lubahn DB, Smithies O, Korach KS. Analysis of transcription and estrogen insensitivity in the female mouse after targeted disruption of the estrogen receptor gene. Mol Endocrinol. 1995;9(11):1441-54.
34. Fritton JC, Myers ER, Wright TM, van der Meulen MC. Bone mass is preserved and cancellous architecture altered due to cyclic loading of the mouse tibia after orchidectomy. J Bone Miner Res. 2008;23(5):663-71.
35. Beamer WG, Donahue LR, Rosen CJ, Baylink DJ. Genetic variability in adult bone density among inbred strains of mice. Bone. 1996;18(5):397-403.
36. Wergedal JE, Sheng MH, Ackert-Bicknell CL, Beamer WG, Baylink DJ. Genetic variation in femur extrinsic strength in 29 different inbred strains of mice is dependent on variations in femur cross-sectional geometry and bone density. Bone. 2005;36(1):111-22.
37. Lee K, Jessop H, Suswillo R, Zaman G, Lanyon L. Endocrinology: bone adaptation requires oestrogen receptor-alpha. Nature. 2003;424(6947):389.
38. Riggs BL, Khosla S, Melton LJ, 3rd. Sex steroids and the construction and conservation of the adult skeleton. Endocr Rev. 2002;23(3):279-302.
39. Wakley GK, Schutte HD, Jr., Hannon KS, Turner RT. Androgen treatment prevents loss of cancellous bone in the orchidectomized rat. J Bone Miner Res. 1991;6(4):325-30.
40. Turner RT, Colvard DS, Spelsberg TC. Estrogen inhibition of periosteal bone formation in rat long bones: down-regulation of gene expression for bone matrix proteins. Endocrinology. 1990;127(3):1346-51.
41. Holguin N, Brodt MD, Sanchez ME, Kotiya AA, Silva MJ. Adaptation of tibial structure and strength to axial compression depends on loading history in both C57BL/6 and BALB/c mice. Calcif Tissue Int. 2013;93(3):211-21.
42. McKenzie JA, Bixby EC, Silva MJ. Differential gene expression from microarray analysis distinguishes woven and lamellar bone formation in the rat ulna following mechanical loading. PLoS One. 2011;6(12):e29328.
43. Xiong J, Onal M, Jilka RL, Weinstein RS, Manolagas SC, O'Brien CA. Matrix-embedded cells control osteoclast formation. Nat Med. 2011;17(10):1235-41.
44. Borjesson AE, Lagerquist MK, Liu C, Shao R, Windahl SH, Karlsson C,

Sjogren K, Moverare-Skrtic S, Antal MC, Krust A, Mohan S, Chambon P, Savendahl L, Ohlsson C. The role of estrogen receptor alpha in growth plate cartilage for longitudinal bone growth. J Bone Miner Res. 2010;25(12):2690-700.

Chapter 4

INHIBITING BMP2/4 SIGNALING INCREASES CANCELLOUS BONE MASS IN FEMALE OSTEOBLAST-SPECIFIC ERα KNOCKOUT MICE AND REDUCES BONE'S RESPONSE TO MECHANICAL LOADING

4.1 Introduction

Estrogen helps regulate bone mass throughout life in both sexes (1, 2). Late in puberty in females, estrogen levels rise to suppress periosteal apposition and enhance endosteal resorption, contributing to the skeletal sexual dimorphism that results in lower peak bone mass in women on average (3). Postmenopausal women, due in part to low estrogen bioavailability, are especially susceptible to osteoporosis and subsequent fracture (4). Classical estrogen signaling in bone is mediated mainly through estrogen receptors ERα and ERβ, which can be involved in further intracellular signaling or can bind to estrogen response elements to directly facilitate gene transcription in the nucleus (5). Because of osteopenia found in a male patient with an inactivating mutation of ERα (6) and reports correlating ERα polymorphisms with bone mineral density and osteoporosis (7, 8), the role of ERα signaling in bone is of particular interest. Multiple pathways have been proposed to interact with ERα in bone, including IGF-1, BMP, and wnt/β-catenin (9-11).

Knockout mouse models are valuable tools for elucidating the role of ERα in bone, but basal bone phenotype results vary among mouse models. In global ERαKO female mouse models, both increased and decreased cortical and cancellous bone mass were reported (12-14). When ERα was deleted at the osteoblast progenitor or precursor stage, cortical bone mass was decreased but cancellous bone mass was unchanged (15). Previously, we and others bred mice lacking ERα in mature osteoblasts and osteoctyes (pOC-ERαKO) (16, 17). In general, female pOC-ERαKO

mice had decreased bone mass compared to littermate controls (LC), while male knockouts had increased bone mass compared to LC. In osteocyte-specific ERαKO female mice, cancellous bone mass was shown to be decreased or maintained, but cortical bone mass was unaffected (18, 19). Furthermore, the response to in vivo mechanical loading was enhanced in female pOC-ERαKO mice in both cortical and cancellous bone (Melville In Review), while the response to loading in osteocyte-specific ERαKO female mice was similar to controls (19). These loading results are in conflict with those from global ERαKO mice, which showed a decreased response to mechanical loading (14, 20), and with exercise studies in postmenopausal women, whose bones were not as mechanoresponsive as estrogen-replete women (21). The effects of removing ERα from the entire body vs. one cell type elicit varying results, supporting the complexity of ERα signaling.

Bone morphogenetic proteins (BMPs) were first discovered as initiators of ectopic bone formation and are members of the TGF-β super family of growth factors. When activated by a BMP, a type II receptor phosphorylates a type I receptor, resulting in Smad 1,5,8 phosphorylation (22). Phosphorylated Smad 1,5,8 (pSmad1/5/8) binds with Smad 4 and this complex mediates gene transcription directly. Secreted by virtually all cells of the body, BMPs are critically involved in cellular development and growth. In bone, BMPs can enhance fracture healing and aid in osteoblastogenesis and osteoclastogensis (23, 24). Furthermore, mechanical stimulation both in vitro and in vivo differentially regulated the expression of BMPs and their receptors (25, 26).

BMPR1a, a type I receptor in BMP signaling, is especially important in bone. When BMPR1a was removed from osteoblasts and osteoclasts in cell-specific KO mice, bone mass was increased through both decreased bone formation and bone resorption, suggesting that signaling through this receptor promotes bone formation

(27, 28). RAP-661, a decoy receptor for BMPR1a, binds with high affinity to BMP-2 and BMP-4, both highly expressed in the skeleton. When administered for 1-6 weeks, RAP-661 increased bone mineral density and bone mass in wildtype mice in a dose- and time-dependent manner (29). Although BMP signaling has been shown to interact with ERα in bone, much of the evidence is in vitro (30-32). The interactions among ERα, BMP signaling, and mechanical loading are not well researched in vivo.

We hypothesized that blocking BMP2/4 signaling through BMPR1a would increase bone mass in pOC-ERαKO and LC females to a similar extent, and that bone mass would increase in response to mechanical loading less in animals in which BMP2/4 signaling is blocked. We bred female pOC-ERαKO and LC mice. At 10 weeks of age, all animals underwent 2 weeks of daily in vivo tibial mechanical loading. Half of the animals from each genotype were injected twice weekly with RAP-661, while the remaining half received an IgG placebo control. Changes in bone mass and architecture from drug administration were determined through micro-computed tomography (microCT) of the L5 vertebra and femur. Also, whole bone strength and stiffness were measured through whole bone mechanical tests. To determine the interactions among osteoblastic ERα, BMPR1a, and mechanical loading, microCT of the cortico-cancellous tibial proximal metaphysis and the cortical tibial midshaft were analyzed. Osteoblast and osteoclast activity were measured at the proximal tibia from immunohistochemistry.

4.2 Methods

4.2.1 Generation of osteoblast-specific ERαKO mice

pOC-ERαKO and littermate control (LC) mice were generated by breeding mice containing a transgene encoding *Cre* recombinase driven by the human osteocalcin promoter (*OC-Cre*, provided by Dr. Thomas Clemens, The Johns Hopkins

University, Baltimore, MD) (33, 34) with mice in which exon 3 of the DNA-binding domain of the ERα gene (*Esr1*) is flanked by loxP sequences ($ER\alpha^{fl/fl}$, provided by Dr. Kahn, University of Cincinnati, Cincinnati, OH) (35). All mice were inbred to the C57Bl/6 strain and genotyped as described (17). Mice were housed 3-5 per cage with ad libitum access to food and water. All animal procedures were approved by Cornell University's Institutional Animal Care and Use Committee.

4.2.2 In vivo tibial mechanical loading

The left tibiae of female LC and pOC-ERαKO mice (n=20 per group) were loaded in compression in vivo 5 days per week for 2 weeks as described previously (36). In brief, a cyclic compressive load was applied at a rate of 4Hz for 1200 cycles per day, 5 days per week, in a triangular waveform with a peak load of -7.0N. A dwell of 100ms at -0.5N was inserted between each load, and the dwell-to-peak time was 75ms. A peak load of -9.0N corresponded to 1200ue at the tibial midshaft from strain gauging but induced woven bone at the tibial midshaft (*Chapter 3*). Therefore, the current experimental mice were loaded at -7.0N. Twice weekly, mice received injections of either RAP-661, a receptor decoy for Type 1 BMP Receptors, (IP, 5 mg/kg, n=10 per group) or a placebo (IgG, IP, 5 mg/kg, n=10 per group) (ref Pearsall). Body mass was recorded daily to monitor well-being. Crown/rump lengths were measured at euthanasia.

4.2.3 Microcomputed tomography

After euthanasia by CO_2 inhalation, left and right tibiae were fixed in 4% paraformaldehyde for 24 hours, and then scanned in 70% ethanol at 15um voxel resolution (μCT35, Scanco Medical AG, Switzerland; 55kVp, 145μA, 600ms integration time). For each tibia, the cancellous core and cortical shell of the

metaphysis scans were separated and analyzed separately, and the cortical midshaft was also analyzed as previously described (17).

Right femora and L5 vertebrae were wrapped in PBS-soaked gauze and stored at -20°C prior to microCT scanning at 15um resolution. To analyze the scans, the cancellous core and cortical shell of the vertebrae and the cortical femoral midshaft were analyzed as previously described (Melville under review).

Cancellous bone outcome measures were bone volume fraction (BV/TV), trabecular thickness (Tb.Th), trabecular separation (Tb.Sp), and cancellous tissue mineral density (cn.TMD). Cortical bone outcome measures were cortical area (Ct.Ar), marrow area (Ma.Ar, tibial and femoral midshaft only), total area (T.Ar, tibial and femoral midshaft only), maximum and minimum moments of inertia (I_{MAX}, I_{MIN}), cortical thickness (Ct.Th), and cortical tissue mineral density (ct.TMD). Mineralized tissue was separated from non-mineralized tissue with bone site-specific thresholds.

4.2.4 Histology

After microCT scanning, left and right tibiae were decalcified in 10% EDTA for two weeks, processed, and embedded in paraffin (n=7 per group). Tibiae were sectioned longitudinally at 6µm using a rotary microtome (Leica RM2255, Germany). Sections were stained for TRAP and pro-collagen I as previously described (17). The number of positively-stained osteoclasts (TRAP) or osteoblasts (pro-collagen I) in the cancellous metaphysis was quantified and normalized to bone surface (2 slides/animal, OsteomeasureXP v3.2.1.7). Growth plate thickness was quantified from sections stained with Safranin O/Fast Green/Alcian Blue by averaging five evenly spaced lines (2 slides per mouse, n=7 mice/group, OsteomeasureXP v3.2.1.7).

4.2.5 Mechanical testing

Prior to mechanical testing, femora and L5 vertebrae were thawed to room temperature and kept moist with PBS. Femora were tested in three-point bending to failure, and vertebrae were tested in compression to failure in the cranial-caudal direction as previously described (858 Mini Bionix, MTS, Eden Prairie, MN) (17). Whole bone strength and stiffness were determined from the load-displacement data for bending and compression.

4.2.6 Statistics

For bone lengths, vertebral and femoral microCT, and mechanical testing data, a two-factor (drug, genotype) ANOVA with interaction was used with a Tukey HSD post-hoc test. For tibial microCT, histology, and IHC data, a repeated measures two-factor ANOVA with interaction was used with a Tukey HSD post-hoc test. The between-subject factors were drug and genotype, and the within-subject factor was loaded/left vs. control/right. Significance was set at $p<0.05$.

4.3 Results

4.3.1 Blocking BMP2/4 signaling increased bone mass and strength in vertebra but not femur

At 10 weeks of age, we administered either RAP-661 drug or IgG control placebo (5mg/kg, IP) twice weekly to female pOC-ERαKO and LC mice. After 2 weeks of treatment, the L5 vertebra and femoral midshaft were evaluated by microCT (**Table 4.1, Figure 4.1**). In the cancellous vertebral core, RAP-661 increased BV/TV (+47% LC, +54% pOC-ERαKO) through both trabecular thickening (+26% LC, +27% pOC-ERαKO) and decreased trabecular separation (-11% LC, -8.9% pOC-ERαKO). Cn.TMD was also significantly increased (+7.1% LC, +7.7% pOC-ERαKO).

Analogous to cancellous changes, in the cortical shell of the vertebra RAP-661 increased all measured parameters: Ct.Ar (+11% LC, +22% pOC-ERαKO), Ct.Th (+20%, LC only), I_{MAX} (+31%, LC only), I_{MIN} (+9.1% LC, +15% pOC-ERαKO), and ct. TMD (+2.9% LC, +1.6% pOC-ERαKO). Because of the drug's effects on both compartments of the coricocancellous vertebra, vertebral strength was increased 38% in LC and 54% in pOC-ERαKO from whole bone compression tests. The increase in vertebral strength was similar between genotypes.

In contrast, in the purely cortical region of the femoral midshaft, RAP-661 treatment did not affect bone mass or strength. Overall Ct.Ar, I_{MAX}, I_{MIN}, and ct.TMD were not altered by blocking BMP2/4 signaling. Two weeks of drug treatment were osteogenic at the endocortical surface, as evident from increased Ct.Th (+8.2%, LC only) due to decreased Ma.Ar (-11%, LC only). Femoral strength and stiffness, measured from whole bone mechanical testing, were unaltered by RAP-661 treatment in both genotypes.

4.3.2 Effects of RAP-661 are partially mediated by ERα in osteoblasts

Cell-specific removal of ERα from mature osteoblasts and osteocytes decreased cortical and cancellous bone mass in female mice as shown by us and others (16, 17). We endeavored to determine if RAP-661 would increase bone mass in pOC-ERαKO animals to a similar extent as LC. In agreement with previous work, placebo-treated pOC-ERαKO female mice had decreased BV/TV (-13%) from decreased Tb.Th (-6.9%) in the cancellous vertebral core, along with decreased Ct.Ar (-8.6%) and ct.TMD (-0.61%) in the vertebral cortical shell (**Figure 4.1, Table 4.1**). Similarly, pOC-ERαKO mice had decreased femoral midshaft Ct.Th (-1.2%) and ct.TMD (-0.39%), but no change in Ct.Ar or moment of inertia compared to LC.

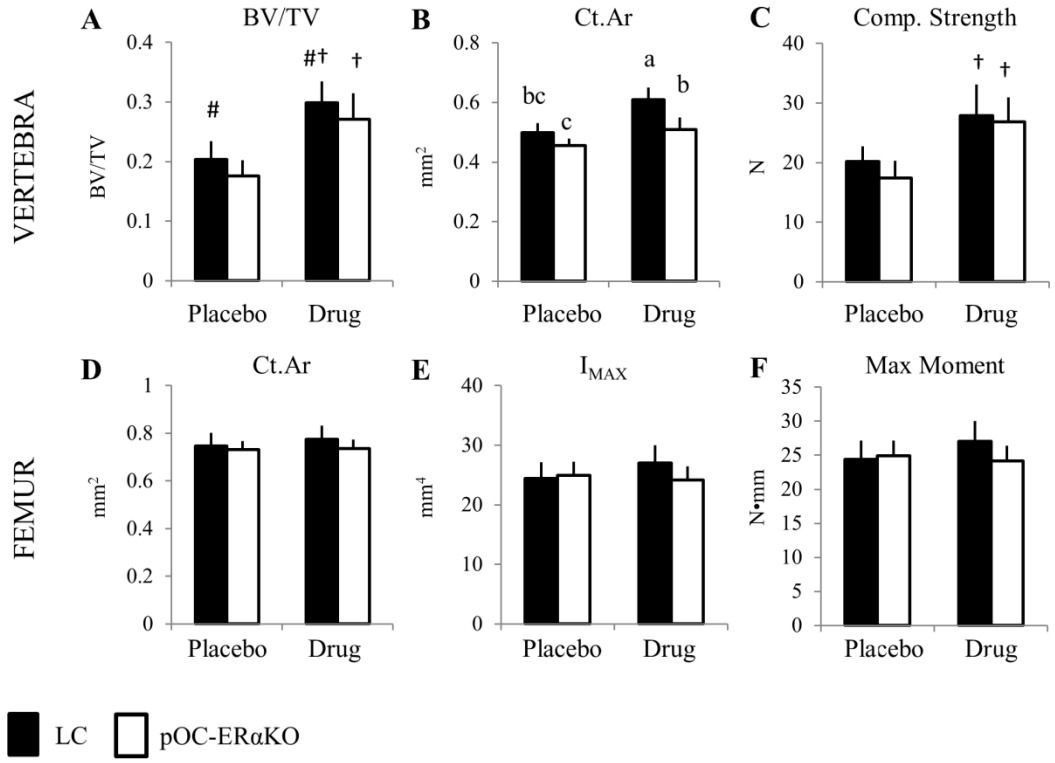

Figure 4.1 RAP-661 and ERα deletion in osteoblasts had differential effects in vertebra and femur from microCT analysis and whole bone mechanical tests in 10-week-old pOC-ERaKO and LC female mice. (A) In the vertebra, cancellous BV/TV was reduced in pOC-ERaKO mice, while RAP-661 treatment increased BV/TV markedly in both genotypes. (B) RAP-661 increased Ct.Ar in the cortical shell more in LC than pOC-ERaKO mice. (C) RAP-661 treatment increased vertebral whole bone strength in both genotypes to a similar extent. In the femur, RAP-661 had no effect on (D) Ct.Ar, (E) IMAX, or (F) maximum moment from whole bone tests. pOC-ERaKO mice were similar to LC mice in all three parameters in the femur.

BV/TV, bone volume fraction; Ct.Ar, cortical area; Comp. Strength, compressive strength; I_{MAX}, maximum moment of inertia; Max, maximum
[#]pOC-ERαKO different from control in corresponding drug-treatment group,
[†]drug-treated different from control in corresponding genotype;
groups not sharing the same letter above bars are significantly different from one another from a Tukey HSD post-hoc where a>b>c.

Table 4.1 Cancellous and cortical parameters measured by microCT for the L5 vertebra and right femoral midshaft in 10-week-old pOC-ERαKO and LC mice injected with either placebo or RAP-661

		Placebo		RAP-661	
		LC	**pOC-ERαKO**	**LC**	**pOC-ERαKO**
Vertebral Body	BV/TV	0.203 ± 0.031	0.176 ± 0.027$^{\#}$	0.299 ± 0.036†	0.271 ± 0.0.044$^{\dagger\#}$
	Tb.Th (μm)	52.9 ± 3.1	49.2 ± 3.4$^{\#}$	66.7 ± 2.9†	62.6 ± 1.4$^{\dagger\#}$
	Tb.Sp (μm)	245 ± 18	236 ± 17	218 ± 26†	215 ± 32†
	cn.TMD (mg HA/cc)	612 ± 18	604 ± 16	656 ± 6.1†	650 ± 9.3†
Vertebral Shell	Ct.Ar (mm^2)	0.498 ± 0.032	0.455 ± 0.024	0.609 ± 0.042†	0.509 ± 0.040$^{\dagger\#}$
	Ct.Th (μm)	84.5 ± 2.9	80.6 ± 4.7	101 ± 3.4†	88.1 ± 3.9$^{\dagger\#}$
	I_{MAX} (mm^4)	0.244 ± 0.034	0.217 ± 0.021	0.320 ± 0.042†	0.238 ± 0.048$^{\#}$
	I_{MIN} (mm^4)	0.0592 ± 0.010	0.0502 ± 0.0051$^{\#}$	0.0645 ± 0.0079†	0.0579 ± 0.0070$^{\#\dagger}$
	ct.TMD (mg HA/cc)	710 ± 8.8	705 ± 11$^{\#}$	730 ± 7.1†	717 ± 14$^{\dagger\#}$
Femoral Midshaft	Ct.Ar (mm^2)	0.747 ± 0.054	0.732 ± 0.034	0.775 ± 0.057	0.736 ± 0.039
	Ma.Ar (mm^2)	0.933 ± 0.075	0.928 ± 0.040	0.828 ± 0.072†	0.903 ± 0.059
	Ct.Th (μm)	181 ± 7.9	179 ± 6.7	196 ± 10†	182 ± 11$^{\#}$
	I_{MAX} (mm^4)	0.208 ± 0.030	0.200 ± 0.021	0.199 ± 0.031	0.197 ± 0.016
	I_{MIN} (mm^4)	0.116 ± 0.017	0.114 ± 0.0074	0.113 ± 0.015	0.112 ± 0.0090
	ct.TMD (mg HA/cc)	948 ± 6.1	944 ± 4.9$^{\#}$	955 ± 15	936 ± 18$^{\#}$

Data are represented as mean ± SD. BV/TV, bone volume fraction; Tb.Th, trabecular thickness; Tb.Sp, trabecular separation; cn.TMD, cancellous tissue mineral density; Ct.Ar, cortical area; Ma.Ar, marrow area; Ct.Th, cortical thickness; I_{MAX} and I_{MIN}, maximum and minimum moments of inertia; ct.TMD, cortical tissue mineral density

$^{\#}$pOC-ERαKO different from LC; †drug different from placebo, $p<0.05$ by repeated measures two-factor ANOVA withinteraction.

Even though RAP-661 increased bone mass and strength in the vertebra, the effects were somewhat genotype-dependent in the cortical shell. Vertebral Ct.Ar and Ct.Th both increased after 2 weeks of drug treatment, but the effects were greater in LC than in pOC-ERαKO mice. Vertebral I_{MAX} was only enhanced by RAP-661 in LC mice. The cancellous core of the vertebra was affected similarly by RAP-661 in both genotypes. At the femoral midshaft, genotype and drug had little effect on bone mass and architecture. Drug treatment increased Ct.Th and decreased Ma.Ar in LC mice only, suggesting only an endosteal effect. Although blocking BMP2/4 signaling increased bone mass, when ERα was absent in osteoblasts and osteocytes, some of the osteogenic effects of RAP-661 were attenuated.

4.3.3 RAP-661 increases bone mass in the cancellous tibial metaphysis but not the cortical tibial metaphysis or cortical midshaft

The bone-building effects of RAP-661 treatment were bone-specific, as evidenced by the increased bone mass in the vertebra but not femur in 10-week-old LC and pOC-ERαKO mice after 2 weeks of treatment. However, the bone effects varied by site even within a single bone from microCT analysis. Comparing the right control tibiae, RAP-661 increased cancellous metaphyseal BV/TV (+60% LC, +68% pOC-ERαKO) due to increased Tb.Th (+19% LC, +18% pOC-ERαKO) **(Figure 4.2, Figure 4.3, Table 4.2**). Cancellous TMD was also increased after 2 weeks of drug treatment, but only in LC animals (+4.3%). The increase in cancellous bone mass appeared to be largely due to decreased osteoclast number rather than increased osteoblast number from TRAP histology and pro-collagen I IHC (**Table 4.3, Figure 4.4**). N.Oc/BS was decreased in control tibiae after 2 weeks of treatment, while RAP-661 did not alter N.Ob/BS. In contrast, in the cortical shell of the tibial metaphysis and the cortical tibial midshaft, bone mass and architecture in right control limbs were

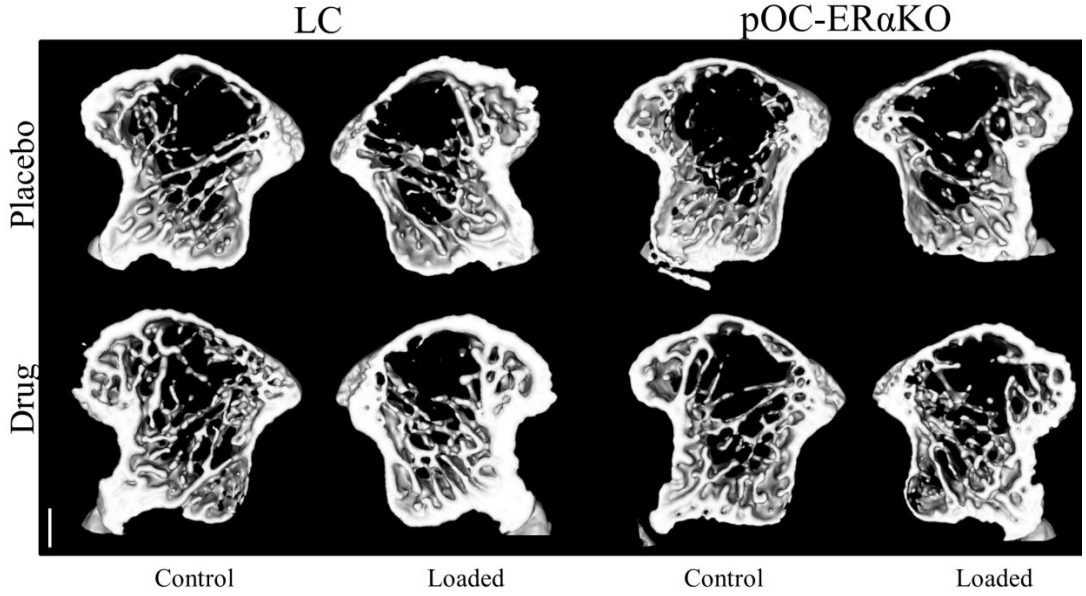

Figure 4.2 Cancellous BV/TV and Ct.Ar were increased with RAP-661 treatment over placebo in both genotypes. Representative images are reconstructed from tibial metaphyseal microCT scans of RAP-661- and placebo-treated 10-week-old pOC-ERaKO and LC female mice after 2 weeks of daily left tibial loading. Mechanical loading increased Ct.Ar more in placebo animals than drug-treated animals for both genotypes, but BV/TV was only increased with loading in pOC-ERαKO placebo animals. Scale bar = 0.5mm, section thickness = 0.51mm.

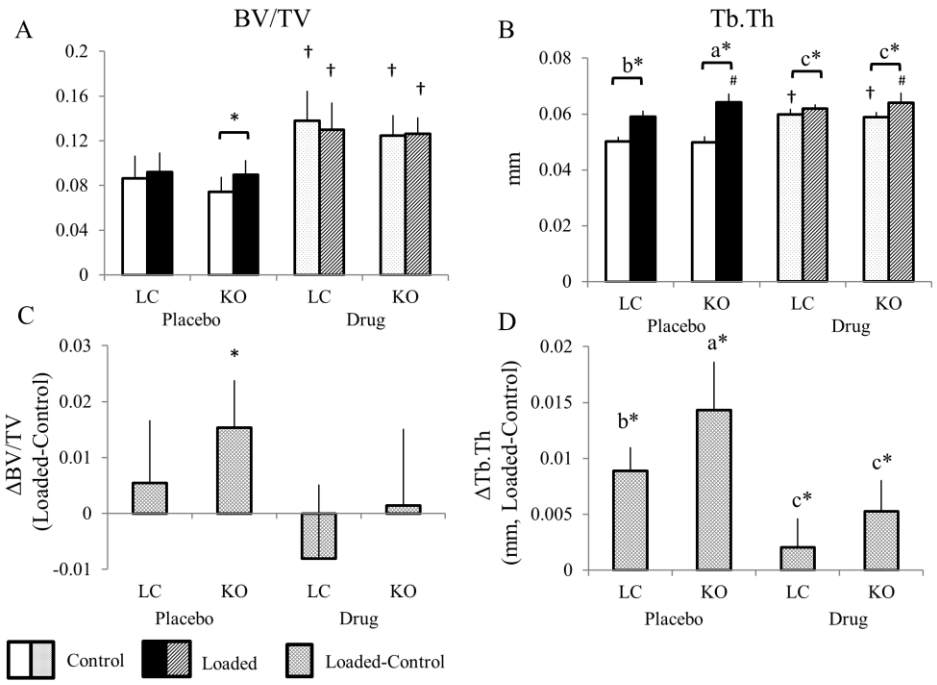

Figure 4.3 RAP-661 drug treatment increased (A) BV/TV in both limbs and (B) Tb.Th in control limbs for 10-week-old female pOC-ERaKO and LC mice from microCT analysis at the tibial metaphysis. Two weeks of daily tibial compression increased (C) BV/TV in placebo-treated pOC-ERaKO mice and (D) Tb.Th in placebo-treated animals of both genotypes. Loading increased Tb.Th more in pOC-ERaKO than LC mice.

Data are mean ± SD for BV/TV, bone volume fraction (A) and Tb.Th, trabecular thickness (B), as well as respective (Loaded-Control) paired differences (C,D).
*loaded greater than control in corresponding genotype and drug-treatment group, $^{\#}$pOC-ERαKO different from LC in corresponding limb and drug-treatment group, †drug-treated different from placebo in corresponding genotype and limb; groups not sharing the same letter above bars are significantly different from one another from a Tukey HSD post-hoc where a>b>c.

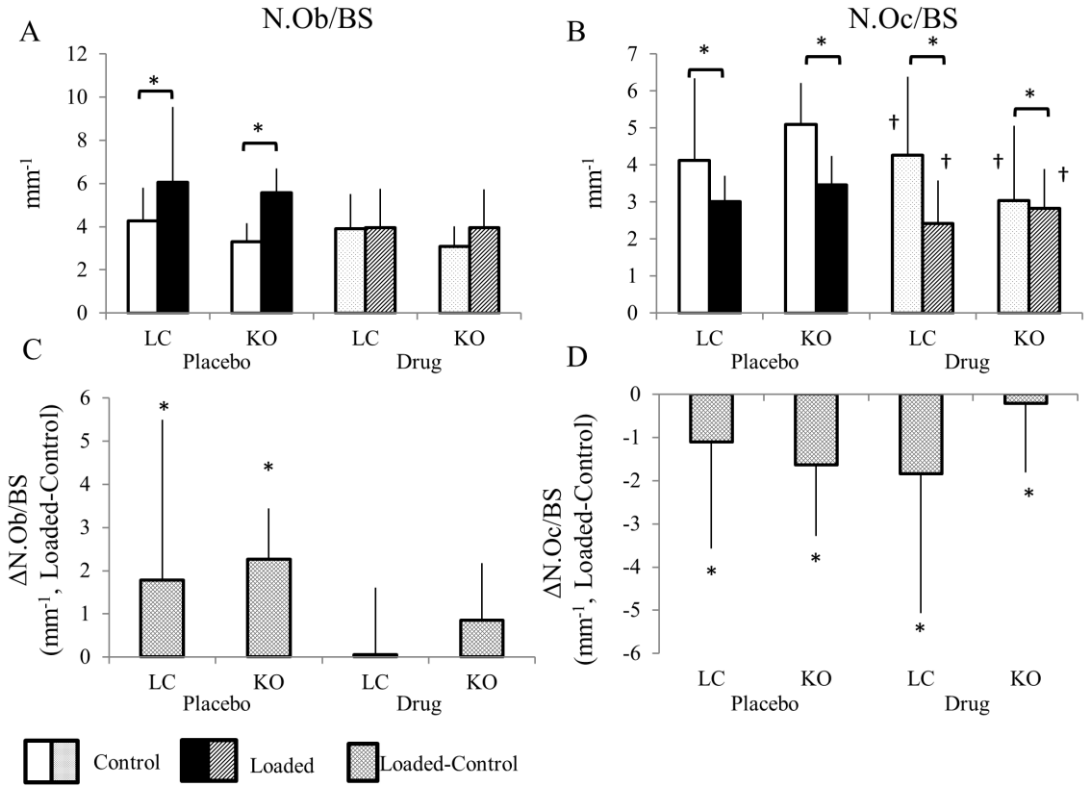

Figure 4.4 RAP-661 treatment decreased osteoclast number but did not affect osteoblast number. Numbers of both cell types were altered with 2 weeks of in vivo tibial loading. (A, C) N.Ob/BS of the cancellous metaphysis was increased with in vivo loading in 10-week-old pOC-ERaKO and LC mice in placebo groups but not in RAP-661 drug-treated groups, measured from pro-collagen I immunohistochemistry. (B,D) N.Oc/BS was decreased in placebo- and RAP-661-treated groups after in vivo loading of both genotypes from TRAP histology. Drug treatment also decreased N.Oc/BS in both pOC-ERaKO and LC.

Data are mean ± SD for N.Ob/BS, number of osteoblasts normalized to bone surface; and N.Oc/BS, number of osteoclasts normalized to bone surface; as well as respective (Loaded-Control) paired differences (C,D).
*loaded different from control in corresponding genotype and drug-treatment group,
†drug-treated different from placebo in corresponding genotype and limb.

Table 4.2 Histology and immunohistochemistry data for the proximal tibia after 2 weeks of left tibial daily loading in 10-wk female pOC-ERαKO and LC mice injected with either placebo or RAP-661

		LC	pOC-ERαKO	LC	pOC-ERαKO
N.Ob/BS	Control	4.27 ± 1.5	3.31 ± 0.84	3.89 ± 1.6	3.09 ± 0.91
	Loaded	6.05 ± 3.5*	5.56 ± 1.1*	3.94 ± 1.8	3.95 ± 1.8
N.Oc/BS	Control	4.12 ± 2.2	5.10 ± 1.1	4.26 ± 2.1†	3.04 ± 2.0†
	Loaded	3.01 ± 0.70*	3.47 ± 0.78*	2.42 ± 1.2*†	2.83 ± 1.1*†

Data are represented as mean ± SD.
*loaded different from control; #pOC-ERαKO different from LC; †drug different from placebo, $p<0.05$ by repeated measures two-factor ANOVA withinteraction

not affected when BMP2/4 signaling was blocked.

4.3.4 RAP-661-treated animals respond less to daily in vivo tibial compression than placebo controls

Because BMPs were upregulated after in vivo and in vitro bone loading, we wanted to see if blocking BMP2/4 signaling would have an effect on how bone responded to in vivo tibial loading with and without ERα signaling in osteoblasts. We subjected pOC-ERαKO and LC female mice to two weeks of daily left tibial compression, while treating animals twice weekly with either RAP-661 or placebo. As has been shown previously, 2 weeks of loading increased cancellous and cortical bone mass in the tibial metaphysis and tibial midshaft in placebo-treated animals. However, RAP-661-treated animals responded differently than their placebo controls, and the loading-drug interactions varied by bone site.

In the cancellous compartment of the tibial metaphysis, 2 weeks of loading increased BV/TV, Tb.Th, and cn.TMD in placebo animals compared to the right control limbs (**Table 4.2, Figure 4.2, Figure 4.3**). However, placebo animals responded more to loading than RAP-661-treated animals. Tb.Th increased 18% in LC and 29% in pOC-ERαKO placebo animals, but only 3.4% in LC and 9.0% in pOC-

ERαKO drug-treated animals. Similarly, cn.TMD increased 2.9% in LC and 4.1% in pOC-ERαKO placebo animals, but only 1.2% in LC and 2.1% in pOC-ERαKO drug-treated animals. Overall BV/TV did not change with loading in drug-treated-animals, and increased 21% in the pOC-ERαKO placebo animals but not in the LC placebo animals. While N.Oc/BS decreased with loading in both treatment groups, N.Ob/BS increased only in placebo animals, suggesting that the drug treatment affected bone formation with loading but not bone resorption with loading (**Figure 4.4**).

Analogous to the cancellous compartment, the cortical shell of the tibial metaphysis responded to loading more in placebo animals than RAP-661-treated animals. After 2 weeks of loading, Ct.Ar, Ct.Th, I_{MAX}, and I_{MIN} all increased in loaded limbs compared to control limbs in placebo animals in both LC and pOC-ERαKO mice (**Figure 4.2, Figure 4.5, Table 4.2**). However, tibial loading increased Ct.Ar, I_{MAX}, and I_{MIN} more in placebo animals than in drug-treated animals for both genotypes, while Ct.Th increased similarly in both treatment groups. For example, Ct.Ar increased 16% in LC 21% in pOC-ERαKO placebo animals with loading, but only 11% in LC and 13% in pOC-ERαKO animals. In contrast, mechanical loading increased ct.TMD in drug-treated groups similarly (+1.5% LC, +1.3% pOC-ERαKO) but had no effect in placebo animals.

Although bone mass was increased at the cortical midshaft with two weeks of tibial loading, the loading effects at this site were not drug-dependent (**Figure 4.6**). Ct.Ar, Ct.Th, I_{MAX}, and I_{MIN} all responded similarly to in vivo loading in placebo and drug-treated LC and pOC-ERαKO mice. ct.TMD and Ma.Ar were unaltered with loading, regardless of treatment group or genotype. Interestingly, the loading effects in RAP-661 treated animals were dampened in the tibial metaphysis but not the midshaft.

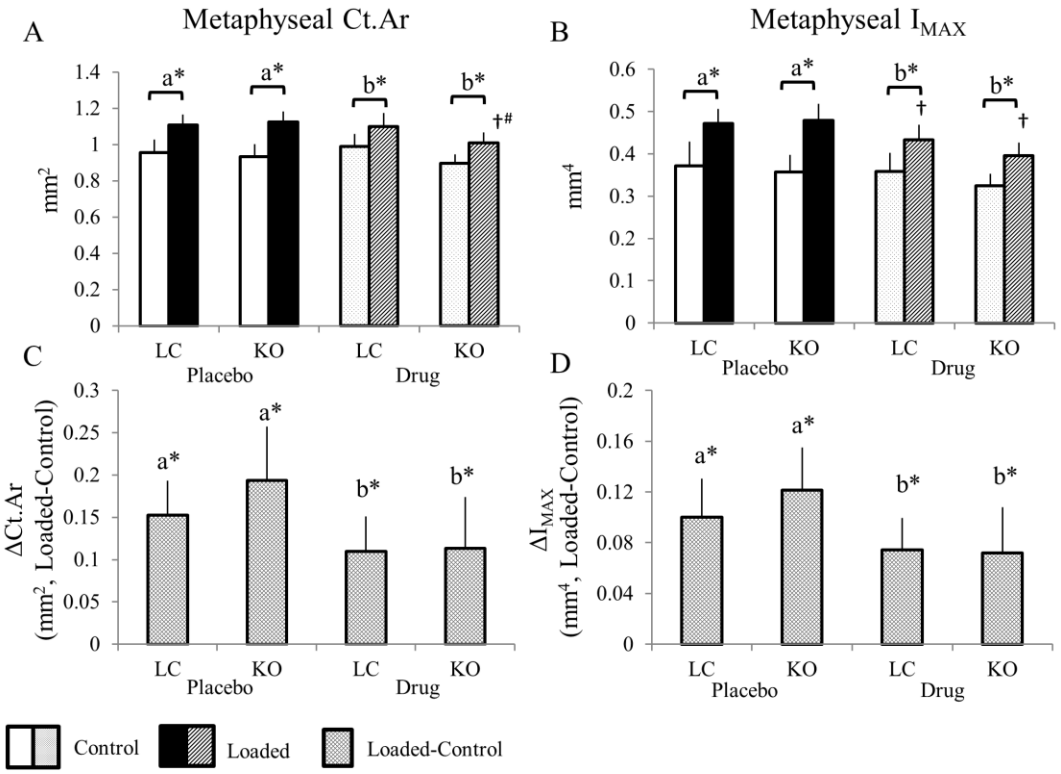

Figure 4.5 (A,B) In the cortical shell of the metaphysis, bone mass increased in 10-week-old pOC-ERaKO and LC female in response to 2 weeks of daily tibial loading from microCT analysis. (C,D) The load-induced increases in Ct.Ar and IMAX were less in RAP-661 drug-treated animals than placebo-treated animals.

Data are mean ± SD. Ct.Ar, cortical area; I_{MAX}, maximum moment of inertia. *loaded different from control in corresponding genotype and drug-treatment group, #pOC-ERαKO different from LC in corresponding limb and drug-treatment group, †RAP661 drug-treated different from placebo in corresponding genotype and limb; groups not sharing the same letter above bars are significantly different from one another from a Tukey HSD post-hoc where a>b>c

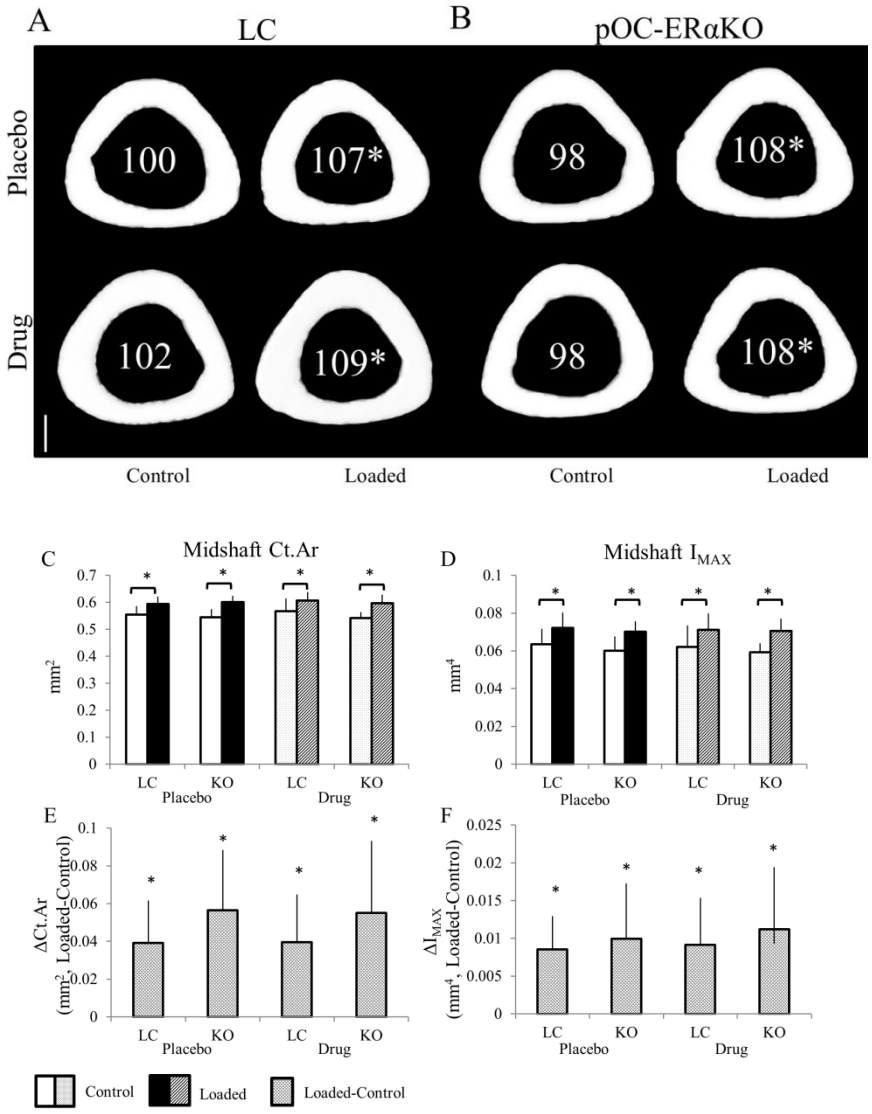

Figure 4.6 Daily tibial loading for two weeks increased Ct.Ar and I_{MAX} in RAP-661- and placebo-treated 10-week-old pOC-ERaKO and LC female mice similarly. (A,B) Representative transverse images are reconstructed from tibial midshaft microCT scans.
Numbers indicate Ct.Ar relative to value in LC, placebo, control limb (100).
*loaded different from control in same genotype and treatment group; section thickness = 45 um; scale bar = 0.25mm.

RAP-661-treated and placebo-treated 10-week-old pOC-ERaKO and LC female mice responded similarly to 2 weeks of daily in vivo tibial loading from microCT analysis at the cortical midshaft for both (C,E) Ct.Ar and (D,F) I_{MAX}. RAP-661 drug treatment did not affect either genotype at this location.

Data are mean ± SD. Ct.Ar, cortical area; I_{MAX}, maximum moment of inertia.
*loaded different from control in corresponding genotype and drug-treatment group.

4.4 Discussion

This work is the first to examine how blocking BMPR1a signaling and removing ERα in osteoblasts affect bone's response to mechanical loading in vivo. At 10 weeks of age, pOC-ERαKO and LC female mice were mechanically loaded in vivo for 5 days a week for 2 weeks in the left tibia with the contralateral limbs as control. Half of the animals in each genotype were administered RAP-661, a soluble BMPR1a receptor that prevents BMP2/4 signaling in bone, twice weekly while the other half received an IgG-matched control during the loading experiment. We found that administering RAP-661 increased bone mass in the cancellous tibial metaphysis and vertebral cortical shell and cancellous body, but not in the cortical tibial metaphysis, tibial midshaft, or femoral midshaft. In addition, the anabolic response to tibial loading was reduced in the cortical and cancellous metaphysis in drug-treated animals, but was normal at the tibial midshaft (**Table 4.4**).

Table 4.3 Two weeks of tibial loading increased bone mass at the tibial metaphysis and tibial midshaft in 10-week-old pOC-ERαKO and LC female mice, as indicated by p-values from a two-factor repeated measures ANOVA. RAP-661 drug treatment only affected the cancellous metaphysis, resulting in significantly increased bone mass over placebo values. In general, placebo-treated animals in the cancellous metaphysis responded more to loading than RAP-661-treated animals. At the tibial midshaft, drug and genotype had no effect.

		Geno	Drug	Load	Geno* Drug	Load* Geno	Load* Drug	Load Geno* Drug
Canc Metaph	BV/TV	N.S.	**<0.0001***	**0.0244***	N.S.	**0.0143***	**0.0012***	N.S.
	Tb.Th	**0.0201***	**<0.0001***	**<0.0001***	N.S.	**0.0001***	**<0.0001***	N.S.
	Tb.Sp	**0.0069***	**0.0008***	N.S.	N.S.	N.S.	N.S.	**0.0053***
	cn.TMD	N.S.	**0.0005***	**<0.0001***	**0.0016***	N.S.	**0.0019***	N.S.
IHC	N.Oc/BS	N.S.	**0.0306***	**0.0472***	0.0904	N.S.	N.S.	N.S.
	N.Ob/BS	N.S.	0.0605	**0.0452***	N.S.	N.S.	**0.0304***	N.S.
Cort Metaph Shell	Ct.Ar	**0.0191***	N.S.	**<0.0001***	**0.0272***	N.S.	**0.0010***	N.S.
	Ct.Th	**0.0078***	N.S.	**<0.0001***	0.0648	N.S.	**0.0026***	0.078
	Imax	N.S.	**0.0013***	**<0.0001***	N.S.	N.S.	**0.0005***	N.S.
	Imin	0.0908	**0.0009***	**<0.0001***	0.0541	N.S.	**0.0001***	N.S.
	ct.TMD	0.0509	N.S.	**0.0034***	0.0658	N.S.	**<0.0001***	N.S.
Cortical Midshaft	Ct.Ar	N.S.	N.S.	**<0.0001***	N.S.	N.S.	N.S.	N.S.
	Ma.Ar	N.S.	0.0663	N.S.	N.S.	N.S.	0.0711	N.S.
	Ct.Th	N.S.	0.0823	**<0.0001***	N.S.	0.0506	N.S.	N.S.
	Imax	N.S.	N.S.	**<0.0001***	N.S.	N.S.	N.S.	N.S.
	Imin	N.S.	N.S.	**<0.0001***	N.S.	N.S.	N.S.	N.S.
	ct.TMD	N.S.	N.S.	N.S.	N.S.	0.0856	N.S.	N.S.

Previously, RAP-661 increased bone mass in the tibial metaphysis in growing C57Bl/6 mice in a time- and dose-dependent manner (29). In the present study, RAP-661 drug treatment also dramatically increased bone mass in the vertebra and cancellous tibial metaphysis along with increased strength in the vertebra, but had no effect at the femoral or cortical midshafts. Our results are consistent with conditional BMPR1a knockout mouse models. In mice with BMPR1a removed from postnatal osteoblasts, bone mass was decreased early in life but increased in adult animals compared to controls (27). In mice with tamoxifen-induced osteoblast-specific ablation of BMPR1a, trabecular bone mass was increased at both 21 days and 22 months of age, while femoral midshaft bone mass was not affected (37). The differential effects of BMPR1a in corticocancellous sites compared to purely cortical sites could be due to a number of reasons. If BMPR1a is mostly acting at the tissue surface, cancellous bone mass will be more easily increased due to its greater surface area. In addition, BMP2 and BMP4, although very highly expressed in bone, are more highly expressed in cancellous bone than in mid-diaphyseal cortical bone, and therefore blocking BMP signaling through this pathway is likely to affect cancellous bone more than cortical bone (38). In OVX mice, treatment with RAP-661 increased femoral maximum load and stiffness back to control animal levels, indicating that the drug can increase bone mass in the bone diaphysis although not observed in the current study (29). However, these treatments were for longer time points (4 and 8 weeks) at a higher dosage (10mg/kg vs. 5 mg/kg for the current study).

In the vertebral cortical shell, pOC-ERαKO mice responded less to two weeks of RAP-661 treatment than LC animals, suggesting that ERα and BMP2/4 signaling in osteoblasts interact. Absence of ERα partially blocked the mechanism that enhanced bone mass with drug treatment was partially blocked when ERα is removed. One

possible explanation is through receptor activator of nuclear factor kappa-B ligand (RANKL), secreted by osteoblasts to regulate osteoclast differentiation and increase bone resorption (39). Osteoprotegrin (OPG), also secreted by osteoblasts, prevents RANKL from binding to RANK to decrease bone resorption. Denosumab, a current osteoporosis therapy, is a RANKL-antibody that reduces bone resorption. Estrogen deficiency also increases RANKL expression (40), which is one mechanism by which post-menopausal women lose bone mass, and therefore may be one mechanism for bone loss found in pOC-ERαKO animals. In OVX mice, RAP-661 treatment decreased serum RANKL levels while increasing serum OPG levels (29). By increasing serum RANKL levels, lack of ERα in osteoblasts could compete with the anabolic mechanism of RAP-661 and explain the reduced response to RAP-661 in the vertebral shell in pOC-ERαKO mice.

Previous work has also shown direct and indirect crosstalk between the BMP2/4 and ER signaling pathways. With estrogen treatment, Smad activity induced by BMP-2 was increased and decreased in mouse myoblasts and breast cancer cells, respectively (31, 32). In mouse myoblastic cells, Smad1/5/8 phophorylation, induced by BMP-2, was enhanced with estrogen treatment (31). On the other hand, BMP treatment increased the expression of both ERα and ERβ, while Smad4, downstream of BMP signaling, repressed estrogen-induced transcriptional activity (30, 32). Translating in vitro cell work in breast cancer and myoblasts cells to in vivo effects in bone is difficult, but it is possible propose that in osteoblasts, lack of ERα could have an impact on the effects of blocking signaling through BMPR1a, possibly by promoting signaling through another BMP receptor pair or through ERβ.

Controlled in vivo loading models have been widely used to study bone adaptation to load (41-43). Our loading model consistently has shown increased bone mass in the proximal tibia and tibial midshaft of growing, adult, male, female, and

genetically altered mice (17, 41, 44, 45). In the current study, we found that mice treated with RAP-661 responded less to loading than placebo animals in the tibial metaphysis, but similarly at the tibial midshaft. One possible explanation is that RAP-661 increased cancellous BV/TV to such a large degree that any further loading-induced increase would be swamped out. A subsequent loading study with a lower drug dosage would help determine if the drug effect is masking the loading effect or attenuating the loading effect. RAP-661 did not affect bone mass in the cortical shell metaphysis, which still responded less to loading in the drug-treated animals than placebo-treated animals. During axial tibial compression at the metaphysis, the cortical shell and cancellous core share the load. We cannot rule out the possibility that the increased cancellous bone mass carried more of the load in drug-treated animals, which resulted in stress shielding for the cortical metaphyseal shell and therefore could explain the shell's decreased anabolic response to loading. However, these results could also suggest that bone's response to mechanical loading may be mediated through BMPR1a. BMPs in general have been associated with bone's response to mechanical loading previously. Osteoblasts subjected to dynamic strain showed increased Smad1/5/8 expression, downstream of BMP signaling (46). After exposure to loading, human fetal osteoblasts showed differential expression of many of the BMPs (47). BMP2 and BMP4 expression were also upregulated after in vivo loading in rodents (26, 48). In support with our findings, osteoblast-like cells from C57Bl/6 mice increased expression of BMPR1a and BMPR1b after fluid shear mechanical stimulation (25). Without BMPR1a, RAP-661-treated mice may not be able to fully convert a mechanical loading stimulus to an osteogenic response.

RAP-661 treatment in LC and pOC-ERαKO mice increased bone mass markedly after two weeks of treatment compared to placebo controls in cortico-cancellous sites but not in cortical diaphyses. Because the greatest risks of

osteoporotic fracture are present in cortico-cancellous sites such as the vertebra or hip, inhibiting signaling through the BMPR1a receptor is a promising future drug treatment option for osteoporosis. Future experiments should further investigate the signaling mechanisms involved, especially in the absence of estrogen, which is the case for many post-menopausal osteoporotic women. Also, because BMPR1a is present in many cell types throughout the body, potential interactions and side effects of the treatment should also be fully explored.

4.5 References

1. Khosla S, Oursler MJ, Monroe DG. Estrogen and the skeleton. Trends Endocrinol Metab. 2012;23(11):576-81.
2. Manolagas SC, Kousteni S, Jilka RL. Sex steroids and bone. Recent Prog Horm Res. 2002;57:385-409.
3. Riggs BL, Khosla S, Melton LJ, 3rd. Sex steroids and the construction and conservation of the adult skeleton. Endocr Rev. 2002;23(3):279-302.
4. Richelson LS, Wahner HW, Melton LJ, 3rd, Riggs BL. Relative contributions of aging and estrogen deficiency to postmenopausal bone loss. N Engl J Med. 1984;311(20):1273-5.
5. Marino M, Galluzzo P, Ascenzi P. Estrogen signaling multiple pathways to impact gene transcription. Curr Genomics. 2006;7(8):497-508.
6. Smith EP, Boyd J, Frank GR, Takahashi H, Cohen RM, Specker B, Williams TC, Lubahn DB, Korach KS. Estrogen resistance caused by a mutation in the estrogen-receptor gene in a man. N Engl J Med. 1994;331(16):1056-61.
7. Kobayashi S, Inoue S, Hosoi T, Ouchi Y, Shiraki M, Orimo H. Association of bone mineral density with polymorphism of the estrogen receptor gene. J Bone Miner Res. 1996;11(3):306-11.
8. Gennari L, Merlotti D, De Paola V, Calabro A, Becherini L, Martini G, Nuti R. Estrogen receptor gene polymorphisms and the genetics of osteoporosis: a HuGE review. Am J Epidemiol. 2005;161(4):307-20.
9. Price JS, Sugiyama T, Galea GL, Meakin LB, Sunters A, Lanyon LE. Role of endocrine and paracrine factors in the adaptation of bone to mechanical loading. Curr Osteoporos Rep. 2011;9(2):76-82.
10. Sunters A, Armstrong VJ, Zaman G, Kypta RM, Kawano Y, Lanyon LE, Price JS. Mechano-transduction in osteoblastic cells involves strain-regulated estrogen receptor alpha-mediated control of insulin-like growth factor (IGF) I receptor sensitivity to Ambient IGF, leading to phosphatidylinositol 3-kinase/AKT-dependent Wnt/LRP5 receptor-independent activation of beta-catenin signaling. J Biol Chem.

2010;285(12):8743-58.
11. Roforth MM, Atkinson EJ, Levin ER, Khosla S, Monroe DG. Dissection of estrogen receptor alpha signaling pathways in osteoblasts using RNA-sequencing. PLoS One. 2014;9(4):e95987.
12. Lindberg MK, Alatalo SL, Halleen JM, Mohan S, Gustafsson JA, Ohlsson C. Estrogen receptor specificity in the regulation of the skeleton in female mice. J Endocrinol. 2001;171(2):229-36.
13. Sims NA, Dupont S, Krust A, Clement-Lacroix P, Minet D, Resche-Rigon M, Gaillard-Kelly M, Baron R. Deletion of estrogen receptors reveals a regulatory role for estrogen receptors-beta in bone remodeling in females but not in males. Bone. 2002;30(1):18-25.
14. Saxon LK, Galea G, Meakin L, Price J, Lanyon LE. Estrogen receptors alpha and beta have different gender-dependent effects on the adaptive responses to load bearing in cancellous and cortical bone. Endocrinology. 2012;153(5):2254-66.
15. Almeida M, Iyer S, Martin-Millan M, Bartell SM, Han L, Ambrogini E, Onal M, Xiong J, Weinstein RS, Jilka RL, O'Brien CA, Manolagas SC. Estrogen receptor-alpha signaling in osteoblast progenitors stimulates cortical bone accrual. J Clin Invest. 2013;123(1):394-404.
16. Maatta JA, Buki KG, Gu G, Alanne MH, Vaaraniemi J, Liljenback H, Poutanen M, Harkonen P, Vaananen K. Inactivation of estrogen receptor alpha in bone-forming cells induces bone loss in female mice. FASEB J. 2012.
17. Melville KM, Kelly NH, Khan SA, Schimenti JC, Ross FP, Main RP, van der Meulen MC. Female mice lacking estrogen receptor-alpha in osteoblasts have compromised bone mass and strength. J Bone Miner Res. 2014;29(2):370-9.
18. Kondoh S, Inoue K, Igarashi K, Sugizaki H, Shirode-Fukuda Y, Inoue E, Yu T, Takeuchi JK, Kanno J, Bonewald LF, Imai Y. Estrogen receptor alpha in osteocytes regulates trabecular bone formation in female mice. Bone. 2014;60:68-77.
19. Windahl SH, Borjesson AE, Farman HH, Engdahl C, Moverare-Skrtic S, Sjogren K, Lagerquist MK, Kindblom JM, Koskela A, Tuukkanen J, Divieti Pajevic P, Feng JQ, Dahlman-Wright K, Antonson P, Gustafsson JA, Ohlsson C. Estrogen receptor-alpha in osteocytes is important for trabecular bone formation in male mice. Proc Natl Acad Sci U S A. 2013;110(6):2294-9.
20. Lee K, Jessop H, Suswillo R, Zaman G, Lanyon L. Endocrinology: bone adaptation requires oestrogen receptor-alpha. Nature. 2003;424(6947):389.
21. Bassey EJ, Rothwell MC, Littlewood JJ, Pye DW. Pre- and postmenopausal women have different bone mineral density responses to the same high-impact exercise. J Bone Miner Res. 1998;13(12):1805-13.
22. Rosen V. BMP2 signaling in bone development and repair. Cytokine Growth Factor Rev. 2009;20(5-6):475-80.
23. Fukuda T, Kokabu S, Ohte S, Sasanuma H, Kanomata K, Yoneyama K, Kato H, Akita M, Oda H, Katagiri T. Canonical Wnts and BMPs cooperatively induce osteoblastic differentiation through a GSK3beta-dependent and beta-catenin-independent mechanism. Differentiation. 2010;80(1):46-52.
24. Canalis E, Economides AN, Gazzerro E. Bone morphogenetic proteins, their antagonists, and the skeleton. Endocr Rev. 2003;24(2):218-35.

25. Lau KH, Kapur S, Kesavan C, Baylink DJ. Up-regulation of the Wnt, estrogen receptor, insulin-like growth factor-I, and bone morphogenetic protein pathways in C57BL/6J osteoblasts as opposed to C3H/HeJ osteoblasts in part contributes to the differential anabolic response to fluid shear. J Biol Chem. 2006;281(14):9576-88.
26. Zaman G, Saxon LK, Sunters A, Hilton H, Underhill P, Williams D, Price JS, Lanyon LE. Loading-related regulation of gene expression in bone in the contexts of estrogen deficiency, lack of estrogen receptor alpha and disuse. Bone. 2010;46(3):628-42.
27. Mishina Y, Starbuck MW, Gentile MA, Fukuda T, Kasparcova V, Seedor JG, Hanks MC, Amling M, Pinero GJ, Harada S, Behringer RR. Bone morphogenetic protein type IA receptor signaling regulates postnatal osteoblast function and bone remodeling. J Biol Chem. 2004;279(26):27560-6.
28. Okamoto M, Murai J, Imai Y, Ikegami D, Kamiya N, Kato S, Mishina Y, Yoshikawa H, Tsumaki N. Conditional deletion of Bmpr1a in differentiated osteoclasts increases osteoblastic bone formation, increasing volume of remodeling bone in mice. J Bone Miner Res. 2011;26(10):2511-22.
29. Baud'huin M, Solban N, Cornwall-Brady M, Sako D, Kawamoto Y, Liharska K, Lath D, Bouxsein ML, Underwood KW, Ucran J, Kumar R, Pobre E, Grinberg A, Seehra J, Canalis E, Pearsall RS, Croucher PI. A soluble bone morphogenetic protein type IA receptor increases bone mass and bone strength. Proc Natl Acad Sci U S A. 2012;109(30):12207-12.
30. Wu L, Wu Y, Gathings B, Wan M, Li X, Grizzle W, Liu Z, Lu C, Mao Z, Cao X. Smad4 as a transcription corepressor for estrogen receptor alpha. J Biol Chem. 2003;278(17):15192-200.
31. Yamamoto T, Saatcioglu F, Matsuda T. Cross-talk between bone morphogenic proteins and estrogen receptor signaling. Endocrinology. 2002;143(7):2635-42.
32. Matsumoto Y, Otsuka F, Takano M, Mukai T, Yamanaka R, Takeda M, Miyoshi T, Inagaki K, Sada KE, Makino H. Estrogen and glucocorticoid regulate osteoblast differentiation through the interaction of bone morphogenetic protein-2 and tumor necrosis factor-alpha in C2C12 cells. Mol Cell Endocrinol. 2010;325(1-2):118-27.
33. Clemens TL, Tang H, Maeda S, Kesterson RA, Demayo F, Pike JW, Gundberg CM. Analysis of osteocalcin expression in transgenic mice reveals a species difference in vitamin D regulation of mouse and human osteocalcin genes. J Bone Miner Res. 1997;12(10):1570-6.
34. Zhang M, Xuan S, Bouxsein ML, von Stechow D, Akeno N, Faugere MC, Malluche H, Zhao G, Rosen CJ, Efstratiadis A, Clemens TL. Osteoblast-specific knockout of the insulin-like growth factor (IGF) receptor gene reveals an essential role of IGF signaling in bone matrix mineralization. J Biol Chem. 2002;277(46):44005-12.
35. Dupont S, Krust A, Gansmuller A, Dierich A, Chambon P, Mark M. Effect of single and compound knockouts of estrogen receptors alpha (ERalpha) and beta (ERbeta) on mouse reproductive phenotypes. Development. 2000;127(19):4277-91.
36. Lynch ME, Main RP, Xu Q, Walsh DJ, Schaffler MB, Wright TM, van der Meulen MC. Cancellous bone adaptation to tibial compression is not sex dependent in growing mice. J Appl Physiol (1985). 2010;109(3):685-91.

37. Kamiya N, Ye L, Kobayashi T, Lucas DJ, Mochida Y, Yamauchi M, Kronenberg HM, Feng JQ, Mishina Y. Disruption of BMP signaling in osteoblasts through type IA receptor (BMPRIA) increases bone mass. J Bone Miner Res. 2008;23(12):2007-17.
38. Kochanowska I, Chaberek S, Wojtowicz A, Marczynski B, Wlodarski K, Dytko M, Ostrowski K. Expression of genes for bone morphogenetic proteins BMP-2, BMP-4 and BMP-6 in various parts of the human skeleton. BMC Musculoskelet Disord. 2007;8:128.
39. Boyce BF, Xing L. The RANKL/RANK/OPG pathway. Curr Osteoporos Rep. 2007;5(3):98-104.
40. Manolagas SC, O'Brien CA, Almeida M. The role of estrogen and androgen receptors in bone health and disease. Nat Rev Endocrinol. 2013;9(12):699-712.
41. Fritton JC, Myers ER, Wright TM, van der Meulen MC. Loading induces site-specific increases in mineral content assessed by microcomputed tomography of the mouse tibia. Bone. 2005;36(6):1030-8.
42. Torrance AG, Mosley JR, Suswillo RF, Lanyon LE. Noninvasive loading of the rat ulna in vivo induces a strain-related modeling response uncomplicated by trauma or periostal pressure. Calcif Tissue Int. 1994;54(3):241-7.
43. De Souza RL, Matsuura M, Eckstein F, Rawlinson SC, Lanyon LE, Pitsillides AA. Non-invasive axial loading of mouse tibiae increases cortical bone formation and modifies trabecular organization: a new model to study cortical and cancellous compartments in a single loaded element. Bone. 2005;37(6):810-8.
44. Fritton JC, Myers ER, Wright TM, van der Meulen MC. Bone mass is preserved and cancellous architecture altered due to cyclic loading of the mouse tibia after orchidectomy. J Bone Miner Res. 2008;23(5):663-71.
45. Lynch ME, Main RP, Xu Q, Schmicker TL, Schaffler MB, Wright TM, van der Meulen MC. Tibial compression is anabolic in the adult mouse skeleton despite reduced responsiveness with aging. Bone. 2011;49(3):439-46.
46. Rath B, Nam J, Deschner J, Schaumburger J, Tingart M, Grassel S, Grifka J, Agarwal S. Biomechanical forces exert anabolic effects on osteoblasts by activation of SMAD 1/5/8 through type 1 BMP receptor. Biorheology. 2011;48(1):37-48.
47. Kopf J, Petersen A, Duda GN, Knaus P. BMP2 and mechanical loading cooperatively regulate immediate early signalling events in the BMP pathway. BMC Biol. 2012;10:37.
48. McKenzie JA, Bixby EC, Silva MJ. Differential gene expression from microarray analysis distinguishes woven and lamellar bone formation in the rat ulna following mechanical loading. PLoS One. 2011;6(12):e29328.

Chapter 5
CONCLUSIONS AND DISCUSSION

5.1 Summary

The objective of this research was to elucidate the function of estrogen receptor alpha (ERα) signaling in osteoblasts. Because decreased circulating estrogen levels are associated with decreased bone mass, understanding estrogen signaling in bone is critical in osteoporosis pathology and developing potential new therapies. However, the roles of ERα and ERβ, the two main hormone receptors involved in estrogen signaling, are not well characterized and vary by cell type. After generating an osteoblast-specific ERα knockout (pOC-ERαKO) mouse model, the role of ERα in osteoblasts in general bone phenotype (Aim 1), bone's response to mechanical loading (Aim 2), and crosstalk with BMPR1a, a type I receptor in bone morphogenetic protein (BMP) signaling (Aim 3), were assessed. In pOC-ERαKO females, bone mass was reduced and the response to mechanical loading was enhanced. In pOC-ERαKO females, bone mass was increased and the response to mechanical loading was unaltered. In females, ERα and BMPR1a were shown to interact in bone, and bone's response to mechanical loading was partially mediated by BMPR1a. This thesis shows that ERα has important, sex-specific roles in bone and bone mechanoadaptation, and that the receptor is involved in other important bone signaling networks. Developing new drugs or technologies that can harness the signaling mechanisms of ERα in bone would advance the clinical field.

Aim 1

Global ERαKO mice have systemic effects that interfere with interpreting the role of ERα in bone (1-4). To combat these confounding effects, cell-specific

knockouts allow the receptor's role to be examined at a particular point of interest in the cell lineage (5-11). An osteoblast-specific ERαKO mouse model was developed to eliminate systemic effects present in the global knockout. We hypothesized that removing ERα at the osteoblast stage of lineage would decrease bone mass in females. Bone mass, architecture, and strength in female pOC-ERαKO and littermate control (LC) mice at 12 and 18 weeks of age were assessed. At both ages, pOC-ERαKO mice had reduced bone volume fraction due to increased trabecular separation in the proximal tibia, L5 vertebra, and distal femur compared to LC. In the vertebra, trabecular thickness was also decreased in knockouts, contributing to the overall decreased bone mass. Osteoblast activity in knockouts was decreased in the cancellous proximal tibia, but osteoclast number was similar to LC. At cortical sites in the tibial midshaft, L5 vertebra, and distal femur, cortical area was decreased in pOC-ERαKO mice at both ages, accompanied by overall decreased cortical thickness. The decreased cortical and cancellous bone mass corresponded to decreased whole bone strength in the femur and vertebra. Osteoblastic ERα regulated both cortical and cancellous bone mass at multiple bone sites.

Aim 2

Healthy bone has the ability to adapt to its mechanical requirements. Increased dynamic mechanical loading, especially in younger populations, can promote bone formation (12, 13). However, in older populations or in bone diseases such as osteoporosis, exercise programs have varied results on increasing bone mass (14-16). To study bone's anabolic response to mechanical forces, controlled in vivo compression of rodent limbs are widely used models (10, 11, 17-19). In global ERαKO mice, the response to loading was attenuated compared to controls, but in bone cell-specific knockouts, the loading response has not been well studied (11, 20,

21). We hypothesized that pOC-ERαKO mice would have decreased bone mass and would respond less to mechanical loading. We bred 10-week-old male and female pOC-ERαKO and LC mice to determine the role of ERα in osteoblasts in bone phenotype and mechanotransduction in both sexes. After measuring bone stiffness at the tibial midshaft, all mice had their left tibiae loaded 5 days a week for 2 weeks with a peak load of –9.0N, which corresponded to 1200με at the midshaft. Lack of ERα in osteoblasts had the opposite effect on bone mass in males than in females, compared to their respective LC. Female pOC-ERαKO mice showed reduced cancellous bone volume fraction in the tibial metaphysis and L5 vertebral body and reduced cortical area in the vertebral cortical shell and femoral midshaft. In contrast, male pOC-ERαKO had increased bone volume fraction in the L5 vertebral body and increased cortical area at both the tibial and femoral midshafts. Reflecting these bone mass changes, female knockouts had decreased whole bone vertebral strength, while males had increased whole bone femoral strength compared to their sex-matched controls. The response to mechanical loading in these animals was evaluated at both the tibial metaphysis and the tibial midshaft. In female pOC-ERαKO mice, cancellous bone volume fraction increased more after 2 weeks of tibial loading than LC mice, while cortical area in the cortical shell of the metaphysis adapted similarly in both genotypes. Furthermore, at the tibial midshaft, cortical area increased more in female knockouts. In males, bone volume fraction did not increase with loading in either genotype, but in the cortical shell of the metaphysis and the cortical midshaft, cortical area and maximum moment of inertia increased similarly in pOC-ERαKO male and LC after loading. ERα in osteoblasts affected bone mass and the response to mechanical loading differentially in males and females.

Aim 3

Cell signaling in bone is complex. Estrogen and its receptors interact with a variety of other signaling pathways. Bone morphogenetic proteins (BMPs) and their signaling effectors have been shown to interact with ERα in non-bone cell types both in vitro and in vivo, and BMPs have also been implicated in bone adaptation (22-26). Throughout development, BMPs regulate a wide variety of cell processes, but BMP2 and 4 have specific roles in bone. Because BMP2 and BMP4 bind highly to the receptor BMPR1a, a soluble BMPR1a receptor, RAP-661, was created to block all signaling through BMPR1a (27). We hypothesized that blocking BMP2/4 signaling would increase bone mass and reduce bone's response to mechanical loading. 10-week-old pOC-ERαKO and LC female mice were administered either RAP-661 or a IgG-matched placebo. All animals underwent left tibial loading for 2 weeks with a peak load of -7.0N to eliminate woven bone that was induced at the tibial midshaft in female animals loaded at -9.0N in Aim 2. RAP-661 treatment increased bone mass in the vertebra and cancellous tibial metaphysis, but not at the cortical shell of the tibial metaphysis, tibial midshaft, or femoral midshaft. Furthermore, RAP-661 increased vertebral cortical area and cortical thickness to a lesser extent in pOC-ERαKO mice than in LC, and vertebral I_{MAX} was only enhanced by RAP-661 in LC mice. In the tibial metaphysis, animals treated with RAP-661 showed a decreased anabolic response to 2 week of tibial loading compared to placebo animals. In contrast, at the tibial midshaft both placebo and RAP-661-treated mice exhibited similar increases in cortical area, cortical thickness, and moments of inertia from loading. In short, RAP-661 treatment affected mostly cancellous regions and reduced bone's response to mechanical loading only in the tibial metaphysis.

5.2 Strengths

Knockout mouse models are valuable tools that allow researchers to study the

role of a particular gene/protein in cellular or whole body function. The pOC-ERαKO mouse model, in which ERα is removed from mature osteoblasts and osteoctyes, is a major strength of this work. Many other bone-cell-specific ERαKO mice have been developed, including those that target ERα deletion in osteoblast progenitors, osteoblasts precursors, committed osteoblasts, osteocytes, osteoclast precursors, and osteoclasts (5-11). To date, only one other group has developed the pOC-ERαKO thus far, and similar effects on male and female bone mass to this work have been reported (8).

The tibial compression model used in this work elicits a reliable, robust increase in bone mass in both cancellous and cortical bone. Other rodent loading models exist that use rats, which cannot be genetically manipulated with the ease that mice can (28), or use the ulna instead of the tibia (19), which only allows for studying cortical bone's adaptation to loading. Although other mouse tibial compression models exist, a different waveform is often used. Instead of loading the tibia 5 days a week, 1200 cycles per day, at a rate of 4Hz, with a 0.1-second rest between cycles (29), other groups may load the tibia 3 days a week, 60 cycles per day, at 2Hz, with 10-second rest between cycles (30). We have consistently shown an osteogenic response to our loading model in male and females, in growing and aged mice, in gonadectomized mice, and in genetically modified mice (17, 29, 31, 32). In contrast, the loading waveform with longer rests and fewer cycles per day has actually been shown to decrease trabecular bone volume fraction in the cancellous metaphysis in aged mice and is not as osteogenic as the model used in the current work (33).

Another strength of this work is the ability to study signaling interactions of ERα in osteoblasts with other important bone pathways, including the BMP pathway using RAP-661, a soluble BMPR1a receptor that blocks signaling through BMP2/4. Currently, a number of osteoporosis drugs are FDA-approved, the majority of which

are classified as anti-resorptive agents. Anti-resorptive agents include selective estrogen receptor modulators (SERMs), bisphosphonates, non-steroidal hormones, and antibodies. The only anabolic agent available for osteoporosis treatment is teriparatide (rhPTH) that acts by increasing bone turnover so that osteoblasts are stimulated to a greater extent and thereby bone mass increases. RAP-661 is another potential anabolic osteoporosis treatment that increases bone mass and strength in mice by increasing osteoblast and osteoclast activity (27). We have also contributed to the efficacy research of this drug through Aim 3, where we administered the drug or placebo to female pOC-ERαKO and LC mice concurrently with daily tibial compression. This study was the first to examine the interactions of ERα in osteoblasts and mechanical loading with BMPR1a.

5.3 Limitations

Every scientific model can only be examined in its specific context, which always introduces limitations. One limitation with the pOC-ERαKO mouse model is the specificity of ERα deletion. Breeding mice containing the osteocalcin-promoted cre recombinase (OC-Cre) (34) with mice that have exon 3 of the ERα gene floxed with loxP sites (3) should remove ERα from only mature osteoblasts and osteoctyes, because osteocalcin is specific to osteoblasts. After OC-Cre mice were crossed with Rosa26-Cre reporter mice and tibia were fixed and embedded, longitudinal tibial sections were stained with X-Gal to detect β-galactosidase activity, which indicates the cre specificity (Figure 5.1). We found distinct staining in osteoblasts and osteocytes, but also found β-galactosidase activity in hypertrophic chondroctyes, consistent with one previous report (35). Although cellular organization appeared normal in pOC-ERαKO growth plates, and growth plate height and long bone lengths did not vary by genotype, if ERα is absent in some hypertrophic chondroctyes in our

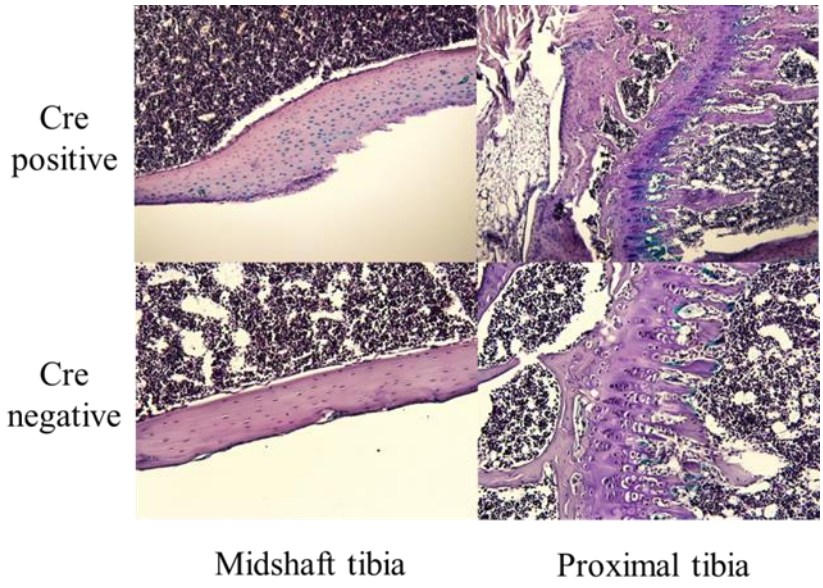

Figure 5.1 Cre expression of OC-Cre mice was found not only in osteoblasts and osteocytes, but also in hypertrophic chondroctyes. OC-Cre mice were crossed with Rosa26-Cre reporter mice, and then tibiae at 10 weeks were embedded, sectioned, and stained with LacZ to detect β-galactosidase activity.

model, then it is potentially also absent from osteoblast precursors, osteoblast progenitors, and committed osteoblasts. The effects on endochondral ossification could be further explored. In a chondrocyte-specific ERαKO mouse, growth plate heights and long bone lengths were not altered compared to controls (36). However, the growth plate height in knockout mice did not decrease in response to estrogen treatment as wildtype mice did. Furthermore, long bones continued to grow past 4 months of age in the cartilage-specific ERαKOs. Similar experiments could be performed on pOC-ERαKO mice to assess the possibility of ERα deletion in chondrocytes by aging the mice to assess long bone growth and treating mice with estrogen to examine growth plate height.

Although knockout mice, especially tissue-specific knockout mice, provide insight into the role of a particular gene in development and cellular processes, one drawback is the compensatory effects that arise from gene deficiency from birth or even in the womb. Many knockout mice are embryonically lethal, including the

global knockouts for BMP2, BMP4, BMPR1a, and Smad1, but other knockout models that are viable develop significant compensatory mechanisms due to the innate redundancy of biological systems (37). For example, when both are present, ERα and ERβ repress functions of one another, but in the absence of ERα, ERβ may compensate and take over some of ERα's functions (38). If ERα were removed from osteoblasts but only in adult animals for a given amount of time, its effects on bone mass could be quite different than when it was removed in utero. Developing a tamoxifen-induced, osteoblast-specific ERαKO mouse would provide interesting insight into the role of ERα in bone development and growth vs. bone maintenance. Tamoxifen-induced knockouts only activate cre recombinase in animals that harbor both a floxed gene and cre recombinase when tamoxifen is administered. An inducible osteoblast-specific BMPR1a knockout mouse already exists that used a tamoxifen-induced *OC-Cre* mouse (39).

In vivo loading models provide controlled, non-invasive environments for studying bone adaptation. Although these models control the magnitude of applied loads very well, the tissue-level strains are much more difficult to characterize, especially in the cancellous bone of the tibial metaphysis. To conduct loading experiments, a peak load is chosen that matches strains experienced on the diaphyseal cortex, measured by strain gauging at the midshaft. In Aim 2, bone stiffness was similar among male and female pOC-ERαKO and LC mice, and so all mice were loaded with a peak load of -9.0N. However, microCT analysis revealed major cortical and cancellous bone differences between genotypes and sex. At the tibial metaphysis, female pOC-ERαKO mice had decreased bone volume fraction than LC, and the knockouts responded more to mechanical loading. This increased anabolic response could be due to higher strains experienced in the cancellous bone in pOC-ERαKO mice, as osteogenic responses have been correlated with bone strain magnitudes (40).

One approach to determine bone stiffness and engendered strains with loading would be to develop finite element models of whole bones in each genotype (29, 32). Another approach would be to design a loading experiment in which the female pOC-ERαKO and LC mice each received a peak load proportional to their baseline bone volume fraction. If the pOC-ERαKO mice still responded more to the loading than LC mice, then the increased response would be due to the genotype rather than different strain environments.

Although RAP-661, a soluble BMPR1a receptor, increased bone mass dramatically in mice, possible side effects on other body systems need further exploration and are a limitation to the possibility of this drug being used as an osteoporosis treatment. BMPR1a, although highly implicated in bone, is widely expressed in many tissues throughout development (41). Its importance is obvious by the embryonic lethality of a BMPR1a global KO mouse (42). As with all drugs, side effects are inevitable, and the relative benefits and risks must be fully evaluated before a drug can be approved by the FDA. Performing long-term drug treatment studies, toxicity studies, and full organ analysis studies would be next steps.

5.4 Future Work

The pOC-ERαKO mouse model developed in this work showed an important role of ERα in bone mass and bone's response to mechanical loading, while also beginning to delve into the signaling mechanisms of the receptor. Future work would expand on ERα signaling knowledge to better understand osteoporosis pathology. Whether the bone phenotype or loading response in growing male and female pOC-ERαKO mice is mirrored in aged mice needs to be determined. Also, more work should focus on elucidating the cellular and molecular mechanisms that drive the genotype-specific responses seen in all three Aims. Other potential future experiments

include performing ovariectomy on pOC-ERαKO female mice, administering RAP-661 in aged mice, and exploring the signaling crosstalk between ERα in osteoblasts and other bone-specific pathways by administering additional signaling blocking agents.

Effects of age in pOC-ERαKO mice

After generating a new knockout mouse model, its characteristics should be studied at multiple ages to determine if a phenomenon is age-specific or if it is consistent throughout the lifespan. This information gives insight into the mechanisms behind the phenotype or response reported. Furthermore, when bone is still modeling during growth, the skeleton behaves differently than when bone is only in the remodeling phase after peak bone mass is achieved, usually around 16 weeks in mice (43). In *Aim 1*, pOC-ERαKO female mice were examined at 12 and 18 weeks of age. In *Aim 2*, male and female pOC-ERαKO mice were examined at 12 weeks of age, both in bone phenotype and bone's response to mechanical loading (10 weeks plus 2 weeks of loading). For pOC-ERαKO, another group examined the bone phenotype of males and females at 3.5 and 6 months of age (8). Although decreases in female bone mass similar to our results were reported at both ages, male pOC-ERαKO mice exhibited similar bone mass to controls at 3.5 months and decreased trabecular bone mass at 6 months of age. Because of this discrepancy, a study utilizing aged pOC-ERαKO female and male mice from the current work would indicate if the decreased bone mass found in females and increased bone mass found in males continues with age. Furthermore, in vivo tibial loading studies should be applied to 6-month old pOC-ERαKO mice of both sexes. Our tibial loading model is anabolic in both growing and aged mice (17, 32); however, a loading model with a different waveform actually reduced bone mass in the tibial metaphysis in aged female mice

(33). In humans, bone's anabolic response to exercise decreases with age (14), and so determining if the controlled loading model can still stimulate bone formation in aged pOC-ERαKO mice, when bone is only remodeling, is a worthwhile endeavor. Furthermore, aged mice may be more relevant to human clinical data, as osteoporosis mostly affects the elderly and is especially present in estrogen-deplete post-menopausal women.

Cellular mechanisms driving the bone phenotype and response to loading in pOC-ERαKO mice

Decreased estrogen levels are a major cause of bone loss in postmenopausal women (44). During puberty, estrogen promotes bone growth, but it also contributes to growth plate closure and suppression of periosteal expansion, indicating multiple functions based on hormone levels, age, and other yet unknown factors (45). Estrogen signaling can occur through classical pathways, involving estrogen's activation of ERα or ERβ and subsequently gene transcription or repression events. However, non-genotropic pathways have also been recognized, which involve the ligand-binding domain of the ERs but are involved in other intracellular signaling pathways instead of direct gene regulation (46). The signaling environments in which estrogens and ERs are involved are poorly understood due to the complexity. In vitro, estrogen and ERα have been proposed to be involved in a number of signaling pathways important to bone, including the wnt/β-catenin pathway, IGF-1 signaling, BMP signaling, and PTH signaling (22, 23, 47).

This work has shown that in pOC-ERαKO female mice, bone mass is reduced and the response to mechanical loading is reduced. In pOC-ERαKO male mice, bone mass is increased and the response to mechanical loading is unchanged. However, by removing ERα from osteoblasts and osteocytes, the signaling environment is perturbed

from before birth. By determining changes in gene expression of bone-related pathways, the in vivo interactions of ERα with other cell signaling systems can be determined. RNAseq is a technique that determines the differential regulation of genes utilizing the entire mouse genome. From this database, an abundant amount of information can be garnered. By analyzing the cancellous compartment of the tibial metaphysis, the cortical shell of the tibial metaphysis, and the cortical diaphysis separately in male and female pOC-ERαKO and LC mice, genes that are affected by lack of ERα in osteoblasts and osteocytes could be determined. For example, expression levels of ERβ may be highly increased in knockouts, as this receptor has been postulated to compensate for loss of ERα in vitro (38). Another hypothesis would involve downregulation of wnt agonists, since ERs and wnts may cooperate with each other in bone (47, 48).

Determining the potential mechanisms behind why female pOC-ERαKO mice responded more to loading would expand on this work. Similarly, RNAseq data could be obtained from cancellous and cortical bone of left, loaded tibia and right, control tibia to compare gene expression profile from both pOC-ERαKO and LC mice. In Aim 2 and Aim 3, two weeks of in vivo tibial loading were used to assess whole tissue changes in bone mass and architecture. The cellular mechanisms that drive tissue-level changes occur on shorter time scales. Some transcription factors can be targeted in under 30 minutes after a stimulus, but osteoblasts do not increase until 24-48 hours after a dynamic loading event, and mineralization does not begin for at least 3 days after the appropriate stimulus. Therefore, obtaining samples for RNAseq data at time points that are 3 hours, 24 hours, and 3 days after single or multiple days of loading would provide much information about all of these processes. Information gained from RNAseq experiments in pOC-ERαKO and LC mice with and without loading could generate ideas for future pathways to target for new drugs in osteoporosis

prevention and treatment.

OVX response in pOC-ERαKO mice

As a model of estrogen deficiency such as with osteoporosis, ovariectomy (OVX) in the rat is the gold standard. This surgery excises the estrogen-producing ovaries and therefore removes most circulating estrogen (49). More recently, mouse OVX models have been frequently implemented due to the ability to manipulate the mouse genome through knockout models, but bone loss varies widely with bone site and mouse strain (50). Bone loss with OVX and bone mass increase with estrogen treatment differ among ERαKO mouse models, indicating bone cell-specific mechanisms for each process. In global ERαKO mice, estrogen treatment after OVX did not increase cortical area or trabecular bone mineral density to the same degree as in ERβKO or WT mice, indicating that estrogen's bone-building effects may be mediated by ERα (51). In mice with ERα removed at the osteoblast precursor or osteoblast progenitor stage which resulted in decreased cortical bone mass, OVX did not lose cortical bone after OVX as wildtype mice did (7). In osteoclast-specific ERαKO mice that had decreased cancellous bone mass, OVX did not induce cancellous bone loss as it did in wildtype mice (5). Our pOC-ERαKO female mice showed decreased cancellous and cortical bone mass, a different phenotype than the other cell-specific ERαKO models. First, an OVX experiment on pOC-ERαKO mice would indicate if ERα in osteoblasts is required for further cancellous or cortical bone loss when all circulating estrogen is removed. Next, estrogen replacement in these mice would show if estrogen can still increase bone mass without osteoblastic ERα, possibly through ERα in other cell types, or through compensatory action of ERβ. Some research has indicated that ERα and ERβ repress a subset of gene transcriptional activity of each other when both are present, but ERβ may take over some of the

activity of ERα in its absence (38, 52).

RAP-661 effects in older animals of both sexes

Exercise programs to increase bone mass are not as effective in post-menopausal women as in pre-menopausal women (14). After menopause, estrogen levels in women decline, which contributes to bone mass and architecture changes, but men experience a decline in hormones with age as well (44, 53, 54). Likewise, in vivo animal models of bone adaptation have been shown to be less responsive in older animals or even promoters of bone loss (32, 55). Whether the reason is because the cells are not sensing the mechanical signal as well or because the cells cannot translate the signal into the correct cellular response is yet to be determined. Other factors may contribute to this phenomenon in humans, including increased serum concentration of sclerostin, a wnt signaling inhibitor, and decreased OPG serum levels with age, which in turn increases osteoclast activity (56).

During bone's modeling phase, the shape of bone is changing and bone mass in increasing during an animal's growth. Once peak bone mass is achieved, bone remodeling persists to delicately balance bone formation and bone resorption to maintain bone mass. Aim 3 examined the effects of RAP-661, a BMPR1a receptor inhibitor, on bone mass in pOC-ERαKO and LC female mice, and in the response to loading in these animals. However, at 10 weeks of age, mice are still rapidly growing and have not yet achieved peak bone mass. Furthermore, only female mice were utilized. To fully characterize the interactions among RAP-661, osteoblastic ERα, and loading, similar experiments should be repeated on older animals of both sexes that are at least skeletally mature or that are aged to 6 months. Experiments on aged mice would give more relevance to the drug's target demographic, as osteoporosis is most prevalent in older populations.

5.5 References

1. Lindberg MK, Alatalo SL, Halleen JM, Mohan S, Gustafsson JA, Ohlsson C. Estrogen receptor specificity in the regulation of the skeleton in female mice. J Endocrinol. 2001;171(2):229-36.
2. Sims NA, Dupont S, Krust A, Clement-Lacroix P, Minet D, Resche-Rigon M, Gaillard-Kelly M, Baron R. Deletion of estrogen receptors reveals a regulatory role for estrogen receptors-beta in bone remodeling in females but not in males. Bone. 2002;30(1):18-25.
3. Dupont S, Krust A, Gansmuller A, Dierich A, Chambon P, Mark M. Effect of single and compound knockouts of estrogen receptors alpha (ERalpha) and beta (ERbeta) on mouse reproductive phenotypes. Development. 2000;127(19):4277-91.
4. Lee HR, Kim TH, Choi KC. Functions and physiological roles of two types of estrogen receptors, ERalpha and ERbeta, identified by estrogen receptor knockout mouse. Lab Anim Res. 2012;28(2):71-6.
5. Nakamura T, Imai Y, Matsumoto T, Sato S, Takeuchi K, Igarashi K, Harada Y, Azuma Y, Krust A, Yamamoto Y, Nishina H, Takeda S, Takayanagi H, Metzger D, Kanno J, Takaoka K, Martin TJ, Chambon P, Kato S. Estrogen prevents bone loss via estrogen receptor alpha and induction of Fas ligand in osteoclasts. Cell. 2007;130(5):811-23.
6. Martin-Millan M, Almeida M, Ambrogini E, Han L, Zhao H, Weinstein RS, Jilka RL, O'Brien CA, Manolagas SC. The estrogen receptor-alpha in osteoclasts mediates the protective effects of estrogens on cancellous but not cortical bone. Mol Endocrinol. 2010;24(2):323-34.
7. Almeida M, Iyer S, Martin-Millan M, Bartell SM, Han L, Ambrogini E, Onal M, Xiong J, Weinstein RS, Jilka RL, O'Brien CA, Manolagas SC. Estrogen receptor-alpha signaling in osteoblast progenitors stimulates cortical bone accrual. J Clin Invest. 2013;123(1):394-404.
8. Maatta JA, Buki KG, Gu G, Alanne MH, Vaaraniemi J, Liljenback H, Poutanen M, Harkonen P, Vaananen K. Inactivation of estrogen receptor alpha in bone-forming cells induces bone loss in female mice. FASEB J. 2012.
9. Melville KM, Kelly NH, Khan SA, Schimenti JC, Ross FP, Main RP, van der Meulen MC. Female mice lacking estrogen receptor-alpha in osteoblasts have compromised bone mass and strength. J Bone Miner Res. 2014;29(2):370-9.
10. Kondoh S, Inoue K, Igarashi K, Sugizaki H, Shirode-Fukuda Y, Inoue E, Yu T, Takeuchi JK, Kanno J, Bonewald LF, Imai Y. Estrogen receptor alpha in osteocytes regulates trabecular bone formation in female mice. Bone. 2014;60:68-77.
11. Windahl SH, Borjesson AE, Farman HH, Engdahl C, Moverare-Skrtic S, Sjogren K, Lagerquist MK, Kindblom JM, Koskela A, Tuukkanen J, Divieti Pajevic P, Feng JQ, Dahlman-Wright K, Antonson P, Gustafsson JA, Ohlsson C. Estrogen

receptor-alpha in osteocytes is important for trabecular bone formation in male mice. Proc Natl Acad Sci U S A. 2013;110(6):2294-9.
12. Fuchs RK, Bauer JJ, Snow CM. Jumping improves hip and lumbar spine bone mass in prepubescent children: a randomized controlled trial. J Bone Miner Res. 2001;16(1):148-56.
13. Kontulainen S, Sievanen H, Kannus P, Pasanen M, Vuori I. Effect of long-term impact-loading on mass, size, and estimated strength of humerus and radius of female racquet-sports players: a peripheral quantitative computed tomography study between young and old starters and controls. J Bone Miner Res. 2003;18(2):352-9.
14. Bassey EJ, Rothwell MC, Littlewood JJ, Pye DW. Pre- and postmenopausal women have different bone mineral density responses to the same high-impact exercise. J Bone Miner Res. 1998;13(12):1805-13.
15. Kerr D, Morton A, Dick I, Prince R. Exercise effects on bone mass in postmenopausal women are site-specific and load-dependent. J Bone Miner Res. 1996;11(2):218-25.
16. Korpelainen R, Keinanen-Kiukaanniemi S, Heikkinen J, Vaananen K, Korpelainen J. Effect of impact exercise on bone mineral density in elderly women with low BMD: a population-based randomized controlled 30-month intervention. Osteoporos Int. 2006;17(1):109-18.
17. Fritton JC, Myers ER, Wright TM, van der Meulen MC. Loading induces site-specific increases in mineral content assessed by microcomputed tomography of the mouse tibia. Bone. 2005;36(6):1030-8.
18. De Souza RL, Matsuura M, Eckstein F, Rawlinson SC, Lanyon LE, Pitsillides AA. Non-invasive axial loading of mouse tibiae increases cortical bone formation and modifies trabecular organization: a new model to study cortical and cancellous compartments in a single loaded element. Bone. 2005;37(6):810-8.
19. Lee KC, Maxwell A, Lanyon LE. Validation of a technique for studying functional adaptation of the mouse ulna in response to mechanical loading. Bone. 2002;31(3):407-12.
20. Lee K, Jessop H, Suswillo R, Zaman G, Lanyon L. Endocrinology: bone adaptation requires oestrogen receptor-alpha. Nature. 2003;424(6947):389.
21. Saxon LK, Galea G, Meakin L, Price J, Lanyon LE. Estrogen receptors alpha and beta have different gender-dependent effects on the adaptive responses to load bearing in cancellous and cortical bone. Endocrinology. 2012;153(5):2254-66.
22. Lau KH, Kapur S, Kesavan C, Baylink DJ. Up-regulation of the Wnt, estrogen receptor, insulin-like growth factor-I, and bone morphogenetic protein pathways in C57BL/6J osteoblasts as opposed to C3H/HeJ osteoblasts in part contributes to the differential anabolic response to fluid shear. J Biol Chem. 2006;281(14):9576-88.
23. Zaman G, Saxon LK, Sunters A, Hilton H, Underhill P, Williams D, Price JS, Lanyon LE. Loading-related regulation of gene expression in bone in the contexts of estrogen deficiency, lack of estrogen receptor alpha and disuse. Bone. 2010;46(3):628-42.
24. McKenzie JA, Bixby EC, Silva MJ. Differential gene expression from microarray analysis distinguishes woven and lamellar bone formation in the rat ulna following mechanical loading. PLoS One. 2011;6(12):e29328.

25. Yamamoto T, Saatcioglu F, Matsuda T. Cross-talk between bone morphogenic proteins and estrogen receptor signaling. Endocrinology. 2002;143(7):2635-42.
26. Matsumoto Y, Otsuka F, Takano M, Mukai T, Yamanaka R, Takeda M, Miyoshi T, Inagaki K, Sada KE, Makino H. Estrogen and glucocorticoid regulate osteoblast differentiation through the interaction of bone morphogenetic protein-2 and tumor necrosis factor-alpha in C2C12 cells. Mol Cell Endocrinol. 2010;325(1-2):118-27.
27. Baud'huin M, Solban N, Cornwall-Brady M, Sako D, Kawamoto Y, Liharska K, Lath D, Bouxsein ML, Underwood KW, Ucran J, Kumar R, Pobre E, Grinberg A, Seehra J, Canalis E, Pearsall RS, Croucher PI. A soluble bone morphogenetic protein type IA receptor increases bone mass and bone strength. Proc Natl Acad Sci U S A. 2012;109(30):12207-12.
28. Torrance AG, Mosley JR, Suswillo RF, Lanyon LE. Noninvasive loading of the rat ulna in vivo induces a strain-related modeling response uncomplicated by trauma or periostal pressure. Calcif Tissue Int. 1994;54(3):241-7.
29. Lynch ME, Main RP, Xu Q, Walsh DJ, Schaffler MB, Wright TM, van der Meulen MC. Cancellous bone adaptation to tibial compression is not sex dependent in growing mice. J Appl Physiol (1985). 2010;109(3):685-91.
30. Brodt MD, Silva MJ. Aged mice have enhanced endocortical response and normal periosteal response compared with young-adult mice following 1 week of axial tibial compression. J Bone Miner Res. 2010;25(9):2006-15.
31. Fritton JC, Myers ER, Wright TM, van der Meulen MC. Bone mass is preserved and cancellous architecture altered due to cyclic loading of the mouse tibia after orchidectomy. J Bone Miner Res. 2008;23(5):663-71.
32. Lynch ME, Main RP, Xu Q, Schmicker TL, Schaffler MB, Wright TM, van der Meulen MC. Tibial compression is anabolic in the adult mouse skeleton despite reduced responsiveness with aging. Bone. 2011;49(3):439-46.
33. Holguin N, Brodt MD, Sanchez ME, Kotiya AA, Silva MJ. Adaptation of tibial structure and strength to axial compression depends on loading history in both C57BL/6 and BALB/c mice. Calcif Tissue Int. 2013;93(3):211-21.
34. Clemens TL, Tang H, Maeda S, Kesterson RA, Demayo F, Pike JW, Gundberg CM. Analysis of osteocalcin expression in transgenic mice reveals a species difference in vitamin D regulation of mouse and human osteocalcin genes. J Bone Miner Res. 1997;12(10):1570-6.
35. Xiong J, Onal M, Jilka RL, Weinstein RS, Manolagas SC, O'Brien CA. Matrix-embedded cells control osteoclast formation. Nat Med. 2011;17(10):1235-41.
36. Borjesson AE, Lagerquist MK, Liu C, Shao R, Windahl SH, Karlsson C, Sjogren K, Moverare-Skrtic S, Antal MC, Krust A, Mohan S, Chambon P, Savendahl L, Ohlsson C. The role of estrogen receptor alpha in growth plate cartilage for longitudinal bone growth. J Bone Miner Res. 2010;25(12):2690-700.
37. Cao X, Chen D. The BMP signaling and in vivo bone formation. Gene. 2005;357(1):1-8.
38. Lindberg MK, Moverare S, Skrtic S, Gao H, Dahlman-Wright K, Gustafsson JA, Ohlsson C. Estrogen receptor (ER)-beta reduces ERalpha-regulated gene transcription, supporting a "ying yang" relationship between ERalpha and ERbeta in

mice. Mol Endocrinol. 2003;17(2):203-8.
39. Kamiya N, Ye L, Kobayashi T, Lucas DJ, Mochida Y, Yamauchi M, Kronenberg HM, Feng JQ, Mishina Y. Disruption of BMP signaling in osteoblasts through type IA receptor (BMPRIA) increases bone mass. J Bone Miner Res. 2008;23(12):2007-17.
40. Sugiyama T, Meakin LB, Browne WJ, Galea GL, Price JS, Lanyon LE. Bones' adaptive response to mechanical loading is essentially linear between the low strains associated with disuse and the high strains associated with the lamellar/woven bone transition. J Bone Miner Res. 2012;27(8):1784-93.
41. Dewulf N, Verschueren K, Lonnoy O, Moren A, Grimsby S, Vande Spiegle K, Miyazono K, Huylebroeck D, Ten Dijke P. Distinct spatial and temporal expression patterns of two type I receptors for bone morphogenetic proteins during mouse embryogenesis. Endocrinology. 1995;136(6):2652-63.
42. Mishina Y, Suzuki A, Ueno N, Behringer RR. Bmpr encodes a type I bone morphogenetic protein receptor that is essential for gastrulation during mouse embryogenesis. Genes Dev. 1995;9(24):3027-37.
43. Beamer WG, Donahue LR, Rosen CJ, Baylink DJ. Genetic variability in adult bone density among inbred strains of mice. Bone. 1996;18(5):397-403.
44. Richelson LS, Wahner HW, Melton LJ, 3rd, Riggs BL. Relative contributions of aging and estrogen deficiency to postmenopausal bone loss. N Engl J Med. 1984;311(20):1273-5.
45. Khosla S, Oursler MJ, Monroe DG. Estrogen and the skeleton. Trends Endocrinol Metab. 2012;23(11):576-81.
46. Kousteni S, Bellido T, Plotkin LI, O'Brien CA, Bodenner DL, Han L, Han K, DiGregorio GB, Katzenellenbogen JA, Katzenellenbogen BS, Roberson PK, Weinstein RS, Jilka RL, Manolagas SC. Nongenotropic, sex-nonspecific signaling through the estrogen or androgen receptors: dissociation from transcriptional activity. Cell. 2001;104(5):719-30.
47. Sunters A, Armstrong VJ, Zaman G, Kypta RM, Kawano Y, Lanyon LE, Price JS. Mechano-transduction in osteoblastic cells involves strain-regulated estrogen receptor alpha-mediated control of insulin-like growth factor (IGF) I receptor sensitivity to Ambient IGF, leading to phosphatidylinositol 3-kinase/AKT-dependent Wnt/LRP5 receptor-independent activation of beta-catenin signaling. J Biol Chem. 2010;285(12):8743-58.
48. Price JS, Sugiyama T, Galea GL, Meakin LB, Sunters A, Lanyon LE. Role of endocrine and paracrine factors in the adaptation of bone to mechanical loading. Curr Osteoporos Rep. 2011;9(2):76-82.
49. Thompson DD, Simmons HA, Pirie CM, Ke HZ. FDA Guidelines and animal models for osteoporosis. Bone. 1995;17(4 Suppl):125S-33S.
50. Bouxsein ML, Myers KS, Shultz KL, Donahue LR, Rosen CJ, Beamer WG. Ovariectomy-induced bone loss varies among inbred strains of mice. J Bone Miner Res. 2005;20(7):1085-92.
51. Lindberg MK, Weihua Z, Andersson N, Moverare S, Gao H, Vidal O, Erlandsson M, Windahl S, Andersson G, Lubahn DB, Carlsten H, Dahlman-Wright K, Gustafsson JA, Ohlsson C. Estrogen receptor specificity for the effects of estrogen in

ovariectomized mice. J Endocrinol. 2002;174(2):167-78.
52. Pettersson K, Delaunay F, Gustafsson JA. Estrogen receptor beta acts as a dominant regulator of estrogen signaling. Oncogene. 2000;19(43):4970-8.
53. Riggs BL, Khosla S, Melton LJ, 3rd. Sex steroids and the construction and conservation of the adult skeleton. Endocr Rev. 2002;23(3):279-302.
54. Khosla S, Amin S, Orwoll E. Osteoporosis in men. Endocr Rev. 2008;29(4):441-64.
55. Meakin LB, Galea GL, Sugiyama T, Lanyon LE, Price JS. Age-Related Impairment of Bones' Adaptive Response to Loading in Mice is Associated with Gender-Related Deficiencies in Osteoblasts But No Change in Osteocytes. J Bone Miner Res. 2014.
56. Modder UI, Hoey KA, Amin S, McCready LK, Achenbach SJ, Riggs BL, Melton LJ, 3rd, Khosla S. Relation of age, gender, and bone mass to circulating sclerostin levels in women and men. J Bone Miner Res. 2011;26(2):373-9.

APPENDIX A. **IN VIVO AXIAL LOADING OF THE MOUSE TIBIA**[2]

A.1 **Introduction**

In the field of bone metabolism, considerable interest exists in elucidating new anabolic pathways that can be targeted therapeutically to improve bone mass and strength. The dysregulation of certain bone-active signaling pathways, manifest in numerous human diseases of bone metabolism as altered bone mass, size and strength, have shed light on the mechanisms of norma7l skeletal homeostasis. More importantly, these observations provide insight into viable molecular targets that can be manipulated in otherwise healthy patients to achieve a therapeutic outcome. Recent efforts in skeletal biology have been focused on uncovering new anabolic, rather than anti-catabolic, pathways that can be manipulated to improve bone mass in skeletally fragile individuals. In addition, certain skeletal diseases have yielded targets for anabolic action in bone (e.g. hyperostosis corticalis, sclerosteosis). However, a much more ubiquitous mechanism of bone formation and accrual, that is not based on disease yet is incredibly anabolic, is available for therapeutic discovery. That mechanism is mechanotransduction, the process by which bone responds and adapts to its mechanical environment by adjusting tissue mass, architecture and material properties.

Repeated increased loading, such as occurs with exercise, has the propensity to induce new bone formation. Conversely, when loads are reduced during conditions such as bed rest, neuromuscular paralysis, and spaceflight, bone mass is lost in the weight-bearing bones. Despite its anabolic potential, our understanding of the cellular and molecular mechanisms that govern this adaptive process is far from complete. To systematically study this process, and eventually identify and clearly define the

[2] Melville KM, Robling AG, van der Meulen MCH (2014) Axial tibial loading of bone. AJ van Wijnen, JJ Westendorf, eds. Osteoporosis and Osteoarthritis, in Methods in Molecular Biology Series, in press

anabolic mechanisms involved, reliable, meaningful, well-characterized, and reproducible physiologic models of mechanical loading are crucial, preferably in intact animals. Towards this end, a number of animal loading models have been developed, including rodent exercise studies, rodent whole body vibration, and *in vivo* loading models such as tibial four-point bending, rodent ulnar axial loading, and mouse tibial axial loading (1-6). An advantage of *in vivo* mechanical loading models is that controlled, repeated mechanical forces are applied to the skeletal site of interest. In contrast, exercise studies are associated with a mechanical environment that is much more difficult to quantify and is less well-controlled.

One in vivo loading model that has been met with broad appeal is the mouse tibial axial loading model. This model applies cyclic, physiologically relevant loads to one tibia while using the contralateral tibia as an internal control (3, 7). This model has several advantages, including the use of the mouse, and the presence of substantial volumes of cortical and cancellous bone. The mouse is a valuable animal model because of the opportunity to study genetic manipulations, including congenic, transgenic, knockout, and knock-in mice. These genetic models can provide critical insights into the underlying mechanisms involved in mechanotransduction. The mouse tibia can provide information about the skeletal response to applied loads across several bone envelopes: cancellous, periosteal, and endocortical.

This chapter describes general methods for cyclic loading of the mouse tibia. The loading can be performed using a load-controlled mechanical testing system or a custom loading device with Labview software. The basic protocol in our laboratories involves loading groups of mice under isoflurane anesthesia for multiple days, and the procedures described are generally applicable and can be modified to suit an investigator's particular goals. Before beginning a loading experiment, a number of items must be considered. Loading protocols reported in the literature use a variety of

different parameters including number of loading sessions per week, number of loading cycles per day, and characteristics of the load waveform including the loading frequency, loading rate, and inclusion of rest periods (8, 9). Maximum or peak compressive load must also be determined prior to loading by using *in vivo* strain gauging techniques to measure bone stiffness at the tibial midshaft. Furthermore, before loading experiments are underway, a sham loading experiment must be performed to confirm the lack of systemic effects in any particular laboratory set-up. These considerations are first described, followed by a general outline of the strain gauging procedures and *in vivo* axial tibial loading methods.

Although not the focus of this chapter, before beginning an experiment, relevant outcome measures must be chosen. This choice will affect experimental design, number of animals, and experiment duration. Common outcomes measures include gene expression via qPCR, bone geometry and morphology via micro-computed tomography, dynamic histomorphometry via injection of bone-seeking fluorescent labels prior to sacrifice, protein and/or RNA localization *via* immunohistochemistry or *in situ* hybridization, mechanical testing, serum measurements via ELISA or RIA, body and organ masses, and many others.

A.2 **Materials**

A.2.1 Animal Model Selection

1. Select mouse strain. The choice of background strain for mouse axial tibial loading will depend on a number of factors. The amount of cancellous bone in the tibial metaphysis varies with mouse strain, as do cortical bone mass, bone mineral density, bone shape, and bone strength (10-14). Tibia length and

mouse size are also items to consider. Furthermore, some mouse strains are more mechanoresponsive than others (15, 16).

2. Select wild type or genetically modified mice. Depending on the research question, genetically modified mice may help identify whether the response to loading depends on the absence, presence, overexpression or modification of a particular gene or set of genes.
3. Select appropriate sex. The research question being asked will guide the decision regarding the use of male or female mice (or both). For example, models of post-menopausal osteoporosis are usually performed in female mice, particularly if ovariectomy will be used. Models of osteoarthritis usually use male mice because of the chondroprotective effect of estrogen (17). Many individual genes or larger quantitative trait loci (QTL) are associated with sex-specific effects, so when dealing with a novel gene or pathway with no *a priori* knowledge of sex interaction, males and females should both be studied.
4. Select mouse age. Again, this choice depends on the research question. Growing animals are still accruing bone mass, until around 16-24 weeks of age, when peak bone mass is reached although the specific age varies with bone site and mouse strain (11, 14). Aged mice are usually in a state of bone loss (18). Mice that have just reached skeletal maturity (e.g., 16 wks of age) are often used for tibia loading because the skeleton is still young enough to elicit a robust anabolic response to mechanical stimulation, and at the same time, the appositional growth on the periosteal surfaces has dropped to very low levels. This latter attribute allows for a less complicated interpretation of the load-induced bone formation effects observed in the loaded limb. At this age at this age the anabolic response is almost exclusively a result of loading,

rather than a combined function of growth and enhanced mechanical input (as occurs in loaded growing bone).

A.2.2 Select appropriate controls.

1. Sham controls. A separate experiment must be performed to ensure that tibial loading does not cause systemic effects, which have been both confirmed and refuted in the literature (19, 20). Confirm that paired contralateral control limbs from loaded mice are not different from control limbs obtained from separate nonloaded animals. This experiment should contain two groups of mice for an experimental duration corresponding to that of the planned *in vivo* tibial loading experiments. The first group of mice should have one tibia loaded while the contralateral limb is used as an internal control. The second group should be put under anesthesia and have one tibia placed in the loading device for the duration of loading just as the first group, but the tibia should not actually be loaded during the experiment (sham loading). If the results from the two sets of control limbs are similar, then paired contralateral limbs are appropriate controls.
2. Paired controls. If no systemic effects are presents, the contralateral, unloaded limb is often used as the control tibia, to which all measurable outcomes will be compared in determining bone's anabolic response to mechanical loading.

A.2.3 Strain Gauging Materials (When not specified, materials can be ordered from Fisher Scientific or similar supplier)

1. 60/40 tin/lead solder, 0.022 inch diameter (Multicore Solders, Westbury, NY)
2. Three-conductor cable (Vishay Micro-Measurements, Wendell, NC, Cat# 336-FTE)

3. Soldering iron (GC Electronics, Rockford, IL, Model# 12-070)
4. Dissecting microscope with light source
5. Dissecting curved jewelers microforceps (Fisher Scientific, Cat# 08-953F)
6. Standard capacity wire stripping system (American Beauty, Clawson, MI, Model# 10503)
7. Tip tinner (MG Chemicals, Burlington, Ontario, Cat# 4910-28G)
8. Rosin Soldering Flux (Radio Shack)
9. Single element strain gauges (Vishay Micro-Measurements, Cat# EA-06-015LA-120)
10. Scalpel holder and #15 scalpel blades
11. Isopropyl alcohol
12. Clear tape
13. Index cards for gauge preparation
14. 1st coat: M Bond Adhesive Resin Type AE (Vishay Micro-Measurements)
15. Catalyst for 1st coat: M Bond Type 10 Curing Agent (Vishay Micro-Measurements)
16. 2nd coat: M Coat D (Vishay Micro-Measurements) (store in refrigerator)
17. 3rd coat: M Coat A (Vishay Micro-Measurements) (store in refrigerator)
18. Weigh boats in which to mix the first coat with the catalyst
19. Cotton swabs to apply isopropyl alcohol
20. Wooden applicator sticks to apply coat coverings
21. Eye dropper or transfer pipettes
22. Xylene, to thin 3rd coat if needed
23. Toluene, to thin 2nd coat if needed
24. Plugs for wires to connect gauge to computer or data acquisition device (Digi-Key, Thief River Falls, MN, Part# A26528-40-ND)

25. 1-min, 3-min, or 5-min curing epoxy
26. Digital multimeter
27. Strain conditioning hardware including bridge excitation, Wheatstone bridge circuit, and signal amplification and filtering. Integrated systems are produced by Vishay Micro-measurements and National Instruments LabView board (Part #'s 781156-01, 779521-01, 194738-01, 779012-01).

A.2.4 Surgical Supplies

1. Surgical tools including scissors, small scalpels and blades, jeweler's forceps, periosteal elevator and small-tooth forceps
2. Small gauze
3. Small animal razor
4. Calipers
5. Cotton swabs
6. Methyl ethyl ketone
7. Cyanoacrylate tissue adhesive

A.2.5 Loading Materials

1. Loading device with actuator, calibrated load cell (or similar)
2. Computer with connections for loading hardware and electronics
3. If using custom loading device, signal conditioning hardware for data acquisition from load cell with Labview software for tibial loading (or similar) (*see* **Note 1**)
4. Loading configuration files to input loading parameters

5. Wooden cylindrical rod (~17mm length) from long cotton swab handle (Fisher Scientific, #23-400-118) for loading program test (*see* **Note 2**)

A.2.6 Mouse Care Materials

1. Rodent cages with food, enrichment (such as a shelter, PVC pipe, running wheel, or hard wood block), nesting material, and water.
2. Rodent anesthesia induction chamber
3. Mouse anesthesia nose cone
4. Isoflurane anesthesia machine with tubing attached to anesthesia chamber and mouse nose cone simultaneously
5. Oxygen tank connected to isoflurane machine
6. Isoflurane
7. Carbon cartridge halogen filters connected to tubing to scavenge isoflurane
8. Sterile petroleum jelly eye ointment (Fisher Scientific, Cat# NC0138063)
9. Extra mouse cage for anesthesia recovery
10. Balance with 0.01g accuracy and maximum capacity of at least 200g

A.3 **Methods**

All animal procedures should be reviewed and approved by your Institutional Animal Care and Use Committee.

Prior to Loading Experiment:

A.3.1 Loading Parameter Selection

1. Select peak or maximum compressive load. Peak or maximum load is the load level that will be reached repeatedly during the cyclic loading. This load can vary depending on age, sex, strain, and genotype. To determine this load level, in vivo strain gaging at the tibial midshaft should be performed. (See 3.2 "Determining in vivo stiffness using strain gauges" below.) By determining tibial bone stiffness at the midshaft, the load to produce a desired strain at the tibial midshaft can be chosen.
2. Select pre-load value. The magnitude of the compressive pre-load should be a small percentage of the maximum or peak load. For example, –0.5N is an appropriate pre-load for a -9.0N compressive peak load (*see* **Note 3**).
3. Select frequency, loading rate, dwell time, and number of cycles for the loading waveform. Triangle waves are generally used because the load is applied at a constant strain rate. For a sinusoidal wave, the loading rate varies throughout the cycle. One commonly used *in vivo* compressive loading protocol for the mouse consists of 1200 cycles per day at 4 Hz, with a load-unload ramp of 0.15 seconds and 0.1s dwell time (**Figure A1**) (8). Another common protocol applies 60 cycles per day at 2Hz, with a load-unload ramp of 0.15 seconds and 10s second dwell time (9). (*see* **Note 4**)
4. Select pause insertion duration. Bone formation is stimulated by inserting pauses in between load cycles, rather than continuous cyclic loading (21). In axial tibial loading of mice, rest insertions have been short (0.1s) or long (10.0s) (8, 9). As described in Step (3) pauses also can be used to achieve the desired loading rate and frequency.
5. Select loading duration. A range of loading durations have been used. Loading 3 or 5 times per week is most common (8, 9). The duration of loading experiments can last from 1 day to 6 weeks and will depend on the research

question and outcome measurements. Shorter time frames are often used when the primary outcome measures are skeletal gene expression changes after mechanical loading. Longer time frames are often used to detect changes in bone morphology, geometry, and cellular activity.

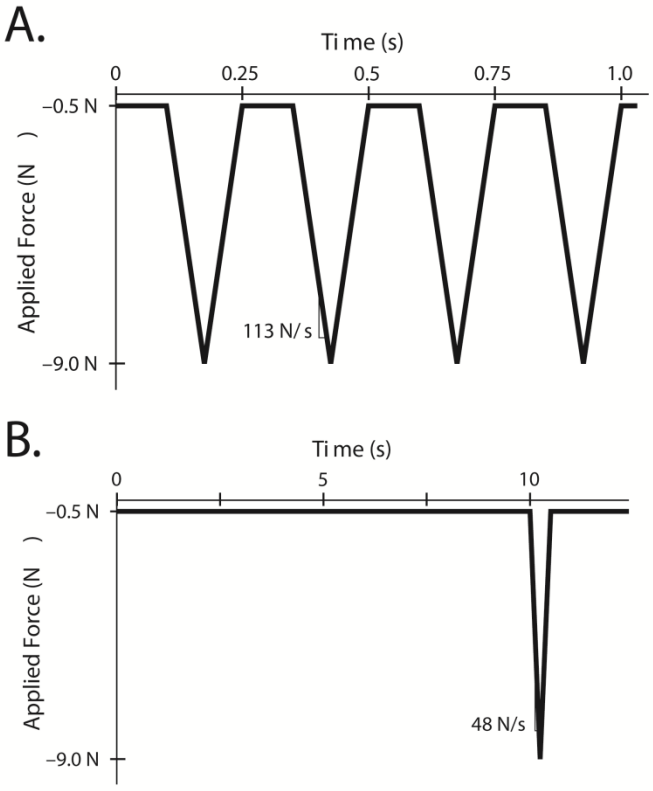

Figure A.1 Common in vivo axial tibial loading triangular waveforms for mice with 9.0N peak compressive load. (A) This waveform is usually run 5 times per week, 1200 cycles per day at a rate of 4Hz, with a 0.1s dwell period, and 113 N/s loading rate. (B) This waveform is run 3 times per week, 60 cycles per day at a rate of 0.1Hz, with a 10.0s dwell period and a 48 N/s loading rate.

A.3.2 Determining in vivo stiffness using strain gauges

Strain gauges are electrical conductors that change resistance when deformed. By rigidly attaching a gauge to the surface of the tibia, the deformation caused by loading

can be measured. Stiffness is then calculated as the applied load per deformation. In practice, the goal is to determine the load required to achieve a desired strain level on the bone surface. For a stiff bone, this load is higher than for a more compliant bone.

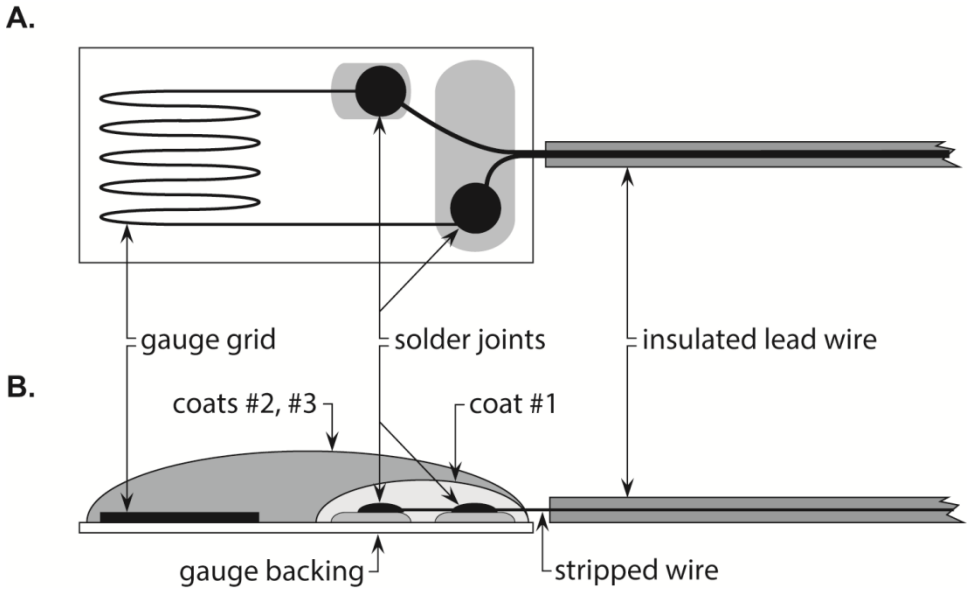

Figure A.2 Trimmed strain gauge assembly. (A) Top view of strain gauge preparation. (B) Side-view schematic of strain gauge preparation. The 1st coat is applied only to the soldering joint and should not touch the gauge grid. The 2nd and 3rd coats are applied to the entire gauge top surface. Stripped wire should not be exposed and can be covered by the coats.

A.3.2.1 Strain gauge preparation (**Figure A.2**)

1. Trim the gauge of unnecessary material. Place gauge on an index card and view using a dissecting microscope. Using a scalpel, remove excess material by cutting just within alignment markings; be careful not to disturb strain-sensitive grid. Use rocking motions, not shearing motions, to trim. Once trimmed, secure and protect grid with scotch tape while leaving terminals exposed.

2. Prepare lead wires. Trim two wires to 17cm in length and strip approximately 0.5cm of insulation from one end of each wire. Dip these ends in solder flux and touch the soldering iron to each wire.
3. Prepare gauge terminals. Apply a minimal amount of solder primer to the end of each wire, then use soldering iron to add tin. Use the dissecting microscope, and be careful to ensure that the added tin is contained within each terminal to prevent a short circuit.
4. Solder lead wires onto gauge terminals using the stripped and tinned ends.
5. Remove tape, and clean gauge with isopropyl alcohol.
6. Bend the gauge wires into an S-shape so that the gauge is slanted with the grid section at the highest point.
7. Apply insulating coats (*see* **Note 5**).
    1. Mix up M-coat AE in a weigh boat 30 minutes before application to gauge leads. Mix a dime-sized amount of resin and two medicine drops of catalyst. After 30 minutes, apply only to the gauge terminals by dabbing small amounts of resin to the leads by touching with a wooden applicator stick. Make sure the resin does not touch the grid. Let the resin catalyze overnight at room temperature.
    2. The following day, apply M-coat D (white, store in refrigerator) with the supplied brush to the entire upper surface of the gauge. Cure overnight at room temperature, or at room temperature for 15minutes and then in an oven for 1hr at 65°C (*see* **Note 6**).
8. The following day, apply M-coat A (clear, stored in refrigerator) to the entire top surface of the gauge using a wooden applicator stick by dab touching. Cure for 4-5 days at room temperature before applying the strain gauges to the bone (*see* **Note 7**).

9. Attach a plug to the wire ends. First apply flux to both the wire tips and the plug leads. Then, apply solder to the plug leads. Last, place the wires on top of the solder-covered plugs and heat with the soldering iron until bonded.
10. Coat plug/wire connections with epoxy.
11. Check the resistance of the gauge. Using a digital multimeter, touch the leads of the device to the ends of the plug. The strain gauge should read 120.0 Ω, but an acceptable range is 118.5-121.5 Ω.

A.3.2.2 In Vivo Load-Strain Calibration

1. Prepare a working area in a fume hood or biosafety cabinet.
2. Anesthetize the mouse using isoflurane (2.5% in 1 L/min O_2). This procedure applies strain gauges as a non-survival surgery, and so the mouse is anesthetized throughout the surgery and data collection and then euthananized.
3. Shave the mouse limb. Fur must be removed at the site of strain gauge application, which is the medial aspect of the hindlimb of interest.
4. Measure the length of the tibia from ankle to knee using calipers. Use the result to approximate the tibial midshaft and mark this location on the skin using a felt-tipped pen.
5. Incise the hindlimb to expose tibia. This exposure is most easily accomplished using scissors. First, make an opening where the midshaft was approximated. Then, using blunt dissection techniques separate skin from underlying muscle working proximally toward the knee and distally toward the ankle. The incision should be as small as possible, but will usually span from just proximal to the ankle joint to just distal to the knee joint. Keep in mind that the knee and ankle will be contact points when load is applied, therefore skin in these areas should remain intact.

6. Retract muscle and skin from implantation site. Use blunt dissection techniques to expose the periosteal surface of the tibia.
7. Prepare the tibial surface for adhesion. Gently scrape the bone with a periosteal elevator to remove the periosteum and debris. Degrease the bone using a cotton swab saturated with methyl ethyl ketone or chloroform.
8. Prepare strain gauge for adhesion. Using a cotton swab saturated with methyl ethyl ketone, degrease the gauge carefully using minimal pressure. Then, grasp the wires with jeweler's forceps just above the gauge.
9. Apply a very small drop of cyanoacrylate adhesive to the back of the gauge and immediately adhere the gauge to the midshaft of the tibia, being sure to align it with the long axis of the diaphysis (**Figure A.3**). Adhering the gauge works best when another laboratory member is firmly holding the tibia in place. Apply gentle pressure for one minute to ensure secure attachment (*see* **Note 8**).
10. Examine the gauge attachment. The grid should be located at the midshaft of the tibia, aligned with the longitudinal axis of the tibia, and not be medial or lateral or rotated.
11. Calibrate the strain gauge. Open Labview or similar data acquisition software. Insert the gauge lead wires into strain conditioner or similar to complete the Wheatstone bridge quarter-bridge. Calibrate the gauge to zero while the mouse lies in a dorsal recumbent position. If calibration fails, a new gauge must be prepared and attached. To do so, the bone must be re-cleaned and the Steps 7-11 repeated.
12. Apply compressive load. Place animal in the loading device actuator and apply a voltage corresponding to approximately a 2N load (*see* **Note 9**). Ascertain the viability of the attached gauge by determining if the results resemble

accurate strain patterns. Apply mechanical loads for varying voltages to produce peak compressive loads from approximately 2.0N to 10.0N (*see* **Note 10**).

13. Once all data have been collected, cut off the wires very close to the gauge, but keep the gauge attached to the bone. The tibia should be imaged using micro-computed tomography to determine if gauge placement was accurate. Gauge positioning is very important to ensure that results are comparable across different animals and ages.
14. Properly euthanize mouse once strain gauge data have been obtained for both limbs.
15. From stiffness data of all animals in a group, calculate the load needed to apply a specific strain to the tibial midshaft. The physiologic range of bone strain across multiple vertebrate species during normal activity is 1000-1500 με in compression (22).
16. If desired, the strain data measured at the gauge location can be combined with a finite element analysis to determine the peak strain within the cortical cross section (9, 23). The strains at the gauge location are generally not the maximum strains for the cortex. This analysis requires solving for the tibial strains using a computational model of the mouse tibia at the section of gauge attachment.

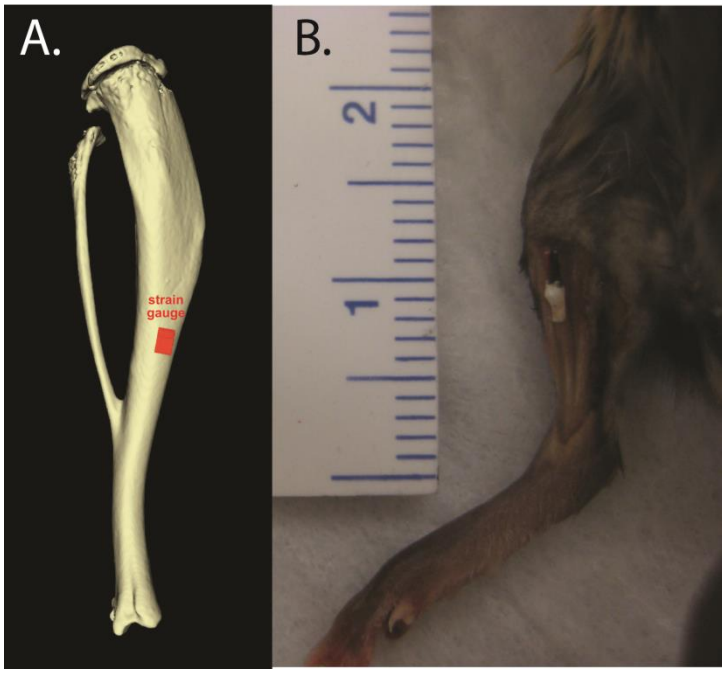

Figure A.3 Proper strain gauge placement at the tibial midshaft. (A) Schematic showing strain gauge positioned at the middiaphysis of tibia. (B) Photograph of surgically-implanted gauge attached to surface of mouse tibia.

A.3.3 In Vivo Axial Tibial Loading Experimental Methods

A.3.3.1 Set Up and Preparation for In Vivo Axial Tibial Loading

1. Connect and power on all electronic signal conditioning components, including the loading device.
2. Open LabView loading program and insert proper loading parameters.
3. Zero the load cell. Check load offset by reading load when load cell is resting without any item positioned in the loading fixtures. Depending on your loading system, either enter the load offset in Newtons if an offset is entered directly or select the option to zero the load cell. The load from load cell should now read 0.0N (*see* **Note 11**).

4. Position a wooden rod in the loading device. Adjust and lock the horizontal position such that the rod is snug between the actuator and the load cell, but not so tight that the load cell is loaded beyond -1.0N.
5. Open and appropriately name the data file.
6. Run practice loading session with rod to warm up components and confirm the loading setup is working correctly and has no unforeseen issues.

Figure A.4 Mouse situated in loading device, ready for in vivo axial loading to be applied to the left tibia.

A.3.3.2 Application of In Vivo Axial Tibial Loading

1. While rod is being loaded, turn on oxygen tank and isoflurane machine. Set oxygen flow to 1L/min and isoflurane flow to 2%, or whatever levels have been established in your protocol and approved by your Institutional Animal Care and Use Committee.
2. Place first mouse to be loaded into anesthesia chamber (Mouse A).
3. When Mouse A is asleep, remove Mouse A from chamber and apply eye ointment to each eye to maintain hydration during anesthesia, loading and recovery.

4. When test of wooden rod completes, promptly loosen fixtures and remove the rod.
5. Immediately check the load cell offset and adjust offset value if necessary so that the resting load cell reads 0.0N.
6. Remove Mouse A from the anesthesia chamber and place nose cone over nose.
7. Position Mouse A in the loading device, and lock the device so that the left tibia is snug. The left knee should be snug at the load cell cup and foot snug at the actuator (**Figure A.4**). Once tibia is positioned and the device adjusted and locked, load cell should not read below -1.0N before loading begins or too much compressive preload is applied to the tibia (*see* **Note 12**).
8. Open a new data file and name the file appropriately to identify experiment, mouse, and date.
9. Begin the loading program when Mouse A's breathing is slowed.
10. Monitor Mouse A during loading to check for continued slow breathing and unconsciousness (*see* **Note 13**).
11. Monitor the load cell and voltage outputs during the loading program (*see* **Note 14**).
12. When 2 to 3 minutes remain in the loading program, place the next mouse (Mouse B) into the isoflurane chamber (*see* **Note 15**).
13. When Mouse B is asleep, remove Mouse B from chamber and apply eye ointment to each eye to maintain hydration during anesthesia, loading and recovery.
14. Once loading program finishes, promptly unlock the loading device, remove Mouse A, and place on balance.
15. Check the load cell offset and adjust offset value if necessary so that the resting load cell reads 0.0N.

16. Record Mouse A body mass and place the animal into anesthesia recovery cage. Use one recovery cage per cage of mice. Once all mice from a single cage have been loaded, make sure all mice are awake and moving around before returning the animals to their original cage.
17. Position Mouse B into loading device, and adjust and lock the device so that left tibia is snug.
18. Repeat steps 7-17 for each subsequent mouse until all mice are loaded (Mouse B becomes Mouse A, and next mouse becomes Mouse B, etc.).
19. If a mouse loses >10% body mass over the course of an experiment, then wet food should be placed in the cage containing that mouse. If a mouse loses 20% body mass, that mouse should no longer be used for the experiment and should be appropriately euthanized.
20. Repeat procedure for each day that mice are to be loaded. Always load the same tibia for each mouse.

A.3.3.3 Clean up

1. Once final mouse is in recovery cage, turn off isoflurane and oxygen.
2. Close loading program software.
3. Turn off all electronic components.

A.3.4 Potential Outcome Measures

1. Cortical and cancellous morphology by microcomputed tomography
2. Gene expression by qRT-PCR
3. Dynamic histomorphometry using fluorochrome labeling
4. Protein localization by immunohistochemistry
5. Serum hormone assays by ELISA

6. Many others

A.4 **Notes**

1. The loads can be applied using a load-controlled mechanical testing system, such as the Bose Enduratec system or similar, or using a custom loading device with load cell and associated electronics signal conditioning hardware (National Instruments) and control software (Labview). When using a mechanical testing system, the loading waveform needs to be programmed within the software interface. Portable systems allow loading to be performed in the animal facility; table top machines require transportation of the animals to the laboratory. Custom loading devices are portable and allow loading in the animal facility. The Labview software can be customized as desired.
2. The practice rod does not have to be made of wood or be exactly 17mm in length. Wooden handles removed from long cotton swabs work well, and approximate the length of a mouse tibia and are less stiff than metal.)
3. A pre-load is required so that the actuator does not lift off at the beginning of loading or during the dwell phase of the cyclic loading.
4. Several loading waveform parameters are coupled. For example, loading rate and frequency are related. However, if the loading rate results in a higher frequency than desired, a dwell period may be included to achieve the desired frequency.
5. Insulating coats are applied to solidify solder bonds and to waterproof the gauge.
6. Toluene may be added to thin M-coat D as necessary.
7. Xylene may be added to thin M-coat A as necessary.

8. Attaching the strain gauge to bone in vivo is a difficult step, and practice runs are recommended.

9. This voltage should be determined prior to beginning strain gauge surgery. By loading a wooden rod in the loading device, the voltage corresponding to 2, 4, 6, 8, 10, and 12N can be determined. These values can then be applied once the strain gauge is applied to the anesthetized mouse.

10. During strain gaging, several items must be monitored: 1) Noise in data. If the gauge is not attached properly or is misaligned, the data will be very noisy (**Figure A.5**). Occasionally this noise will decrease at higher voltages. If the noise does not disappear, then a new gauge needs to be attached and data collection must be repeated. 2) Strain levels. During loading, the bone strain should be approximated by determining the difference between the peak and valley of the strain read out. If the applied strain exceeds 2000 με as the voltage increases, then the higher voltages should be excluded for this particular mouse/strain/limb. At very high strain levels, the bone could fracture. 3) Mouse status. Be sure that the mouse is in deep anesthesia and that its nose remains in the nose cone at all times.

11. The offset load for the load cell should stay relatively constant throughout the day and throughout the entire experiment. If large changes are noted, the load cell should be recalibrated or replaced. The offset load value should also be relatively low compared to the peak load applied to the tibia, at least <10% but ideally <5%.)

12. The tibia is positioned horizontally in our loading device at Cornell, and so the mouse will be positioned on its back. If the tibia is positioned vertically, the mouse will be positioned differently.

13. If the mouse's breathing becomes rapid, quickly increase the isoflurane to 2.5-3% for a period of about 20 seconds. For the next mouse, be sure to wait longer for slower breathing before beginning the loading program.

14. Both the voltage input and load output should be steady cyclic wave patterns. Make sure peak load is being reached consistently. If using Labview and input and/or output are jumpy, Hardware Configuration PID settings may need to be altered. If load cell is not reading, immediately stop program and check that all wires are connected.

15. This time to start anesthesia may vary depending on how quickly anesthesia takes effect on mice and will differ by age, sex and genotype.

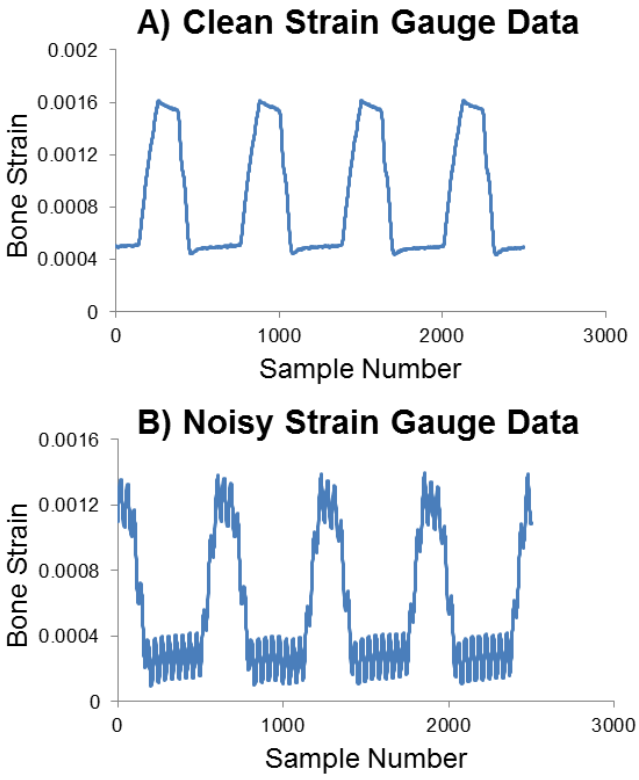

Figure A.5 Sample strain gauge data. (A) Clean data with clear values, indicating proper gauge attachment. (B) Data with high frequency noise evident likely because

the gauge is poorly attached or may be aligned off-axis. A new gauge should be used.

A.5 **References**

1. Turner CH, Akhter MP, Raab DM, Kimmel DB, Recker RR. A noninvasive, in vivo model for studying strain adaptive bone modeling. Bone. 1991;12(2):73-9.
2. Lee KC, Maxwell A, Lanyon LE. Validation of a technique for studying functional adaptation of the mouse ulna in response to mechanical loading. Bone. 2002;31(3):407-12.
3. Fritton JC, Myers ER, Wright TM, van der Meulen MC. Loading induces site-specific increases in mineral content assessed by microcomputed tomography of the mouse tibia. Bone. 2005;36(6):1030-8.
4. Wallace JM, Rajachar RM, Allen MR, Bloomfield SA, Robey PG, Young MF, Kohn DH. Exercise-induced changes in the cortical bone of growing mice are bone- and gender-specific. Bone. 2007;40(4):1120-7.
5. Prisby RD, Lafage-Proust MH, Malaval L, Belli A, Vico L. Effects of whole body vibration on the skeleton and other organ systems in man and animal models: What we know and what we need to know. Ageing Research Reviews. 2008;7(4):319-29.
6. Iwamoto J, Takeda T, Sato Y. Effect of treadmill exercise on bone mass in female rats. Exp Anim. 2005;54(1):1-6.
7. De Souza RL, Matsuura M, Eckstein F, Rawlinson SC, Lanyon LE, Pitsillides AA. Non-invasive axial loading of mouse tibiae increases cortical bone formation and modifies trabecular organization: a new model to study cortical and cancellous compartments in a single loaded element. Bone. 2005;37(6):810-8.
8. Lynch ME, Main RP, Xu Q, Walsh DJ, Schaffler MB, Wright TM, van der Meulen MC. Cancellous bone adaptation to tibial compression is not sex dependent in growing mice. J Appl Physiol. 2010;109(3):685-91.
9. Brodt MD, Silva MJ. Aged mice have enhanced endocortical response and normal periosteal response compared with young-adult mice following 1 week of axial tibial compression. J Bone Miner Res. 2010;25(9):2006-15.
10. Sheng MH, Baylink DJ, Beamer WG, Donahue LR, Rosen CJ, Lau KH, Wergedal JE. Histomorphometric studies show that bone formation and bone mineral apposition rates are greater in C3H/HeJ (high-density) than C57BL/6J (low-density) mice during growth. Bone. 1999;25(4):421-9.
11. Klein RF, Shea M, Gunness ME, Pelz GB, Belknap JK, Orwoll ES. Phenotypic characterization of mice bred for high and low peak bone mass. J Bone Miner Res. 2001;16(1):63-71.
12. Wergedal JE, Sheng MH, Ackert-Bicknell CL, Beamer WG, Baylink DJ. Genetic variation in femur extrinsic strength in 29 different inbred strains of mice is dependent on variations in femur cross-sectional geometry and bone density. Bone.

2005;36(1):111-22.
13. Sabsovich I, Clark JD, Liao G, Peltz G, Lindsey DP, Jacobs CR, Yao W, Guo TZ, Kingery WS. Bone microstructure and its associated genetic variability in 12 inbred mouse strains: microCT study and in silico genome scan. Bone. 2008;42(2):439-51.
14. Beamer WG, Donahue LR, Rosen CJ, Baylink DJ. Genetic variability in adult bone density among inbred strains of mice. Bone. 1996;18(5):397-403.
15. Robling AG, Turner CH. Mechanotransduction in bone: genetic effects on mechanosensitivity in mice. Bone. 2002;31(5):562-9.
16. Saxon LK, Robling AG, Castillo AB, Mohan S, Turner CH. The skeletal responsiveness to mechanical loading is enhanced in mice with a null mutation in estrogen receptor-beta. Am J Physiol Endocrinol Metab. 2007;293(2):E484-91.
17. Nielsen RH, Christiansen C, Stolina M, Karsdal MA. Oestrogen exhibits type II collagen protective effects and attenuates collagen-induced arthritis in rats. Clinical and Experimental Immunology. 2008;152(1):21-7.
18. Glatt V, Canalis E, Stadmeyer L, Bouxsein ML. Age-related changes in trabecular architecture differ in female and male C57BL/6J mice. J Bone Miner Res. 2007;22(8):1197-207.
19. Sample SJ, Collins RJ, Wilson AP, Racette MA, Behan M, Markel MD, Kalscheur VL, Hao Z, Muir P. Systemic effects of ulna loading in male rats during functional adaptation. J Bone Miner Res. 2010;25(9):2016-28.
20. Sugiyama T, Price JS, Lanyon LE. Functional adaptation to mechanical loading in both cortical and cancellous bone is controlled locally and is confined to the loaded bones. Bone. 2010;46(2):314-21.
21. Srinivasan S, Ausk BJ, Poliachik SL, Warner SE, Richardson TS, Gross TS. Rest-inserted loading rapidly amplifies the response of bone to small increases in strain and load cycles. J Appl Physiol. 2007;102(5):1945-52.
22. Rubin CT, Lanyon LE. Dynamic strain similarity in vertebrates; an alternative to allometric limb bone scaling. J Theor Biol. 1984;107(2):321-7.
23. Christiansen BA, Bayly PV, Silva MJ. Constrained tibial vibration in mice: a method for studying the effects of vibrational loading of bone. J Biomech Eng. 2008;130(4):044502.

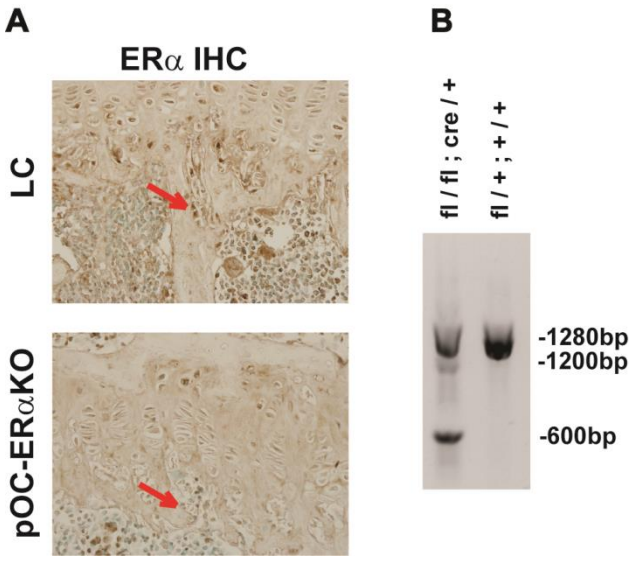

Figure B.1 ERα deletion confirmation. (A) LC mice have positively stained osteoblasts for ERα, while cKO mice do not. (B) Genomic femur DNA PCR confirmed the presence of the knockout allele (600bp) in cKO mice but not in LC mice.

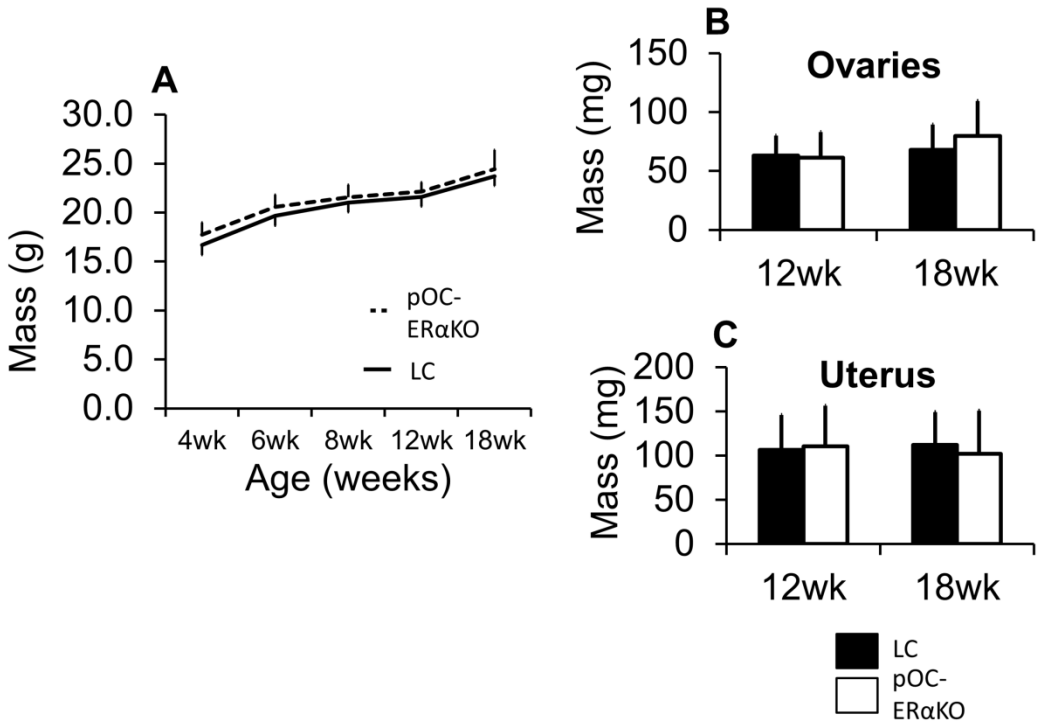

Figure B.2 Unlike the global ERαKO, pOC-ERαKO female mice had normal body (A), ovarian (B) and uterine (C) masses at 12 and 18 weeks of age compared to LC mice.

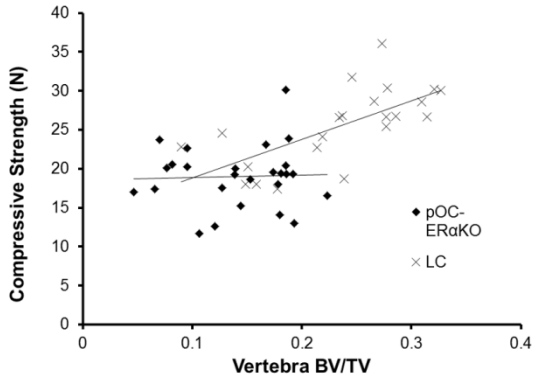

Figure B.3 Vertebral compressive strength correlated linearly with BV/TV for LC but not pOC-ERαKO mice through regression analysis. BV/TV accounted for 43% of the variation in vertebral compressive strength for LC mice (p=0.0006) but BV/TV had no predictive value for vertebral strength in pOC-ERαKO mice.

Table B.1: Phenotype measurements for female pOC-ERαKO and LC mice

	12wk		**18wk**	
	LC	**cKO**	**LC**	**cKO**
Crown/Rump Length (mm)	84.0 ± 4.2	85.0 ± 3.0	88.2 ± 3.7	90.0 ± 2.3
Ovary Mass (mg)	63.3 ± 17	61.4 ± 22	68.0 ± 22	80.0 ± 30
Uterus Mass (mg)	106 ± 39	111 ± 46	112 ± 37	102 ± 49
Right Femur Length (mm)	17.8 ± 0.38	17.8 ± 0.46	18.3 ± 0.65	18.5 ± 0.39
Right Tibia Length (mm)	15.4 ± 0.38	15.1 ± 0.66	15.7 ± 0.37	16.0 ± 0.43

Data are represented as mean ± SD.

Table B.2 Indices of cancellous bone determined by microCT analysis of VOIs from the right proximal tibial metaphysis of female pOC-ERαKO and LC mice.

Animal ID	Age	cKO or LC	BV/TV	Tb.Th (mm)	Tb.Sp (mm)	cn.TMD (mgHA/cc)
15-02	16wk	LC	0.1323	0.0581	0.3175	
15-15	16wk	LC	0.1139	0.0559	0.3581	
16-03	16wk	LC	0.1534	0.0641	0.3073	735.313
17-11	16wk	LC	0.1125	0.0606	0.3326	744.558
17-02	16wk	LC	0.1449	0.0721	0.4168	747.618
17-03	16wk	LC	0.1486	0.0748	0.48	751.46
18-08	16wk	LC	0.1175	0.059	0.3342	723.528
19-06	16wk	LC	0.1089	0.0621	0.3211	775.941
20-03	16wk	LC	0.1665	0.0694	0.3206	761.226
21_04	16wk	LC	0.1402	0.066	0.3321	758.231
16-01	16wk	cKO	0.1539	0.0715	0.4412	733.294
16-02	16wk	cKO	0.1181	0.0639	0.4056	744.754
17-07	16wk	cKO	0.1682	0.0762	0.432	711.026
17-10	16wk	cKO	0.136	0.0679	0.62	728.541
18-02	16wk	cKO	0.0719	0.061	0.7517	749.507
19-04	16wk	cKO	0.1096	0.0704	0.6239	753.804
21-07	16wk	cKO	0.1423	0.0718	0.5716	740.521
18-04	16wk	cKO	0.0609	0.0596	0.6602	730.885
21-05	16wk	cKO	0.1481	0.0721	0.4519	
22-01	16wk	cKO	0.1416	0.0707	0.6751	
1203	12wk	LC	0.0854	0.0494	0.334	761.974
1205	12wk	LC	0.0874	0.0496	0.2949	787.942
1216	12wk	LC	0.0983	0.0488	0.2971	765.504
1304	12wk	LC	0.0904	0.0499	0.3203	752.141
1306	12wk	LC	0.0773	0.0504	0.3668	803.132
1410	12wk	LC	0.0643	0.0445	0.34	774.454
1201	12wk	cKO	0.0508	0.049	0.3859	786.682
1204	12wk	cKO	0.0617	0.0506	0.5242	798.846
1208	12wk	cKO	0.0543	0.0467	0.4667	788.699
804	12wk	cKO	0.0583	0.0465	0.4771	771.996
1107	12wk	cKO	0.0362	0.0445	0.5281	782.711
1301	12wk	cKO	0.0566	0.0491	0.5422	804.771
1403	12wk	cKO	0.0304	0.0453	0.5299	761.281

Table B.2 continued:

Animal ID	Age	cKO or LC	BV/TV	Tb.Th (mm)	Tb.Sp (mm)	cn.TMD (mgHA/cc)
A26-06	12wk	LC	0.1277	0.0521	0.2714	766.826
A27-07	12wk	LC	0.1171	0.0558	0.3601	761.812
A28-02	12wk	LC	0.1321	0.056	0.2768	760.25
A29-04	12wk	LC	0.0571	0.0463	0.4388	757.189
B31-04	12wk	LC	0.0887	0.0483	0.3272	762.073
B34-12	12wk	LC	0.0985	0.0475	0.3323	770.277
B33-07	12wk	LC	0.0855	0.0517	0.363	748.074
C34-11	12wk	LC	0.13	0.0573	0.2794	790.265
C32-07	12wk	LC	0.0824	0.0546	0.3794	780.629
C35-14	12wk	LC	0.1196	0.0596	0.3511	798.665
D27-03	12wk	cKO	0.07	0.0546	0.4882	773.337
D27-13	12wk	cKO	0.0875	0.0562	0.4842	769.626
D28-04	12wk	cKO	0.0815	0.0506	0.4263	764.612
D32-01	12wk	cKO	0.0607	0.0492	0.4799	740.196
E29-09	12wk	cKO	0.0844	0.0503	0.4636	766.24
E30-06	12wk	cKO	0.0666	0.0485	0.4339	762.594
E31-01	12wk	cKO	0.0594	0.0507	0.5039	780.173
F31-02	12wk	cKO	0.0594	0.0518	0.5613	783.038
F29-03	12wk	cKO	0.0778	0.0504	0.5005	741.824
F33-01	12wk	cKO	0.0759	0.054	0.4279	794.693

Table B.3 Indices of cortical bone determined by microCT analysis of VOIs from the right tibial midshaft of female pOC-ERαKO and LC mice.

Animal ID	Age	cKO or LC	I_{MAX} (mm^4)	I_{MIM} (mm^4)	Ct.Ar. (mm^2)	ct.TMD (mgHA/cc)
15-02	16wk	LC	0.06847	0.04026	0.63177	1038.791
15-15	16wk	LC	0.06999	0.04573	0.60843	1025.444
16-03	16wk	LC	0.11252	0.06485	0.7709	1032.866
17-11	16wk	LC	0.05921	0.04392	0.64991	1030.783
17-02	16wk	LC	0.0699	0.05407	0.68306	1050.837
17-03	16wk	LC	0.06537	0.0444	0.68001	1058.845
18-08	16wk	LC	0.07438	0.0508	0.65304	1040.875
19-06	16wk	LC	0.11552	0.0684	0.78482	1042.307
20-03	16wk	LC	0.07076	0.04665	0.62202	1019.258
21_04	16wk	LC	0.08952	0.05177	0.69098	1027.137
16-01	16wk	cKO	0.10778	0.06594	0.74552	1026.485
16-02	16wk	cKO	0.07439	0.04275	0.66412	1038.27
17-07	16wk	cKO	0.06508	0.04235	0.62457	1026.55
17-10	16wk	cKO	0.05394	0.02863	0.54642	1024.467
18-02	16wk	cKO	0.07106	0.04926	0.57425	1001.158
19-04	16wk	cKO	0.07077	0.04087	0.61317	1038.596
21-07	16wk	cKO	0.06927	0.03648	0.6037	1034.494
18-04	16wk	cKO	0.06633	0.03631	0.55627	1013.203
21-05	16wk	cKO	0.09809	0.05656	0.69015	1004.543
22-01	16wk	cKO	0.08759	0.03946	0.65746	1006.952
1203	12wk	LC	0.07441	0.05773	0.66708	1029.788
1205	12wk	LC	0.11077	0.06313	0.73495	1024.115
1216	12wk	LC	0.07463	0.05221	0.63534	1018.884
1304	12wk	LC	0.06415	0.04081	0.60024	1041.827
1306	12wk	LC	0.06724	0.0458	0.59784	1024.683
1410	12wk	LC	0.07785	0.04534	0.61215	1021.216
1201	12wk	cKO	0.07204	0.03624	0.57111	991.4658
1204	12wk	cKO	0.09218	0.0503	0.63899	994.7433
1208	12wk	cKO	0.07964	0.03981	0.59108	987.3689
804	12wk	cKO	0.07202	0.0452	0.58164	994.4282
1107	12wk	cKO	0.07103	0.03428	0.6007	1029.788
1301	12wk	cKO	0.07359	0.0441	0.5826	1013.589
1403	12wk	cKO	0.08152	0.04013	0.63131	1004.891

Table B.3 continued:

Animal ID	Age	cKO or LC	I_{MAX} (mm^4)	I_{MIM} (mm^4)	Ct.Ar. (mm^2)	ct.TMD (mgHA/cc)
A26-06	12wk	LC	0.08266	0.06087	0.66278	1009.557
A27-07	12wk	LC	0.07199	0.05427	0.65666	1017.305
A28-02	12wk	LC	0.08954	0.06929	0.7291	977.5226
A29-04	12wk	LC	0.07179	0.04314	0.58724	996.8603
B31-04	12wk	LC	0.09052	0.05577	0.7086	1026.876
B34-12	12wk	LC	0.05554	0.03922	0.58343	1026.42
B33-07	12wk	LC	0.06139	0.03971	0.59453	994.321
C34-11	12wk	LC	0.09904	0.05714	0.73524	1023.686
C32-07	12wk	LC	0.07562	0.04124	0.63462	
C35-14	12wk	LC	0.09791	0.05698	0.72146	993.2792
D27-03	12wk	cKO	0.05382	0.03555	0.54065	988.2658
D27-13	12wk	cKO	0.06361	0.03723	0.59139	988.2658
D28-04	12wk	cKO	0.07767	0.05596	0.60907	966.1934
D32-01	12wk	cKO	0.06399	0.03333	0.58976	997.7718
E29-09	12wk	cKO	0.06605	0.03542	0.57537	1008.059
E30-06	12wk	cKO	0.04475	0.02577	0.48159	
E31-01	12wk	cKO	0.0996	0.05219	0.68641	
F31-02	12wk	cKO	0.12201	0.06696	0.8173	1007.408
F29-03	12wk	cKO	0.06938	0.03359	0.5545	
F33-01	12wk	cKO	0.06699	0.0398	0.57519	

Table B.3 continued:

Animal ID	Age	cKO or LC	T.Ar (mm^2)	Mar.Ar (mm^2)	Ct.Ar/ T.Ar	Ct.Th (mm)
15-02	16wk	LC	0.84091	0.20914	0.75129	0.252
15-15	16wk	LC	0.88649	0.27806	0.68634	0.227
16-03	16wk	LC	1.08062	0.30972	0.71338	0.262
17-11	16wk	LC	0.81591	0.166	0.79654	0.273
17-02	16wk	LC	0.90806	0.225	0.75222	0.265
17-03	16wk	LC	0.83544	0.15543	0.81395	0.28
18-08	16wk	LC	0.91599	0.26295	0.71293	0.245
19-06	16wk	LC	1.10215	0.31733	0.71208	0.264
20-03	16wk	LC	0.88548	0.26346	0.70247	0.237
21_04	16wk	LC	0.95965	0.26867	0.72004	0.251
16-01	16wk	cKO	1.08159	0.33607	0.68929	0.251
16-02	16wk	cKO	0.8679	0.20378	0.7652	0.258
17-07	16wk	cKO	0.84244	0.21787	0.74138	0.251
17-10	16wk	cKO	0.72618	0.17976	0.75246	0.236
18-02	16wk	cKO	0.92579	0.35154	0.62028	0.203
19-04	16wk	cKO	0.85849	0.24532	0.71425	0.238
21-07	16wk	cKO	0.82775	0.22405	0.72933	0.236
18-04	16wk	cKO	0.83302	0.27675	0.66778	0.213
21-05	16wk	cKO	1.02086	0.33071	0.67605	0.24
22-01	16wk	cKO	0.88463	0.22717	0.7432	0.244
1203	12wk	LC	0.94704	0.27996	0.70439	0.247
1205	12wk	LC	1.07922	0.34427	0.681	0.243
1216	12wk	LC	0.93971	0.30437	0.6761	0.223
1304	12wk	LC	0.83842	0.23818	0.71591	0.235
1306	12wk	LC	0.88423	0.28639	0.67611	0.226
1410	12wk	LC	0.91441	0.30226	0.66945	0.221
1201	12wk	cKO	0.84716	0.27605	0.67415	0.216
1204	12wk	cKO	0.98451	0.34552	0.64904	0.22
1208	12wk	cKO	0.89489	0.30381	0.6605	0.217
804	12wk	cKO	0.90301	0.32137	0.64412	0.212
1107	12wk	cKO	0.82179	0.22109	0.73096	0.239
1301	12wk	cKO	0.91257	0.32997	0.63842	0.214
1403	12wk	cKO	0.88773	0.25642	0.71115	0.234

Table B.3 continued:

Animal ID	Age	cKO or LC	T.Ar (mm^2)	Mar.Ar (mm^2)	Ct.Ar/ T.Ar	Ct.Th (mm)
A26-06	12wk	LC	0.99821	0.33543	0.66396	0.234
A27-07	12wk	LC	0.91786	0.2612	0.71542	0.245
A28-02	12wk	LC	1.03259	0.30349	0.70609	0.256
A29-04	12wk	LC	0.87744	0.2902	0.66926	0.217
B31-04	12wk	LC	0.98157	0.27297	0.72191	0.258
B34-12	12wk	LC	0.78732	0.20389	0.74103	0.236
B33-07	12wk	LC	0.81245	0.21792	0.73178	0.237
C34-11	12wk	LC	0.99386	0.25862	0.73978	0.265
C32-07	12wk	LC	0.85024	0.21562	0.7464	
C35-14	12wk	LC	1.00111	0.27965	0.72066	0.253
D27-03	12wk	cKO	0.77251	0.23186	0.69986	0.219
D27-13	12wk	cKO	0.80919	0.2178	0.73083	0.233
D28-04	12wk	cKO	0.98081	0.37174	0.62099	0.213
D32-01	12wk	cKO	0.77711	0.18735	0.75891	0.235
E29-09	12wk	cKO	0.80744	0.23207	0.71258	0.226
E30-06	12wk	cKO	0.67457	0.19298	0.71393	
E31-01	12wk	cKO	0.99247	0.30606	0.69161	
F31-02	12wk	cKO	1.08744	0.27014	0.75158	
F29-03	12wk	cKO	0.81295	0.25845	0.68209	
F33-01	12wk	cKO	0.83401	0.25882	0.68966	

Table B.4 Indices of cancellous bone determined by microCT analysis of VOIs from the L5 vertebral body of female pOC-ERαKO and LC mice.

Animal ID	Age	cKO or LC	BV/TV	Tb.Th (mm)	Tb.Sp (mm)	cn.TMD (mgHA/cc)
15-02	16wk	LC	0.297	0.0616	0.2177	649.172
15-15	16wk	LC	0.2262	0.0549	0.2649	652.297
16-03	16wk	LC				
17-11	16wk	LC	0.2028	0.0526	0.2473	639.861
17-02	16wk	LC	0.3154	0.0665	0.2787	682.378
17-03	16wk	LC	0.3288	0.0928	0.2268	719.0355
18-08	16wk	LC	0.3071	0.0615	0.2123	672.807
19-06	16wk	LC	0.2616	0.0637	0.2534	700.674
20-03	16wk	LC				
21_04	16wk	LC	0.2342	0.0572	0.2881	678.406
16-01	16wk	cKO	0.1315	0.0523	0.3781	682.834
16-02	16wk	cKO	0.1754	0.0503	0.2808	657.115
17-07	16wk	cKO	0.1578	0.0495	0.3248	646.893
17-10	16wk	cKO	0.1639	0.0509	0.2875	653.795
18-02	16wk	cKO	0.1185	0.0453	0.3061	645.07
19-04	16wk	cKO	0.1306	0.0492	0.3054	665.645
21-07	16wk	cKO	0.1753	0.0519	0.288	668.119
18-04	16wk	cKO	0.1247	0.05	0.3729	650.148
21-05	16wk	cKO	0.1812	0.0508	0.269	654.836
22-01	16wk	cKO	0.1771	0.0562	0.3011	679.578
1203	12wk	LC	0.2366	0.0507	0.2084	701.52
1205	12wk	LC				
1216	12wk	LC				
1304	12wk	LC	0.1985	0.0489	0.2478	714.412
1306	12wk	LC	0.2278	0.0508	0.1989	740.066
1410	12wk	LC	0.1517	0.0453	0.2503	710.766
1201	12wk	cKO	0.1161	0.043	0.3272	714.412
1204	12wk	cKO	0.1381	0.0432	0.2706	706.534
1208	12wk	cKO	0.1261	0.0432	0.2984	697.288
804	12wk	cKO	0.1234	0.0434	0.2934	721.965
1107	12wk	cKO	0.1439	0.0443	0.2505	706.208
1301	12wk	cKO	0.0923	0.0391	0.2829	696.181
1403	12wk	cKO	0.1505	0.0492	0.298	738.242

Table B.4 continued:

Animal ID	Age	cKO or LC	BV/TV	Tb.Th (mm)	Tb.Sp (mm)	cn.TMD (mgHA/cc)
A26-06	12wk	LC	0.2864	0.0558	0.2058	638.233
A27-07	12wk	LC	0.2541	0.0576	0.2536	643.637
A28-02	12wk	LC	0.3338	0.0668	0.2323	637.322
A29-04	12wk	LC	0.194	0.0535	0.2348	601.055
B31-04	12wk	LC	0.3053	0.0607	0.2177	647.479
B34-12	12wk	LC	0.1729	0.0503	0.3001	625.667
B33-07	12wk	LC	0.2514	0.059	0.296	620.003
C34-11	12wk	LC	0.2951	0.0599	0.2137	643.898
C32-07	12wk	LC	0.2343	0.0571	0.2446	664.408
C35-14	12wk	LC	0.2976	0.0587	0.1961	611.799
D27-03	12wk	cKO	0.1184	0.0443	0.2868	624.951
D27-13	12wk	cKO	0.1961	0.0514	0.243	643.898
D28-04	12wk	cKO	0.1956	0.0491	0.2384	620.523
D32-01	12wk	cKO	0.1958	0.0534	0.2445	649.758
E29-09	12wk	cKO	0.2419	0.0533	0.2134	633.611
E30-06	12wk	cKO	0.1586	0.0491	0.2915	632.829
E31-01	12wk	cKO	0.1672	0.0497	0.2571	636.801
F31-02	12wk	cKO	0.2052	0.0518	0.2328	640.382
F29-03	12wk	cKO	0.1338	0.0478	0.2975	618.57
F33-01	12wk	cKO	0.2094	0.0534	0.2488	655.748

Table B.5 Indices of cortical bone determined by microCT analysis of VOIs from the L5 vertebral cortical shell of female pOC-ERαKO and LC mice.

Animal ID	Age	cKO or LC	I_{MAX} (mm^4)	I_{MIM} (mm^4)	Ct.Ar. (mm^2)	ct.TMD (mgHA/cc)
15-02	16wk	LC	0.14429	0.04228	0.41737	675.281
15-15	16wk	LC	0.18351	0.05935	0.46886	687.066
16-03	16wk	LC				
17-11	16wk	LC	0.26954	0.05635	0.52003	732.4481
17-02	16wk	LC	0.18454	0.06786	0.47931	732.969
17-03	16wk	LC	0.23372	0.06479	0.51822	711.2874
18-08	16wk	LC	0.20634	0.06288	0.50952	733.0341
19-06	16wk	LC	0.30799	0.07835	0.60089	771.5793
20-03	16wk	LC				
21_04	16wk	LC	0.22072	0.06514	0.49315	748.921
16-01	16wk	cKO	0.27194	0.07831	0.49666	735.247
16-02	16wk	cKO	0.21473	0.07129	0.46524	740.652
17-07	16wk	cKO	0.22104	0.08022	0.47007	699.502
17-10	16wk	cKO	0.2301	0.06604	0.48186	737.005
18-02	16wk	cKO	0.16063	0.05208	0.38773	706.013
19-04	16wk	cKO	0.18478	0.06004	0.42483	738.503
21-07	16wk	cKO	0.23081	0.05398	0.46968	745.665
18-04	16wk	cKO	0.16977	0.05041	0.38506	684.266
21-05	16wk	cKO	0.19299	0.05688	0.42155	725.351
22-01	16wk	cKO	0.21694	0.05828	0.45041	741.498
1203	12wk	LC	0.23139	0.06985	0.54893	725.6767
1205	12wk	LC				
1216	12wk	LC				
1304	12wk	LC	0.23676	0.09418	0.57687	733.555
1306	12wk	LC	0.19703	0.05131	0.46964	735.1827
1410	12wk	LC	0.20218	0.05332	0.4803	723.5931
1201	12wk	cKO	0.31721	0.08602	0.59337	707.315
1204	12wk	cKO	0.16176	0.05844	0.42405	701.651
1208	12wk	cKO	0.20507	0.08787	0.4945	709.854
804	12wk	cKO	0.18304	0.05576	0.42276	714.347
1107	12wk	cKO	0.1899	0.05635	0.43219	731.406
1301	12wk	cKO	0.22484	0.05328	0.47113	735.833
1403	12wk	cKO	0.19332	0.06458	0.48216	723.202

Table B.5 continued:

Animal ID	Age	cKO or LC	I_{MAX} (mm^4)	I_{MIM} (mm^4)	Ct.Ar. (mm^2)	ct.TMD (mgHA/cc)
A26-06	12wk	LC	0.20471	0.05657	0.44181	702.106
A27-07	12wk	LC	0.16019	0.05172	0.42843	715.259
A28-02	12wk	LC	0.24584	0.09944	0.60734	744.9493
A29-04	12wk	LC	0.09925	0.05111	0.35761	640.838
B31-04	12wk	LC	0.18097	0.05348	0.44502	682.118
B34-12	12wk	LC	0.22282	0.07841	0.49859	721.5096
B33-07	12wk	LC	0.18644	0.04264	0.43935	692.665
C34-11	12wk	LC	0.19473	0.06444	0.48328	721.705
C32-07	12wk	LC	0.19921	0.04356	0.42743	723.9187
C35-14	12wk	LC	0.20962	0.04888	0.47919	709.0085
D27-03	12wk	cKO	0.14813	0.03908	0.36838	683.159
D27-13	12wk	cKO	0.2728	0.05912	0.53092	702.432
D28-04	12wk	cKO	0.25132	0.04774	0.50024	708.031
D32-01	12wk	cKO	0.23109	0.04652	0.46545	729.843
E29-09	12wk	cKO	0.15297	0.03882	0.38658	673.132
E30-06	12wk	cKO	0.23398	0.05567	0.46359	694.814
E31-01	12wk	cKO	0.25294	0.05907	0.47871	707.38
F31-02	12wk	cKO	0.15821	0.04191	0.37708	675.802
F29-03	12wk	cKO	0.24822	0.07284	0.49796	714.022
F33-01	12wk	cKO	0.18981	0.05452	0.43189	711.482

Table B.5 continued:

Animal ID	Age	cKO or LC	T.Ar (mm^2)	Ct.Ar/ T.Ar	Ct.Th (mm)
15-02	16wk	LC	0.81274	0.51354	0.089
15-15	16wk	LC	1.0235	0.45809	0.088
16-03	16wk	LC			
17-11	16wk	LC	1.11058	0.46825	0.096
17-02	16wk	LC	0.94279	0.50839	0.097
17-03	16wk	LC	1.10616	0.46848	0.097
18-08	16wk	LC	1.03733	0.49118	0.093
19-06	16wk	LC	1.16024	0.5179	0.104
20-03	16wk	LC			
21_04	16wk	LC			0.094
16-01	16wk	cKO			0.085
16-02	16wk	cKO	1.06589	0.43648	0.082
17-07	16wk	cKO	1.15495	0.40701	0.079
17-10	16wk	cKO	1.22556	0.39317	0.086
18-02	16wk	cKO	0.97832	0.39632	0.075
19-04	16wk	cKO	0.95407	0.44528	0.082
21-07	16wk	cKO			0.088
18-04	16wk	cKO	0.98036	0.39277	0.073
21-05	16wk	cKO	1.02796	0.41008	0.081
22-01	16wk	cKO	1.0462	0.43052	0.085
1203	12wk	LC	1.04104	0.52729	0.102
1205	12wk	LC			
1216	12wk	LC			
1304	12wk	LC	1.18473	0.48692	0.1
1306	12wk	LC	0.91607	0.51267	0.095
1410	12wk	LC	0.98318	0.48852	0.093
1201	12wk	cKO	1.27599	0.46503	0.085
1204	12wk	cKO	0.98543	0.43032	0.08
1208	12wk	cKO	1.09165	0.45299	0.084
804	12wk	cKO	0.9556	0.4424	0.082
1107	12wk	cKO	0.92525	0.46711	0.082
1301	12wk	cKO	1.1063	0.42587	0.086
1403	12wk	cKO	1.01346	0.47576	0.089

Table B.5 continued:

Animal ID	Age	cKO or LC	T.Ar (mm^2)	Ct.Ar/ T.Ar	Ct.Th (mm)
A26-06	12wk	LC	0.994	0.44448	0.084
A27-07	12wk	LC	0.95887	0.44681	0.09
A28-02	12wk	LC	1.20574	0.50371	0.112
A29-04	12wk	LC	0.96039	0.37236	0.072
B31-04	12wk	LC	1.07941	0.41228	0.086
B34-12	12wk	LC	1.12616	0.44274	0.09
B33-07	12wk	LC	1.17111	0.37515	0.085
C34-11	12wk	LC	1.09002	0.44337	0.094
C32-07	12wk	LC	1.11008	0.38505	0.078
C35-14	12wk	LC	1.0572	0.45326	0.091
D27-03	12wk	cKO	1.09307	0.33701	0.073
D27-13	12wk	cKO	1.09551	0.48463	0.094
D28-04	12wk	cKO	1.12973	0.44279	0.084
D32-01	12wk	cKO	1.09447	0.42528	0.082
E29-09	12wk	cKO	0.95339	0.40548	0.075
E30-06	12wk	cKO	1.27044	0.36491	0.08
E31-01	12wk	cKO			0.081
F31-02	12wk	cKO	1.08269	0.34828	0.071
F29-03	12wk	cKO			0.083
F33-01	12wk	cKO	1.17535	0.36746	0.078

Table B.6 Indices of cortical bone determined by microCT analysis of VOIs from the right distal femoral cortical shell of female pOC-ERαKO and LC mice.

Animal ID	Age	cKO or LC	I_{MAX} (mm^4)	I_{MIM} (mm^4)	Ct.Ar. (mm^2)	ct.TMD (mgHA/cc)
15-02	16wk	LC	0.64162	0.30152	1.22466	909.5477
15-15	16wk	LC	0.56416	0.31608	1.07306	858.2408
16-03	16wk	LC	0.7635	0.39455	1.27132	899.5858
17-11	16wk	LC	0.54662	0.25603	1.1785	920.6815
17-02	16wk	LC	0.63703	0.29757	1.24998	893.791
17-03	16wk	LC	0.66353	0.34139	1.2784	889.7542
18-08	16wk	LC	0.65774	0.30612	1.19553	912.5427
19-06	16wk	LC	0.76157	0.41478	1.32699	904.4691
20-03	16wk	LC	0.56116	0.28626	1.07574	888.452
21_04	16wk	LC	0.6336	0.30195	1.19324	914.8867
16-01	16wk	cKO	0.75379	0.373	1.1733	871.1326
16-02	16wk	cKO	0.5158	0.27288	0.97678	894.1817
17-07	16wk	cKO	0.6499	0.31147	1.13601	865.6634
17-10	16wk	cKO	0.52161	0.2378	1.00472	884.2849
18-02	16wk	cKO	0.44002	0.24414	0.84817	846.4559
19-04	16wk	cKO	0.59157	0.29265	1.06602	875.3648
21-07	16wk	cKO	0.54313	0.25651	1.00654	867.0307
18-04	16wk	cKO	0.46669	0.23333	0.93283	880.2481
21-05	16wk	cKO	0.67451	0.29953	1.1587	888.6473
22-01	16wk	cKO	0.57097	0.32545	1.08628	879.2714
1203	12wk	LC	0.61655	0.24506	1.17409	913.7147
1205	12wk	LC	0.67736	0.25043	1.22117	925.4996
1216	12wk	LC	0.50093	0.20047	1.01734	881.6805
1304	12wk	LC	0.45755	0.19578	1.00913	923.2208
1306	12wk	LC	0.48048	0.21548	1.00847	909.2872
1410	12wk	LC	0.44295	0.20589	0.97205	920.8768
1201	12wk	cKO	0.4841	0.20133	0.96687	878.5552
1204	12wk	cKO	0.52005	0.21602	0.9624	879.7923
1208	12wk	cKO	0.43853	0.15718	0.95259	883.4384
804	12wk	cKO	0.50865	0.23083	1.03966	910.0034
1107	12wk	cKO	0.39661	0.19155	0.97875	937.7403
1301	12wk	cKO	0.63766	0.27046	1.22135	905.055
1403	12wk	cKO	0.31813	0.1651	0.85515	928.1691

Table B.6 continued:

Animal ID	Age	cKO or LC	I_{MAX} (mm^4)	I_{MIM} (mm^4)	Ct.Ar. (mm^2)	ct.TMD (mgHA/cc)
A26-06	12wk	LC	0.59063	0.33478	1.12329	838.7729
A27-07	12wk	LC	0.50503	0.26509	1.0412	877.7739
A28-02	12wk	LC	0.73055	0.38119	1.30273	855.2458
A29-04	12wk	LC	0.40862	0.22949	0.90521	864.8821
B31-04	12wk	LC	0.62473	0.38995	1.16253	870.6769
B34-12	12wk	LC	0.44902	0.24973	0.92818	847.6279
B33-07	12wk	LC	0.50727	0.3263	1.11291	881.4201
C34-11	12wk	LC	0.71039	0.3976	1.26025	858.3711
C32-07	12wk	LC	0.5169	0.24707	1.05445	894.4421
C35-14	12wk	LC	0.63791	0.30324	1.13154	849.1254
D27-03	12wk	cKO				
D27-13	12wk	cKO	0.37839	0.19075	0.80423	837.3405
D28-04	12wk	cKO	0.54754	0.2779	0.99996	830.504
D32-01	12wk	cKO	0.40489	0.21152	0.89364	854.0087
E29-09	12wk	cKO	0.39266	0.26572	0.86041	836.6894
E30-06	12wk	cKO	0.35114	0.20788	0.82928	825.7509
E31-01	12wk	cKO	0.57063	0.29255	1.01599	855.1156
F31-02	12wk	cKO	0.64635	0.34277	1.02458	820.1514
F29-03	12wk	cKO	0.39311	0.22121	0.83868	836.1035
F33-01	12wk	cKO	0.44511	0.24652	0.91841	867.3563

Table B.6 continued:

Animal ID	Age	cKO or LC	T.Ar (mm^2)	Ct.Ar/ T.Ar	Ct.Th (mm)
15-02	16wk	LC	1.81194	0.67588	0.183
15-15	16wk	LC	1.71274	0.62652	0.152
16-03	16wk	LC			0.17
17-11	16wk	LC	1.85138	0.63655	0.183
17-02	16wk	LC	1.82486	0.68497	0.191
17-03	16wk	LC	1.93686	0.66003	0.186
18-08	16wk	LC	1.81877	0.65733	0.174
19-06	16wk	LC	1.99529	0.66506	0.184
20-03	16wk	LC	1.76785	0.6085	0.153
21_04	16wk	LC	1.81029	0.65914	0.178
16-01	16wk	cKO	1.93865	0.60521	0.156
16-02	16wk	cKO	1.56682	0.62341	0.146
17-07	16wk	cKO	1.8064	0.62888	0.155
17-10	16wk	cKO			0.152
18-02	16wk	cKO	1.56305	0.54264	0.128
19-04	16wk	cKO	1.67579	0.63613	0.154
21-07	16wk	cKO	1.60399	0.62753	0.146
18-04	16wk	cKO	1.62155	0.57527	0.147
21-05	16wk	cKO			0.163
22-01	16wk	cKO	1.79717	0.60444	0.155
1203	12wk	LC	1.69319	0.69342	0.186
1205	12wk	LC	1.69914	0.7187	0.192
1216	12wk	LC	1.44241	0.7053	0.173
1304	12wk	LC	1.37536	0.73372	0.179
1306	12wk	LC	1.41741	0.71149	0.167
1410	12wk	LC	1.45601	0.66762	0.171
1201	12wk	cKO	1.71204	0.56475	0.166
1204	12wk	cKO	1.61779	0.59489	0.162
1208	12wk	cKO	1.49177	0.63856	0.175
804	12wk	cKO	1.51987	0.68405	0.176
1107	12wk	cKO	1.42524	0.68672	0.183
1301	12wk	cKO	1.77951	0.68634	0.202
1403	12wk	cKO	1.37777	0.62068	0.172

Table B.6 continued:

Animal ID	Age	cKO or LC	T.Ar (mm^2)	Ct.Ar/ T.Ar	Ct.Th (mm)
A26-06	12wk	LC	1.86567	0.60209	0.153
A27-07	12wk	LC	1.73823	0.599	0.159
A28-02	12wk	LC	2.04498	0.63704	0.181
A29-04	12wk	LC	1.56739	0.57753	0.145
B31-04	12wk	LC	1.90014	0.61181	0.163
B34-12	12wk	LC	1.57254	0.59024	0.143
B33-07	12wk	LC	1.86643	0.59627	0.168
C34-11	12wk	LC	1.91904	0.65671	0.174
C32-07	12wk	LC	1.68237	0.62677	0.164
C35-14	12wk	LC	1.7871	0.63317	0.162
D27-03	12wk	cKO			
D27-13	12wk	cKO	1.47523	0.54515	0.126
D28-04	12wk	cKO			0.147
D32-01	12wk	cKO	1.51812	0.58865	0.144
E29-09	12wk	cKO	1.51831	0.56669	0.129
E30-06	12wk	cKO	1.35701	0.61111	0.135
E31-01	12wk	cKO	1.65133	0.61525	0.148
F31-02	12wk	cKO	1.81934	0.56316	0.133
F29-03	12wk	cKO			0.129
F33-01	12wk	cKO	1.5591	0.58907	0.14

Table B.7 Indices of cancellous bone determined by microCT analysis of VOIs from the distal femur of female pOC-ERαKO and LC mice.

Animal ID	Age	cKO or LC	BV/TV	Tb.Th (mm)	Tb.Sp (mm)	cn.TMD (mgHA/cc)
15-02	16wk	LC	0.0932	0.0501	0.2991	733.945
15-15	16wk	LC	0.0908	0.0524	0.352	741.889
16-03	16wk	LC	0.0855	0.0518	0.2999	732.643
17-11	16wk	LC	0.0903	0.048	0.2667	721.249
17-02	16wk	LC	0.1225	0.0602	0.2845	728.997
17-03	16wk	LC	0.1658	0.0702	0.3063	758.947
18-08	16wk	LC	0.0932	0.0497	0.2772	721.053
19-06	16wk	LC	0.1063	0.0586	0.2945	716.821
20-03	16wk	LC	0.0608	0.0464	0.3323	718.709
21_04	16wk	LC	0.0592	0.0496	0.3654	745.144
16-01	16wk	cKO	0.0777	0.0546	0.4438	717.993
16-02	16wk	cKO	0.0669	0.0529	0.3944	736.81
17-07	16wk	cKO	0.0839	0.0527	0.3949	715.91
17-10	16wk	cKO	0.0678	0.0512	0.636	714.217
18-02	16wk	cKO	0.0378	0.0507	0.7385	708.617
19-04	16wk	cKO	0.0488	0.0524	0.5998	705.492
21-07	16wk	cKO	0.0801	0.0563		738.633
18-04	16wk	cKO	0.0248	0.0424	0.5895	703.018
21-05	16wk	cKO	0.097	0.0637	0.4631	760.38
22-01	16wk	cKO	0.0636	0.0551	0.6209	721.249
1203	12wk	LC	0.1529	0.0614	0.227	688.824
1205	12wk	LC	0.1663	0.0597	0.2308	701.651
1216	12wk	LC	0.13	0.0583	0.2584	675.997
1304	12wk	LC	0.1338	0.0515	0.2434	759.664
1306	12wk	LC	0.0992	0.0515	0.2708	724.7
1410	12wk	LC	0.0971	0.0561	0.2942	701.976
1201	12wk	cKO	0.0654	0.0451	0.3656	714.673
1204	12wk	cKO	0.0804	0.0492	0.4094	717.537
1208	12wk	cKO	0.0716	0.0484	0.364	700.348
804	12wk	cKO	0.1083	0.0556	0.2649	724.765
1107	12wk	cKO	0.0879	0.052	0.2729	753.739
1301	12wk	cKO	0.1341	0.0534	0.2182	712.459
1403	12wk	cKO	0.063	0.0569	0.3529	739.675

Table B.7 continued:

Animal ID	Age	cKO or LC	BV/TV	Tb.Th (mm)	Tb.Sp (mm)	cn.TMD (mgHA/cc)
A26-06	12wk	LC	0.1279	0.0577	0.2509	698.2
A27-07	12wk	LC	0.1052	0.0538	0.2611	726.783
A28-02	12wk	LC	0.1578	0.0568	0.2095	688.889
A29-04	12wk	LC	0.0747	0.0588	0.3242	717.993
B31-04	12wk	LC	0.1016	0.0512	0.2769	684.527
B34-12	12wk	LC	0.0965	0.0517	0.2756	691.819
B33-07	12wk	LC	0.091	0.0546	0.2995	693.968
C34-11	12wk	LC	0.1541	0.0598	0.2316	710.961
C32-07	12wk	LC	0.09	0.0541	0.3037	727.304
C35-14	12wk	LC	0.1049	0.057	0.2595	700.869
D27-03	12wk	cKO				
D27-13	12wk	cKO	0.0667	0.0543	0.4392	687.066
D28-04	12wk	cKO	0.0799	0.052	0.3512	691.884
D32-01	12wk	cKO	0.0792	0.0541	0.4044	724.179
E29-09	12wk	cKO	0.088	0.0546	0.4169	697.418
E30-06	12wk	cKO	0.0666	0.0533	0.4087	685.438
E31-01	12wk	cKO	0.075	0.0539	0.4013	706.339
F31-02	12wk	cKO	0.074	0.053	0.4856	697.418
F29-03	12wk	cKO	0.066	0.0495	0.4793	682.508
F33-01	12wk	cKO	0.1049	0.057	0.2595	700.869

Table B.8 Indices of serum makers determined by ELISAs for female pOC-ERαKO and LC mice.

Animal ID	Age	cKO or LC	TRACP5b (U/L)	IGF-1 (ng/mL)	OC (ng/mL)	E2 (pg/mL)
15-02	16wk	LC	49.8	187	49.8	
15-15	16wk	LC	35.2	231	35.2	
16-03	16wk	LC	32.5	220	32.5	
17-11	16wk	LC	20.9	242	20.9	
17-02	16wk	LC	52.7	236	52.7	
17-03	16wk	LC	59.8	242	59.8	
18-08	16wk	LC	39.8	230	39.8	
19-06	16wk	LC	28.4	224	28.4	
20-03	16wk	LC	27.8	234	27.8	
21_04	16wk	LC	33.3	213	33.3	
16-01	16wk	cKO	15.6	266	15.6	
16-02	16wk	cKO	16.1	222	16.1	
17-07	16wk	cKO	59.7	291	59.7	
17-10	16wk	cKO	22.6	253	22.6	
18-02	16wk	cKO	32.3	243	32.3	
19-04	16wk	cKO	22.3	260	22.3	
21-07	16wk	cKO	14.3	225	14.3	
18-04	16wk	cKO	17	218	17	
21-05	16wk	cKO	21.3	141	21.3	
22-01	16wk	cKO	19.1	315	19.1	
1203	12wk	LC				6.9645
1205	12wk	LC				12.696
1216	12wk	LC				6.416
1304	12wk	LC				7.593
1306	12wk	LC				9.341
1410	12wk	LC				7.573
1201	12wk	cKO				6.669
1204	12wk	cKO				10.256
1208	12wk	cKO				9.918
804	12wk	cKO				9.634
1107	12wk	cKO				9.719
1301	12wk	cKO				9.391
1403	12wk	cKO				15.717

Table B.8 continued:

Animal ID	Age	cKO or LC	TRACP5b (U/L)	IGF-1 (ng/mL)	OC (ng/mL)	E2 (pg/mL)
A26-06	12wk	LC	20	378	121	
A27-07	12wk	LC	23.7	353	120	
A28-02	12wk	LC	19.2	429	93	
A29-04	12wk	LC	14.2	334	132	
B31-04	12wk	LC	27.5	349	81	
B34-12	12wk	LC	18.1	288	91	
B33-07	12wk	LC	17.7	398	110	
C34-11	12wk	LC	17.8	313	111	
C32-07	12wk	LC	23.8	409	126	
C35-14	12wk	LC		394	105	
D27-03	12wk	cKO	8	309	83	
D27-13	12wk	cKO		384	75	
D28-04	12wk	cKO	16.1	306	89	
D32-01	12wk	cKO	12.5	373	139	
E29-09	12wk	cKO	15.9	236	111	
E30-06	12wk	cKO	12	390	104	
E31-01	12wk	cKO	10.5	265	86	
F31-02	12wk	cKO	29.1	395	85	
F29-03	12wk	cKO	15.2	427	133	
F33-01	12wk	cKO	10.4	318	98	

Table B.9 Indices of body, ovarian, and uterine masses for female pOC-ERαKO and LC mice.

Animal ID	Age	cKO or LC	Body mass (g)	Ovarian mass(g)	Uterine mass(g)
15-02	16wk	LC	22.52	0.0559	0.0711
15-15	16wk	LC	23.8	0.0875	0.1075
16-03	16wk	LC	26.78	0.0775	0.0956
17-11	16wk	LC	21.44	0.0448	0.078
17-02	16wk	LC	24.51	0.0754	0.1225
17-03	16wk	LC	22.57	0.0332	0.1473
18-08	16wk	LC	23.41	0.0942	0.0866
19-06	16wk	LC	26.03	0.0894	0.1854
20-03	16wk	LC	21.33	0.0448	0.0817
21_04	16wk	LC	24.73	0.0769	0.143
16-01	16wk	cKO	27.07	0.1244	0.0765
16-02	16wk	cKO	24.88	0.0629	0.067
17-07	16wk	cKO	24.7	0.0445	0.2217
17-10	16wk	cKO	22.98	0.0708	0.069
18-02	16wk	cKO	20.03	0.0431	0.077
19-04	16wk	cKO	25.07	0.0836	0.1271
21-07	16wk	cKO	23.56	0.0546	0.0948
18-04	16wk	cKO	23.82	0.0886	0.0516
21-05	16wk	cKO	26.16	0.1026	0.1187
22-01	16wk	cKO	25.99	0.1217	0.1157
1203	12wk	LC	21.59	0.044	0.075
1205	12wk	LC	21.6	0.072	0.169
1216	12wk	LC	21.65	0.094	0.109
1304	12wk	LC	22.3	0.083	0.089
1306	12wk	LC	20.93	0.051	0.101
1410	12wk	LC	21.6	0.068	0.07
1201	12wk	cKO	22.03	0.048	0.14
1204	12wk	cKO	22.56	0.064	0.13
1208	12wk	cKO	21.9	0.057	0.108
804	12wk	cKO	21.56	0.06	0.128
1107	12wk	cKO	20.79	0.076	0.24
1301	12wk	cKO	22.14	0.084	0.085
1403	12wk	cKO	23.95	0.055	0.124

Table B.9 continued:

Animal ID	Age	cKO or LC	Body mass (g)	Ovarian mass(g)	Uterine mass(g)
A26-06	12wk	LC	22.04	0.05	0.06
A27-07	12wk	LC	20.04	0.04	0.06
A28-02	12wk	LC	24.45	0.07	0.07
A29-04	12wk	LC	19.69	0.05	0.12
B31-04	12wk	LC	26.31	0.09	0.14
B34-12	12wk	LC	20.15	0.08	0.1
B33-07	12wk	LC	21.39	0.05	0.17
C34-11	12wk	LC	23.2	0.06	0.18
C32-07	12wk	LC	22.42	0.05	0.1
C35-14	12wk	LC	23.21	0.06	0.09
D27-03	12wk	cKO	18.47	0.04	0.11
D27-13	12wk	cKO	19.39	0.04	0.16
D28-04	12wk	cKO	21.77	0.06	0.07
D32-01	12wk	cKO	20.81	0.04	0.08
E29-09	12wk	cKO	19.77	0.05	0.15
E30-06	12wk	cKO	19.57	0.03	0.08
E31-01	12wk	cKO	23.27	0.09	0.07
F31-02	12wk	cKO	24.52	0.09	0.07
F29-03	12wk	cKO	19.87	0.05	0.07
F33-01	12wk	cKO	23.53	0.11	0.06

Table B.10 Indices of crown/rump and long bone lengths of female pOC-ERαKO and LC mice.

Animal ID	Age	cKO or LC	Crown/rump (mm)	R tibia (mm)	R femur (mm)
15-02	16wk	LC	89.5	15.87	19.5
15-15	16wk	LC	85.8	15.62	18.24
16-03	16wk	LC	89.6	15.74	18.69
17-11	16wk	LC	81.7	15.34	17.34
17-02	16wk	LC	87.5	15.8	18.09
17-03	16wk	LC	89.1	15.74	18.06
18-08	16wk	LC	88.9	15.52	18
19-06	16wk	LC	93.9	16.28	19.11
20-03	16wk	LC	83.9	14.98	17.7
21_04	16wk	LC	92.2	16.07	18.51
16-01	16wk	cKO	92	16.69	19.14
16-02	16wk	cKO	89.1	16.07	18.42
17-07	16wk	cKO	89.2	16.32	18.84
17-10	16wk	cKO	91	16.16	18.42
18-02	16wk	cKO	84.6	15.43	17.91
19-04	16wk	cKO	89.1	16.36	18.9
21-07	16wk	cKO	91.8	15.85	18.27
18-04	16wk	cKO	89.4	15.35	18.18
21-05	16wk	cKO	92.4	15.63	18.12
22-01	16wk	cKO	91.3	15.91	18.45
1203	12wk	LC		15.39	17.73
1205	12wk	LC		15.93	18.27
1216	12wk	LC		15.82	18.15
1304	12wk	LC		15.2	17.55
1306	12wk	LC		15.38	17.97
1410	12wk	LC		15.23	18.21
1201	12wk	cKO		15.53	17.88
1204	12wk	cKO		16.12	18.72
1208	12wk	cKO		15.44	17.88
804	12wk	cKO		15.78	18.15
1107	12wk	cKO		15.63	17.52
1301	12wk	cKO		15.1	18.06
1403	12wk	cKO		15.39	18.57

Table B.10 continued:

Animal ID	Age	cKO or LC	Crown/rump (mm)	R tibia (mm)	R femur (mm)
A26-06	12wk	LC	88.82	15.41	18.06
A27-07	12wk	LC	80.62	15.52	17.7
A28-02	12wk	LC	85.97	15.63	17.82
A29-04	12wk	LC	76.42	15.07	17.58
B31-04	12wk	LC	89.76	15.45	17.94
B34-12	12wk	LC	79.9	14.69	17.4
B33-07	12wk	LC	82.27	14.81	17.64
C34-11	12wk	LC	84.93	15.72	18.03
C32-07	12wk	LC	84.76	14.83	16.86
C35-14	12wk	LC	86.5	15.81	18.39
D27-03	12wk	cKO	82.24	13.48	17.16
D27-13	12wk	cKO	83.58	14.38	17.55
D28-04	12wk	cKO	86.37	15.29	17.37
D32-01	12wk	cKO	80.79	14.37	17.16
E29-09	12wk	cKO	86.04	14.8	17.49
E30-06	12wk	cKO	83.22	15.42	18.15
E31-01	12wk	cKO	84.56	15.36	18.06
F31-02	12wk	cKO	91.89	15.5	18.18
F29-03	12wk	cKO	84.56	15.18	17.67
F33-01	12wk	cKO	86.43	14.28	17.34

Table B.11 Indices of histology and IHC data for female pOC-ERαKO and LC mice.

Animal ID	Age	cKO or LC	N.Ob/BS (mm^{-1})	N.Oc/BS (mm^{-1})	Gp.Th (mm)
15-02	16wk	LC	2.36	2.867448	0.10563
15-15	16wk	LC	1.08	1.382762	0.09245
16-03	16wk	LC			
17-11	16wk	LC			
17-02	16wk	LC			
17-03	16wk	LC	0.98	2.495536	0.12852
18-08	16wk	LC	2.86	2.702598	0.110413
19-06	16wk	LC			
20-03	16wk	LC	3.05	1.476561	0.10653
21_04	16wk	LC	2.52	1.751456	0.08962
16-01	16wk	cKO	0.55		0.086463
16-02	16wk	cKO			0.0907
17-07	16wk	cKO			
17-10	16wk	cKO			
18-02	16wk	cKO	0.22		0.0862
19-04	16wk	cKO			
21-07	16wk	cKO	2.74	1.712516	0.12894
18-04	16wk	cKO	2.09	1.670796	0.13898
21-05	16wk	cKO	1.2	0.902501	0.09701
22-01	16wk	cKO			
1203	12wk	LC			0.12057
1205	12wk	LC	5.33	3.533224	0.11778
1216	12wk	LC	2.46		0.10797
1304	12wk	LC	1.53	3.584055	0.11948
1306	12wk	LC	4.44	3.203233	0.11882
1410	12wk	LC			
1201	12wk	cKO	2.99	3.029201	0.11506
1204	12wk	cKO	0.911	3.409571	0.11934
1208	12wk	cKO	1.63	3.660773	0.11422
804	12wk	cKO	2.81	2.618107	0.11719
1107	12wk	cKO		3.745557	0.10848
1301	12wk	cKO			
1403	12wk	cKO	1.65	4.327819	0.11226

Table B.12 Indices of femur and vertebra mechanical testing data for female pOC-ERαKO and LC mice.

Animal ID	Age	cKO or LC	Compressive Strength (N)	Compressive Stiffness (N)	Bending Strength (N)	Bending Stiffness ($N \cdot mm^2$)
15-02	16wk	LC	28.578	103.8904	33.678	1074.243
15-15	16wk	LC	18.697	305.3106	24.78	699.83
16-03	16wk	LC			38.214	1083.659
17-11	16wk	LC	22.739	373.2911	35.143	1111.282
17-02	16wk	LC	30.093	421.6552	39.084	1200.667
17-03	16wk	LC	30.333	479.2656	42.296	1193.437
18-08	16wk	LC	30.24	511.8893	33.088	1038.062
19-06	16wk	LC	36.065	399.4248	38.232	1255.336
20-03	16wk	LC	24.049	248.9949	22.704	836.328
21_04	16wk	LC	31.788	536.362	32.713	1132.686
16-01	16wk	cKO	20.012	274.2806	35.358	777.816
16-02	16wk	cKO	20.431	377.0363	29.756	871.938
17-07	16wk	cKO	23.113	398.924	36.604	1114.085
17-10	16wk	cKO	19.594	178.0772	28.582	983.447
18-02	16wk	cKO	17.526	291.137	26.498	694.513
19-04	16wk	cKO	19.256	345.072	30.216	1025.179
21-07	16wk	cKO	19.332	392.6172	29.297	992.692
18-04	16wk	cKO			27.567	713.822
21-05	16wk	cKO	19.354	177.4108	28.842	958.379
22-01	16wk	cKO	30.121	433.449	32.329	949.633
1203	12wk	LC	20.219	327.3722	29.852	850.369
1205	12wk	LC			33.01	820.189
1216	12wk	LC	24.013	379.507	25.39	758.404
1304	12wk	LC	24.567	495.1576	28.23	873.911
1306	12wk	LC	18.039	584.3264	24.383	721.598
1410	12wk	LC	22.819	325.4188	21.926	701.304
1201	12wk	cKO	17.416	201.7724	25.511	716.661
1204	12wk	cKO	20.119	140.1533	26.524	721.101
1208	12wk	cKO	20.23	632.702	27.171	759.793
804	12wk	cKO	23.755	288.4784	27.718	773.605
1107	12wk	cKO	20.549	364.4803	21.371	645.551
1301	12wk	cKO	17.025	205.215	27.482	684.986
1403	12wk	cKO	22.686	252.1339	25.163	703.881

Table B.12 continued:

Animal ID	Age	cKO or LC	Compressive Strength (N)	Compressive Stiffness (N)	Bending Strength (N)	Bending Stiffness ($N \cdot mm^2$)
A26-06	12wk	LC	28.655	329.133	24.632	697.853
A27-07	12wk	LC	26.817	191.4022	23.824	774.6
A28-02	12wk	LC	26.7	182.1428	36.46	821.303
A29-04	12wk	LC	17.386	146.5738	19.635	595.092
B31-04	12wk	LC	26.713	224.2436	30.204	625.039
B34-12	12wk	LC	18.036	106.2432	22.684	608.673
B33-07	12wk	LC	26.599	194.148	23.962	667.121
C34-11	12wk	LC	26.67	199.4929	30.73	877.487
C32-07	12wk	LC	24.121	230.216	26.579	756.158
C35-14	12wk	LC	25.459	296.3981	30.126	802.994
D27-03	12wk	cKO	11.711	61.53558	19.961	543.797
D27-13	12wk	cKO	14.105	101.8058	22.943	548.801
D28-04	12wk	cKO	18.012	163.0534	25.376	595.605
D32-01	12wk	cKO	19.392	294.4854	25.503	559.089
E29-09	12wk	cKO	16.515	78.80144	21.876	618.729
E30-06	12wk	cKO	15.253	255.1193	19.117	559.196
E31-01	12wk	cKO	18.669	221.999	26.048	806.559
F31-02	12wk	cKO	23.847	291.5137	24.702	574.879
F29-03	12wk	cKO	12.588	83.62522	19.689	564.95
F33-01	12wk	cKO	13.039	164.1078	21.497	675.028

APPENDIX C. **CHAPTER 3 SUPPLEMENTARY FIGURES AND DATA**

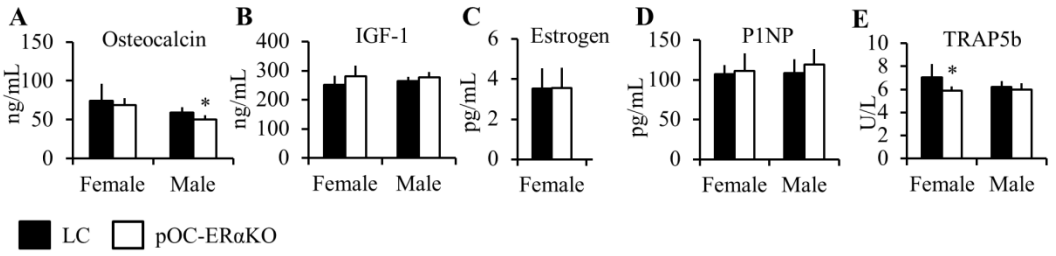

Figure C.1 Serum marker measurements in male and female LC and pOC-ERαKO mice. Female pOC-ERαKO mice had similar levels of osteocalcin, IGF-1, estrogen, and P1NP as LC, but TRAP5b serum levels were lower. Male pOC-ERαKO mice had decreased serum osteocalcin levels but similar IGF-1, P1NP, and TRAP5b levels to LC.

Table C.1 Length and mass measurements for female and male LC and pOC-ERαKO mice. Data are mean ± SD. n=6-14 per group. *pOC-ERαKO different from LC, $p<0.05$ by one-way ANOVA for each sex.

	Female		Male	
	LC	pOC-ERαKO	LC	pOC-ERαKO
Crown/Rump Length (mm)	82.4 ± 1.8	81.8 ± 1.6	89.4 ± 1.9	90.1 ± 2.5
Body mass (g)	18.8 ± 0.82	19.0 ± 0.79	25.0 ± 1.0	25.9 ± 1.4
Loaded tibia length (mm)	17.4 ± 0.19	17.4 ± 0.18	18.0 ± 0.16	17.9 ± 0.13
Control tibia length (mm)	17.3 ± 0.30	17.4 ± 0.26	18.1 ± 0.11	18.1 ± 0.13
Right femur length (mm)	15.0 ±0.29	15.0 ± 0.29	15.5 ± 0.30	15.8 ± 0.21*
Ovarian mass (mg)	154 ± 47	168 ± 48	N/A	N/A
Uterine mass (mg)	597 ± 160	744 ± 290	N/A	N/A

Table C.2 Indices of cancellous bone determined by microCT analysis of VOIs from loaded left (L) and control right (R) proximal tibial metaphysis of 12-week-old female and male pOC-ERαKO and LC mice.

Animal ID	Male or Female	cKO or LC	BV/TV.L	BV/TV.R	Tb.Th.L (mm)	Tb.Th.R (mm)
H1314	F	LC	0.0975	0.0922	0.0618	0.0488
H1411	F	LC	0.0845	0.0587	0.0629	0.0476
H1504	F	LC	0.1043	0.0639	0.0644	0.0499
H1708	F	LC	0.116	0.1196	0.0628	0.0491
I1710	F	LC	0.1175	0.0712	0.0694	0.0456
I2007	F	LC	0.0849	0.0535	0.0622	0.0467
I2205	F	LC	0.114	0.0778	0.0694	0.0519
I2209	F	LC	0.1252	0.081	0.072	0.0514
J2304	F	LC	0.1237	0.0819	0.0672	0.0476
J2306	F	LC	0.1066	0.0622	0.0761	0.0449
J2413	F	LC	0.1328	0.1001	0.0648	0.0482
K2501	F	LC	0.1175	0.0526	0.0723	0.0451
K2503	F	LC	0.1221	0.0866	0.0707	0.0519
K2606	F	LC	0.1118	0.0899	0.0659	0.049
L1707	F	cKO	0.1152	0.0623	0.0725	0.0438
L1804	F	cKO	0.1151	0.0554	0.0772	0.047
L1808	F	cKO	0.1214	0.0598	0.0741	0.0477
L1813	F	cKO	0.1332	0.073	0.0699	0.0476
M2113	F	cKO	0.093	0.0591	0.0717	0.0473
M2216	F	cKO	0.1203	0.071	0.073	0.0463
M2303	F	cKO	0.1047	0.046	0.0735	0.0446
M2310	F	cKO	0.1484	0.0417	0.0737	0.0415
N2311	F	cKO	0.1034	0.0586	0.0719	0.0489
N2404	F	cKO	0.1089	0.0669	0.0693	0.0489
N2406	F	cKO	0.1139	0.0487	0.0796	0.0477
N2410	F	cKO	0.1063	0.0585	0.0842	0.0459

Table C.2 continued:

Animal ID	Male or Female	cKO or LC	BV/TV.L	BV/TV.R	Tb.Th.L (mm)	Tb.Th.R (mm)
O1412	M	LC	0.1607	0.1705	0.0573	0.0536
O1507	M	LC	0.1651	0.1361	0.0633	0.0476
O1610	M	LC	0.1717	0.1652	0.0562	0.0486
O1701	M	LC	0.1515	0.1797	0.0585	0.0541
P1801	M	LC	0.1734	0.1293	0.0583	0.0492
P1910	M	LC	0.1255	0.1043	0.0557	0.0413
P2003	M	LC				
P2117	M	LC				
Q2202	M	LC	0.0944	0.0673	0.0538	0.0401
Q2309	M	LC	0.1043	0.0562	0.0593	0.0394
Q2403	M	LC	0.1535	0.1145	0.0594	0.0429
R2412	M	LC	0.0948	0.0651	0.0637	0.0406
R2506	M	LC	0.1535	0.1329	0.0623	0.0493
R2611	M	LC	0.1679	0.1307	0.0571	0.0449
S1306	M	cKO	0.1473	0.1207	0.0644	0.0475
S1307	M	cKO	0.1541	0.154	0.0548	0.0483
S1401	M	cKO	0.1843	0.1543	0.0614	0.0481
S1805	M	cKO	0.1305	0.0913	0.0683	0.0488
T1607	M	cKO	0.1583	0.2072	0.0584	0.0581
T1806	M	cKO	0.1707	0.2102	0.062	0.062
T1811	M	cKO	0.1698	0.2001	0.054	0.0526
T2101	M	cKO	0.1421	0.1911	0.0588	0.0587
U2108	M	cKO	0.1564	0.1342	0.056	0.0457
U2402	M	cKO	0.1381	0.1443	0.0558	0.0471
U2505	M	cKO	0.1711	0.1562	0.0675	0.0536
V2507	M	cKO	0.1552	0.1815	0.0707	0.0587
V2602	M	cKO				
V2608	M	cKO				

Table C.2 continued:

Animal ID	Male or Female	cKO or LC	Tb.Sp.L (mm)	Tb.Sp.R (mm)	cn.TMD.L (mgHA/cc)	cn.TMD.R (mgHA/CC)
H1314	F	LC	0.3054	0.2983	781.866	753.869
H1411	F	LC	0.3892	0.3379	793.195	769.3
H1504	F	LC	0.2978	0.3744	801.725	786.684
H1708	F	LC	0.3203	0.2543	780.304	750.158
I1710	F	LC	0.2858	0.3088	809.799	762.529
I2007	F	LC	0.365	0.3484	786.88	773.011
I2205	F	LC	0.3528	0.3247	788.638	787.791
I2209	F	LC	0.2959	0.3122	803.353	762.463
J2304	F	LC	0.3235	0.3225	807.715	777.048
J2306	F	LC	0.3221	0.3364	800.683	753.022
J2413	F	LC	0.2929	0.2746	787.27	748.53
K2501	F	LC	0.35	0.3715	815.658	755.822
K2503	F	LC	0.3648	0.3548	813.249	782.713
K2606	F	LC	0.3121	0.3022	798.404	777.634
L1707	F	cKO	0.3784	0.3595	765.003	737.591
L1804	F	cKO	0.4747	0.4777	805.762	768.909
L1808	F	cKO	0.4009	0.4299	790.135	759.599
L1813	F	cKO	0.4087	0.3781	798.404	768.909
M2113	F	cKO	0.4535	0.3788	799.12	758.557
M2216	F	cKO	0.3665	0.4206	797.948	754.715
M2303	F	cKO	0.4523	0.4499	782.973	767.672
M2310	F	cKO	0.3774	0.3745	769.821	750.613
N2311	F	cKO	0.4553	0.4351	806.087	751.59
N2404	F	cKO	0.4237	0.3716	807.455	782.582
N2406	F	cKO	0.5034	0.4765	797.493	740
N2410	F	cKO	0.5321	0.4097	770.016	739.87

Table C.2 continued:

Animal ID	Male or Female	cKO or LC	Tb.Sp.L	Tb.Sp R	cn.TMD.L	cn.TMD.R
O1412	M	LC	0.2279	0.2067	798.665	765.393
O1507	M	LC	0.2218	0.2127	798.209	776.918
O1610	M	LC	0.1876	0.2001	790.982	765.133
O1701	M	LC	0.2276	0.2262	812.468	776.462
P1801	M	LC	0.1886	0.2176	787.856	764.742
P1910	M	LC	0.2172	0.2034	790.331	771.123
P2003	M	LC				
P2117	M	LC				
Q2202	M	LC	0.2605	0.2605	791.698	764.221
Q2309	M	LC	0.253	0.2675	795.735	768.063
Q2403	M	LC	0.1945	0.2029	794.693	764.742
R2412	M	LC	0.2893	0.2814	820.086	764.156
R2506	M	LC	0.2284	0.2332	791.893	762.463
R2611	M	LC	0.1978	0.2074	775.941	740.717
S1306	M	cKO	0.2561	0.2681	798.404	781.541
S1307	M	cKO	0.1986	0.1972	781.606	759.403
S1401	M	cKO	0.1936	0.1909	800.097	758.166
S1805	M	cKO	0.3083	0.2909	810.45	805.501
T1607	M	cKO	0.2208	0.2043	788.377	782.387
T1806	M	cKO	0.2367	0.2376	800.944	790.786
T1811	M	cKO	0.1907	0.1914	776.006	764.677
T2101	M	cKO	0.2615	0.2699	777.113	773.728
U2108	M	cKO	0.1951	0.1976	792.284	755.041
U2402	M	cKO	0.2225	0.1958	779.718	765.133
U2505	M	cKO	0.2121	0.2056	808.952	768.909
V2507	M	cKO	0.2615	0.2532	810.58	782.127
V2602	M	cKO				
V2608	M	cKO				

Table C.3 Indices of cortical bone determined by microCT analysis of VOIs from loaded left (L) and control right (R) tibial midshaft of 12-week-old female and male pOC-ERαKO and LC mice.

Animal ID	Male or Female	cKO or LC	I_{MAX}.L (mm4)	I_{MAX}.R (mm4)	I_{MIN}.L (mm4)	I_{MIN}.R (mm4)
H1314	F	LC	0.09647	0.05995	0.06344	0.05181
H1411	F	LC	0.0722	0.05977	0.0545	0.05064
H1504	F	LC	0.08801	0.06697	0.06235	0.04923
H1708	F	LC	0.07719	0.05276	0.0606	0.0462
I1710	F	LC	0.08574	0.05325	0.05396	0.04449
I2007	F	LC	0.09717	0.06048	0.06796	0.05286
I2205	F	LC				
I2209	F	LC	0.10162	0.06108	0.07811	0.05594
J2304	F	LC	0.09608	0.05239	0.0661	0.04642
J2306	F	LC	0.09626	0.07	0.06252	0.0531
J2413	F	LC	0.08858	0.05848	0.06849	0.04841
K2501	F	LC	0.10658	0.06021	0.06858	0.05027
K2503	F	LC	0.10068	0.06238	0.06949	0.0545
K2606	F	LC	0.0966	0.06647	0.06424	0.05197
L1707	F	cKO	0.09298	0.05238	0.06225	0.04354
L1804	F	cKO	0.1083	0.05679	0.07276	0.04868
L1808	F	cKO	0.09682	0.06321	0.06194	0.04453
L1813	F	cKO		0.06872		0.05708
M2113	F	cKO	0.11851	0.05908	0.07309	0.04491
M2216	F	cKO	0.09614	0.06272	0.06032	0.04628
M2303	F	cKO	0.11756	0.04817	0.07466	0.04249
M2310	F	cKO	0.10734	0.05678	0.07237	0.04183
N2311	F	cKO	0.09849	0.07031	0.0652	0.05082
N2404	F	cKO	0.10735	0.06514	0.07091	0.05343
N2406	F	cKO	0.0996	0.05726	0.06627	0.04562
N2410	F	cKO	0.11366	0.05738	0.07604	0.04511

Table C.3 continued:

Animal ID	Male or Female	cKO or LC	I_{MAX}.L (mm4)	I_{MAX}.R (mm4)	I_{MIN}.L (mm4)	I_{MIN}.R (mm4)
O1412	M	LC	0.12617	0.11634	0.08948	0.08733
O1507	M	LC	0.13942	0.12962	0.09474	0.08379
O1610	M	LC	0.13251	0.14426	0.0975	0.10701
O1701	M	LC	0.14357	0.14495	0.09945	0.10315
P1801	M	LC	0.12454	0.1199	0.08375	0.08282
P1910	M	LC	0.11093	0.12456	0.07822	0.08466
P2003	M	LC	0.14377	0.13826	0.08833	0.09529
P2117	M	LC	0.13808	0.14168	0.10428	0.09663
Q2202	M	LC	0.13063	0.09848	0.08508	0.06852
Q2309	M	LC	0.09368	0.0772	0.07059	0.06026
Q2403	M	LC	0.12299	0.12696	0.08965	0.08873
R2412	M	LC	0.10443	0.08228	0.07183	0.06478
R2506	M	LC	0.11783	0.12524	0.08335	0.07984
R2611	M	LC	0.15439	0.13115	0.09954	0.08611
S1306	M	cKO	0.14111	0.15141	0.09106	0.08569
S1307	M	cKO	0.18662	0.16167	0.10825	0.08958
S1401	M	cKO	0.14223	0.15312	0.09885	0.09768
S1805	M	cKO	0.13376	0.13952	0.08172	0.09561
T1607	M	cKO	0.14149	0.14429	0.11186	0.10581
T1806	M	cKO	0.16421	0.16911	0.10399	0.11046
T1811	M	cKO	0.17147	0.14641	0.11484	0.10043
T2101	M	cKO	0.16086	0.13504	0.10249	0.09322
U2108	M	cKO	0.13737	0.13265	0.09775	0.09257
U2402	M	cKO	0.15639	0.15125	0.1099	0.10329
U2505	M	cKO	0.14981	0.13213	0.10008	0.09111
V2507	M	cKO	0.12179	0.12028	0.09205	0.0816
V2602	M	cKO	0.10884	0.10252	0.07021	0.07004
V2608	M	cKO	0.14811	0.13789	0.09646	0.09307

Table C.3 continued:

Animal ID	Male or Female	cKO or LC	CtAr.L (mm2)	Ct.Ar.R (mm2)	ct.TMD.L (mgHA/cc)	ct.TMD.R (mgHA/cc)
H1314	F	LC	0.72629	0.56607	1009.166	1022.904
H1411	F	LC	0.65553	0.56859	1015.938	1016.003
H1504	F	LC	0.677	0.57549	1027.722	1018.086
H1708	F	LC	0.66011	0.50429	974.3322	990.6749
I1710	F	LC	0.71031	0.52449	1023.556	1018.802
I2007	F	LC	0.73966	0.57546	1012.226	1029.285
I2205	F	LC				
I2209	F	LC	0.74972	0.57748	1014.505	1029.22
J2304	F	LC	0.7244	0.52613	997.5114	1015.677
J2306	F	LC	0.70094	0.59131	1009.817	1022.774
J2413	F	LC	0.73273	0.53151	1009.036	1005.194
K2501	F	LC	0.75772	0.56373	1020.886	1033.322
K2503	F	LC	0.75355	0.57058	1023.165	1030.848
K2606	F	LC	0.73238	0.60161	1053.441	1057.608
L1707	F	cKO	0.71827	0.50818	1001.548	1018.672
L1804	F	cKO	0.77843	0.5251	1011.054	1017.891
L1808	F	cKO	0.72437	0.53545	1007.018	1021.928
L1813	F	cKO		0.57005		1015.091
M2113	F	cKO	0.81455	0.54376	1004.804	1027.657
M2216	F	cKO	0.72057	0.54895	1012.357	1023.49
M2303	F	cKO	0.82934	0.49464	993.0187	1031.238
M2310	F	cKO	0.74387	0.49986	993.4745	1000.897
N2311	F	cKO	0.71226	0.56958	1026.03	1024.793
N2404	F	cKO	0.72339	0.56505	1031.694	1022.318
N2406	F	cKO	0.74325	0.52153	1006.562	1011.185
N2410	F	cKO	0.79538	0.52701	996.4697	1010.989

Table C.3 continued:

Animal ID	Male or Female	cKO or LC	CtAr.L (mm2)	Ct.Ar.R (mm2)	ct.TMD.L (mgHA/cc)	ct.TMD.R (mgHA/cc)
O1412	M	LC	0.78024	0.77414	1044.651	1055.264
O1507	M	LC	0.83357	0.78705	1045.042	1050.511
O1610	M	LC	0.82751	0.85469	1057.543	1038.335
O1701	M	LC	0.84272	0.87523	1040.94	1055.85
P1801	M	LC	0.76538	0.73595	1048.818	1029.741
P1910	M	LC	0.7429	0.75633	1040.744	1032.671
P2003	M	LC	0.82669	0.85087	1039.703	1046.604
P2117	M	LC	0.83599	0.84284	1023.36	1034.168
Q2202	M	LC	0.76651	0.66826	1016.979	1024.402
Q2309	M	LC	0.70693	0.62194	1034.364	1027.788
Q2403	M	LC	0.79971	0.78398	1042.828	1041.265
R2412	M	LC	0.71203	0.63316	1028.634	1020.756
R2506	M	LC	0.77521	0.79321	1047.581	1056.566
R2611	M	LC	0.86051	0.79424	1040.549	1044.391
S1306	M	cKO	0.83093	0.83869	1049.73	1046.344
S1307	M	cKO	0.91831	0.85328	1039.573	1045.758
S1401	M	cKO	0.83175	0.82829	1049.209	1034.689
S1805	M	cKO	0.78077	0.80608	1045.888	1044.846
T1607	M	cKO	0.84464	0.86271	1058.129	1060.473
T1806	M	cKO	0.87855	0.92101	1058.129	1064.119
T1811	M	cKO	0.89452	0.85995	1048.232	1073.104
T2101	M	cKO	0.8512	0.81242	1039.377	1044.846
U2108	M	cKO	0.81914	0.78113	1052.399	1039.377
U2402	M	cKO	0.85718	0.8561	1039.247	1048.102
U2505	M	cKO	0.84451	0.81876	1053.311	1055.199
V2507	M	cKO	0.78013	0.7542	1042.242	1049.013
V2602	M	cKO	0.71181	0.70156	1020.235	998.9438
V2608	M	cKO	0.83609	0.82369	1037.294	1041.786

Table C.3 continued:

Animal ID	Male or Female	cKO or LC	Ct.Th.L (mm)	Ct.Th.R (mm)	Mar.Ar.L (mm2)	Ma.Ar.R (mm2)
H1314	F	LC	0.254	0.207	0.31538	0.32459
H1411	F	LC	0.246	0.21	0.27414	0.31902
H1504	F	LC	0.235	0.209	0.33606	0.32942
H1708	F	LC	0.235	0.184	0.32566	0.35499
I1710	F	LC	0.267	0.197	0.25268	0.31666
I2007	F	LC	0.263	0.211	0.3193	0.32191
I2205	F	LC				
I2209	F	LC	0.251	0.211	0.36623	0.34554
J2304	F	LC	0.252	0.198	0.32857	0.32131
J2306	F	LC	0.24	0.209	0.33405	0.344
J2413	F	LC	0.259	0.192	0.30749	0.36132
K2501	F	LC	0.26	0.207	0.32909	0.32815
K2503	F	LC	0.268	0.205	0.32236	0.35275
K2606	F	LC	0.257	0.22	0.30444	0.30877
L1707	F	cKO	0.254	0.19	0.30635	0.33054
L1804	F	cKO	0.266	0.189	0.3299	0.36158
L1808	F	cKO	0.254	0.194	0.30835	0.34505
L1813	F	cKO		0.197		0.3958
M2113	F	cKO	0.274	0.203	0.30353	0.31792
M2216	F	cKO	0.256	0.201	0.30894	0.33611
M2303	F	cKO	0.281	0.188	0.29678	0.32569
M2310	F	cKO	0.246	0.183	0.3524	0.35603
N2311	F	cKO	0.243	0.2	0.34129	0.36185
N2404	F	cKO	0.238	0.2	0.38523	0.35906
N2406	F	cKO	0.258	0.19	0.313	0.34905
N2410	F	cKO	0.266	0.194	0.33436	0.33932

Table C.3 continued:

Animal ID	Male or Female	cKO or LC	Ct.Th.L (mm)	Ct.Th.R (mm)	Mar.Ar.L (mm2)	Ma.Ar.R (mm2)
O1412	M	LC	0.238	0.246	0.44124	0.42179
O1507	M	LC	0.256	0.247	0.42981	0.4233
O1610	M	LC	0.253	0.253	0.42247	0.4568
O1701	M	LC	0.254	0.266	0.44593	0.4232
P1801	M	LC	0.238	0.227	0.43453	0.47111
P1910	M	LC	0.24	0.231	0.39815	0.45037
P2003	M	LC	0.253	0.262	0.41672	0.40345
P2117	M	LC	0.246	0.258	0.45853	0.43637
Q2202	M	LC	0.235	0.217	0.4422	0.42149
Q2309	M	LC	0.239	0.215	0.34519	0.36611
Q2403	M	LC	0.252	0.235	0.40745	0.43949
R2412	M	LC	0.233	0.213	0.38877	0.39871
R2506	M	LC	0.247	0.254	0.39958	0.38075
R2611	M	LC	0.257	0.244	0.44447	0.43025
S1306	M	cKO	0.255	0.259	0.39703	0.41635
S1307	M	cKO	0.259	0.257	0.47196	0.43495
S1401	M	cKO	0.248	0.24	0.46451	0.49194
S1805	M	cKO	0.242	0.24	0.4356	0.48156
T1607	M	cKO	0.247	0.257	0.48768	0.44261
T1806	M	cKO	0.257	0.27	0.47088	0.44939
T1811	M	cKO	0.251	0.26	0.50874	0.44194
T2101	M	cKO	0.246	0.249	0.48665	0.44663
U2108	M	cKO	0.245	0.233	0.45601	0.47438
U2402	M	cKO	0.246	0.252	0.49972	0.46585
U2505	M	cKO	0.251	0.255	0.46313	0.42175
V2507	M	cKO	0.24	0.235	0.43475	0.42912
V2602	M	cKO	0.231	0.231		
V2608	M	cKO	0.25	0.253		

Table C.4 Indices of cortical bone determined by microCT analysis of VOIs from loaded left (L) and control right (R) tibial metaphyseal cortical shell of 12-week-old female and male pOC-ERαKO and LC mice.

Animal ID	Male or Female	cKO or LC	I_{MAX}.L (mm4)	I_{MAX}.R (mm4)	I_{MIN}.L (mm4)	I_{MIN}.R (mm4)
H1314	F	LC	0.57359	0.32878	0.44911	0.25657
H1411	F	LC	0.51219	0.36795	0.40061	0.27276
H1504	F	LC	0.50291	0.34614	0.37988	0.27035
H1708	F	LC	0.42567	0.28728	0.32648	0.22976
I1710	F	LC	0.41664	0.33107	0.34874	0.28633
I2007	F	LC	0.49526	0.4088	0.40883	0.34163
I2205	F	LC	0.56225	0.42348	0.45574	0.33683
I2209	F	LC	0.59722	0.39047	0.50905	0.33781
J2304	F	LC	0.51779	0.33194	0.43504	0.28143
J2306	F	LC	0.50904	0.34181	0.42391	0.28619
J2413	F	LC	0.50649	0.35117	0.41288	0.3029
K2501	F	LC	0.67133	0.36821	0.54306	0.29178
K2503	F	LC	0.56751	0.50031	0.47631	0.36604
K2606	F	LC	0.61455	0.44076	0.49907	0.35653
L1707	F	cKO	0.52075	0.32361	0.4085	0.26
L1804	F	cKO	0.61293	0.33886	0.48187	0.25965
L1808	F	cKO	0.50702	0.34045	0.41831	0.24684
L1813	F	cKO	0.598	0.38121	0.48934	0.33032
M2113	F	cKO	0.5357	0.3458	0.42933	0.27037
M2216	F	cKO	0.53159	0.36688	0.42241	0.27818
M2303	F	cKO	0.5093	0.28829	0.40294	0.2115
M2310	F	cKO	0.51133	0.30318	0.41132	0.23405
N2311	F	cKO	0.49477	0.33532	0.41845	0.29395
N2404	F	cKO	0.63298	0.39581	0.48813	0.29929
N2406	F	cKO	0.51793	0.34188	0.38695	0.2293
N2410	F	cKO	0.51098	0.30075	0.39227	0.22785

Table C.4 continued:

Animal ID	Male or Female	cKO or LC	I_{MAX}.L (mm4)	I_{MAX}.R (mm4)	I_{MIN}.L (mm4)	I_{MIN}.R (mm4)
O1412	M	LC	0.66493	0.59319	0.52239	0.44572
O1507	M	LC	0.6776	0.53349	0.52996	0.42294
O1610	M	LC	0.70305	0.57387	0.57859	0.43031
O1701	M	LC	0.70228	0.63236	0.5529	0.47034
P1801	M	LC	0.61714	0.5974	0.48387	0.3903
P1910	M	LC	0.66092	0.49858	0.49654	0.40133
P2003	M	LC	0.767	0.68585	0.61828	0.57444
P2117	M	LC	0.72984	0.66952	0.58568	0.42463
Q2202	M	LC	0.58799	0.4198	0.4149	0.35455
Q2309	M	LC	0.53522	0.41842	0.41402	0.32538
Q2403	M	LC	0.68857	0.52809	0.54015	0.39098
R2412	M	LC	0.61392	0.44391	0.501	0.3565
R2506	M	LC	0.72174	0.53762	0.61364	0.43244
R2611	M	LC	0.71661	0.61214	0.56626	0.46745
S1306	M	cKO	0.63754	0.49085	0.46876	0.3424
S1307	M	cKO	0.79347	0.57638	0.62135	0.40546
S1401	M	cKO	0.73987	0.60811	0.59074	0.42608
S1805	M	cKO	0.69332	0.47215	0.55421	0.37936
T1607	M	cKO	0.84467	0.7649	0.65139	0.56008
T1806	M	cKO	1.05651	0.78747	0.79125	0.53589
T1811	M	cKO	0.84393	0.65226	0.67676	0.46565
T2101	M	cKO	0.88742	0.79133	0.6575	0.50722
U2108	M	cKO	0.65356	0.53871	0.52029	0.43032
U2402	M	cKO	0.77898	0.52505	0.6318	0.40316
U2505	M	cKO	0.79574	0.66302	0.58972	0.46773
V2507	M	cKO	0.73819	0.58173	0.59525	0.39781
V2602	M	cKO	0.72907	0.57578	0.56404	0.44528
V2608	M	cKO	0.60402	0.55442	0.46251	0.39984

Table C.4 continued:

Animal ID	Male or Female	cKO or LC	Ct.Ar.L (mm2)	Ct.Ar.R (mm2)	T.Ar.L (mm2)	T.Ar.R (mm2)
H1314	F	LC	1.28537	0.90588	1.81258	1.31204
H1411	F	LC	1.25535	0.94869	1.76172	1.48042
H1504	F	LC	1.2209	0.89409	1.63005	1.35724
H1708	F	LC	1.11363	0.80816	1.57935	1.30491
I1710	F	LC	1.14391	0.91536	1.47666	1.37854
I2007	F	LC	1.28217	1.05066	1.82107	1.681
I2205	F	LC	1.3723	1.05903	2.16429	1.81098
I2209	F	LC	1.39062	1.02918	2.23547	1.80653
J2304	F	LC	1.28429	0.9192	2.06701	1.61957
J2306	F	LC	1.28222	0.93065	2.08891	1.612
J2413	F	LC	1.15407	0.86418	1.79973	1.43346
K2501	F	LC	1.42173	0.9652	1.99868	1.56539
K2503	F	LC	1.36287	1.1221	2.13231	1.92811
K2606	F	LC	1.36568	1.08793	2.24392	1.88868
L1707	F	cKO	1.287	0.86942	2.18722	1.68859
L1804	F	cKO	1.37102	0.86386	2.36889	1.73989
L1808	F	cKO	1.17182	0.8367	2.33303	1.87888
L1813	F	cKO	1.31356	0.93236	2.34444	2.0739
M2113	F	cKO	1.31744	0.891	2.01309	1.59248
M2216	F	cKO	1.27969	0.92345	2.05297	1.66322
M2303	F	cKO	1.25569	0.78995	1.96529	1.40003
M2310	F	cKO	1.28612	0.78701	1.98796	1.46447
N2311	F	cKO	1.23474	0.88407	1.92446	1.66017
N2404	F	cKO	1.27355	0.93424	2.25259	1.81014
N2406	F	cKO	1.25433	0.84785	1.85662	1.42551
N2410	F	cKO	1.24248	0.83235	1.82539	1.42101

Table C.4 continued:

Animal ID	Male or Female	cKO or LC	Ct.Ar.L (mm2)	Ct.Ar.R (mm2)	T.Ar.L (mm2)	T.Ar.R (mm2)
O1412	M	LC	1.33529	1.21426		
O1507	M	LC	1.33187	1.1153		
O1610	M	LC	1.36541	1.19876		
O1701	M	LC	1.36123	1.2445		
P1801	M	LC	1.25308	1.09968		
P1910	M	LC	1.25881	1.0378		
P2003	M	LC	1.41538	1.32636		
P2117	M	LC	1.35615	1.20298		
Q2202	M	LC	1.20311	0.94107		
Q2309	M	LC	1.12699	0.90789		
Q2403	M	LC	1.27135	1.06541		
R2412	M	LC	1.2283	0.97985		
R2506	M	LC	1.41122	1.12315		
R2611	M	LC	1.36739	1.13505		
S1306	M	cKO	1.26785	1.03303		
S1307	M	cKO	1.3619	1.08136		
S1401	M	cKO	1.33563	1.10263		
S1805	M	cKO	1.38011	0.98856		
T1607	M	cKO	1.4634	1.38642		
T1806	M	cKO	1.65962	1.43201		
T1811	M	cKO	1.44696	1.27471		
T2101	M	cKO	1.4736	1.36656		
U2108	M	cKO	1.26754	1.08839		
U2402	M	cKO	1.37946	1.05454		
U2505	M	cKO	1.41302	1.21701		
V2507	M	cKO	1.43739	1.17058		
V2602	M	cKO	1.34455	1.17504		
V2608	M	cKO	1.23305	1.11136		

Table C.4 continued:

Animal ID	Male or Female	cKO or LC	Ct.Th.L (mm)	Ct.Th.R (mm)	ctTIMD.L (mgHA/cc)	ct.TMD.R (mgHA/cc)
H1314	F	LC	0.168	0.138	823.0163	825.816
H1411	F	LC	0.185	0.147	846.9117	824.1883
H1504	F	LC	0.181	0.138	856.6131	849.1906
H1708	F	LC	0.172	0.125	844.8933	800.4882
I1710	F	LC	0.177	0.138	882.5921	834.2803
I2007	F	LC	0.196	0.151	864.4914	840.9216
I2205	F	LC	0.192	0.151	846.4559	833.8246
I2209	F	LC	0.179		819.1097	872.3204
J2304	F	LC	0.173	0.135	837.0801	838.187
J2306	F	LC	0.186	0.143	854.0087	833.1083
J2413	F	LC	0.154	0.118	800.8788	774.5743
K2501	F	LC	0.182	0.147	827.6391	840.8564
K2503	F	LC	0.185	0.147	849.3208	844.8282
K2606	F	LC	0.17	0.15	843.7864	847.2372
L1707	F	cKO	0.179	0.128	819.891	792.8703
L1804	F	cKO	0.173	0.125	828.6808	820.6723
L1808	F	cKO	0.16	0.124	821.5187	825.23
L1813	F	cKO	0.17	0.128	841.3773	816.6355
M2113	F	cKO	0.186	0.128	839.424	807.5852
M2216	F	cKO	0.181	0.136	840.8564	820.3468
M2303	F	cKO	0.178	0.124	846.2606	842.8749
M2310	F	cKO	0.173	0.118	805.0459	778.0903
N2311	F	cKO	0.178	0.125	838.1218	836.6894
N2404	F	cKO	0.155	0.129	837.2754	830.8295
N2406	F	cKO	0.18	0.13	837.8614	801.0742
N2410	F	cKO	0.179	0.135	842.4191	821.7792

Table C.4 continued:

Animal ID	Male or Female	cKO or LC	Ct.Th.L (mm)	Ct.Th.R (mm)	ctTIMD.L (mgHA/cc)	ct.TMD.R (mgHA/cc)
O1412	M	LC	0.153	0.141	826.6625	820.477
O1507	M	LC	0.158	0.135	831.2202	819.6306
O1610	M	LC	0.16	0.14	839.6194	826.7927
O1701	M	LC		0.148	872.3204	840.5309
P1801	M	LC	0.151	0.131	835.6476	807.3899
P1910	M	LC	0.15	0.13	814.4869	820.2166
P2003	M	LC	0.168	0.154	826.6625	825.8812
P2117	M	LC	0.168	0.157	815.9193	824.9045
Q2202	M	LC	0.157	0.122	829.4622	803.6786
Q2309	M	LC	0.145	0.117	818.5237	804.9157
Q2403	M	LC	0.148	0.116	820.477	821.5839
R2412	M	LC	0.147	0.121	827.7042	813.7056
R2506	M	LC	0.163	0.132	814.6171	801.9206
R2611	M	LC	0.155	0.125	799.9673	808.8223
S1306	M	cKO	0.155	0.13	828.6158	818.0028
S1307	M	cKO	0.149	0.13	814.2264	807.8456
S1401	M	cKO	0.15	0.128	816.5053	801.8555
S1805	M	cKO	0.164	0.12	830.6342	812.1429
T1607	M	cKO	0.166	0.157	815.4635	818.9144
T1806	M	cKO	0.171	0.173	814.9426	839.0334
T1811	M	cKO	0.158	0.151	806.4132	829.5924
T2101	M	cKO	0.168	0.16	816.0495	830.6993
U2108	M	cKO	0.145	0.125	808.8223	801.5951
U2402	M	cKO	0.155	0.132	808.9525	808.9525
U2505	M	cKO	0.157	0.135	821.5839	811.3616
V2507	M	cKO	0.166	0.149	815.5938	825.0998
V2602	M	cKO	0.158	0.145	812.9243	812.8591
V2608	M	cKO	0.148	0.133	802.116	786.7499

Table C.5 Indices of cancellous bone from microCT analysis of L5 vertebral body of 12-week-old male and female pOC-ERαKO and LC mice.

Animal ID	Male or Female	cKO or LC	BV/TV	Tb.Th (mm)	Tb.Sp (mm)	cn.TMD (mgHA/cc)
H1314	F	LC	0.1941	0.0479	0.227	612.84
H1411	F	LC	0.171	0.0471	0.2432	629.639
H1504	F	LC				
H1708	F	LC	0.2464	0.053	0.195	644.419
I1710	F	LC	0.2022	0.0463	0.1974	626.969
I2007	F	LC	0.1843	0.0487	0.2385	639.21
I2205	F	LC	0.1697	0.0469	0.2397	641.749
I2209	F	LC	0.1495	0.0452	0.2471	630.681
J2304	F	LC				
J2306	F	LC				
J2413	F	LC				
K2501	F	LC				
K2503	F	LC	0.1957	0.0515	0.2156	632.178
K2606	F	LC				
L1707	F	cKO				
L1804	F	cKO				
L1808	F	cKO	0.1427	0.0443	0.2256	653.99
L1813	F	cKO	0.1543	0.046	0.2401	641.424
M2113	F	cKO	0.1727	0.0456	0.2116	638.168
M2216	F	cKO	0.181	0.0459	0.2154	629.574
M2303	F	cKO				
M2310	F	cKO				
N2311	F	cKO				
N2404	F	cKO	0.1437	0.0457	0.2468	638.559
N2406	F	cKO	0.1689	0.0458	0.2095	634.327
N2410	F	cKO	0.1552	0.0439	0.2434	637.647

Table C.5 continued:

Animal ID	Male or Female	cKO or LC	BV/TV	Tb.Th (mm)	Tb.Sp (mm)	cn.TMD (mgHA/cc)
O1412	M	LC	0.2741	0.0542	0.1671	664.343
O1507	M	LC				
O1610	M	LC	0.2558	0.0506	0.1712	644.875
O1701	M	LC				
P1801	M	LC				
P1910	M	LC	0.2185	0.0467	0.1872	629.834
P2003	M	LC	0.3025	0.058	0.1591	679.253
P2117	M	LC	0.2654	0.0525	0.1654	656.529
Q2202	M	LC	0.1859	0.0438	0.1923	631.462
Q2309	M	LC	0.2014	0.0458	0.1834	618.635
Q2403	M	LC				
R2412	M	LC				
R2506	M	LC				
R2611	M	LC				
S1306	M	cKO				
S1307	M	cKO	0.266	0.0509	0.158	647.479
S1401	M	cKO				
S1805	M	cKO	0.2124	0.0459	0.1666	638.168
T1607	M	cKO	0.331	0.0603	0.1615	674.955
T1806	M	cKO				
T1811	M	cKO	0.3102	0.0546	0.146	652.232
T2101	M	cKO	0.3466	0.0606	0.1401	680.425
U2108	M	cKO	0.2803	0.051	0.154	635.043
U2402	M	cKO				
U2505	M	cKO				
V2507	M	cKO	0.2882	0.0559	0.1677	656.529
V2602	M	cKO				
V2608	M	cKO	0.2707	0.0517	0.1679	642.596

Table C.6 Indices of cortical bone from microCT analysis of L5 cortical vertebral shell in 12-week-old male and female pOC-ERαKO and LC mice.

Animal ID	Male or Female	cKO or LC	I_{MAX} (mm^4)	I_{MIN} (mm^4)	Ct.Ar (mm^2)	T.Ar (mm^2)
H1314	F	LC	0.13658	0.02985	0.31723	0.86805
H1411	F	LC	0.14528	0.02941	0.32793	0.83764
H1504	F	LC				
H1708	F	LC	0.1498	0.031	0.33396	0.90138
I1710	F	LC	0.15246	0.03507	0.33806	0.86011
I2007	F	LC	0.12518	0.02653	0.31715	0.79824
I2205	F	LC	0.14054	0.02948	0.32907	0.94037
I2209	F	LC	0.14059	0.02872	0.32651	0.89089
J2304	F	LC				
J2306	F	LC				
J2413	F	LC				
K2501	F	LC				
K2503	F	LC	0.14857	0.02712	0.33918	0.92831
K2606	F	LC				
L1707	F	cKO				
L1804	F	cKO				
L1808	F	cKO	0.12517	0.0247	0.27646	0.83946
L1813	F	cKO	0.15817	0.03115	0.29619	0.91385
M2113	F	cKO	0.13044	0.02963	0.29314	0.87508
M2216	F	cKO	0.15025	0.03071	0.31722	0.93925
M2303	F	cKO				
M2310	F	cKO				
N2311	F	cKO	0.1457	0.02903	0.30141	0.89386
N2404	F	cKO	0.11959	0.02528	0.26487	0.79025
N2406	F	cKO				
N2410	F	cKO	0.14108	0.0283	0.29683	0.84429

Table C.6 continued:

Animal ID	Male or Female	cKO or LC	I_{MAX} (mm^4)	I_{MIN} (mm^4)	Ct.Ar (mm^2)	T.Ar (mm^2)
O1412	M	LC	0.16991	0.04364	0.38706	0.88151
O1507	M	LC				
O1610	M	LC	0.12998	0.03248	0.31724	0.84998
O1701	M	LC				
P1801	M	LC				
P1910	M	LC	0.12451	0.02851	0.29031	0.85824
P2003	M	LC	0.13775	0.03893	0.35583	0.91451
P2117	M	LC	0.15298	0.03897	0.34399	0.90543
Q2202	M	LC	0.12067	0.02641	0.28047	0.72351
Q2309	M	LC	0.11669	0.02436	0.27425	0.79627
Q2403	M	LC				
R2412	M	LC				
R2506	M	LC				
R2611	M	LC				
S1306	M	cKO				
S1307	M	cKO	0.13641	0.03212	0.31698	0.7995
S1401	M	cKO				
S1805	M	cKO	0.11409	0.02955	0.28478	0.85277
T1607	M	cKO	0.17668	0.04296	0.36066	0.93344
T1806	M	cKO				
T1811	M	cKO	0.13704	0.03354	0.32638	0.8027
T2101	M	cKO	0.1629	0.0376	0.3805	0.9643
U2108	M	cKO	0.12942	0.03104	0.31716	0.89323
U2402	M	cKO				
U2505	M	cKO				
V2507	M	cKO	0.13541	0.03229	0.32073	0.81465
V2602	M	cKO				
V2608	M	cKO	0.1369	0.03156	0.32411	0.85734

Table C.6 continued:

Animal ID	Male or Female	cKO or LC	Ct.Ar/ T.Ar	Ct.Th (mm)	ct.TMD (mgHA/cc)
H1314	F	LC	0.36545	0.062	774.574
H1411	F	LC	0.39149	0.068	798.925
H1504	F	LC			
H1708	F	LC	0.3705	0.064	793.586
I1710	F	LC	0.39305	0.061	791.763
I2007	F	LC	0.39731	0.069	795.67
I2205	F	LC	0.34994	0.065	790.656
I2209	F	LC	0.3665	0.067	788.963
J2304	F	LC			
J2306	F	LC			
J2413	F	LC			
K2501	F	LC			
K2503	F	LC	0.36537	0.068	795.8
K2606	F	LC			
L1707	F	cKO			
L1804	F	cKO			
L1808	F	cKO	0.32933	0.057	801.79
L1813	F	cKO	0.32411	0.058	791.698
M2113	F	cKO	0.33499	0.059	788.638
M2216	F	cKO	0.33774	0.059	777.048
M2303	F	cKO			
M2310	F	cKO			
N2311	F	cKO	0.3372	0.06	786.88
N2404	F	cKO	0.33518	0.054	779.783
N2406	F	cKO			
N2410	F	cKO	0.35157	0.059	786.489

Table C.6 continued:

Animal ID	Male or Female	cKO or LC	Ct.Ar/ T.Ar	Ct.Th (mm)	ct.TMD (mgHA/cc)
O1412	M	LC	0.43909	0.069	798.99
O1507	M	LC			
O1610	M	LC	0.37323	0.063	796.776
O1701	M	LC			
P1801	M	LC			
P1910	M	LC	0.33827	0.057	791.112
P2003	M	LC	0.38909	0.068	805.176
P2117	M	LC	0.37992	0.062	791.568
Q2202	M	LC	0.38765	0.059	785.773
Q2309	M	LC	0.34442	0.057	792.87
Q2403	M	LC			
R2412	M	LC			
R2506	M	LC			
R2611	M	LC			
S1306	M	cKO			
S1307	M	cKO	0.39648	0.063	798.73
S1401	M	cKO			
S1805	M	cKO	0.33394	0.056	787.921
T1607	M	cKO	0.38638	0.066	805.762
T1806	M	cKO			
T1811	M	cKO	0.4066	0.065	805.436
T2101	M	cKO	0.39459	0.07	812.012
U2108	M	cKO	0.35507	0.062	790.331
U2402	M	cKO			
U2505	M	cKO			
V2507	M	cKO	0.3937	0.064	790.135
V2602	M	cKO			
V2608	M	cKO	0.37804	0.063	792.675

Table C.7 Indices of cortical bone from microCT analysis of femoral midshaft in 12-week-old male and female pOC-ERαKO and LC mice.

Animal ID	Male or Female	cKO or LC	I_{MAX} (mm^4)	I_{MIN} (mm^4)	Ct.Ar (mm^2)	T.Ar (mm^2)
H1314	F	LC				
H1411	F	LC	0.20554	0.1078	0.73707	1.64374
H1504	F	LC				
H1708	F	LC				
I1710	F	LC	0.18875	0.09982	0.7176	1.56852
I2007	F	LC				
I2205	F	LC	0.18427	0.10503	0.7257	1.57486
I2209	F	LC	0.22747	0.11149	0.76358	1.69098
J2304	F	LC	0.16089	0.09425	0.6755	1.49048
J2306	F	LC				
J2413	F	LC				
K2501	F	LC	0.18592	0.10753	0.7092	1.61537
K2503	F	LC	0.20099	0.10899	0.72732	1.64662
K2606	F	LC	0.20812	0.12013	0.75252	1.699
L1707	F	cKO				
L1804	F	cKO				
L1808	F	cKO	0.16229	0.10588	0.66771	1.57536
L1813	F	cKO	0.19192	0.11394	0.71074	1.67157
M2113	F	cKO	0.1538	0.09657	0.65532	1.50025
M2216	F	cKO				
M2303	F	cKO	0.16969	0.09542	0.6721	1.53472
M2310	F	cKO	0.17473	0.09919	0.67914	1.56418
N2311	F	cKO				
N2404	F	cKO	0.19918	0.11264	0.7005	1.70093
N2406	F	cKO	0.17482	0.09822	0.64796	1.52265
N2410	F	cKO	0.17586	0.10155	0.66817	1.59634

Table C.7 continued:

Animal ID	Male or Female	cKO or LC	I_{MAX} (mm^4)	I_{MIN} (mm^4)	Ct.Ar (mm^2)	T.Ar (mm^2)
O1412	M	LC	0.38018	0.17477	0.99391	2.14234
O1507	M	LC	0.32796	0.17206	0.94187	2.07344
O1610	M	LC				
O1701	M	LC				
P1801	M	LC	0.31672	0.14607	0.86047	2.01197
P1910	M	LC	0.32654	0.16579	0.89962	2.08083
P2003	M	LC				
P2117	M	LC	0.48215	0.21835	1.09071	2.44105
Q2202	M	LC				
Q2309	M	LC				
Q2403	M	LC				
R2412	M	LC	0.27373	0.11929	0.80844	1.81559
R2506	M	LC	0.32406	0.15278	0.89257	2.02434
R2611	M	LC	0.37527	0.18801	0.98292	2.20117
S1306	M	cKO	0.40187	0.17208	1.04793	2.1204
S1307	M	cKO	0.42396	0.21136	1.03238	2.36015
S1401	M	cKO				
S1805	M	cKO				
T1607	M	cKO	0.43891	0.24014	1.08811	2.44166
T1806	M	cKO	0.5603	0.25639	1.22987	2.57149
T1811	M	cKO	0.43499	0.21962	1.06601	2.38652
T2101	M	cKO	0.486	0.22883	1.14984	2.41592
U2108	M	cKO				
U2402	M	cKO				
U2505	M	cKO				
V2507	M	cKO				
V2602	M	cKO	0.32178	0.13796	0.91304	1.92117
V2608	M	cKO	0.37422	0.1849	0.98119	2.18814

Table C.7 continued:

Animal ID	Male or Female	cKO or LC	Ct.Ar/ T.Ar	Ct.Th (mm)	ct.TMD (mgHA/cc)	Ma.Ar (mm^2)
H1314	F	LC				
H1411	F	LC	0.44841	0.18	956.492	0.90667
H1504	F	LC				
H1708	F	LC				
I1710	F	LC	0.4575	0.179	945.1629	0.85092
I2007	F	LC				
I2205	F	LC	0.4608	0.185	955.32	0.84916
I2209	F	LC	0.45156	0.184	951.9343	0.9274
J2304	F	LC	0.45321	0.173	932.7269	0.81498
J2306	F	LC				
J2413	F	LC				
K2501	F	LC	0.43903	0.176	936.2427	0.90617
K2503	F	LC	0.4417	0.178	938.6518	0.9193
K2606	F	LC	0.44292	0.182	943.6653	0.94648
L1707	F	cKO				
L1804	F	cKO				
L1808	F	cKO	0.42385	0.169	942.2328	0.90765
L1813	F	cKO	0.4252	0.174	934.4197	0.96083
M2113	F	cKO	0.43681	0.17	937.8054	0.84493
M2216	F	cKO				
M2303	F	cKO	0.43793	0.171	937.4799	0.86262
M2310	F	cKO	0.43418	0.171	924.6531	0.88504
N2311	F	cKO				
N2404	F	cKO	0.41183	0.168	914.6262	1.00043
N2406	F	cKO	0.42555	0.144	929.862	0.87469
N2410	F	cKO	0.41857	0.165	938.9774	0.92817

Table C.7 continued:

Animal ID	Male or Female	cKO or LC	Ct.Ar/ T.Ar	Ct.Th (mm)	ct.TMD (mgHA/cc)	Ma.Ar (mm^2)
O1412	M	LC	0.46394	0.201	929.4714	1.14843
O1507	M	LC	0.45426	0.201	932.3361	1.13157
O1610	M	LC				
O1701	M	LC				
P1801	M	LC	0.42767	0.185	940.0191	1.1515
P1910	M	LC	0.43234	0.189	915.7982	1.18121
P2003	M	LC				
P2117	M	LC	0.44682	0.194	921.5279	1.35034
Q2202	M	LC				
Q2309	M	LC				
Q2403	M	LC				
R2412	M	LC	0.44528	0.182	917.8166	1.00715
R2506	M	LC	0.44092	0.192	925.3694	1.13177
R2611	M	LC	0.44654	0.202	920.0303	1.21825
S1306	M	cKO	0.49422	0.203	928.9505	1.07247
S1307	M	cKO	0.43742	0.188	933.6384	1.32777
S1401	M	cKO				
S1805	M	cKO				
T1607	M	cKO	0.44565	0.204	937.9356	1.35355
T1806	M	cKO	0.47827	0.211	933.2477	1.34162
T1811	M	cKO	0.44668	0.196	934.4197	1.32051
T2101	M	cKO	0.47594	0.221	934.5499	1.26608
U2108	M	cKO				
U2402	M	cKO				
U2505	M	cKO				
V2507	M	cKO				
V2602	M	cKO	0.47525	0.192	921.2674	1.00813
V2608	M	cKO	0.44842	0.198	919.1188	1.20695

Table C.8 Indices of serum markers in 12-week-old female and male pOC-ERαKO and LC mice.

Animal ID	Male or Female	cKO or LC	TRACP5b (U/L)	IGF-1 (ng/mL)	OC (ng/mL)	P1NP (pg/mL)	E2 (pg/mL)
H1314	F	LC				108.4487	
H1411	F	LC	6.2	244	55		3.448049
H1504	F	LC				116.7179	
H1708	F	LC	5.9	192	54		3.271478
I1710	F	LC				99.28205	
I2007	F	LC	6.4	255	95		3.549684
I2205	F	LC				96.84615	
I2209	F	LC	7.2	301	91		2.487657
J2304	F	LC				97.35897	
J2306	F	LC	7.1	282	111		2.419775
J2413	F	LC	9.4	245	56		6.004602
K2501	F	LC	6.2	250	65		3.574322
K2503	F	LC				123.7692	
K2606	F	LC	8	237	64		3.59913
L1707	F	cKO				117.9359	
L1804	F	cKO				105.1795	
L1808	F	cKO	5.4	255	61		3.285083
L1813	F	cKO	5.9	341	76		6.515233
M2113	F	cKO				84.79487	
M2216	F	cKO	5.7	297	71		3.358604
M2303	F	cKO	5.7	254	85		2.669501
M2310	F	cKO	5.9	231	65	145.8205	3.830296
N2311	F	cKO	6.5	290	56		2.896515
N2404	F	cKO				92.16667	
N2406	F	cKO	5.6	315	65	122.0385	2.721704
N2410	F	cKO	6.3	268	71		3.195441

Table C.8 continued:

Animal ID	Male or Female	cKO or LC	TRACP5b (U/L)	IGF-1 (ng/mL)	OC (ng/mL)	P1NP (pg/mL)	E2 (pg/mL)
O1412	M	LC	5.9	270	73		
O1507	M	LC	6	264	55	113.1923	
O1610	M	LC	6.3	261	59		
O1701	M	LC	6.5	251	66		
P1801	M	LC	6.1	297	54		
P1910	M	LC	6	262	57		
P2003	M	LC				92.87179	
P2117	M	LC				91.97436	
Q2202	M	LC				139.6667	
Q2309	M	LC				95.5641	
Q2403	M	LC				120.1795	
R2412	M	LC				108.4487	
R2506	M	LC	7.3	264	55		
R2611	M	LC	5.6	251	55		
S1306	M	cKO	5.2	285	54		
S1307	M	cKO	6.6	287	43	101.2051	
S1401	M	cKO	6.2	294	50		
S1805	M	cKO	6.4	295	58	94.47436	
T1607	M	cKO	6.1	283	47		
T1806	M	cKO	6.2	279	45		
T1811	M	cKO				96.39744	
T2101	M	cKO				136.9744	
U2108	M	cKO				134.9872	
U2402	M	cKO				144.859	
U2505	M	cKO	5.2	249	48		
V2507	M	cKO	6.1	248	56		
V2602	M	cKO				128.1923	
V2608	M	cKO				116.9744	

Table C.9 Indices of body, ovarian, and uterine masses in 12-week-old female and male pOC-ERαKO and LC mice.

Animal ID	Male or Female	cKO or LC	Body mass (g)	Ovarian mass (g)	Uterine mass (g)
H1314	F	LC	18.66	147	486
H1411	F	LC	19.07		458
H1504	F	LC		112	850
H1708	F	LC	19.18	179	511
I1710	F	LC	17.45	122	480
I2007	F	LC	18.89	138	473
I2205	F	LC	19.28	246	912
I2209	F	LC	19.39	238	721
J2304	F	LC	17.49	164	578
J2306	F	LC	19.19	95	822
J2413	F	LC	20.55		578
K2501	F	LC	18.47	132	561
K2503	F	LC	18.28	140	500
K2606	F	LC	18.64	132	429
L1707	F	cKO	17.47	148	602
L1804	F	cKO	19.54	248	997
L1808	F	cKO	18.41	132	505
L1813	F	cKO	20.55	167	1090
M2113	F	cKO	18.44	241	811
M2216	F	cKO	19.14	120	878
M2303	F	cKO	18.71	185	507
M2310	F	cKO	18.8	124	1272
N2311	F	cKO	19.67	229	458
N2404	F	cKO	19.61	154	913
N2406	F	cKO	19.25	150	444
N2410	F	cKO	18.66	113	455

Table C.9 continued:

Animal ID	Male or Female	cKO or LC	Body mass (g)	Ovarian mass (g)	Uterine mass (g)
O1412	M	LC	24.59	N/A	N/A
O1507	M	LC	24.36	N/A	N/A
O1610	M	LC	25.35	N/A	N/A
O1701	M	LC	26.36	N/A	N/A
P1801	M	LC	24.6	N/A	N/A
P1910	M	LC	25.7	N/A	N/A
P2003	M	LC	25.8	N/A	N/A
P2117	M	LC	26.56	N/A	N/A
Q2202	M	LC	23.79	N/A	N/A
Q2309	M	LC	23.17	N/A	N/A
Q2403	M	LC	26.18	N/A	N/A
R2412	M	LC	24.41	N/A	N/A
R2506	M	LC	24.2	N/A	N/A
R2611	M	LC	25.3	N/A	N/A
S1306	M	cKO	24.9	N/A	N/A
S1307	M	cKO	26.14	N/A	N/A
S1401	M	cKO	25.5	N/A	N/A
S1805	M	cKO	26.02	N/A	N/A
T1607	M	cKO	26.87	N/A	N/A
T1806	M	cKO	28.72	N/A	N/A
T1811	M	cKO	27.28	N/A	N/A
T2101	M	cKO	26.73	N/A	N/A
U2108	M	cKO	25.07	N/A	N/A
U2402	M	cKO	27.19	N/A	N/A
U2505	M	cKO	25.18	N/A	N/A
V2507	M	cKO	23.25	N/A	N/A
V2602	M	cKO	24.61	N/A	N/A
V2608	M	cKO	24.86	N/A	N/A

Table C.10 Indices of crown/rump and long bone lengths in 12-week-old female and male pOC-ERαKO and LC mice.

Animal ID	Male or Female	cKO or LC	Crown/rump length (mm)	L tibia length (mm)	R tibia length (mm)	R femur length (mm)
H1314	F	LC	81.34	17.58	17.46	14.97
H1411	F	LC	80.81	17.55	17.61	15.12
H1504	F	LC	80.59	17.25	16.92	14.59
H1708	F	LC	81.17	17.4	17.61	
I1710	F	LC	82.52	17.13	17.01	14.86
I2007	F	LC	80.4		17.19	14.86
I2205	F	LC	83.81			15.21
I2209	F	LC	85.14			15.12
J2304	F	LC				14.29
J2306	F	LC	80.58			14.74
J2413	F	LC	85.95			15.4
K2501	F	LC	83.04			15.18
K2503	F	LC	82.86			15.02
K2606	F	LC	83.25			15.04
L1707	F	cKO	79.23	17.16	17.25	14.77
L1804	F	cKO	80.4	17.55	17.46	14.97
L1808	F	cKO	81.83	17.46	17.07	14.88
L1813	F	cKO	82.08		17.82	15.54
M2113	F	cKO	81.48	17.52	17.61	15.03
M2216	F	cKO	83.69	17.49	17.4	15.29
M2303	F	cKO	78.53			15.2
M2310	F	cKO	81.95			14.81
N2311	F	cKO	83.22			
N2404	F	cKO	83.31			14.96
N2406	F	cKO	82.36			15.14
N2410	F	cKO	82.97			14.44

Table C.10 continued:

Animal ID	Male or Female	cKO or LC	Crown/rump length (mm)	L tibia length (mm)	R tibia length (mm)	R femur length (mm)
O1412	M	LC	88.53	17.67	17.7	15.62
O1507	M	LC	89.37	18	17.97	15.53
O1610	M	LC	90.52	17.94	17.82	15.79
O1701	M	LC	92.18	18.12	18.03	15.52
P1801	M	LC	88.7	18.06	17.97	15.52
P1910	M	LC	90.92	18.06	18	16.02
P2003	M	LC	92.34			15.41
P2117	M	LC	89.86			15.06
Q2202	M	LC	86.55			14.89
Q2309	M	LC	86.2			
Q2403	M	LC	91.77			15.3
R2412	M	LC	88.11			15.38
R2506	M	LC	89.35			15.75
R2611	M	LC	87.96			15.66
S1306	M	cKO	88.25	18.09	18.09	
S1307	M	cKO	94.42	18.18	18.03	15.91
S1401	M	cKO	91.86	18.03	17.88	15.58
S1805	M	cKO	91.03	18.15	18.18	
T1607	M	cKO	91.79	17.88	18	16.12
T1806	M	cKO	91.12	18.15	18.24	15.95
T1811	M	cKO	89.71			15.85
T2101	M	cKO	90.84			15.97
U2108	M	cKO	86.46			16.03
U2402	M	cKO	93.18			15.71
U2505	M	cKO	91.57			15.68
V2507	M	cKO	86.47			15.61
V2602	M	cKO	88.71			15.68
V2608	M	cKO	86.47			15.39

Table C.11 Indices of L5 vertebral geometries in 12-week-old female and male pOC-ERαKO and LC mice.

Animal ID	Male or Female	cKO or LC	Height (mm)	Length (mm)	Width (mm)
H1314	F	LC	3.05	2.09	1.17
H1411	F	LC	3.51	2.1	1.29
H1504	F	LC	3.09	2.04	1.16
H1708	F	LC			
I1710	F	LC	2.56	2.13	
I2007	F	LC	3.11	1.93	1.11
I2205	F	LC	3.46	2.28	1.14
I2209	F	LC	2.55	2.12	1.05
J2304	F	LC	3.27	1.72	1.09
J2306	F	LC	2.64	2.11	1.18
J2413	F	LC	3.13	2.09	1.37
K2501	F	LC	3.03	2.14	1.11
K2503	F	LC	3.16	1.93	1.13
K2606	F	LC	2.81	2.16	1.08
L1707	F	cKO	3.44	2.5	1.24
L1804	F	cKO	2.29		
L1808	F	cKO			
L1813	F	cKO	3.6	2.09	1.24
M2113	F	cKO	3.03	2.03	1.37
M2216	F	cKO			
M2303	F	cKO	2.9	2	1.36
M2310	F	cKO	2.96	1.84	1.34
N2311	F	cKO	3.22	2	1.13
N2404	F	cKO			
N2406	F	cKO	3.53	2.17	1.08
N2410	F	cKO	3.15	2.01	1.22

Table C.11 continued:

Animal ID	Male or Female	cKO or LC	Height (mm)	Length (mm)	Width (mm)
O1412	M	LC	3.33		
O1507	M	LC	3.19	2.12	1.25
O1610	M	LC	3.47	2.29	1.16
O1701	M	LC			
P1801	M	LC			
P1910	M	LC	3.13	2.1	1.23
P2003	M	LC	3.06	1.88	1.39
P2117	M	LC	3.16	2.1	1.23
Q2202	M	LC	3.14	1.97	1.22
Q2309	M	LC	2.96	2.15	1.23
Q2403	M	LC			
R2412	M	LC			
R2506	M	LC			
R2611	M	LC	3.1	2.24	1.1
S1306	M	cKO			
S1307	M	cKO	3.41	2.1	1.26
S1401	M	cKO	3.37		
S1805	M	cKO	3.14	2.16	1.27
T1607	M	cKO			
T1806	M	cKO			
T1811	M	cKO	3.18	2.26	1.33
T2101	M	cKO	3.36	2.21	1.27
U2108	M	cKO	3.2		
U2402	M	cKO			
U2505	M	cKO			
V2507	M	cKO	3.34		
V2602	M	cKO			
V2608	M	cKO	3.04	2.16	1.34

Table C.12 Indices of mechanical testing data in right femur and L5 vertebra in 12-week-old female and male pOC-ERαKO and LC mice.

Animal ID	Male or Female	cKO or LC	Compressive strength (N)	Compressive stiffness (N)	Max moment (N·mm)	Bending stiffness ($N \cdot mm^2$)
H1314	F	LC	21.3	150.6544	26.45956	47.82056
H1411	F	LC	20.766	109.4184	25.74407	43.95674
H1504	F	LC	18.134	82.10611	27.89319	81.61951
H1708	F	LC				
I1710	F	LC	26.93	252.5554	21.09659	29.34121
I2007	F	LC			22.28689	25.30023
I2205	F	LC	21.272	122.2372	26.32479	33.80898
I2209	F	LC	20.483	274.5931	24.28274	42.12473
J2304	F	LC	20.585	85.57881	23.32698	26.60421
J2306	F	LC	18.736	165.7116	20.4339	32.82371
J2413	F	LC	22.007	113.9209	21.21159	21.70257
K2501	F	LC	25.11	80.60002	24.7689	53.47599
K2503	F	LC	27.897	305.9099	22.47223	29.29675
K2606	F	LC	17.712	112.9539	27.0933	48.04753
L1707	F	cKO	18.221	91.96649	25.44859	84.99117
L1804	F	cKO	15.156	64.02484	22.76094	41.17293
L1808	F	cKO	19.767		22.8981	25.30077
L1813	F	cKO	19.915	201.664	22.8981	25.30077
M2113	F	cKO	20.068	176.0935	21.7013	30.49013
M2216	F	cKO	17.899		23.44835	46.86691
M2303	F	cKO	15.319	85.21682	25.27342	23.90771
M2310	F	cKO	12.911	56.38142	20.66681	47.71993
N2311	F	cKO	17.072	97.98532		
N2404	F	cKO	18.929		22.5519	49.52684
N2406	F	cKO	18.65	120.9425	25.73869	34.59623
N2410	F	cKO	19.75	71.8018	22.15127	71.86923

Table C.12 continued:

Animal ID	Male or Female	cKO or LC	Compressive Strength (N)	Compressive Stiffness (N)	Max moment (N·mm)	Bending stiffness (N·mm^2)
O1412	M	LC	24.867	220.4127	38.07199	209.9159
O1507	M	LC	17.817	227.6033	38.55323	217.3116
O1610	M	LC	26.674	149.6611	34.91419	79.94756
O1701	M	LC				
P1801	M	LC			28.06262	172.7391
P1910	M	LC	20.376	213.3878	30.12318	48.3166
P2003	M	LC	29.249	248.2333	38.12461	43.45768
P2117	M	LC	29.432	532.1187	39.20994	83.67157
Q2202	M	LC	18.686	128.5139	28.64428	78.05465
Q2309	M	LC	26.619	115.955	25.56948	87.14018
Q2403	M	LC			32.64057	47.16066
R2412	M	LC			25.56114	23.12665
R2506	M	LC			35.86112	29.42739
R2611	M	LC	21.46	366.5595	37.82316	136.8459
S1306	M	cKO			34.92784	86.85404
S1307	M	cKO	22.451	159.9802	36.12844	97.87588
S1401	M	cKO	21.626	147.1915	32.50593	65.07007
S1805	M	cKO	17.645	157.9703		
T1607	M	cKO	38.346	301.7728	40.69047	101.328
T1806	M	cKO			44.81976	206.1935
T1811	M	cKO	25.315	264.9894	43.57968	228.4519
T2101	M	cKO	34.458	389.7634	42.58247	151.7351
U2108	M	cKO	22.737	254.0512	37.19725	96.73706
U2402	M	cKO			38.98755	63.46775
U2505	M	cKO			38.56435	129.4197
V2507	M	cKO	26.402	177.5177	41.05285	31.21829
V2602	M	cKO			30.67679	35.12127
V2608	M	cKO			38.22918	261.5301

Table C.13 Indices of histology and IHC in the left loaded (L) and right control (R) cancellous tibial metaphysis of 12-week-old female and male pOC-ERαKO and LC mice.

Animal ID	Male or Female	cKO or LC	N.Oc/BS.L (mm^{-1})	N.Oc/BS.R (mm^{-1})	Oc.S/BS.L	Oc.S/BS.L
H1314	F	LC	3.306435	1.625295	0.062143	0.02833
H1411	F	LC	1.396418	2.626927	0.025033	0.055065
H1504	F	LC	2.718334		0.05735	
H1708	F	LC	1.00334	1.382218	0.016908	0.025269
I1710	F	LC	2.837096	4.478723	0.059442	0.11618
I2007	F	LC	2.520633	1.19772	0.045665	0.025919
I2205	F	LC	3.063762	3.545493	0.073225	0.094126
I2209	F	LC				
J2304	F	LC				
J2306	F	LC				
J2413	F	LC				
K2501	F	LC				
K2503	F	LC				
K2606	F	LC				
L1707	F	cKO	2.857316	0.63389	0.076545	0.012516
L1804	F	cKO	3.044763	2.611393	0.062592	0.043461
L1808	F	cKO	2.397827	1.120268	0.045548	0.018749
L1813	F	cKO	1.180976	2.824179	0.022639	0.061743
M2113	F	cKO	3.321339	2.994283	0.06272	0.059232
M2216	F	cKO	1.316706	1.65151	0.021361	0.02745
M2303	F	cKO				
M2310	F	cKO				
N2311	F	cKO				
N2404	F	cKO				
N2406	F	cKO				
N2410	F	cKO				

Table C.13 continued:

Animal ID	Male or Female	cKO or LC	N.Oc/BS.L (mm^{-1})	N.Oc/BS.R (mm^{-1})	Oc.S/BS.L	Oc.S/BS.L
O1412	M	LC	4.413818	1.519655	0.102097	0.023419
O1507	M	LC	2.714064	3.401465	0.054702	0.069983
O1610	M	LC	4.840309	2.636878	0.112848	0.055795
O1701	M	LC	5.009117	3.217296	0.113281	0.063754
P1801	M	LC	5.535407	4.042086	0.122497	0.080494
P1910	M	LC	2.007029	3.585239	0.03893	0.075761
P2003	M	LC	2.433492	1.868339	0.056071	0.036255
P2117	M	LC				
Q2202	M	LC				
Q2309	M	LC				
Q2403	M	LC				
R2412	M	LC				
R2506	M	LC				
R2611	M	LC				
S1306	M	cKO	4.321684	5.231241	0.110984	0.113817
S1307	M	cKO				
S1401	M	cKO				
S1805	M	cKO	3.851248	3.145757	0.079168	0.062854
T1607	M	cKO	3.912146	2.684461	0.070692	0.064413
T1806	M	cKO				
T1811	M	cKO	4.608856	3.363916	0.10483	0.069227
T2101	M	cKO				
U2108	M	cKO				
U2402	M	cKO				
U2505	M	cKO				
V2507	M	cKO				
V2602	M	cKO	3.991309	2.95816	0.094434	0.062854
V2608	M	cKO	5.583881	3.460954	0.142686	0.08068

Table C.13 continued:

Animal ID	Male or Female	cKO or LC	N.Ob/BS.L (mm^{-1})	N.Ob/BS.R (mm^{-1})	Gp.Th.L (mm)	Gp.Th.R (mm)
H1314	F	LC	2.13716	0.927	0.18175	0.10051
H1411	F	LC	2.60249	1.6907	0.18295	0.11383
H1504	F	LC	2.51905		0.1731	
H1708	F	LC	3.96817	3.51719	0.17581	0.11314
I1710	F	LC	1.82915	0.98188	0.18441	0.0922
I2007	F	LC	3.61003	2.45755	0.17195	0.10997
I2205	F	LC	4.48204	2.67077	0.17652	0.11025
I2209	F	LC				
J2304	F	LC				
J2306	F	LC				
J2413	F	LC				
K2501	F	LC				
K2503	F	LC				
K2606	F	LC				
L1707	F	cKO	2.89942	1.23876	0.22718	0.11614
L1804	F	cKO	2.54611	1.40857	0.1742	0.11754
L1808	F	cKO	2.43955	1.17164	0.1963	0.11643
L1813	F	cKO	2.44367	1.10779	0.19482	0.12271
M2113	F	cKO	4.20884	1.66701	0.203	0.11756
M2216	F	cKO	2.5242	1.0485	0.19229	0.12101
M2303	F	cKO				
M2310	F	cKO				
N2311	F	cKO				
N2404	F	cKO				
N2406	F	cKO				
N2410	F	cKO				

Table C.13 continued:

Animal ID	Male or Female	cKO or LC	N.Ob/BS.L mm^{-1}	N.Ob/BS.R mm^{-1}	Gp.Th (mm)	Gp.Th (mm)
O1412	M	LC	4.413818	1.519655	0.102097	0.023419
O1507	M	LC	2.714064	3.401465	0.054702	0.069983
O1610	M	LC	4.840309	2.636878	0.112848	0.055795
O1701	M	LC	5.009117	3.217296	0.113281	0.063754
P1801	M	LC	5.535407	4.042086	0.122497	0.080494
P1910	M	LC	2.007029	3.585239	0.03893	0.075761
P2003	M	LC	2.433492	1.868339	0.056071	0.036255
P2117	M	LC				
Q2202	M	LC				
Q2309	M	LC				
Q2403	M	LC				
R2412	M	LC				
R2506	M	LC				
R2611	M	LC				
S1306	M	cKO	4.321684	5.231241	0.110984	0.113817
S1307	M	cKO				
S1401	M	cKO				
S1805	M	cKO	3.851248	3.145757	0.079168	0.062854
T1607	M	cKO	3.912146	2.684461	0.070692	0.064413
T1806	M	cKO				
T1811	M	cKO	4.608856	3.363916	0.10483	0.069227
T2101	M	cKO				
U2108	M	cKO				
U2402	M	cKO				
U2505	M	cKO				
V2507	M	cKO				
V2602	M	cKO	3.991309	2.95816	0.094434	0.062854
V2608	M	cKO	5.583881	3.460954	0.142686	0.08068

Table C.14 Indices of dynamic histomorphometry measurements in the left loaded (L) and right control (R) cancellous tibial metaphysis of 12-week-old female and male pOC-ERαKO and LC mice.

Animal ID	Male or Female	cKO or LC	MS.L (mm/mm)	MS.R (mm/mm)	MAR.L (um/day)	MAR.R (um/day)
H1314	F	LC				
H1411	F	LC				
H1504	F	LC				
H1708	F	LC				
I1710	F	LC				
I2007	F	LC				
I2205	F	LC				
I2209	F	LC				
J2304	F	LC	0.36814	0.17952	1.66825	1.34253
J2306	F	LC	0.2711	0.20297	2.31127	1.44191
J2413	F	LC	0.29248	0.19234	1.49875	1.64009
K2501	F	LC	0.34931	0.20789	2.04939	1.43749
K2503	F	LC	0.34405	0.26526	1.73354	1.66952
K2606	F	LC				
L1707	F	cKO				
L1804	F	cKO				
L1808	F	cKO				
L1813	F	cKO				
M2113	F	cKO				
M2216	F	cKO				
M2303	F	cKO	0.28104	0.17665	1.85725	1.06099
M2310	F	cKO		0.28374		1.11657
N2311	F	cKO	0.27266	0.20494	2.03331	1.06495
N2404	F	cKO	0.3012	0.26762	1.79311	1.33764
N2406	F	cKO	0.31534	0.22273	2.47846	1.25661
N2410	F	cKO	0.22565	0.2292	2.39834	1.2479

Table C.14 continued:

Animal ID	Male or Female	cKO or LC	MS.L (mm/mm)	MS.R (mm/mm)	MAR.L (um/day)	MAR.R (um/day)
O1412	M	LC				
O1507	M	LC				
O1610	M	LC				
O1701	M	LC				
P1801	M	LC				
P1910	M	LC				
P2003	M	LC				
P2117	M	LC				
Q2202	M	LC	0.32247	0.29417	1.45196	1.24966
Q2309	M	LC	0.33269	0.31072	1.24601	1.177
Q2403	M	LC	0.34949	0.20056	1.13762	0.91171
R2412	M	LC	0.31561	0.26573	1.14046	1.09377
R2506	M	LC				
R2611	M	LC	0.28149	0.30917	0.97261	1.03749
S1306	M	cKO				
S1307	M	cKO	0.22169	0.22382	1.10307	1.03546
S1401	M	cKO				
S1805	M	cKO				
T1607	M	cKO				
T1806	M	cKO	0.31743	0.30816	1.13217	1.37931
T1811	M	cKO				
T2101	M	cKO				
U2108	M	cKO	0.13779	0.14226	0.40597	0
U2402	M	cKO	0.37353	0.27162	1.1498	0.92006
U2505	M	cKO	0.28728	0.26711	1.28026	1.30245
V2507	M	cKO	0.33851	0.28514	1.54796	1.42769
V2602	M	cKO				
V2608	M	cKO				

Table C.14 continued:

Animal ID	Male or Female	cKO or LC	BFR.L (day^{-1})	BFR.R (day^{-1})
H1314	F	LC		
H1411	F	LC		
H1504	F	LC		
H1708	F	LC		
I1710	F	LC		
I2007	F	LC		
I2205	F	LC		
I2209	F	LC		
J2304	F	LC	0.09684	0.05675
J2306	F	LC	0.07645	0.03718
J2413	F	LC	0.04506	0.03953
K2501	F	LC	0.15581	0.06204
K2503	F	LC	0.07456	0.07931
K2606	F	LC		
L1707	F	cKO		
L1804	F	cKO		
L1808	F	cKO		
L1813	F	cKO		
M2113	F	cKO		
M2216	F	cKO		
M2303	F	cKO	0.08833	0.03194
M2310	F	cKO		0.05321
N2311	F	cKO	0.06534	0.04746
N2404	F	cKO	0.09562	0.08144
N2406	F	cKO	0.09422	0.04214
N2410	F	cKO	0.06884	0.04472

Table C.14 continued:

Animal ID	Male or Female	cKO or LC	BFR.L (day^{-1})	BFR.R (day^{-1})
O1412	M	LC		
O1507	M	LC		
O1610	M	LC		
O1701	M	LC		
P1801	M	LC		
P1910	M	LC		
P2003	M	LC		
P2117	M	LC		
Q2202	M	LC	0.04972	0.04065
Q2309	M	LC	0.0545	0.05559
Q2403	M	LC	0.03057	0.01539
R2412	M	LC	0.04354	0.02996
R2506	M	LC		
R2611	M	LC	0.01959	0.02366
S1306	M	cKO		
S1307	M	cKO	0.0221	0.01955
S1401	M	cKO		
S1805	M	cKO		
T1607	M	cKO		
T1806	M	cKO	0.02657	0.03841
T1811	M	cKO		
T2101	M	cKO		
U2108	M	cKO	0.0042	0
U2402	M	cKO	0.03147	0.02285
U2505	M	cKO	0.03528	0.0272
V2507	M	cKO	0.04265	0.05175
V2602	M	cKO		
V2608	M	cKO		

Table C.15 Indices of dynamic histomorphometry measurements in the left loaded (L) and right control (R) endosteal tibial midshaft of 12-week-old female and male pOC-ERαKO and LC mice.

Animal ID	Male or Female	cKO or LC	MS.L (mm/mm)	MS.R (mm/mm)	MAR.L (um/day)	MAR.R (um/day)
H1314	F	LC				
H1411	F	LC				
H1504	F	LC				
H1708	F	LC				
I1710	F	LC				
I2007	F	LC				
I2205	F	LC				
I2209	F	LC				
J2304	F	LC	0.74158	0.62317	2.06334	0.62317
J2306	F	LC	0.57502	0.56692	1.45973	0.56692
J2413	F	LC	0.66269	0.61338	2.77227	0.61338
K2501	F	LC	0.46109	0.56907	2.53442	0.56907
K2503	F	LC	0.34209	0.56066	1.57995	0.56066
K2606	F	LC				
L1707	F	cKO				
L1804	F	cKO				
L1808	F	cKO				
L1813	F	cKO				
M2113	F	cKO				
M2216	F	cKO				
M2303	F	cKO	0.33789	0.6252	1.80393	0.6252
M2310	F	cKO	0.42726	0.73957	0.99638	0.73957
N2311	F	cKO	0.56091	0.30863	1.40117	0.30863
N2404	F	cKO	0.34655	0.63301	1.61171	0.63301
N2406	F	cKO	0.32133	0.32533	0.98014	0.32533
N2410	F	cKO	0.28444	0.67411	2.03405	0.67411

Table C.15 continued:

Animal ID	Male or Female	cKO or LC	MS.L (mm/mm)	MS.R (mm/mm)	MAR.L (um/day)	MAR.R (um/day)
O1412	M	LC				
O1507	M	LC				
O1610	M	LC				
O1701	M	LC				
P1801	M	LC				
P1910	M	LC				
P2003	M	LC				
P2117	M	LC				
Q2202	M	LC	0.40617	0.53644	1.30601	0.68835
Q2309	M	LC	0.46877	0.5127	1.33834	0.48391
Q2403	M	LC	0.2012	0.34364	0	0.5355
R2412	M	LC	0.45123	0.45681	0	0
R2506	M	LC		0.05235		0
R2611	M	LC	0.03225	0.23777	0	0.92234
S1306	M	cKO				
S1307	M	cKO	0.22764	0.27243	0.85997	0.55954
S1401	M	cKO				
S1805	M	cKO				
T1607	M	cKO				
T1806	M	cKO	0.05634	0.14543	0	0
T1811	M	cKO				
T2101	M	cKO				
U2108	M	cKO	0.09989	0.05609	0	0
U2402	M	cKO	0.12076	0.15321	0	0.50896
U2505	M	cKO	0.16582	0.14199	0	0
V2507	M	cKO	0.1541	0.39863	0	0.85279
V2602	M	cKO				
V2608	M	cKO				

Table C.15 continued:

Animal ID	Male or Female	cKO or LC	BFR.L (day^{-1})	BFR.R (day^{-1})	Wo.Ar.L (mm^2)	Wo.Ar.R (mm^2)
H1314	F	LC				
H1411	F	LC				
H1504	F	LC				
H1708	F	LC				
I1710	F	LC				
I2007	F	LC				
I2205	F	LC				
I2209	F	LC				
J2304	F	LC	0.63796	0.22393	0	0
J2306	F	LC	0.32024	0.14427	0	0
J2413	F	LC	0.83405	0.21079	0	0
K2501	F	LC	0.55813	0.14335	0.02007	0
K2503	F	LC	0.36691	0.19464	0.03255	0
K2606	F	LC				
L1707	F	cKO				
L1804	F	cKO				
L1808	F	cKO				
L1813	F	cKO				
M2113	F	cKO				
M2216	F	cKO				
M2303	F	cKO	0.35209	0.21735	0.04524	0
M2310	F	cKO	0.18316	0.26836	0.01437	0
N2311	F	cKO	0.32695	0.08164	0.01119	0
N2404	F	cKO	0.20391	0.25185	0.0108	0
N2406	F	cKO	0.21358	0	0.02212	0
N2410	F	cKO	0.43818	0.17609	0.03057	0

Table C.15 continued:

Animal ID	Male or Female	cKO or LC	BFR.L (day^{-1})	BFR.R (day^{-1})	Wo.Ar.L (mm^2)	Wo.Ar.R (mm^2)
O1412	M	LC				
O1507	M	LC				
O1610	M	LC				
O1701	M	LC				
P1801	M	LC				
P1910	M	LC				
P2003	M	LC				
P2117	M	LC				
Q2202	M	LC	0.19287	0.1275	0	0
Q2309	M	LC	0.25025	0.08698	0	0
Q2403	M	LC	0	0.05483	0	0
R2412	M	LC	0	0	0	0
R2506	M	LC		0		0
R2611	M	LC	0	0.06133	0	0
S1306	M	cKO				
S1307	M	cKO	0.0464	0.04971	0	0
S1401	M	cKO				
S1805	M	cKO				
T1607	M	cKO				
T1806	M	cKO	0	0	0	0
T1811	M	cKO				
T2101	M	cKO				
U2108	M	cKO	0	0	0	0
U2402	M	cKO	0	0.0242	0	0
U2505	M	cKO	0	0	0	0
V2507	M	cKO	0	0.10072	0	0
V2602	M	cKO				
V2608	M	cKO				

Table C.16 Indices of dynamic histomorphometry measurements in the left loaded (L) and right control (R) periosteal tibial midshaft of 12-week-old female and male pOC-ERαKO and LC mice.

Animal ID	Male or Female	cKO or LC	MS.L (mm/mm)	MS.R (mm/mm)	MAR.L (um/day)	MAR.R (um/day)
H1314	F	LC				
H1411	F	LC				
H1504	F	LC				
H1708	F	LC				
I1710	F	LC				
I2007	F	LC				
I2205	F	LC				
I2209	F	LC				
J2304	F	LC	0.32211	0.04132	2.37324	0
J2306	F	LC	0.10212	0.15179	2.61944	0
J2413	F	LC	0.20765	0.12335	2.3402	0
K2501	F	LC	0.25128	0.16569	2.11839	0
K2503	F	LC	0.24823	0.04073	2.22811	0
K2606	F	LC				
L1707	F	cKO				
L1804	F	cKO				
L1808	F	cKO				
L1813	F	cKO				
M2113	F	cKO				
M2216	F	cKO				
M2303	F	cKO	0.09287	0.06929	0	0
M2310	F	cKO	0.31946	0.03921	1.91439	0
N2311	F	cKO	0.38956	0.07851	1.5714	0
N2404	F	cKO	0.32679	0.11145	2.7089	0
N2406	F	cKO	0.22034	0.12717	2.11904	0
N2410	F	cKO	0.21226	0.07056	1.88384	0

Table C.16 continued:

Animal ID	Male or Female	cKO or LC	MS.L (mm/mm)	MS.R (mm/mm)	MAR.L (um/day)	MAR.R (um/day)
O1412	M	LC				
O1507	M	LC				
O1610	M	LC				
O1701	M	LC				
P1801	M	LC				
P1910	M	LC				
P2003	M	LC				
P2117	M	LC				
Q2202	M	LC	0.55087	0.08429	1.43845	0
Q2309	M	LC	0.51949	0.13136	1.91359	0
Q2403	M	LC	0.22665	0.0662	0	0
R2412	M	LC	0.69662	0.14282	1.7518	0
R2506	M	LC		0.04827		0
R2611	M	LC	0.16264	0.0304	0	0
S1306	M	cKO				
S1307	M	cKO	0.54829	0.1373	1.17717	0
S1401	M	cKO				
S1805	M	cKO				
T1607	M	cKO				
T1806	M	cKO	0.46807	0.54246	0.79333	0.88301
T1811	M	cKO				
T2101	M	cKO				
U2108	M	cKO	0.1884	0.1065	0	0
U2402	M	cKO	0.29555	0.14247	0.4237	0
U2505	M	cKO	0.57935	0.19892	1.10236	0
V2507	M	cKO	0.39777	0.13925	1.15115	0
V2602	M	cKO				
V2608	M	cKO				

Table C.16 continued:

Animal ID	Male or Female	cKO or LC	BFR.L (day^{-1})	BFR.R (day^{-1})	Wo.Ar.L (mm^2)	Wo.Ar.R (mm^2)
H1314	F	LC				
H1411	F	LC				
H1504	F	LC				
H1708	F	LC				
I1710	F	LC				
I2007	F	LC				
I2205	F	LC				
I2209	F	LC				
J2304	F	LC	0.34195	0	0.11831	0
J2306	F	LC	0.19643	0	0.15287	0
J2413	F	LC	0.27022	0	0.1087	0
K2501	F	LC	0.24548	0	0.17849	0
K2503	F	LC	0.26639	0	0.1423	0
K2606	F	LC				
L1707	F	cKO				
L1804	F	cKO				
L1808	F	cKO				
L1813	F	cKO				
M2113	F	cKO				
M2216	F	cKO				
M2303	F	cKO	0	0	0.25725	0
M2310	F	cKO	0.28681	0	0.16585	0
N2311	F	cKO	0.20206	0	0.13243	0
N2404	F	cKO	0.27638	0	0.11363	0
N2406	F	cKO	0.27855	0	0.16307	0
N2410	F	cKO	0.22883	0	0.162	0

Table C.16 continued:

Animal ID	Male or Female	cKO or LC	BFR.L (day^{-1})	BFR.R (day^{-1})	Wo.Ar.L (mm^2)	Wo.Ar.R (mm^2)
O1412	M	LC				
O1507	M	LC				
O1610	M	LC				
O1701	M	LC				
P1801	M	LC				
P1910	M	LC				
P2003	M	LC				
P2117	M	LC				
Q2202	M	LC	0.1828	0	0	0
Q2309	M	LC	0.30253	0	0.02625	0
Q2403	M	LC	0	0	0	0
R2412	M	LC	0.27055	0	0	0
R2506	M	LC		0		0
R2611	M	LC	0	0	0	0
S1306	M	cKO				
S1307	M	cKO	0.09763	0	0	0
S1401	M	cKO				
S1805	M	cKO				
T1607	M	cKO				
T1806	M	cKO	0.07874	0.09804	0	0
T1811	M	cKO				
T2101	M	cKO				
U2108	M	cKO	0	0	0	0
U2402	M	cKO	0.0276	0	0	0
U2505	M	cKO	0.13621	0	0	0
V2507	M	cKO	0.10311	0	0	0
V2602	M	cKO				
V2608	M	cKO				

Table C.17 Indices of bone stiffness from strain gauge data in left and right tibia of male and female pOC-ERαKO (KO) and LC mice

Animal ID	L bone stiffness (N/ε)	R bone stiffness (N/ε)	L and R average
KOF1	N/A	-0.00781	-0.00781
KOF2	-0.00832	-0.00552	-0.00692
KOF3	-0.00683	-0.00777	-0.0073
KOF4	-0.00763	-0.00934	-0.00849
LCF1	-0.00777	-0.0064	-0.00708
LCF2	-0.00775	-0.00535	-0.00655
LCF3	-0.00571	-0.00538	-0.00555
LCF4	-0.01179	-0.00509	-0.00844
LCF5	-0.00709	-0.00662	-0.00686
LCF6	-0.006	-0.0056	-0.0058
KOM1	-0.00555	-0.01237	-0.00896
KOM2	-0.00668	-0.00635	-0.00651
KOM3	-0.00796	-0.01031	-0.00914
KOM4	-0.00536	-0.00555	-0.00545
KOM5	-0.00908	-0.00746	-0.00827
LCM1	-0.00552	-0.00566	-0.00559
LCM2	-0.01629	-0.00945	-0.01287
LCM3	-0.00575	-0.00668	-0.00621
LCM4	-0.00539	-0.00408	-0.00474
LCM5	-0.00935	-0.00785	-0.0086
LCM6	-0.00727	-0.00791	-0.00759

APPENDIX D. **CHAPTER 4 DATA**

Table D.1 Indices of cancellous bone from microCT analysis of tibial metaphysis in 12-week-old female pOC-ERαKO and LC mice treated with RAP-661 or placebo

Animal ID	cKO or LC	Drug or placebo	BV/TV.R (BV/TV)	Tb.Th.R (mm)	Tb.Sp.R (mm)	cn.TMD.R (mg HA/cc)
A4204	LC	placebo	0.0636	0.0482	0.3855	678.341
A4406	LC	placebo	0.1173	0.0537	0.3159	685.308
A4415	LC	placebo	0.0831	0.05	0.3661	647.805
A4502	LC	placebo	0.0586	0.0486	0.4159	686.024
A4508	LC	placebo	0.0688	0.0502	0.4413	692.991
B4807	LC	placebo	0.0749	0.0516	0.3747	706.729
B5012	LC	placebo	0.0953	0.0512	0.2814	695.4
B5108	LC	placebo	0.0883	0.0496	0.3605	677.169
B5110	LC	placebo	0.1023	0.0498	0.2896	695.075
B5302	LC	placebo	0.1122	0.049	0.2766	676.323
C5203	LC	drug	0.103	0.0581	0.3187	718.514
C5605	LC	drug	0.1158	0.0588	0.3006	712.068
C5702	LC	drug	0.1429	0.0617	0.3006	717.537
C5915	LC	drug	0.1369	0.0579	0.263	712.068
C6010	LC	drug	0.1416	0.0632	0.2817	715.259
D6105	LC	drug	0.1308	0.0581	0.2962	697.288
D6312	LC	drug	0.1682	0.06	0.2279	702.562
D6407	LC	drug	0.1935	0.0625	0.2456	702.041
D6509	LC	drug	0.1138	0.0576	0.2841	726.848
D6603	LC	drug	0.1323	0.0605	0.2897	728.736
E4112	cKO	placebo	0.0985	0.0503	0.327	692.47
E4209	cKO	placebo	0.0582	0.0453	0.3989	678.797
E4213	cKO	placebo	0.0715	0.0491	0.3922	682.378
E4301	cKO	placebo	0.0644	0.0513	0.4883	712.003
E4307	cKO	placebo	0.0734	0.0482	0.4262	680.034
F4409	cKO	placebo	0.0941	0.0533	0.303	698.525
F4512	cKO	placebo	0.0555	0.0494	0.4531	693.512
F4901	cKO	placebo	0.0724	0.0495	0.3199	702.497
F4904	cKO	placebo	0.0762	0.0515	0.3518	703.409
F5008	cKO	placebo	0.0772	0.051	0.3932	698.525

Table D.1 continued

Animal ID	cKO or LC	Drug or placebo	BV/TV.R (BV/TV)	Tb.Th.R (mm)	Tb.Sp.R (mm)	cn.TMD.R (mg HA/cc)
G5013	cKO	drug	0.1015	0.0591	0.3687	709.529
G5502	cKO	drug	0.1436	0.0597	0.2861	686.35
G5504	cKO	drug	0.1318	0.0574	0.2982	694.033
G5601	cKO	drug	0.1146	0.0609	0.3818	708.227
G5709	cKO	drug	0.1335	0.06	0.2945	720.663
H5812	cKO	drug	0.1051	0.0561	0.3555	703.213
H6007	cKO	drug	0.1534	0.0554	0.2756	672.937
H6415	cKO	drug	0.109	0.0586	0.4072	713.175
H6503	cKO	drug	0.114	0.0592	0.354	705.297
H6608	cKO	drug	0.1406	0.0613	0.3882	705.622

Table D.1 continued

Animal ID	cKO or LC	Drug or placebo	BV/TV.L (BV/TV)	Tb.Th.L (mm)	Tb.Sp.L (mm)	cn.TMD.L (mg HA/cc)
A4204	LC	placebo	0.0824	0.0591	0.3415	711.157
A4406	LC	placebo	0.12	0.0599	0.26	708.943
A4415	LC	placebo	0.1021	0.0622	0.3187	704.906
A4502	LC	placebo	0.079	0.0578	0.4043	698.851
A4508	LC	placebo	0.0591	0.0601	0.4468	715.389
B4807	LC	placebo	0.0884	0.0616	0.3497	724.114
B5012	LC	placebo	0.0949	0.0579	0.2912	709.399
B5108	LC	placebo	0.094	0.0572	0.3475	677.234
B5110	LC	placebo				
B5302	LC	placebo	0.1072	0.0559	0.2923	684.657
C5203	LC	drug	0.0892	0.0632	0.3818	730.95
C5605	LC	drug	0.1175	0.0591	0.2925	725.806
C5702	LC	drug	0.1191	0.0592	0.2782	716.821
C5915	LC	drug	0.1456	0.0624	0.2494	729.778
C6010	LC	drug	0.1282	0.0635	0.2795	725.611
D6105	LC	drug	0.1336	0.0629	0.2769	714.608
D6312	LC	drug	0.1717	0.0627	0.2405	715.128
D6407	LC	drug	0.1602	0.0623	0.2681	710.44
D6509	LC	drug	0.1069	0.062	0.2903	729.843
D6603	LC	drug	0.1259	0.0613	0.3399	718.449

Table D.1 continued

Animal ID	cKO or LC	Drug or placebo	BV/TV.L (BV/TV)	Tb.Th.L (mm)	Tb.Sp.L (mm)	cn.TMD.L (mg HA/cc)
E4112	cKO	placebo	0.1177	0.0616	0.3367	709.985
E4209	cKO	placebo	0.0828	0.0674	0.3883	733.424
E4213	cKO	placebo	0.0788	0.0652	0.4391	714.152
E4301	cKO	placebo	0.082	0.0679	0.5091	750.418
E4307	cKO	placebo	0.1001	0.0666	0.4396	728.346
F4409	cKO	placebo	0.0945	0.0647	0.326	717.993
F4512	cKO	placebo	0.0737	0.0664	0.45	712.719
F4901	cKO	placebo	0.0815	0.0581	0.3475	715.91
F4904	cKO	placebo	0.0974	0.0632	0.3273	727.89
F5008	cKO	placebo	0.0862	0.0609	0.3563	718.123
G5013	cKO	drug	0.1315	0.0693	0.3053	721.77
G5502	cKO	drug				
G5504	cKO	drug	0.1163	0.0647	0.324	727.499
G5601	cKO	drug	0.1119	0.0674	0.3442	712.133
G5709	cKO	drug	0.1391	0.0634	0.2829	720.533
H5812	cKO	drug	0.1234	0.0609	0.3488	705.036
H6007	cKO	drug	0.1525	0.0605	0.2674	700.739
H6415	cKO	drug	0.1054	0.059	0.3168	720.402
H6503	cKO	drug	0.1206	0.063	0.3248	714.998
H6608	cKO	drug	0.1349	0.0681	0.4008	723.723

Table D.2 Indices of cortical bone from microCT analysis of tibial metaphysis in 12-week-old female pOC-ERαKO and LC mice treated with RAP-661 or placebo

Animal ID	cKO or LC	Drug or placebo	M.Imax.R (mm^4)	M.Imin.R (mm^4)	M.Ct.Ar.R (mm^2)	M. Ct.Th.R (mm)	ct.TMD (mgHA/ cc)
A4204	LC	placebo	0.36455	0.28647	0.93021	0.136	768.715
A4406	LC	placebo	0.51052	0.32993	1.1096	0.146	799.121
A4415	LC	placebo	0.33987	0.28156	0.93631	0.136	781.671
A4502	LC	placebo	0.38646	0.32148	0.9605	0.135	779.458
A4508	LC	placebo	0.40699	0.33749	0.99686	0.137	787.596
B4807	LC	placebo	0.31619	0.25253	0.86214	0.127	773.272
B5012	LC	placebo	0.32786	0.28524	0.93958	0.14	775.551
B5108	LC	placebo	0.38996	0.33555	1.01485	0.144	798.275
B5110	LC	placebo	0.3393	0.27045	0.93999	0.14	782.908
B5302	LC	placebo	0.3337	0.27023	0.87545	0.121	753.348

Table D.2 continued

Animal ID	cKO or LC	Drug or placebo	M.Imax.R (mm^4)	M.Imin.R (mm^4)	M.Ct.Ar.R (mm^2)	M. Ct.Th.R (mm)	ct.TMD (mgHA/ cc)
C5203	LC	drug	0.3734	0.32412	1.02452	0.148	801.27
C5605	LC	drug	0.28518	0.24921	0.91506	0.145	783.299
C5702	LC	drug	0.37148	0.28679	1.01891	0.149	796.061
C5915	LC	drug	0.40015	0.34707	1.0355	0.139	775.551
C6010	LC	drug	0.36772	0.29337	1.01803	0.152	776.398
D6105	LC	drug	0.39867	0.32377	1.05918	0.153	796.061
D6312	LC	drug	0.33193	0.28562	0.89438	0.122	738.113
D6407	LC	drug	0.29725	0.24449	0.86791	0.122	743.842
D6509	LC	drug	0.41171	0.35293	1.04615	0.141	792.349
D6603	LC	drug	0.35387	0.28852	1.01712	0.152	786.75
E4112	cKO	placebo	0.35417	0.27332	0.98737	0.149	791.829
E4209	cKO	placebo	0.34564	0.29201	0.88313	0.122	762.92
E4213	cKO	placebo	0.34111	0.30208	0.91589	0.127	777.374
E4301	cKO	placebo	0.35274	0.28332	0.90036	0.125	785.383
E4307	cKO	placebo	0.28535	0.23974	0.82319	0.123	780.955
F4409	cKO	placebo	0.42642	0.35802	1.05352	0.141	785.057
F4512	cKO	placebo	0.32827	0.27554	0.87006	0.123	769.105
F4901	cKO	placebo	0.38276	0.31834	0.99413	0.137	800.098
F4904	cKO	placebo	0.40518	0.35106	0.98897	0.129	777.049
F5008	cKO	placebo	0.35486	0.29783	0.91694	0.125	775.551
G5013	cKO	drug	0.32409	0.25647	0.92812	0.142	781.151
G5502	cKO	drug	0.27578	0.2219	0.87525	0.135	776.072
G5504	cKO	drug	0.35365	0.29013	0.96814	0.134	772.296
G5601	cKO	drug	0.30134	0.2554	0.83306	0.126	766.826
G5709	cKO	drug	0.37269	0.30276	0.94001	0.125	757.385
H5812	cKO	drug	0.29584	0.24979	0.86608	0.129	754.846
H6007	cKO	drug	0.3392	0.24225	0.82357	0.109	720.924
H6415	cKO	drug	0.3339	0.2877	0.95501	0.14	772.491
H6503	cKO	drug	0.33168	0.28321	0.89979	0.124	764.157
H6608	cKO	drug	0.31732	0.24231	0.88369	0.128	762.269

Table D.2 continued

Animal ID	cKO or LC	Drug or placebo	M.Imax.L (mm^4)	M.Imin.L (mm^4)	M.Ct.Ar.L (mm^2)	M. Ct.Th.L (mm)	ct.TMD (mgHA/ cc)
A4204	LC	placebo	0.47391	0.36975	1.10116	0.149	782.453
A4406	LC	placebo	0.53998	0.43276	1.22484	0.159	783.95
A4415	LC	placebo	0.47644	0.35069	1.10555	0.15	777.7
A4502	LC	placebo	0.47999	0.39456	1.09159	0.145	779.002
A4508	LC	placebo	0.47459	0.36561	1.07318	0.149	784.927
B4807	LC	placebo	0.41395	0.33223	1.05043	0.146	768.649
B5012	LC	placebo	0.43331	0.35126	1.05334	0.143	763.05
B5108	LC	placebo	0.48232	0.38999	1.13433	0.153	783.494
B5110	LC	placebo	0.49607	0.40923	1.19092	0.162	779.653
B5302	LC	placebo	0.44539	0.34792	1.06947	0.144	770.407
C5203	LC	drug	0.47335	0.36961	1.1425	0.158	808.953
C5605	LC	drug	0.40741	0.33825	1.11173	0.158	798.795
C5702	LC	drug	0.43466	0.32952	1.08938	0.152	797.754
C5915	LC	drug	0.46359	0.37418	1.13685	0.149	786.88
C6010	LC	drug	0.42511	0.32757	1.09346	0.158	794.889
D6105	LC	drug	0.4682	0.38122	1.19795	0.17	808.887
D6312	LC	drug	0.4313	0.32456	1.03197	0.136	760.185
D6407	LC	drug	0.35202	0.26837	0.92438	0.129	754.065
D6509	LC	drug	0.45204	0.37347	1.13378	0.162	801.53
D6603	LC	drug	0.4283	0.33914	1.13407	0.161	798.34
E4112	cKO	placebo	0.48679	0.38883	1.20284	0.166	776.267
E4209	cKO	placebo	0.49835	0.37871	1.08608	0.14	762.659
E4213	cKO	placebo	0.44116	0.35947	1.05158	0.142	765.264
E4301	cKO	placebo	0.53848	0.41742	1.20528	0.159	787.01
E4307	cKO	placebo	0.43562	0.33056	1.10991	0.156	781.151
F4409	cKO	placebo	0.53759	0.42574	1.20796	0.155	772.361
F4512	cKO	placebo	0.44052	0.3536	1.07708	0.146	773.142
F4901	cKO	placebo	0.45565	0.34876	1.10683	0.154	795.084
F4904	cKO	placebo	0.49849	0.38928	1.13045	0.146	775.616
F5008	cKO	placebo	0.45796	0.37703	1.09225	0.143	768.129

Table D.2 continued

Animal ID	cKO or LC	Drug or placebo	M.Imax.L (mm^4)	M.Imin.L (mm^4)	M.Ct.Ar.L (mm^2)	M. Ct.Th.L (mm)	ct.TMD (mgHA/ cc)
A4204	LC	placebo	0.42883	0.31373	1.11308	0.16	792.545
A4406	LC	placebo					
A4415	LC	placebo	0.41868	0.32468	1.06545	0.148	779.197
A4502	LC	placebo	0.4032	0.31097	1.0042	0.14	784.146
A4508	LC	placebo	0.39956	0.31825	1.01348	0.137	764.938
B4807	LC	placebo	0.40767	0.32325	1.05129	0.141	764.092
B5012	LC	placebo	0.41864	0.30497	0.95962	0.122	748.596
B5108	LC	placebo	0.36895	0.30845	0.98244	0.139	777.635
B5110	LC	placebo	0.39292	0.30282	0.97616	0.132	769.821
B5302	LC	placebo	0.33203	0.25637	0.9282	0.134	774.249

Table D.2 continued

Animal ID	cKO or LC	Drug or placebo	M.Imax.L (mm^4)	M.Imin.L (mm^4)	M.Ct.Ar.L (mm^2)	M. Ct.Th.L (mm)	ct.TMD (mgHA/ cc)
C5203	LC	drug	0.47335	0.36961	1.1425	0.158	808.953
C5605	LC	drug	0.40741	0.33825	1.11173	0.158	798.795
C5702	LC	drug	0.43466	0.32952	1.08938	0.152	797.754
C5915	LC	drug	0.46359	0.37418	1.13685	0.149	786.88
C6010	LC	drug	0.42511	0.32757	1.09346	0.158	794.889
D6105	LC	drug	0.4682	0.38122	1.19795	0.17	808.887
D6312	LC	drug	0.4313	0.32456	1.03197	0.136	760.185
D6407	LC	drug	0.35202	0.26837	0.92438	0.129	754.065
D6509	LC	drug	0.45204	0.37347	1.13378	0.162	801.53
D6603	LC	drug	0.4283	0.33914	1.13407	0.161	798.34
E4112	cKO	placebo	0.48679	0.38883	1.20284	0.166	776.267
E4209	cKO	placebo	0.49835	0.37871	1.08608	0.14	762.659
E4213	cKO	placebo	0.44116	0.35947	1.05158	0.142	765.264
E4301	cKO	placebo	0.53848	0.41742	1.20528	0.159	787.01
E4307	cKO	placebo	0.43562	0.33056	1.10991	0.156	781.151
F4409	cKO	placebo	0.53759	0.42574	1.20796	0.155	772.361
F4512	cKO	placebo	0.44052	0.3536	1.07708	0.146	773.142
F4901	cKO	placebo	0.45565	0.34876	1.10683	0.154	795.084
F4904	cKO	placebo	0.49849	0.38928	1.13045	0.146	775.616
F5008	cKO	placebo	0.45796	0.37703	1.09225	0.143	768.129

Table D.2 continued

Animal ID	cKO or LC	Drug or placebo	M.Imax.L (mm^4)	M.Imin.L (mm^4)	M.Ct.Ar.L (mm^2)	M. Ct.Th.L (mm)	ct.TMD (mgHA/ cc)
G5013	cKO	drug	0.42883	0.31373	1.11308	0.16	792.545
G5502	cKO	drug					
G5504	cKO	drug	0.41868	0.32468	1.06545	0.148	779.197
G5601	cKO	drug	0.4032	0.31097	1.0042	0.14	784.146
G5709	cKO	drug	0.39956	0.31825	1.01348	0.137	764.938
H5812	cKO	drug	0.40767	0.32325	1.05129	0.141	764.092
H6007	cKO	drug	0.41864	0.30497	0.95962	0.122	748.596
H6415	cKO	drug	0.36895	0.30845	0.98244	0.139	777.635
H6503	cKO	drug	0.39292	0.30282	0.97616	0.132	769.821
H6608	cKO	drug	0.33203	0.25637	0.9282	0.134	774.249

Table D.3 Indices of tibial midshaft bone from microCT of 12-week-old female pOC-ERαKO and LC mice, treated with RAP-661 or placebo

Animal ID	cKO or LC	Drug or placebo	Imax.R (mm^4)	Imin.R (mm^4)	Ct.Ar.R (mm^2)	T.Ar.R (mm^2)
A4204	LC	placebo	0.06597	0.05287	0.5598	0.93653
A4406	LC	placebo	0.08064	0.05961	0.61561	1.01202
A4415	LC	placebo	0.06018	0.05132	0.54348	0.90561
A4502	LC	placebo	0.06332	0.05307	0.56604	0.91549
A4508	LC	placebo	0.06922	0.05061	0.56796	0.92863
B4807	LC	placebo	0.0603	0.04459	0.52375	0.87795
B5012	LC	placebo	0.0525	0.04144	0.5214	0.81663
B5108	LC	placebo	0.06959	0.05689	0.59279	0.95739
B5110	LC	placebo	0.05473	0.04536	0.5382	0.84735
B5302	LC	placebo	0.05914	0.04717	0.52403	0.88237
C5203	LC	drug	0.08171	0.05812	0.63319	0.98843
C5605	LC	drug	0.04629	0.03841	0.53012	0.76143
C5702	LC	drug	0.06323	0.05345	0.58465	0.90436
C5915	LC	drug	0.06374	0.04744	0.57164	0.87747
C6010	LC	drug	0.06824	0.05414	0.58403	0.93496
D6105	LC	drug	0.06914	0.06256	0.60533	0.97397
D6312	LC	drug	0.05471	0.04316	0.50589	0.84936
D6407	LC	drug	0.04381	0.03759	0.48748	0.76266
D6509	LC	drug	0.07052	0.05959	0.60615	0.96119
D6603	LC	drug	0.05915	0.05168	0.56714	0.88975

Table D.3 continued

Animal ID	cKO or LC	Drug or placebo	Imax.R (mm^4)	Imin.R (mm^4)	Ct.Ar.R (mm^2)	T.Ar.R (mm^2)
E4112	cKO	placebo	0.0568	0.04933	0.54946	0.86897
E4209	cKO	placebo	0.07234	0.05136	0.57582	0.9395
E4213	cKO	placebo	0.06305	0.05	0.5362	0.90681
E4301	cKO	placebo	0.05601	0.04403	0.51335	0.85819
E4307	cKO	placebo	0.05848	0.04798	0.52835	0.88068
F4409	cKO	placebo	0.07336	0.05791	0.59666	0.97346
F4512	cKO	placebo	0.05088	0.04461	0.50159	0.84212
F4901	cKO	placebo	0.0577	0.04998	0.56586	0.87252
F4904	cKO	placebo	0.0605	0.05046	0.56255	0.88884
F5008	cKO	placebo	0.0519	0.04411	0.51642	0.83396
G5013	cKO	drug	0.0589	0.04365	0.54457	0.84549
G5502	cKO	drug	0.05275	0.04116	0.52536	0.81472
G5504	cKO	drug	0.06291	0.05176	0.56444	0.90731
G5601	cKO	drug	0.06233	0.04788	0.56717	0.88219
G5709	cKO	drug				
H5812	cKO	drug	0.06023	0.04611	0.5313	0.88076
H6007	cKO	drug	0.05194	0.04257	0.50655	0.82956
H6415	cKO	drug	0.06408	0.04984	0.56378	0.90497
H6503	cKO	drug	0.06181	0.04715	0.53453	0.89764
H6608	cKO	drug				

Table D.3 continued

Animal ID	cKO or LC	Drug or placebo	Imax.L (mm^4)	Imin.L (mm^4)	Ct.Ar.L (mm^2)	T.Ar.L (mm^2)
A4204	LC	placebo	0.0772	0.06084	0.61844	0.98824
A4406	LC	placebo	0.08802	0.06688	0.63771	1.057
A4415	LC	placebo	0.07321	0.0571	0.60768	0.95901
A4502	LC	placebo	0.07975	0.06024	0.6091	1.00517
A4508	LC	placebo	0.07178	0.05306	0.55608	0.96684
B4807	LC	placebo	0.06587	0.04551	0.56264	0.87962
B5012	LC	placebo	0.06066	0.04704	0.56963	0.86492
B5108	LC	placebo	0.07393	0.05834	0.6168	0.96559
B5110	LC	placebo	0.06638	0.05052	0.588	0.90364
B5302	LC	placebo	0.06443	0.05443	0.57827	0.92029

Table D.3 continued

Animal ID	cKO or LC	Drug or placebo	Imax.L (mm^4)	Imin.L (mm^4)	Ct.Ar.L (mm^2)	T.Ar.L (mm^2)
C5203	LC	drug	0.08031	0.0623	0.63888	1.00448
C5605	LC	drug	0.06629	0.04855	0.60309	0.88167
C5702	LC	drug	0.06918	0.05268	0.6179	0.91434
C5915	LC	drug	0.07482	0.05753	0.60391	0.96166
C6010	LC	drug	0.07899	0.06023	0.64066	0.98643
D6105	LC	drug				
D6312	LC	drug	0.07181	0.05336	0.59156	0.9381
D6407	LC	drug	0.0519	0.04659	0.53871	0.83561
D6509	LC	drug	0.07809	0.05925	0.62574	0.97938
D6603	LC	drug	0.06952	0.05586	0.60314	0.93635
E4112	cKO	placebo	0.06532	0.05109	0.60069	0.89737
E4209	cKO	placebo	0.06974	0.05011	0.59063	0.9152
E4213	cKO	placebo	0.06787	0.05102	0.57164	0.92248
E4301	cKO	placebo	0.07402	0.06006	0.62829	0.97216
E4307	cKO	placebo	0.07912	0.0564	0.62985	0.9719
F4409	cKO	placebo	0.0784	0.06365	0.63003	1.00175
F4512	cKO	placebo	0.06729	0.05193	0.56934	0.91925
F4901	cKO	placebo	0.0621	0.05095	0.60185	0.88638
F4904	cKO	placebo	0.07149	0.05505	0.60285	0.95004
F5008	cKO	placebo	0.06544	0.04921	0.58625	0.8943
G5013	cKO	drug	0.07767	0.0589	0.65326	0.96616
G5502	cKO	drug	0.05948	0.04492	0.5486	0.86027
G5504	cKO	drug	0.07034	0.05364	0.60692	0.93335
G5601	cKO	drug	0.06721	0.05107	0.58704	0.90998
G5709	cKO	drug	0.08031	0.0623	0.63888	1.00448
H5812	cKO	drug	0.06629	0.04855	0.60309	0.88167
H6007	cKO	drug	0.06918	0.05268	0.6179	0.91434
H6415	cKO	drug	0.07482	0.05753	0.60391	0.96166
H6503	cKO	drug	0.07899	0.06023	0.64066	0.98643
H6608	cKO	drug				

Table D.3 continued

Animal ID	cKO or LC	Drug or placebo	Ct.Th.R (mm)	ct.TMD.R (mgHA/cc)	Ma.Ar.R (mm^2)
A4204	LC	placebo	0.197	949.46	0.37673
A4406	LC	placebo	0.208	962.222	0.39641
A4415	LC	placebo	0.194	948.484	0.36213
A4502	LC	placebo	0.202	958.445	0.34945
A4508	LC	placebo	0.199	959.617	0.36067
B4807	LC	placebo	0.19	951.804	0.3542
B5012	LC	placebo	0.2	957.404	0.29523
B5108	LC	placebo	0.206	962.287	0.3646
B5110	LC	placebo	0.203	964.566	0.30915
B5302	LC	placebo	0.188	937.48	0.35834
C5203	LC	drug	0.218	968.993	0.35524
C5605	LC	drug	0.218	970.686	0.23131
C5702	LC	drug	0.212	972.704	0.31971
C5915	LC	drug	0.212	960.789	0.30583
C6010	LC	drug	0.207	961.896	0.35093
D6105	LC	drug	0.21	961.571	0.36864
D6312	LC	drug	0.186	927.779	0.34347
D6407	LC	drug	0.195	940.996	0.27518
D6509	LC	drug	0.214	958.185	0.35504
D6603	LC	drug			0.32261
E4112	cKO	placebo	0.203	962.222	0.31951
E4209	cKO	placebo	0.202	958.185	0.36368
E4213	cKO	placebo	0.188	939.498	0.37061
E4301	cKO	placebo	0.189	945.489	0.34484
E4307	cKO	placebo	0.19	951.739	0.35233
F4409	cKO	placebo	0.206	955.06	0.3768
F4512	cKO	placebo	0.187	945.619	0.34053
F4901	cKO	placebo	0.212	970.165	0.30666
F4904	cKO	placebo	0.207	963.459	0.32629
F5008	cKO	placebo	0.195	948.093	0.31754

Table D.3 continued

Animal ID	cKO or LC	Drug or placebo	Ct.Th.R (mm)	ct.TMD.R (mgHA/cc)	Ma.Ar.R (mm^2)
G5013	cKO	drug	0.205	954.083	0.30092
G5502	cKO	drug	0.203	964.045	0.28936
G5504	cKO	drug	0.204	959.357	0.34287
G5601	cKO	drug	0.211	961.636	0.31502
G5709	cKO	drug			
H5812	cKO	drug	0.19	941.061	0.34946
H6007	cKO	drug	0.19	938.587	0.32301
H6415	cKO	drug	0.206	951.218	0.34119
H6503	cKO	drug	0.192	931.294	0.36311
H6608	cKO	drug			

Table D.3 continued

Animal ID	cKO or LC	Drug or placebo	Ct.Th.L (mm)	ct.TMD.L (mgHA/cc)	Ma.Ar.L (mm^2)
A4204	LC	placebo	0.212	955.906	0.3698
A4406	LC	placebo	0.209	945.163	0.41929
A4415	LC	placebo	0.213	955.581	0.35133
A4502	LC	placebo	0.207	951.023	0.39607
A4508	LC	placebo	0.19	948.874	0.41076
B4807	LC	placebo	0.208	953.367	0.31698
B5012	LC	placebo	0.214	961.115	0.29529
B5108	LC	placebo	0.219	968.147	0.34879
B5110	LC	placebo	0.215	961.636	0.31564
B5302	LC	placebo	0.207	947.832	0.34202
C5203	LC	drug	0.22	967.691	0.3656
C5605	LC	drug	0.226	970.947	0.27858
C5702	LC	drug	0.228	976.22	0.29644
C5915	LC	drug	0.21	941.386	0.35775
C6010	LC	drug	0.227	963.849	0.34577
D6105	LC	drug			
D6312	LC	drug	0.208	942.038	0.34654
D6407	LC	drug	0.205	936.568	0.2969
D6509	LC	drug	0.22	956.101	0.35364
D6603	LC	drug	0.217	959.031	0.33321

Table D.3 continued

Animal ID	cKO or LC	Drug or placebo	Ct.Th.L (mm)	ct.TMD.L (mgHA/cc)	Ma.Ar.L (mm^2)
E4112	cKO	placebo	0.228	977.653	0.29668
E4209	cKO	placebo	0.216	970.1	0.32457
E4213	cKO	placebo	0.206	953.302	0.35084
E4301	cKO	placebo	0.222	949.721	0.34387
E4307	cKO	placebo	0.222	952.325	0.34205
F4409	cKO	placebo	0.218	953.627	0.37172
F4512	cKO	placebo	0.201	947.181	0.34991
F4901	cKO	placebo	0.23	975.765	0.28453
F4904	cKO	placebo	0.216	966.584	0.34719
F5008	cKO	placebo	0.218	960.789	0.30805
G5013	cKO	drug	0.236	958.836	0.3129
G5502	cKO	drug	0.209	951.153	0.31167
G5504	cKO	drug	0.22	971.532	0.32643
G5601	cKO	drug	0.213	954.799	0.32294
G5709	cKO	drug			
H5812	cKO	drug	0.217	954.669	0.32747
H6007	cKO	drug	0.206	939.563	0.3939
H6415	cKO	drug	0.207	955.711	0.35564
H6503	cKO	drug			
H6608	cKO	drug			

Table D.4 IHC and histology indices for the cancellous tibial metaphysis of 12-week-old female pOC-ERαKO and LC mice

Animal ID	cKO or LC	Drug or placebo	N.Ob/BS.R (mm^{-1})	N.Ob/BS.L (mm^{-1})	N.Oc/BS.R (mm^{-1})	N.Oc/BS.L (mm^{-1})
A4204	LC	placebo	5.46579	6.50849		3.0187
A4406	LC	placebo	2.54777	2.39893	2.07743	3.76326
A4415	LC	placebo	3.58722	12.4482	5.45062	3.92354
A4502	LC	placebo		4.79951		
A4508	LC	placebo				
B4807	LC	placebo			4.59136	2.69503
B5012	LC	placebo	5.5711		1.93756	
B5108	LC	placebo	5.83622	6.24583	2.99133	2.18484
B5110	LC	placebo	2.59642	3.88438	7.6661	2.49904
B5302	LC	placebo				

Table D.4 continued

Animal ID	cKO or LC	Drug or placebo	N.Ob/BS.R (mm^{-1})	N.Ob/BS.L (mm^{-1})	N.Oc/BS.R (mm^{-1})	N.Oc/BS.L (mm^{-1})
C5203	LC	drug	1.93641	2.69687	1.2377	4.05683
C5605	LC	drug	5.54803		5.52692	3.3957
C5702	LC	drug		7.41239	3.63786	
C5915	LC	drug				
C6010	LC	drug	1.90743	3.32022	2.73674	2.69268
D6105	LC	drug	4.68363	2.3533	5.44437	1.74729
D6312	LC	drug	5.34769	3.84114		1.13419
D6407	LC	drug				
D6509	LC	drug	3.93944	4.03362	7.0032	1.51255
D6603	LC	drug				
E4112	cKO	placebo				
E4209	cKO	placebo	3.91936	5.49151	6.41444	2.94263
E4213	cKO	placebo	2.66057	3.44162	5.20834	
E4301	cKO	placebo	2.29501	5.9205	6.3175	3.80454
E4307	cKO	placebo				
F4409	cKO	placebo	4.31775		4.20317	2.54669
F4512	cKO	placebo		5.8581		2.86903
F4901	cKO	placebo	2.74065	5.90659	4.81099	4.26763
F4904	cKO	placebo				
F5008	cKO	placebo	3.91564	6.77309	3.64236	4.37372
G5013	cKO	drug				
G5502	cKO	drug				
G5504	cKO	drug		2.84617		2.01678
G5601	cKO	drug	2.43069	2.86424	2.08325	2.85902
G5709	cKO	drug				
H5812	cKO	drug	4.19626	3.78159		4.82041
H6007	cKO	drug	3.19986	2.1283	0.61042	1.86188
H6415	cKO	drug		6.90793	5.14352	2.83774
H6503	cKO	drug	3.68551	5.15355	5.13376	
H6608	cKO	drug	1.9588		2.23412	2.57204

Table D.5 Indices of cancellous vertebra measured by microCT in 12-week-old female LC and pOC-ERαKO mice, drug- and placebo-treated

Animal ID	cKO or LC	Drug or placebo	BV/TV	Tb.Th (mm)	Tb.Sp (mm)	cn.TMD (mgHA/cc)
A4204	LC	placebo	0.1913	0.053	0.2421	630.225
A4406	LC	placebo	0.2445	0.0571	0.2451	631.722
A4415	LC	placebo	0.2279	0.0553	0.2301	622.672
A4502	LC	placebo	0.1691	0.0523	0.2721	623.779
A4508	LC	placebo	0.1784	0.051	0.2701	591.029
B4807	LC	placebo	0.1679	0.0479	0.2444	591.615
B5012	LC	placebo	0.2134	0.0505	0.2232	590.052
B5108	LC	placebo	0.234	0.0557	0.2303	618.505
B5110	LC	placebo				
B5302	LC	placebo				
C5203	LC	drug	0.2334	0.0627	0.2588	656.204
C5605	LC	drug	0.3261	0.069	0.1974	661.087
C5702	LC	drug	0.3013	0.0665	0.2226	648.065
C5915	LC	drug	0.2963	0.0655	0.2277	653.925
C6010	LC	drug	0.3259	0.068	0.2144	651.32
D6105	LC	drug	0.2579	0.0632	0.2472	652.102
D6312	LC	drug	0.3185	0.0672	0.1917	655.618
D6407	LC	drug	0.333	0.0714	0.1875	667.663
D6509	LC	drug				
D6603	LC	drug				
E4112	cKO	placebo	0.2245	0.0555	0.2209	631.722
E4209	cKO	placebo	0.1374	0.0475	0.2683	608.804
E4213	cKO	placebo	0.1917	0.0488	0.2098	602.293
E4301	cKO	placebo	0.171	0.0478	0.2285	603.53
E4307	cKO	placebo	0.1653	0.0467	0.2379	583.476
F4409	cKO	placebo	0.1931	0.0534	0.2408	618.31
F4512	cKO	placebo	0.1664	0.0466	0.2364	591.094
F4901	cKO	placebo	0.158	0.0474	0.2449	590.182
F4904	cKO	placebo				
F5008	cKO	placebo	0.1913	0.053	0.2421	630.225

Table D.5 continued

Animal ID	cKO or LC	Drug or placebo	BV/TV	Tb.Th (mm)	Tb.Sp (mm)	cn.TMD (mgHA/cc)
G5013	cKO	drug	0.2253	0.0611	0.2417	653.99
G5502	cKO	drug	0.2844	0.0608	0.2064	631.267
G5504	cKO	drug	0.2755	0.0634	0.2095	655.943
G5601	cKO	drug	0.2256	0.0612	0.2434	657.18
G5709	cKO	drug	0.2687	0.063	0.2015	657.962
H5812	cKO	drug	0.3339	0.0648	0.1801	652.623
H6007	cKO	drug	0.3278	0.0632	0.1724	641.359
H6415	cKO	drug	0.2263	0.063	0.2651	651.776
H6503	cKO	drug				
H6608	cKO	drug				

Table D.6 Indices of cortical shell vertebra from microCT of 12-week-old female LC and pOC-ERαKO drug- and placebo- treated animals

Animal ID	cKO or LC	Drug or placebo	Imax (mm^4)	Imin (mm^4)	Ct.Ar (mm^2)	Ct.Th (mm)	ct.TMD (mgHA/cc)
A4204	LC	placebo	0.26117	0.05955	0.51325	0.088	713.891
A4406	LC	placebo	0.27988	0.05808	0.53126	0.087	711.482
A4415	LC	placebo	0.18706	0.06892	0.46403	0.083	707.38
A4502	LC	placebo	0.24936	0.05539	0.50241	0.086	715.063
A4508	LC	placebo	0.23612	0.05666	0.48912	0.082	703.148
B4807	LC	placebo	0.20438	0.04311	0.43944	0.08	695.921
B5012	LC	placebo	0.28375	0.05393	0.5216	0.083	704.841
B5108	LC	placebo	0.24643	0.07777	0.52445	0.087	724.7
B5110	LC	placebo					
B5302	LC	placebo					
C5203	LC	drug	0.38075	0.07862	0.64874	0.098	722.161
C5605	LC	drug	0.33246	0.06262	0.62473	0.107	739.089
C5702	LC	drug	0.35647	0.06153	0.65455	0.104	724.7
C5915	LC	drug	0.32748	0.06444	0.62303	0.102	737.462
C6010	LC	drug	0.30841	0.06351	0.61061	0.102	730.69
D6105	LC	drug	0.24017	0.05118	0.52246	0.099	738.243
D6312	LC	drug	0.30836	0.07103	0.59903	0.097	724.895
D6407	LC	drug	0.30386	0.06339	0.58917	0.099	724.635
D6509	LC	drug					
D6603	LC	drug					

Table D.6 continued

Animal ID	cKO or LC	Drug or placebo	Imax (mm^4)	Imin (mm^4)	Ct.Ar (mm^2)	Ct.Th (mm)	ct.TMD (mgHA/ cc)
E4112	cKO	placebo	0.20164	0.04875	0.47311	0.088	720.012
E4209	cKO	placebo	0.25712	0.06135	0.48674	0.081	707.966
E4213	cKO	placebo	0.23399	0.05039	0.47062	0.082	711.547
E4301	cKO	placebo	0.22472	0.05213	0.44234	0.074	696.116
E4307	cKO	placebo	0.20257	0.04534	0.42003	0.076	696.312
F4409	cKO	placebo	0.21732	0.05101	0.47454	0.086	720.858
F4512	cKO	placebo	0.19521	0.04708	0.43703	0.079	695.66
F4901	cKO	placebo	0.20043	0.04565	0.43907	0.079	693.317
F4904	cKO	placebo					
F5008	cKO	placebo					
G5013	cKO	drug	0.24281	0.05684	0.49645	0.088	729.257
G5502	cKO	drug	0.19103	0.05032	0.45614	0.083	695.075
G5504	cKO	drug	0.31461	0.06387	0.56978	0.092	724.44
G5601	cKO	drug	0.27516	0.06269	0.53668	0.089	728.671
G5709	cKO	drug	0.18643	0.04843	0.47486	0.091	713.241
H5812	cKO	drug	0.18998	0.05218	0.47302	0.088	724.895
H6007	cKO	drug	0.28025	0.0675	0.53873	0.082	695.335
H6415	cKO	drug	0.22772	0.06145	0.52888	0.092	721.249
H6503	cKO	drug					
H6608	cKO	drug					

Table D.7 Indices of femoral midshafts from microCT of 12-week-old female LC and pOC-ERαKO drug- and placebo- treated animals

Animal ID	cKO or LC	Drug or placebo	Imax (mm^4)	Imin (mm^4)	Ct.Ar (mm^2)	T.Ar (mm^2)
A4204	LC	placebo	0.21274	0.12064	0.73939	1.73815
A4406	LC	placebo	0.25641	0.13663	0.82178	1.84992
A4415	LC	placebo	0.18893	0.10593	0.70045	1.62548
A4502	LC	placebo	0.21832	0.12233	0.77089	1.72423
A4508	LC	placebo	0.20726	0.13273	0.76646	1.7481
B4807	LC	placebo	0.15507	0.09633	0.65852	1.49796
B5012	LC	placebo	0.19518	0.09126	0.71653	1.53112
B5108	LC	placebo	0.22688	0.12569	0.80157	1.72183
B5110	LC	placebo				
B5302	LC	placebo				

Table D.7 continued

Animal ID	cKO or LC	Drug or placebo	Imax (mm^4)	Imin (mm^4)	Ct.Ar (mm^2)	T.Ar (mm^2)
C5203	LC	drug	0.24289	0.12941	0.83576	1.75328
C5605	LC	drug	0.16072	0.1	0.74087	1.44707
C5702	LC	drug	0.21143	0.11259	0.80698	1.60969
C5915	LC	drug	0.20395	0.1132	0.76835	1.63017
C6010	LC	drug	0.21538	0.12308	0.81978	1.65985
D6105	LC	drug	0.22603	0.13171	0.82292	1.73625
D6312	LC	drug	0.17736	0.09837	0.73773	1.502
D6407	LC	drug	0.15608	0.09345	0.66803	1.48467
D6509	LC	drug				
D6603	LC	drug				
E4112	cKO	placebo	0.17332	0.11275	0.72662	1.57179
E4209	cKO	placebo	0.21681	0.11083	0.7446	1.6836
E4213	cKO	placebo	0.18933	0.10983	0.70509	1.64434
E4301	cKO	placebo	0.17901	0.10175	0.68018	1.5941
E4307	cKO	placebo	0.19262	0.12006	0.71825	1.68642
F4409	cKO	placebo	0.2387	0.12686	0.79651	1.77149
F4512	cKO	placebo	0.19998	0.1149	0.73583	1.66705
F4901	cKO	placebo	0.20637	0.11425	0.74874	1.66494
F4904	cKO	placebo				
F5008	cKO	placebo				
G5013	cKO	drug	0.18982	0.11763	0.76324	1.61414
G5502	cKO	drug	0.17264	0.09866	0.6988	1.52715
G5504	cKO	drug	0.21956	0.12403	0.78981	1.7124
G5601	cKO	drug	0.20752	0.11166	0.76521	1.63244
G5709	cKO	drug	0.18528	0.10374	0.67451	1.63924
H5812	cKO	drug	0.213	0.12164	0.74666	1.73399
H6007	cKO	drug	0.20185	0.10515	0.70942	1.65459
H6415	cKO	drug	0.18921	0.11027	0.74024	1.59983
H6503	cKO	drug				
H6608	cKO	drug				

Table D.7 continued

Animal ID	cKO or LC	Drug or placebo	Ct.Th (mm)	ct.TMD (mgHA/cc)	Ma.Ar (mm^2)
A4204	LC	placebo	0.176	946.4	0.99876
A4406	LC	placebo	0.188	945.684	1.02814
A4415	LC	placebo	0.172	940.801	0.92503
A4502	LC	placebo	0.184	950.437	0.95334
A4508	LC	placebo	0.184	955.515	0.98164
B4807	LC	placebo	0.17	939.498	0.83944
B5012	LC	placebo	0.182	949.656	0.81459
B5108	LC	placebo	0.193	955.776	0.92026
B5110	LC	placebo			
B5302	LC	placebo			
C5203	LC	drug	0.201	959.813	0.91752
C5605	LC	drug	0.201	961.766	0.7062
C5702	LC	drug	0.205	970.426	0.80271
C5915	LC	drug	0.192	951.088	0.86182
C6010	LC	drug	0.204	964.305	0.84007
D6105	LC	drug	0.199	966.714	0.91333
D6312	LC	drug	0.192	944.707	0.76427
D6407	LC	drug	0.174	924.393	0.81664
D6509	LC	drug			
D6603	LC	drug			
E4112	cKO	placebo	0.185	944.056	0.84517
E4209	cKO	placebo	0.179	948.679	0.939
E4213	cKO	placebo	0.173	945.163	0.93925
E4301	cKO	placebo	0.169	939.173	0.91392
E4307	cKO	placebo	0.174	936.243	0.96817
F4409	cKO	placebo	0.189	946.856	0.97498
F4512	cKO	placebo	0.179	942.624	0.93122
F4901	cKO	placebo	0.183	951.283	0.9162
F4904	cKO	placebo			
F5008	cKO	placebo			

Table D.7 continued

Animal ID	cKO or LC	Drug or placebo	Ct.Th (mm)	ct.TMD (mgHA/cc)	Ma.Ar (mm^2)
G5013	cKO	drug	0.194	951.479	0.8509
G5502	cKO	drug	0.177	939.368	0.82835
G5504	cKO	drug	0.192	945.554	0.92259
G5601	cKO	drug	0.19	959.748	0.86723
G5709	cKO	drug	0.164	912.999	0.96473
H5812	cKO	drug	0.177	921.333	0.98733
H6007	cKO	drug	0.173	912.608	0.94517
H6415	cKO	drug	0.187	944.902	0.85959
H6503	cKO	drug			
H6608	cKO	drug			

Table D.8 Indices of femur and vertebra mechanical testing from 12-week-old female pOC-ERαKO and LC mice, drug- and placebo-treated

Animal ID	cKO or LC	Drug or placebo	Fem.Max Moment (Nmm)	Fem.Bend Stiffness (Nmm^2)	Vert. Comp Strength (N)	Vert. Comp Stiffness (N)
A4204	LC	placebo	24.0465	2647.93	18.894	114.906
A4406	LC	placebo	28.5765	2559.08	24.855	243.724
A4415	LC	placebo	24.525	3038.98	19.796	98.3205
A4502	LC	placebo	24.204	2053.74	19.781	240.338
A4508	LC	placebo	27.219	2097.68	17.157	127.68
B4807	LC	placebo	22.1685	3575.71	16.207	99.7807
B5012	LC	placebo	22.4565	2832.24	19.619	175.981
B5108	LC	placebo	28.002	2489.38	20.962	175.716
B5110	LC	placebo	22.3755		21.252	121.678
B5302	LC	placebo	20.439		22.631	160.303
C5203	LC	drug	31.2135	2900.54	25.987	270.517
C5605	LC	drug	27.111	2986.36	27.369	198.733
C5702	LC	drug	30.789	3223.51	26.244	213.037
C5915	LC	drug	24.651	2159.54	15.864	136.377
C6010	LC	drug	27.6225	3428.38	31.825	224.676
D6105	LC	drug	27.117	2491.92	25.559	309.731
D6312	LC	drug	25.3485	2606	28.7	248.193
D6407	LC	drug	20.8455	3225.46	29.452	314.864
D6509	LC	drug	27.792		35.023	362.387
D6603	LC	drug	27.741		32.78	230.372

Table D.8 continued

Animal ID	cKO or LC	Drug or placebo	Fem.Max Moment (Nmm)	Fem.Bend Stiffness (Nmm^2)	Vert. Comp Strength (N)	Vert. Comp Stiffness (N)
E4112	cKO	placebo	26.568	3948.19	23.968	229.26
E4209	cKO	placebo	26.3565	2519.5	18.447	103.077
E4213	cKO	placebo	22.935	1567.71	18.296	161.636
E4301	cKO	placebo	24.381	2880.55	12.96	74.9212
E4307	cKO	placebo	23.355	1993	15.859	145.302
F4409	cKO	placebo	28.878	2882.7	15.974	118.472
F4512	cKO	placebo			16.423	128.614
F4901	cKO	placebo	23.8365	2080.3	16.32	133.579
F4904	cKO	placebo	26.424		17.017	118.212
F5008	cKO	placebo	21.855		16.816	69.8506
G5013	cKO	drug	28.533	2471.42	26.052	183.216
G5502	cKO	drug	24.0975	2804.33	22.267	152.496
G5504	cKO	drug	24.567	2457.47	32.234	216.045
G5601	cKO	drug	25.5975	2422.18	21.608	141.178
G5709	cKO	drug	21.0345	2257.61	28.926	230.166
H5812	cKO	drug	24.306	2543.74	30.567	221.496
H6007	cKO	drug	21.1815	1567.38	24.159	288.486
H6415	cKO	drug	26.0535	2418.43	33.033	222.641
H6503	cKO	drug	22.2945		24.026	151.583
H6608	cKO	drug	23.634		25.82	201.053